The role of BET attenuation in melanoma



Elizabeth K. Henderson

Balliol College,

University of Oxford

A thesis submitted for the degree of

Doctor of Philosophy in Clinical Medicine

Trinity 2020

Acknowledgements

I would like to thank Prof. Panagis Filippakopoulos for his supervision and mentorship throughout my PhD and for all the collaborative opportunities. Especially, thanks for his patience when imparting computational knowledge, and thank you for all the invaluable lessons he has taught me. Prof. Colin Goding for his role as a second supervisor, providing me with direction and guidance. I would also like to thank all Ludwig support staff for all their support.

To past members of the Filippakopoulos lab: I would like to thank Dr Pavel Savitsky for all his patience, encouragement and invaluable supervision. In particular, amongst many lab-lessons, thank you for imparting cloning and troubleshooting wisdom. Takao, Sarah and Chen-Yi, many thanks for all your help and support.

Thank you to Elphire for all your friendship, our encouraging discussions, and laughter. Thanks for encouraging me to keep going when things were tough and for making the last four years brighter.

Thank you to all members of the Goding lab for scientific chats, camaraderie and making the lab a fun and happy place to work. Paka, thank you for all your advice and always listening to my worries, whether lab-related or not, and most times providing a solution, even when you're busy. Yurena and Rom, thank you for encouraging discussions and helpful advice. Diogo and Sizhu for all the times you've had my back. Sarah thank you for all the times you've made me laugh, and hosted me, and for the very delicious breakfasts, your kindness made travelling logistics a lot easier!

To Mark Shipman and Richard Lisle, thank you for patience and microscopy expertise. Richard, thank you for all the encouragement, patience in explaining microscopy things to me multiple times, and making me feel that little bit better when things didn't work.

Thank you to my friends: thank you for all the chats, encouragement, kindness, patience and for knowing when I needed a cup of tea or a G+T.

To my family: thank you for listening to me talk about science things for much longer than just four years. Thank you for encouraging me to go for it, not to give up, and for instilling in me that even when things are hard, I can do it.

Lastly, John. What a star you are. Thank you for reminding me that no matter how my work turns out, I am more than that, and it will be okay. Thank you for being with me every step of the way, for knowing me so well and making me laugh no matter what.

Unless the Lord builds the house, the builders labour in vain.

Psalm 127:1

Disclaimer

I declare that this submission is my own work. To the best of my knowledge, it contains no material that has been written by another or previously submitted in the same or a different form as academic work, to this or any other university.

The data presented in this thesis are the result of my own work, with the exception of *in vitro* data surrounding BET BRD inhibitor affinity presented in Table 4.1, generated by Dr Sarah Picaud.

The U-2 OS cells used in Figure 7.7 were genetically modified by Dr Takao Fujisawa, a post-doctoral scientist previously in the Filippakopoulos lab.

Material from “BET mechanisms in cancer” (Henderson, E & Filippakopoulos, Chapter 5 of the book Histone Modifications in Therapy, has been reused in this thesis, with permission from the co-author and Elsevier, the publisher.

COVID Statement

Owing to pre-existing medical conditions I was deemed “clinically extremely vulnerable” to Coronavirus; therefore, I was shielding from mid-March until July. Additionally, owing to unique personal circumstances I was unable to carry out lab work from August onwards; therefore, experiments I had planned to carry out as part of this thesis are detailed in the Appendix, indicating which experiments pertain to each results chapter. I have also described further work that could have been carried out to extend the work of this thesis. It may have been possible to carry out some of this work under normal circumstances, hence inclusion of these future plans in this thesis.

Abstract

Bromodomain and extra-terminal (BETs) proteins function as epigenetic readers by docking onto acetylated lysine residues (Kac) on histone tails via tandem bromodomains (BRDs), and recruiting protein binding partners via an extra-terminal recruitment domain (ET). Targeting BET BRDs is efficacious in different malignancy models; however, the underlying mechanisms remain largely unknown in solid tumours. Together with concerns over toxicity, this calls for a greater understanding of BET protein biology and alternative targeting approaches. p53 influences the phenotype observed in haematopoietic cells following BET BRD inhibition, so it was investigated whether p53 has a similar regulatory role in melanoma. Here, I show that melanoma cells undergo senescence or apoptosis following BET BRD inhibition, and that p53 mutation status potentially correlates with this cell fate decision. Furthermore, BET inhibition up-regulates autophagic flux in melanoma and prostate cancer cells. However, the effect of concomitant autophagy inhibition on cellular proliferation is heterogeneous. Finally, ET domain inhibition leads to autophagy-dependent senescence in melanoma, which provides proof-of-principle that both Kac-dependent and independent targeting of BETs yield a loss of cell viability.

Table of Contents

Acknowledgements ii
Disclaimer iv
COVID Statement iv
Abstract v
List of Abbreviations 1
Chapter 1: Introduction 6
1.1 Chromatin 6
1.2 Histone acetylation 6
1.3 Recognition of histone acetylation 7
1.4 BETs proteins and their role in transcription 8
1.5 BETs in cellular homeostasis 11
1.5.1 Role of BRD2 in cellular homeostasis 12
1.5.2 Role of BRD3 in cellular homeostasis 13
1.5.3 Role of BRD4 in cellular homeostasis 14
1.6 Pharmacological BET BRD targeting in cancer 15
1.6.1 Proof of principle 17
1.6.2 Mechanisms of BET BRD inhibition 18
1.6.3 Problems with BET BRD targeting 24
1.7 Melanoma 32
1.7.1 Melanoma biology 32
1.7.2 Current treatments for metastatic melanoma 33
1.8 BETs in melanoma 38
1.8.1 Rationale for BET targeting 38
1.8.2 BET inhibition in melanoma 39
1.9 Summary and questions 46
Chapter 2: Materials and Methods 49
2.1 Materials 49
2.1.1 Cell lines 49
2.1.2 siRNAs and primers 50
2.1.3 Antibodies 53
2.1.4 Buffers and reagents 55

2.1.5 Commercially available kits....60
2.1.6 Pharmacological BET inhibitors....60
2.2 Methods....61
2.2.1 Cell biology....61
2.2.2 Molecular Biology....75
2.2.3 Protein biology....78
2.2.4 Statistical analyses....79
Chapter 3: Mechanism of inhibition following BRD inhibition in melanoma....80
3.1 Introduction....80
3.2 Results....83
3.2.1 Melanoma cell lines display different sensitivities to BET BRD inhibition....83
3.2.2 p53 mutation correlates with loss of p21 up-regulation in melanoma cells....88
3.2.3 BET BRD inhibition causes a p53-dependent G1 cell cycle arrest....97
3.2.4 BET BRD inhibition leads to p53-independent activation of autophagy in melanoma cell lines....109
3.2.5 p53 mutation status correlates with cell fate and role of autophagy in melanoma cell lines following BET BRD inhibition....117
3.3 Discussion....134
Chapter 4: Mechanism of action induced by novel BET BRD inhibitor in prostate cancer....141
4.1 Introduction....141
4.2 Results....144
4.2.1 Novel BET BRD inhibitor leads to enhanced loss of cellular proliferation in vitro in prostate cancer cells....144
4.2.2 Loss of cellular proliferation induced by novel BET BRD inhibitor is independent of cell death in prostate cancer....148
4.2.3 Loss of prostate tumour growth is independent of loss of AR signalling....150
4.2.4 BET BRD inhibition leads to up-regulation of autophagy in LNCaP cells....153
4.2.5 BET BRD inhibition yields changes in cell morphology and motility, underpinned by autophagy, in LNCaP prostate cancer cells....164
4.2.6 Concomitant BET BRD inhibition and blockade of the autophagic pathway increases loss of cellular proliferation and G1 cell cycle arrest in LNCaP prostate cancer cells....170
4.3 Discussion....175
Chapter 5: Targeting of BET proteins via the ET-domain leads to autophagy-dependent senescence in a melanoma model....179

5.1 Introduction 179
5.2 Results 181
5.2.1 Generation and validation of stable, doxycycline-inducible PepX expression in a melanoma cell line 181
5.2.2 PepX-mediated ET-domain inhibition decreases cell proliferation in 501mel melanoma cells 187
5.2.3 Loss of cellular proliferation following PepX expression may be p53-independent and p21-independent 189
5.2.4 ET-domain inhibition of BETs induces cell cycle arrest 190
5.2.5 BET ET-domain inhibition induces autophagy-dependent senescence 201
5.3 Discussion 211
Chapter 6: Discussion 216
6.1 Role of autophagy following BET inhibition 216
6.1.1 Autophagy is up-regulated in prostate cancer and melanoma following BET inhibition 217
6.1.2 The dichotomy of autophagy in cancer 218
6.1.3 Autophagy and p53 220
6.2 ET-domain and BRD inhibition lead to autophagy-dependent senescence in 501mel cells 221
6.2.1 Up-regulation of the p53 pathway 222
6.2.2 Senescence induction 222
6.2.3 Transcriptional regulation by BETs in melanoma 223
6.3 Clinical applications 225
6.4 Conclusions 226
Chapter 7: Appendix 227
7.1 Supplementary Figures 227
7.2 Supplemental methods 235
7.2.1 Time lapse microscopy 235
7.2.2 Scratch wound assay 235
7.2.3 LacOLacI Co-localisation assay 235
7.2.4 Cloning pcDNA5-eGFP -PepX, -KRR, and -LIL 237
7.2.5 Cloning BRD4ΔET-mCherry-LacR-NLS 238
7.3 Future Plans relating to results chapters 3-5 242
7.3.1 Future plans relating to Chapter 3 242
7.3.2 Future plans relating to Chapter 4 245

7.3.3 Future plans relating to Chapter 5 246
7.4 Future Plans to extend thesis findings 250
7.4.1 Thesis summary.....250
7.4.2 Unanswered questions 250
7.4.3 BET-G9a axis regulation of autophagy gene expression in melanoma and prostate cancer 253
Bibliography 271

List of Abbreviations

A	Alanine
A375M	A375 metastatic cell line
AKT	RAC-alpha serine/threonine-protein kinase/protein kinase B/AKT
AML	Acute myeloid leukaemia
AMPK	Adenosine monophosphate-activated protein kinase
AR	Androgen receptor
ATG12	Autophagy-related 12
ATG4B	Autophagy-related 4B cysteine peptidase
ATR	Ataxia-telangiectasia and Rad3-related
BafA	Bafilomycin A
BCL-XL	B-cell lymphoma extra large
BCL2	B-cell lymphoma 2
Bdf1	Bromodomain-containing factor 1
BET	Bromo and extra-terminal domain protein
BFP	Blue fluorescent protein
BNIP3	BCL2 interacting protein 3
BNIP3L	BCL2 interacting protein 3 like
BRAF	B-Raf proto-oncogene, serine/threonine kinase
BRD	Bromodomain
BRD2	Bromodomain containing 2
BRD3	Bromodomain containing 3
BRD4	Bromodomain containing 4
BRD4S	Short isoform of BRD4
BRD4SB	Short isoform of BRD4 B
BSA	Bovine serum albumin
C	Cystein
C-terminal	Carboyxl-terminal
C-terminus	Carboxyl-terminus
CDK9	Cyclin dependent kinase 9
CDKN1A	Cyclin dependent kinase inhibitor 1A

CDKN2D	Cyclin dependent kinase inhibitor 2D
cDNA	Complementary DNA
CEBPβ	CCAAT/enhancer-binding protein beta
ChIP	Chromatin immunoprecipitation
ChIP-seq	Chromatin immunoprecipitation followed by sequencing
Cl.	Cleaved
CLCN7	Chloride voltage-gated channel 7
Co-IP	Co-immunoprecipitation
CQ	Chloroquine
CTCF	CCCTC-binding factor
CTLA-4	Cytotoxic T-lymphocyte-associated protein 4
CTM	Carboxyl-terminal motif
CTSF	Cathepsin F
D	Aspartic acid
DAPI	4′, 6-diamidino-2-phenylindole
DMEM	Dulbecco’s modified eagle medium
DMSO	Dimethyl sulfoxide
DNA	Deoxyribonucleic acid
dNTP	Deoxyribonucleotide triphosphate
Dox	Doxycycline
DTT	Dithiothreitol
E2F2	E2F Transcription factor 2
EHMT2	Euchromatic histone lysine methyltransferase 2
ERK	Mitogen-activated protein kinase
ET	Extra-terminal domain
ETV-1	ETS variant transcription factor 1
FACS	Fluorescence activate cell sorting
FL	Full length
FPKM	Fragments per kilobase per million mapped reads
GAPDH	Glyceraldehyde-3-phosphate dehydrogenase
GATA1	GATA binding protein 1
GFP	Green fluorescent protein

GO	Gene ontology
gp100	Glycoprotein 100
GSEA	Gene set enrichment analysis
h	Hours
H	Histidine
H3K9	Histone 3 lysine 9
H3K9me2	Dimethylated lysine 9 of histone 3
H4K5ac	Acetylated Histone 4 lysine 5
HAT	Histone acetyltransferase
HDAC	Histone deactyltransferase
HEXIM1	HEXIM P-TEFb complex subunit 1
HP1	Heterochromatin protein 1
I	Isoleucine
IF	Immunofluorescence
IgG	Immunoglobulin G
IGR37	Institut Gustave Roussy-37
IGR39	Institut Gustave Roussy-39
IP	Immunoprecipitation
JMJD6	Arginine demethylase and lysine hydroxylase
K	Lysine
Kac	Acetylated lysine
kDa	Kilodalton
L	Leucine
LacI	Lac repressor protein
LacO	Lac operator
LacR	Lac repressor protein
LC3B	Microtubule associated protein 1 light chain 3 beta
LFCs	Log2fold changes
LNCaP	Lymph node carcinoma of the prostate
lncRNA	long, non-coding RNA
LSD1	Lysine-specific histone demethylase 1
m-TOR	Mechanistic target of rapamycin

Min	Minutes
miR	microRNA
MITF	Microphthalmia-associated transcription factor
MLL	Mixed lineage leukaemia
MLV	Murine leukaemia virus
MM	Multiple Myeloma
mM	Millimolar
MYC	MYC proto-oncogene
NEU1	Neuraminidase 1
nM	Nanomolar
nm	Nanometre
NMC	NUT-midline carcinoma
NPM1	Nucleophosmin
NRAS	NRAS proto-oncogene, GTPase
NSD3	Nuclear receptor binding SET domain protein 3
NuRD	Nucleosome and remodelling complex
NUT	Nuclear protein in testis
OIS	Oncogene induced senescence
p-mTOR	Phospho-mTOR
p70S6K	Ribosomal S6 Kinase Beta 1
PAGE	Polyacrylamide gel electrophoresis
PARP	Poly(ADP-ribose) polymerase
PBS	Phosphate buffered saline
PC3	Prostate cancer cell line
PCR	Polymerase chain reaction
PD-1	Programmed cell death protein 1
PE	Phosphatidylethanolamine
PI	Propidium iodide
PROTACs	Proteolysis targeting chimeras
PS	Phosphatidylserine
PTEF-b	Positive transcription elongation factor b
PTEN	Phosphatase and tensin homologue

PTM	Post translational modification
qPCR	Quantitative polymerase chain reaction
R	Arginine
RNA	Ribonucleic acid
RNA-seq	RNA-sequencing
RNAi	RNA interference
RPMI	Roswell Park Memorial Institute
S.O.C.	Super optimal broth with catabolic repressor
SDS	Sodium dodecyl sulphate
shRNA	Short-hairpin RNA
siNC	Negative control small-interfering RNA
siRNA	Small-interfering RNA
SLC1A5	Solute carrier family 1 member 5
SLC3A2	Solute carrier family 3 member 2
Stau	Staurosporine
TAD	Topologically associated domain
TAE	Tris-acetate-EDTA
TAZ	Tafazzin
TBS	Tris buffered saline
TBS-T	Tris buffered saline with 0.1% Tween 20
TSA	Trichostatin A
TSC2	Tuberous sclerosis complex
TSS	Transcription start site
ULK1	Unc-51 like autophagy activating kinase 1
V	Valine
v/v	Volume by volume
W	Tryptophan
WT	Wild type
YAP	Yes-associated protein
γH2AX	Gamma H2A.X variant histone
µg	Microgram
µM	Micromolar

Chapter 1: Introduction

1.1 Chromatin

Chromatin is the structure in which DNA is contained within nuclei of interphase cells [1]. Genomic DNA is arranged into nucleosomes, which consist of 146bp of DNA wrapped around an octamer of histone proteins and a linker histone, H1 [2]. The octamer comprises two each of histone proteins H2A, H2B, H3 and H4, and one linker histone, H1, which stabilises the DNA and octamer through internucleosome binding [2]. The tails of the histone proteins are modified through the deposition of post-translational modifications (PTMs), which impact upon histone-histone and histone-DNA interactions, and higher-order chromatin organisation. Consequently, the accessibility of DNA, and subsequent gene expression is profoundly impacted by histone PTMs.

Chromatin can be divided into two structurally and functional distinct states. Euchromatin is defined by histone 3 lysine 4 methylation, and H3 and H4 acetylation [3, 4]. These PTMs render chromatin de-condensed, accessible to transcriptional machinery and the DNA amenable to transcription. Heterochromatin is defined by methylation at lysine 9 on histone 3, the recruitment of heterochromatin protein 1 (HP1) and chromatin condensation [5]. Thus the stretches of DNA between nucleosomes are much shorter and the DNA is much less accessible to transcriptional machinery through steric exclusion, therefore transcription is repressed in these regions [4, 5].

1.2 Histone acetylation

PTMs are abundant throughout the proteome, providing a versatile and reversible layer of regulation, and acetylation is no exception. PTMs enable the initiation or blocking of protein:protein interactions, thereby orchestrating the assembly of complexes that execute complicated molecular functions. Acetylation of lysine residues (Kac) in particular serves

as a link between metabolism and cellular functions, affecting protein stability, localisation and subsequent interactions [6]. Kac found on histone proteins relaxes their interaction with DNA, facilitating the formation of euchromatin and allowing for the recruitment of transcriptional complexes leading to the subsequent activation of gene expression.

Histone acetylation it is associated with active gene transcription. For example, H2AK9ac, H2BK5ac, H3K9ac, H3K18ac, H3K36ac and H4K91ac are located in close proximity to transcription start sites [7]. H2BK12ac, H2BK20ac, H2BK120ac, H3K4ac, H4K5ac, H4K8ac, H4K12ac and H4K16ac are found at promoters and in transcribed regions of gene bodies [7], and H3K27ac is the mark of an active enhancer, but can also be found near transcription start sites [7-9]. Histone acetylation and, therefore, chromatin availability and gene expression, is tightly regulated by histone acetyltransferase (HAT) enzymes and histone deacetyltransferase (HDAC) enzymes [10]. Aberrant histone hypoacetylation and HDAC over-expression compared with normal tissue have been observed across multiple malignancies [11-17], hence the emergence of histone deactylase inhibitors (HDACis) as anti-cancer therapies.

1.3 Recognition of histone acetylation

Recognition of Kac is mediated primarily through bromodomains (BRDs), an evolutionarily conserved domain [18]. In human, 61 BRDs are present in 42 proteins, enabling recognition and docking to Kac through a hydrophobic pocket consisting of four alpha helices (αZ, αA, αB, αC) flanked by two loops (ZA and BC) [19, 20]. BRDs are often found in proteins with a multi-domain architecture. They are sometimes linked to domains with catalytic functions, or other domains that allow for protein-protein interactions, facilitating complex and multifaceted protein functions. Once bound to Kacs, BRD-containing proteins can function as transcription modulators, chromatin remodellers and modifiers, providing a scaffolding platform which enables the aggregation of larger complexes [Reviewed in 21,

22]. Bromo and extra-terminal (BET) proteins belong to this super-class of modular proteins; thus, BETs are linked to important transcriptional phenotypes.

1.4 BETs proteins and their role in transcription

The BET sub-family of proteins consists of BRD2, BRD3, BRD4 (of which there are short and long isoforms), and testis-specific BRDT [Reviewed in 23]. BETs share a common domain architecture with characteristic tandem N-terminal BRDs (Figure 1.1A) that can recognise Kac on histones (Figure 1.1B) and other proteins. BET BRDs exhibit higher affinity towards tandem Kac marks on histones tails, such as H4K5acK8ac, enabled by their large hydrophobic Kac-recognition cavity, rather than single acetylation marks [24, 25]. Once bound to chromatin, BETs act as platforms onto which additional transcriptional machinery can dock, and subsequently modulate transcription [23]. Accordingly, they are referred to as “epigenome readers” [26].

Moreover, BET BRDs initiate interactions with a number of acetylated transcription factors, including NFκB, GATA1, TWIST, ERG and STAT3, contributing to their recruitment to target loci and affecting the transcription of their target genes [27-31]. Interactions with other acetylated proteins, including CyclinT1 [32], ZMYND8 [33] and possibly the androgen receptor (AR – note that an acetylation site has not been mapped yet, but the association between BRD4 and AR is sensitive to BET BRD targeting with small molecule inhibitors) [34] suggest a broader role in recruitment initiated by BET BRDs. Indeed, proteomic studies suggest that several chromatin related proteins contain multiple acetylated lysines, thereby exhibiting similar sequence patterns to those found on histones, providing a structural rationale for recognition and engagement by BET BRDs [35, 36].

Additionally, BET proteins contain an extra-terminal (ET) domain and (in the case of the longer isoforms of BRD4 and BRDT) a C-terminal motif (CTM) (Figure 1.1A). While the

CTM enables interaction with PTEF-b, facilitating the phosphorylation of Ser2 on the RNA polymerase 2 heptad repeat leading to transcriptional elongation [37-39], the ET domain allows for the recruitment of transcriptional modulators, including NSD3 and JMJD6, enabling PTEF-b-independent transcription [40]. The role of BET proteins in PTEF-b-independent transcription remains relatively under explored compared to the PTEF-b-dependent counterpart. BET ET domains recognise conserved short linear motifs found on several proteins providing a rationale for the aggregation of larger transcriptional complexes (Figures 1.1A-1B) [36, 41].

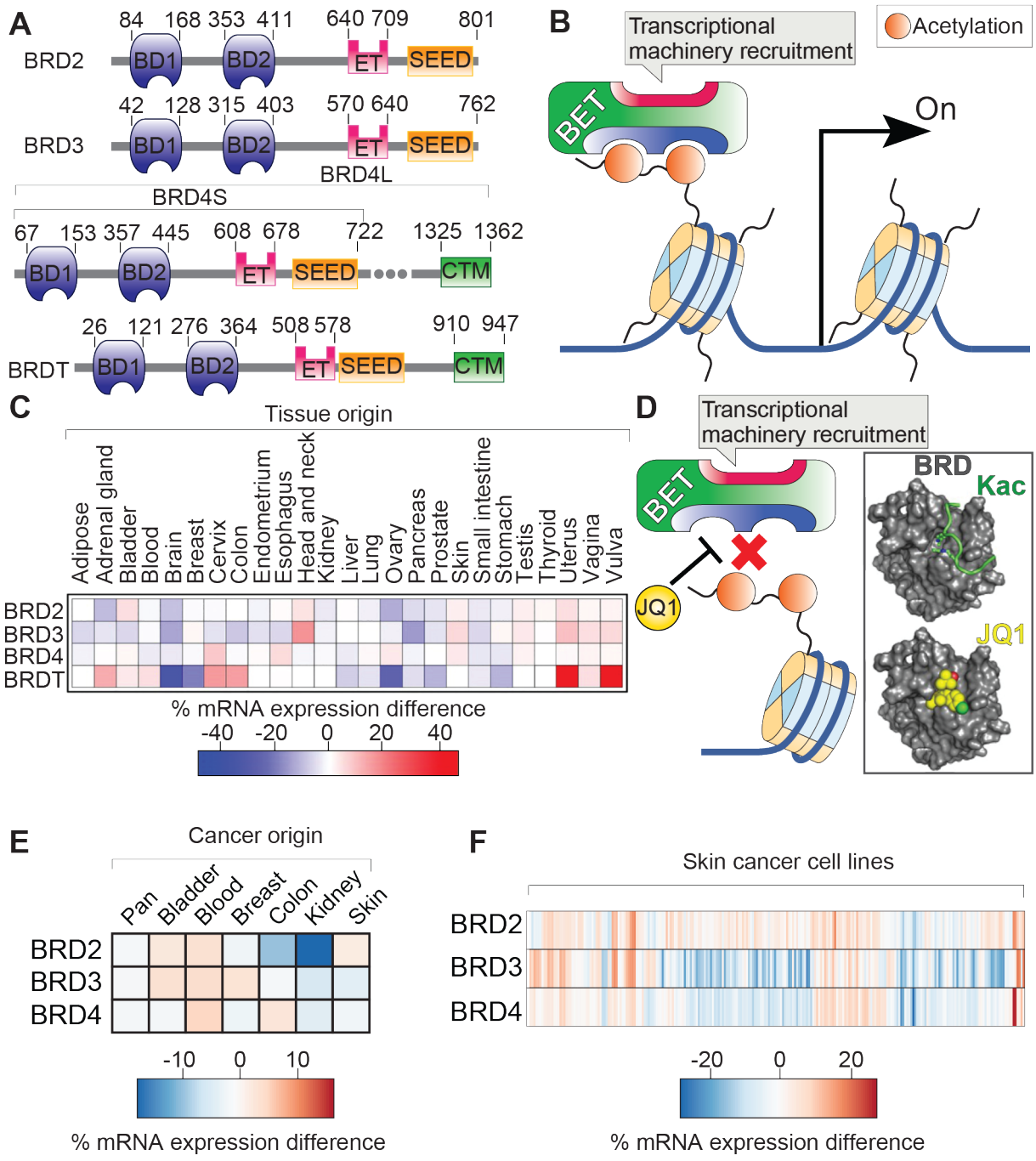


Figure 1.1: *BET protein domain organisation and mechanism. (**A**) Domain organisation of BET proteins showing the two N-terminal BRD modules, ET domain and CTM together with domain boundaries. BRD4SB structure depicted, shown as BRD4S. Figure adapted from [42]. (**B**) Cartoon schematic of BET transcriptional role. BET proteins recognise Kac on histones via BRDs (blue) and transcription factors facilitating chromatin engagement and tethering complexes via ET-domain (pink) and CTM-mediated interactions. (**C**) Deregulation of BET mRNA levels between the normal and the diseased tissue in cancer.*

*Data from [43, 44], figure adapted from [42]. (**D**) Small molecule inhibitors targeting the BRD Kac binding cavity (for example, the thieno-diazepine, (+)-JQ1) compete for Kac binding perturbing BET associations, thereby affecting transcriptional programs. Figure adapted from [42]. (**E**) Mean BRD -2, -3, and -4 mRNA expression levels in pan-cancer cell lines compared with mean BRD -2, -3, and -4 mRNA expression in healthy cell lines from the same origin. Data from [43, 44]. (**F**) BRD -2, -3, and -4 mRNA expression levels in skin cancer cell lines compared with mean BRD -2, -3, and -4 mRNA expression in healthy skin cells. Data from [43, 44].*

1.5 BETs in cellular homeostasis

BET protein expression is ubiquitous, with the exception of BRDT [42, 45]. Since BRDT expression is restricted to the testis [42, 45], BRD2, BRD3 and BRD4 will be the focus of this thesis. While a $Brd3^{-/-}$ mouse not been reported, Brd2 or Brd4 knockout are embryonic lethal in murine development [46, 47]. $Brd2^{-/-}$ mice die by E13.5, suggesting Brd2 is required to complete embryogenesis [46]. $Brd2^{+/-}$ mice are viable, and while cells proliferate more slowly *in vitro* compared to wild type (WT) counterparts, $Brd2^{+/-}$ mice grow up to a size comparable with WT littermates [46, 47]. $Brd4^{-/-}$ mice die *in utero*, shortly after implantation, when trophoblast giant cells and inner cell mass grow into distinct populations; therefore, at least one copy of BRD4 is required to maintain inner cell mass [48]. This is likely underpinned by a defect in mitosis caused by lack of Brd4 expression [48].

Functional redundancy may explain why BET protein mutant mice survive for several days during gestation. BETs exhibit functional redundancy, yet their roles do not entirely overlap, with each BET protein maintaining a subset of distinct roles [42]. At E8.5, neuronal proliferation is initiated and without functional Brd2 expression, mice exhibit neural growth defects [46]. Perhaps, $Brd2^{-/-}$ mice survive until mid-gestation because, until neural

proliferation, other BET protein family members can compensate the role of Brd2. Therefore, when Brd2 is required to carry out a non-redundant function, for example, to drive neural development, it is at this point the effects of Brd2 nullizygosity become clear, and mice undergo organism death. Similarly, in the case of Brd4, of the BET proteins, it alone is able to maintain inner cell mass; however, potentially Brd2 and Brd3 are able to drive cellular proliferation until the point at which inner cell mass maintenance is required. While their shared multi-domain structure affords similar Kac recognition behaviour to the BET family members, BETs and their isoforms have context-specific functions, which draws attention to the complexity of their roles and suggests that they have distinct contributions to cellular homeostasis.

1.5.1 Role of BRD2 in cellular homeostasis

BRD2 has several cellular functions linking to cell cycle progression, metabolism, adipogenesis and transcriptional scaffolding. BRD2 function ensures normal neuronal differentiation, while genetic knockout accelerates cell cycle progression and impairs cell cycle exit in murine models [49]. Regarding metabolism, Brd2 knockdown *in vivo* leads to severe obesity and metabolic alterations in mice [50]. *In vitro*, BRD2 plays a role in differentiation of adipocytes. Knockdown of BRD2 promotes differentiation and is accompanied by an increase in adipocyte differentiation-specific transcription factor expression. Conversely, over-expression of BRD2 leads to a decrease in differentiation and a decrease in adipogenesis [51]. BRD2 plays a scaffolding role in transcription via its interaction with CCCTC-binding factor (CTCF), a protein which compartmentalises topologically associated domains (TADs) [52]. Recruitment of CTCF and BRD2 to chromatin regulates the influence of enhancers on adjacent gene expression. BRD2 depletion partially abrogates the function of these boundaries and allows regulation of

enhancers to aberrantly spread to adjacent genes, indicated by the increase in correlation of the adjacent genes' expression levels [53].

1.5.2 Role of BRD3 in cellular homeostasis

The role of BRD3 *in vivo* is yet to be fully elucidated; however, it has been linked to erythropoiesis via its interaction with acetylated GATA1. Erythroid maturation, the development from erythropoietic stem cells to mature red blood cells, is lost when the BRD3-GATA1 Kac-dependent interaction is disrupted, either through pharmacological inhibition of the BRD3 Kac-binding pocket, or mutations of the GATA1 Kac sites. BRD3 recruits GATA1 to active as well as repressed target genes in a Kac-specific manner [28]. *In vitro* studies demonstrated that BRD3 associates with lysines K312 and K315 on GATA1 following their acetylation [54]. It is possible that BRD2 and BRD4 also play a role in erythroid gene expression, as targeting their expression led to an attenuation of erythroid genes, highlighting the potential functional overlap shared by BET family members [55].

A BRD3 isoform lacking the extra-terminal domain, BRD3R, was found to act as a reprogramming factor [56]. Somatic cells expressing OCT4, KLF4, SOX2 and BRD3R produced a population of induced pluripotent cell colonies. The addition of BRD3R alongside the three essential reprogramming factors, OCT4, KLF4 and SOX2, led to quicker pluripotent reprogramming. Conversely, attenuation of BRD3R function by shRNA led to a 58% decrease in reprogramming, indicating that BRD3R over-expression enhances reprogramming efficiency. BRD3R up-regulated mitotic genes, in such a way that was reminiscent of a pluripotency genetic signature. Interestingly, BRD3R also bound to acetylated histones, showing affinity for tetra-acetylated histone marks; however, it is unclear how this impacts upon its role in cellular reprogramming [56]. There is also evidence suggesting that BRD3 may be directly involved in cell cycle progression by negatively regulating the Rb/E2F pathway; over-expression of BRD3 led to decreased Rb

phosphorylation, and decreased expression of cyclin D1 and E2F3 [57]. While further studies are needed to properly address this functional link, this indication suggests BRD3 may function as a tumour suppressor.

1.5.3 Role of BRD4 in cellular homeostasis

BRD4 exhibits multi-faceted behaviour in cells, particularly since it exists in several different isoforms. Besides its interaction with the transcriptional machinery via its ET domain and CTM, BRD4 and its isoforms have multiple unique roles within the cell. It has been implicated in development, cell cycle progression, DNA damage signalling, and macroautophagy (hereafter referred to as autophagy).

BRD4 is essential for development; while Brd4 null mice die *in utero*, $Brd4^{+/-}$ animals exhibit severe anatomical abnormalities [48]. Transgenic animals expressing inducible short hairpin RNAs (shRNAs) targeting Brd4 display severe defects in several tissues, decreased cellular diversity and stem cell depletion in the small intestine, alopecia, epidermal hyperplasia, sensitivity to organ stress and impaired regeneration following irradiation, establishing a strong developmental role for BRD4 [58]. BRD4 is also involved in cerebellum development and its conditional deletion leads to morphological defects and ataxia [59].

Regarding cell cycle, BRD4 has been implicated in cell cycle progression; it is required for G2 to M transition [60], its expression seems to control the G1 to S transition [61] and over-expression of a short isoform of BRD4 (BRD4S) causes G0/G1 cell cycle arrest [62]. BRD4 is recruited transcriptional start sites during mitosis [60, 63], facilitating transcriptional reactivation following mitosis, and acting as a “bookmark”, seemingly through subsequent chromatin de-compaction of these sites [64]. Accordingly, BRD4 knockdown led to global chromatin decompaction [65]. However, despite the genome-wide distribution of BRD4 over mitotic sites in erythroid cells, coinciding with the distribution of

several histone marks, removal of BRD4 from mitotic chromatin does not impair post-mitotic transcriptional activation. This finding suggests that BRD4 may only transiently bind lineage specific genes, while the true “bookmarks” are the histone Kac patterns that are responsible for post-mitotic re-activation of these genes [66].

Short isoform of BRD4 B (BRD4SB) has been shown to recruit the condensin II complex and insulate chromatin which prevents the propagation of DNA damage signalling upon treatment with ionising radiation, whereas neither BRD4SA nor BRD4SC exhibit this function. Suppression of BRD4SB through shRNA expression lead to increased γH2AX phosphorylation and DNA damage signalling. Over-expression of this isoform also led to compacted chromatin, increased cell death and cell cycle arrest while reduction of BRD4SB led to the inverse phenotype [67].

Silencing of the BET orthologue Bdf1 following an RNAi screen in Drosophila cells, resulted in an increase in LC3B puncta, a marker of autophagy [68]. Similarly, knockdown of BET family members in pancreatic cancer cells demonstrated that specifically knockdown of BRD4, but not BRD2 or BRD3, led to an increase in LC3B puncta and LC3B expression. Indeed, BRD4 knockdown led to the increase in autophagy-related gene expression, and its over-expression prevented the expression of these genes, implicating BRD4 as a suppressor of autophagy [68]. BRD4 suppressed autophagy through interacting with G9a, a histone methyltransferase, at the promoters of autophagy-related genes, which resulted in their down-regulation [68]. Therefore, BRD4 plays a role in gene repression, as well as transcriptional activation.

1.6 Pharmacological BET BRD targeting in cancer

Despite their similar domain architecture, BET proteins seem to adopt unique as well as overlapping roles in different contexts. Although this provides a level of functional redundancy, the exact contribution of each BET protein to particular processes and

phenotypes is unclear. Genome-wide CRISPR screens have demonstrated that BRD4 is one of the common essential genes for sustaining life and BRDT plays a similar role, although in a lineage restricted manner [69]. Given their central role in development and transcription, and their expression in disease is deregulated, there is a strong rationale for therapeutic BET targeting (Figure 1.1C, [42]).

The large hydrophobic Kac-recognition cavity found on BET bromodomains has provided an attractive opportunity for the development of Kac-competitive small molecule inhibitors. Following initial reports by Mitsubishi Pharmaceuticals [70], thieno- (e.g. (+)-JQ1) and benzo-diazepine (e.g. I-BET762) ligands were developed that tightly bound to BET BRDs, displacing histone peptides *in vitro* and removing BET proteins from chromatin *in cellulo*, while affecting transcriptional output [71, 72] (Figure 1.1D). Since the disclosure of the first inhibitors, many chemotypes have been developed that show selectivity and specificity towards BETs as well as other BRDs [Reviewed in 73, 74, 75]. Notably, several inhibitors targeting kinases potently bind to and inhibit BRD4 *in vitro* and *in vivo* [76-79]. Interestingly, the core chemotype scaffolds maintained the same topologies when bound to the kinase target or within the BRD4 cavity, suggesting that it would be possible to design dual kinase/BET targeting inhibitors to harness both kinase and BET responses. Dual polo kinase 1 (PLK1) and BRD4 inhibitors developed with high activity towards both proteins are examples in this direction [80]. It remains to be seen how these interesting tools will contribute to targeted therapies.

Binding of small molecule inhibitors to either BRD leads to context specific displacement of BET proteins from chromatin, along with any recruited interactors. This was demonstrated in the case of BRD4, which binds promoter and enhancer regions throughout chromatin. However, pharmacological targeting of the BRD4 BRDs has a stronger impact in removing the protein from chromatin at “super-enhancers”, regions that contain multiple enhancers which are engaged by an array of transcription factors, in both liquid and solid

malignancies [81]. This subsequently leads to the simultaneous attenuation of multiple transcriptional networks, hence BET BRD inhibitors became an attractive drug candidate.

1.6.1 Proof of principle

Nuclear protein in testis (NUT)-midline carcinoma (NMC) provided proof of principle that targeting BET BRDs in cancer leads to a clinically therapeutic response. NMCs represent rare, aggressive and poorly differentiated squamous carcinomas, which originate in the midline of children and adults. Almost all patients fail to respond to intense chemo- and radio-therapeutic regimens, highlighting NMC as an area of urgent unmet clinical need [82]. The molecular basis for NMC is underpinned by a 15p/19q translocation that was initially described in 1991 [83]. Nearly a decade later, it was shown using fluorescence *in situ* hybridisation (FISH), that the BRD4 gene on chromosome 19 can be interrupted and fused to chromosome 15, giving the t(15;19)(q13;p13.1) translocation [84]. Further FISH experiments revealed the presence of BRD3-NUT fusions in about a third of the known NMC cases. Knockdown experiments targeting the BRD3- or BRD4-NUT fusion proteins showed that these fusion products were drivers of cellular proliferation and prevented differentiation [85]. Expression of the BRD4-NUT fusion leads to p300 recruitment to target loci, resulting in hyper-acetylated domains and leading to p53 inactivation [86]. Following BRD4-NUT recruitment of p300, nearby chromatin is consequently acetylated. This leads to ectopic gene expression, potentially driven by PVT1, MED24 and TP63 [87]. Based on the evidence surrounding the role of BET proteins in driving NMC, they were selected as therapeutic targets. The first *in vivo* study showing BRD4 targeting with (+)-JQ1 led to NMC tumour regression in mice, using cell line and patient-derived xenografts, demonstrating that targeting BET protein function via the BRDs can have a therapeutically beneficial response. *In vitro* experiments established that BET BRD inhibition led to decrease in cell proliferation, G1 cell cycle arrest, time- and dose-dependent

differentiation, both in terms of morphology and squamous tissue gene expression, with terminal differentiation achieved after a week's incubation with (+)-JQ1 in media. Importantly, similar effects on differentiation were not observed in BRD4-independent *in vitro* models of NMC. Patient-derived NMC cells also showed a cessation in growth and cell cycle progression when treated with (+)-JQ1 *in vitro* or when implanted into a mouse xenograft model [71]. Further studies defining the cellular phenotype of BET BRD inhibition in NMC have implicated reprogramming factors in the maintenance of proliferation and absence of differentiation of this carcinoma. (+)-JQ1 led to reduction of MYC and SOX2 expression, stem-cell–like proliferation, colony formation and increased cellular differentiation [88-90]. In fact, SOX2 over-expression protected cells from the cellular differentiation induced by (+)-JQ1 [90]. A study in patients has shown proof of concept, that BRD inhibitors targeting the BRD4-NUT oncogenic fusion protein is clinically beneficial [91]. Following these promising results, BET BRD inhibitors have been tested in a range of malignancies.

1.6.2 Mechanisms of BET BRD inhibition

The phenotypes that arise following BET BRD inhibition across multiple cancer types are similar, yet subtly different. There is considerable inter- and intratumour heterogeneity, with a broad range of sensitivities exhibited to BRD inhibitors and cellular responses, including loss of cell viability, cell cycle arrest and down-regulation of the oncogene, MYC [92-96]. As such, cancer types were evaluated individually so as to appreciate the subtle nuances of each cancer's response to BRD inhibition, the variation of response within tumour types, and to highlight the lack of a clear, universal mechanism by which BET BRD inhibition acts. Table 1.1 summarises the phenotypes observed in each cancer, and mechanisms underpinning sensitivity or resistance.

Cancer Type	Phenotype	Mechanism	References
NUT-midline carcinoma	*In vitro*: Decrease in cell proliferation, G1 cell cycle arrest, BRD4 dependent time- and dose-dependent differentiation, reduction in MYC and SOX2 expression, reduction in colony formation and stem-cell-like proliferation, increased cellular differentiation. *In vivo*: Tumour regression using either cell line or patient-derived xenografts.	15p/19q translocation yielding BRD4-NUT fusion protein. BRD3 –NUT fusions also drive oncogenesis. BRD4 dependent guidance of p300 to loci and subsequent gene activation, and p53 inactivation. BRD3/4-NUT fusion proteins are inhibited upon treatment with BET BRD inhibitor. (+)-JQ1 and siRNA targeting of NUT led to displacement of BRD4 and BRD4-NUT from the SOX2 core promoter and enhancers	[71, 83-86, 88-90]
Acute myeloid leukaemia	*In vitro*: Cell cycle arrest, MYC and target gene down-regulation, BCL2 dependent loss of cell viability, induction of apoptosis. *In vivo*: Enhanced murine survival, reduced tumour burden, MYC down-regulation.	BRD4 displacement from the MYC promoter and transcriptional start site led to down-regulation of MYC. Over-expression of MYC protected cells from cell cycle arrest, and in some cases, cell death or differentiation. Wnt β-catenin pathway drives resistance through β-catenin chromatin occupation in the place of BRD4. BRD4 displacement from transcriptional pause sites on a sensitive cell line-specific set of genes may mediate sensitivity.	[92, 93, 97-102]

Multiple Myeloma	*In vitro*: Loss of cell viability, induction of senescence, G1 cell cycle arrest, MYC down-regulation, p21 up-regulation. *In vivo*: Enhanced murine longevity and decreased MYC expression.	IgH enhancer inserted into MYC locus. Heavy occupation of BRD4 on this enhancer leads to increased MYC expression.	[103-107]
Neuroblastoma	*In vitro* in MYCN amplified cells*:* Decrease in proliferation, G0-G1 cell cycle arrest, increase in apoptosis, MYC and MYCN down-regulation. *In vivo* using xenografts harbouring MYCN amplification: Increased murine survival, decrease in MYCN expression.	BRD4 drives MYCN expression through its occupation of the MYCN promoter and a potential enhancer region in MYCN-amplified cells	[94, 108-112]
Glioblastoma	*In vitro*: Cell cycle arrest, increase in apoptosis, MYC RNA down-regulation, E2F1 gene set down-regulation, p21 up-regulation, BCL-XL pro-apoptotic protein down-regulation. *In vivo*: Decreased rate of tumour growth.	HOTAIR down-regulation led to cell cycle arrest and apoptosis	[113-119]

Colorectal	*In vitro*: G1 to S phase cell cycle perturbation, decrease in colony size formation, modest increase in apoptotic population, MYC down-regulation, p16 and p21 up-regulation, miR-21 down-regulation, Nkd2 up-regulation. *In vivo*: Enhanced murine survival and reduced tumour burden.	BRD4 and Wnt components drive MYC expression	[120-124]
Ovarian	*In vitro*: Non-uniform cell cycle perturbation, decrease in clonogenic growth and cell viability (in cell lines harbouring cMYC amplification), down-regulation of one or both of MYC and FOSL. *In vivo* using xenografts harbouring cMYC amplification: Reduced tumour growth, enhanced murine survival.	PI3K and ERK activation to stabilise MYC and FOSL. FOXM1 expression in xenografts protects against effects of (+)-JQ1.	[123, 125-128]
Breast	*In vitro*: G0/G1 cell cycle arrest, dose dependent loss of cell viability, MYC down-regulation. *In vivo*: Reduction of tumour burden.	BRD4 hyper-phosphorylation by CK2 leads to greater nuclear retention.	[92, 96, 123]

Lung	*In vitro*: Loss of cell viability, G1 cell cycle arrest, apoptosis induction reduction in colony formation, heterogeneous MYC down- regulation and p21 up-regulation. *In vivo* in mice harbouring $LKB1^{WT}$ xenografts: Reduction of tumour burden in mouse models, decrease in MYC mRNA expression.	LKB1 mutation protects against loss of MYC expression when BRD4 function is abrogated. BRD4 can drive FOSL1 expression. FOSL over-expression only partially rescued the cells when treated with BET BRD inhibitor.	[129-133]
Endometrial cancer	*In vitro*: Loss of cell viability *in vitro*, induction of apoptosis, decreased colony formation, cell cycle arrest, reduction of MYC expression. *In vivo*: Reduced tumour growth, decrease in MYC expression in xenografts.	SPOP gain-of-function mutation partially relies on FOSL function, and leads to greater BET degradation and increased sensitivity to BET BRD inhibition. PTEN-positive cells were more senstive than PTEN-negative counterparts to BET BRD inhibition.	[134-136]
Liver cancer	*In vitro*: Loss of cell viability, down-regulation of E2F2, G1 cell cycle arrest, induction of apoptosis, decrease in MYC expression, reduced clonogenic growth and wound healing. *In vivo*: Reduction in tumour burden, E2F2 mRNA down-regulation in xenografts.	BRD4 binds to the E2F2 promoter and is displaced by BET BRD inhibitors. BET BRD inhibition leads to reduction of MYC expression in EGFR WT cells.	[137-141]

Head and neck cancer	*In vitro*: Reduced cell viability, G0/G1 cell cycle arrest, reduction in colony formation, migration, invasion, induction of senescence, decrease in BRD4 expression, heterogeneous reduction in cMYC expression. *In vivo*: Reduced tumour burden and metastasis, induction of senescence in cells from the xenograft.		[82, 142-145]
Prostate	*In vitro* in AR positive cells: Loss of cell viability, G1 cell cycle arrest and apoptosis, AR and MYC down-regulation. Knockdown of BETs leads to inconsistent loss of cell viability. *In vivo*: Reduction in rate of tumour growth and enhanced murine survival.	Over-expression of MYC inconsistently protects cells from BET BRD inhibitor effects on cell growth. AR, not *AR*, expression correlates with sensitivity to BET BRD inhibition	[34, 135, 146-150]
Melanoma	*In vitro*: Loss of cell viability and clonogenic growth, p21-induced cell cycle arrest, BIM and caspase dependent cell death. MYC down-regulation, decrease of melanoma cell growth in 3D skin mimetic model *In vivo*: Decreased tumour growth and metastasis.	BRD4 perturbation leads to loss of AMIGO2 expression, the loss of which led to decreased tumour burden in mice. Over-expression of MYC did not protect from BET BRD inhibition.	[95, 151-154]

Table 1.1**:** Targeting of BET BRDs in different tumour types elicits different phenotypic responses with distinct mechanisms.

In some cancers, the mechanism by which BET protein inhibition acts is well understood; in multiple myeloma an IgH insertion within the MYC locus, proximal to the transcription start site, has been found in several patient-derived cell lines. Heavy occupation of BRD4 at the IgH enhancer leads to up-regulation of MYC expression [103]. In neuroblastoma, (+)-JQ1 treatment leads to the displacement of BRD4 from the MYCN promoter, as well as a potential enhancer region [94]. Studies in acute myeloid leukaemia (AML) demonstrate that displacement of BRD4 from several loci, including -2kb from the *MYC* promoter, the *MYC* promoter itself, and proximally downstream of the *MYC* transcription start site after 4 h of (+)-JQ1 treatment, leads to reduction of MYC expression [92, 98]. BCL2 expression is also lost upon BET BRD inhibition, and the dependence of AML cells on MYC and BCL2 even goes so far as MYC or BCL2 over-expression protects cell lines from BET BRD inhibition [92, 98].

So far, mechanisms involved in cell death, senescence and autophagy have been linked to the cellular response to BET BRD inhibition across a range of malignancies, as have a range of transcription factors. Continuing to unpick the mechanisms that determine the cell fate is critical, if we are to utilise BET BRD inhibitors to their fullest potential as an experimental tool and clinical treatment.

1.6.3 Problems with BET BRD targeting

While BET BRD inhibitors have come to the fore as a useful tool for *in vitro* and *in vivo* investigations, and have entered into clinical trials (Table 1.2), there have been problems with BET BRD inhibitors, specifically with toxicity and resistance. These are detailed below and highlight a need for a more thorough understanding of BET protein biology and alternative BET targeting.

Compound	Phase	Start Date	Reference	Status	Conditions
BMS-986158	I	June 30, 2019	NCT03936465	Recruiting	Solid Tumor, Childhood Lymphoma Brain Tumor, Pediatric
MK-8628	I	October 23, 2014	NCT02259114	Completed	NUT Midline Carcinoma Triple Negative Breast Cancer Non-small Cell Lung Cancer With Rearranged ALK Gene/Fusion Protein or KRAS Mutation Castrate-resistant Prostate Cancer Pancreatic Ductal Adenocarcinoma
OTX015/ MK-8628	I	December 14, 2012	NCT01713582	Completed	Acute Myeloid Leukemia Diffuse Large B-cell Lymphoma Acute Lymphoblastic Leukemia Multiple Myeloma
CPI-0610	I	September 2013	NCT01949883	Completed	Lymphoma
CPI-0610	I	July 2014	NCT02157636	Completed	Multiple Myeloma
RO6870810| Biological: daratumumab	I	June 26, 2017	NCT03068351	Completed	Multiple Myeloma
Azacitidine| BRD4 Inhibitor PLX51107	I	July 31, 2019	NCT04022785	Recruiting	Acute Myeloid Leukemia Myelodysplastic Syndrome Myelodysplastic/ Myeloproliferative Neoplasm Myeloproliferative Neoplasm
CPI-0610	II	May 5, 2017	NCT02986919	Withdrawn	Peripheral Nerve Tumors
MK-8628 Dose A| MK-8628 Dose B	I	May 19, 2016	NCT02698189	Active, not recruiting	AML Including AML de Novo and AML Secondary to MDS DLBCL
MK-8628	I	May 4, 2016	NCT02698176	Terminated	NUT Midline Carcinoma (NMC) Triple Negative Breast Cancer (TNBC) Non-small Cell Lung Cancer (NSCLC) Castration-resistant Prostate Cancer (CRPC)

SF1126| Nivolumab	I	March 27, 2017	NCT03059147	Recruiting	Advanced Hepatocellular Carcinoma
MK-8628	II	October 29, 2014	NCT02296476	Terminated	Glioblastoma Multiforme
BMS-986158 Biological: Nivolumab	I/II	June 5, 2015	NCT02419417	Recruiting	Advanced Tumors
OTX015 Vidaza (azacitidine)	I/II	January 2015	NCT02303782	Withdrawn	Acute Myeloid Leukemia
ABBV-075 Venetoclax	I	April 14, 2015	NCT02391480	Completed	Cancer Breast Cancer Non-Small Cell Lung Cancer Acute Myeloid Leukemia (AML) Multiple Myeloma Prostate Cancer Small Cell Lung Cancer Non-Hodgkins Lymphoma
ZEN003694 Talazoparib	II	April 2019	NCT03901469	Recruiting	Triple Negative Breast Cancer
CPI-0610 Ruxolitinib	I/II	June 2014	NCT02158858	Recruiting	Myelofibrosis Leukemia, Myelocytic, Acute Myelodysplastic/ Myeloproliferative Neoplasm Myelodysplastic Syndrome (MDS)
RO6870810	I	November 6, 2014	NCT02308761	Completed	Acute Myeloid Leukemia Myelodysplastic Syndromes
GSK2820151	I	April 25, 2016	NCT02630251	Terminated	Cancer
GSK525762 Besylate tablets Trametinib tablets	II	November 27, 2017	NCT03266159	Withdrawn	Solid Tumours
BAY 1238097	I	March 2015	NCT02369029	Terminated	Neoplasms
Azacitidine Pembrolizumab Epacadostat INCB057643| INCB059872	I/II	January 26, 2017	NCT02959437	Active, not recruiting	Solid Tumors Advanced Malignancies Metastatic Cancer
RO6870810	I	October 16, 2013	NCT01987362	Completed	Solid Tumors, Advanced Solid Tumors

CC-90010	I	July 24, 2017	NCT03220347	Recruiting	Lymphoma, Non-Hodgkin Neoplasms
INCB059872	I	June 27, 2018	NCT03514407	Recruiting	Relapsed Ewing Sarcoma
ZEN003694 Enzalutamide	I/II	December 2016	NCT02711956	Active, not recruiting	Metastatic Castration-Resistant Prostate Cancer
ZEN003694	I	May 2016	NCT02705469	Completed	Metastatic Castration-Resistant Prostate Cancer
GSK525762	I	March 28, 2012	NCT01587703	Completed	Carcinoma, Midline
INCB054329 Monotherapy	I/II	April 14, 2015	NCT02431260	Terminated	Solid Tumors and Hematologic Malignancy
INCB057643 Gemcitabine Paclitaxel Rucaparib Abiraterone Ruxolitinib Azacitidine	I/II	May 2016	NCT02711137	Terminated	Solid Tumors
GSK525762	II	May 14, 2014	NCT01943851	Completed	Neoplasms
FT-1101 Azacitidine	I	September, 2015	NCT02543879	Completed	Acute Myeloid Leukemia Acute Myelogenous Leukaemia Myelodysplastic syndrome Non-Hodgkin Lymphoma
CC-95775	I	October 24, 2019	NCT04089527	Recruiting	Lymphoma, Non-Hodgkin

Entinostat Molibresib	I	May 2020	NCT03925428	Not yet recruiting	Advanced Lymphoma Advanced Malignant Solid Neoplasm Ann Arbor Stage III B-Cell Non-Hodgkin Lymphoma Ann Arbor Stage III T-Cell Non-Hodgkin Lymphoma Ann Arbor Stage IV B-Cell Non-Hodgkin Lymphoma Ann Arbor Stage IV T-Cell Non-Hodgkin Lymphoma Refractory B-Cell Non-Hodgkin Lymphoma Refractory Lymphoma Refractory Malignant Solid Neoplasm Refractory Pancreatic Carcinoma Refractory T-Cell Non-Hodgkin Lymphoma Stage II Pancreatic Cancer AJCC v8 Stage IIA Pancreatic Cancer AJCC v8 Stage IIB Pancreatic Cancer AJCC v8 Stage III Pancreatic Cancer AJCC v8 Stage IV Pancreatic Cancer AJCC v8 Unresectable Pancreatic Carcinoma
Cisplatin Etoposide Etoposide Phosphate Molibresib Molibresib Besylate	I/II	March 2020	NCT04116359	Not yet recruiting	Metastatic NUT Carcinoma Unresectable NUT Carcinoma
AZD9150 AcalabrutinibA ZD6738 Hu5F9-G4 Rituximab AZD5153	I	June 19, 2018	NCT03527147	Recruiting	NHL DLBCL Non-Hodgkin’s Lymphoma Diffuse Large B Cell Lymphoma
AZD5153 Olaparib	I	June 30, 2017	NCT03205176	Recruiting	Malignant Solid Tumours Lymphoma Ovarian Cancer
ABBV-744	I	March 16, 2018	NCT03360006	Recruiting	Prostate Cancer Acute Myeloid Leukaemia (AML)
ODM-207	I/II	December 22, 2016	NCT03035591	Completed	Solid Tumors

Table 1.2: Clinical studies seeking to exploit BET BRD targeting in multiple disease settings. Data compiled from [155].

1.6.3.1 Toxicity arising from BET BRD targeting in cancer

Given the ubiquitous expression of BETs throughout the human body and their central role in transcription [45], it is perhaps unsurprising that attenuation of their function may lead to adverse side effects. BET BRD inhibition has been met with mixed tolerance: mice harbouring AML [98], neuroblastoma [94], melanoma [95], and prostate [34] malignancies tolerated (+)-JQ1 treatment with little to no adverse effect. In glioblastoma studies, mice tolerated the BET BRD inhibitors OXT015 [115], I-BET151 [113] and (+)-JQ1 [156] well, with no significant weight loss. This is particularly promising owing to the different chemotypes of BET BRD inhibitor used, providing orthogonality. However, mice in a colorectal murine xenograft study showed signs of toxicity: mice exhibited weight loss following daily (+)-JQ1 treatments after 12 days; subsequently, a drug holiday was introduced to allow recovery from the weight loss [120].

There are additional concerns surrounding *in vitro* toxicity. BET BRD inhibition can lead to a reduction in colony formation in embryonic stem cells [157]. (+)-JQ1 can also reduce normal neuronal function through transcriptional changes [158], which corroborates with *in vivo* findings showing that (+)-JQ1 can easily permeate the blood-brain barrier [159] and long term pan-BET inhibition can lead to long-term memory deficits [158]. (+)-JQ1 also leads to decreased seizure severity and faster recovery to normal movement [158]. Although this may seem like a benefit, it is also indicative of neuronal transcriptional rewiring, which may have deleterious effects.

In vivo investigations into (+)-JQ1 as a potential male contraceptive demonstrated reversible effects on male anatomical features, including testis size, spermatozoa motility

and number on male mice treated with pan-BET inhibitor [34, 159]. Conversely, hormone levels, mating behaviour and body weight remained unaffected [159]. While these are promising findings for a potential male contraceptive, perhaps the effects on testis size and spermatozoa motility and number might be perceived as adverse should BET BRD inhibitors be used with a different purpose in mind, for example, as an anti-cancer therapy.

Dissection of the *in vivo* mechanism underpinning toxicity revealed that Brd4 silencing induced reversible toxicities, namely, reduced ability to recover from irradiation, alopecia, depletion of lymphoid haematopoetic compartments [58]. Toxicities have also been observed in Phase I clinical trials for liquid tumours including diarrhoea and fatigue [160, 161]. Similar toxicities were observed in patients in a trial for BET BRD inhibitor use in NMC [91].

Circumventing toxicity by predicting patient response to therapy, developing targeted therapies, or developing alternative BET-protein targeting strategies will ensure cytotoxic effects are selective to malignant cells; thus, improving patient care.

1.6.3.2 Resistance to BET BRD inhibitors

Acquired resistance mechanisms across different malignancies converge upon Wnt β-catenin signalling. In colorectal cancer, BRD4 is recruited, along with Wnt signalling and ERK signalling transcription factors, to the *MYC* super enhancer. Upon (+)-JQ1 treatment, BRD4 is displaced from the super enhancer and MYC expression decreases, which coincides with growth inhibition [120]. However, (+)-JQ1 does not lead to uniform down-regulation of components of the Wnt pathway, but when components of the Wnt pathway are knocked down in combination with (+)-JQ1 treatment, this attenuates MYC expression further [120]. In AML, Wnt β-catenin can drive expression of MYC in place of BRD4, affording cells resistance to BET BRD inhibitors [93, 99]. This brings to light potential targets that may enable restoration of sensitivity to BET BRD inhibitors.

In a breast cancer model, attempts to identify mechanisms underpinning resistance to BET BRD inhibitors began with the generation of resistant cell lines through long term exposure to BRD inhibitors of increasing concentrations. Resistant cells displayed increased number of super enhancers and increased BRD4 occupation on these loci. This led to an increase in BCL-XL expression. BRD4 phosphorylation by CK2 leads to BRD4 stability and localisation in the nucleus, and resistant cells showed BRD4 hyper-phosphorylation. Treatment with (+)-JQ1 with the addition of a CK2 inhibitor led to reduced cell growth compared to (+)-JQ1 alone. Corroborating with this finding, when the reciprocal phosphatase, PP2A, was down-regulated, this also led to resistance to (+)-JQ1 in sensitive cells. Resistant cell lines remain dependent on wild-type BRD4 but also showed that sensitivity to BET BRD inhibitors can be MYC independent [96].

Similarly, BET BRD inhibitor resistance has been induced in an ovarian cancer cell line through chronic exposure to (+)-JQ1 [125]. In these cell lines, resistance to BET BRD inhibition is mediated through kinome reprogramming through activation of pro-survival receptor tyrosine kinases [125]. Indeed, cells with induced resistance to BET BRD inhibitors show greater sensitivity to PI3K/mTOR inhibitors than their sensitive counterparts. Enhanced PI3K and ERK activation leads to increased MYC and FOSL stabilisation; therefore, increased (+)-JQ1 doses are insufficient to decrease FOSL and MYC levels in cells lines with induced resistance, which in turn sustain cell growth. Accordingly, dual targeting of PI3K and ERK, along with BETs, leads to increased sensitivity to (+)-JQ1 [125].

In ovarian and lung cancer models with SMARCA4 and SMARCA2 depletion, cell lines that are sensitive to BET BRD inhibition have been identified, and SMARCA2/4 re-expression leads to resistance to BET BRD inhibitors [162]. These data indicate that wild-type SWI/SNF components are not tumour suppressive, as has been previously suggested [163], highlighting the therapeutic potential of a combinatorial targeting strategy.

The resistance mechanisms that arise in experimental models serve as evidence to suggest BET BRD inhibitors have achieved their aim of targeting multiple pathways simultaneously. The resistance mechanisms also highlight the plasticity of cancer cells and their ability to adapt to new stresses. Our understanding of innate and acquired resistance mechanisms to BET BRD inhibitors bolsters our knowledge of factors that underpin cellular sensitivity to BET BRD inhibitors. Addressing this gap in our understanding would enable the prediction of patients who would be most likely to respond to BET BRD inhibitors.

1.7 Melanoma

1.7.1 Melanoma biology

Malignant melanoma arises in the skin from pigment-producing melanocytes in the skin [164]. With over 200,000 new cases per year, metastatic cases remain largely incurable and is one of the few types of cancer rising in incidence and mortality rate [165]. Only 10% of skin cancer cases are classified as melanoma, but melanoma accounts for 80% of skin-cancer-related deaths [164].

10% of cases arise due to inherited mutations across 20 genes [164]; the vast majority of cases arise in a step-wise fashion, often beginning with an activating MAPK pathway mutation such as BRAF or NRAS [166]. Approximately 50% melanomas harbour a BRAF mutation, ~ 20% melanomas harbour an NRAS mutation, ~12% melanomas harbour an NF1 mutation, which all lead to MAPK pathway activation [167]. NRAS mutations also lead to PI3K/AKT pathway activation, as do PTEN mutations or PTEN losses, which occur in ~20% and ~10% of melanomas, respectively [167]. When mutations or epigenetic alterations coincide, often as a result of UV radiation, senescence bypass, increased proliferation and inhibition of apoptosis occur [166, 168].

In tandem with gradual genetic and epigenetic alterations, step-wise histopathological changes, described by the Clark model, occur during melanoma development, wherein benign naevi (moles) transition, in stages, to metastatic melanoma: (i) benign nevus; (ii) dysplastic nevus; (iii) radial-growth phase melanoma; (iv) vertical-growth phase melanoma; and (v) metastatic melanoma [168]. Cells become progressively more invasive and lose E-cadherin expression and increase N-cadherin expression, which enables metastasis and the onset of generally incurable disease [168].

1.7.2 Current treatments for metastatic melanoma

Several treatment options exist for melanoma patients, including surgical resection and radiotherapy. Surgery is the preferred treatment option, but this is dependent on the melanoma stage [168, 169]. Radiotherapy can be used for patients with skin, bone or brain metastases [169]. Chemotherapeutic agents, such as dacarbazine and paclitaxel, are the most common therapeutic strategy, but patients often develop resistance, with only 11.2% of metastatic melanoma patients achieving durable remission following treatment with dacarbazine [169, 170].

Many melanomas exhibit oncogene addiction, wherein recurring mutations afford cells a proliferative advantage. Thus, the inhibition of the single oncogene is sufficient to halt proliferation in many melanomas; 50% of patients harbour BRAF mutations, and of these, ~85% of these mutations are $BRAF^{V600E}$ [167]. Other less common BRAF mutations in BRAF occur in melanoma (for example V600K, V600R, V600D), and also lead to MAPK pathway activation, demonstrating a clear rationale for targeted therapies against BRAF, such as vemurafenib or dabrafenib [171]. While the progression-free survival afforded to patients by targeted inhibitors as a single therapy is greater than that which is afforded by dacarbazine, the median progression-free survival remains less than half a year [167, 172, 173]. Approximately half of $BRAF^{V600\text{-mutant}}$ advanced melanoma patients do not respond to

these treatments, and most patients develop resistance within a year; therefore, much is still to be desired in terms of an effective treatment for many melanoma patients [167, 168, 172, 173].

NRAS mutations lead to both MAPK and PI3K/AKT pathway activation, making NRAS an ideal target; however, NRAS itself is currently considered undruggable [174]. MEK inhibitors, such as trametinib, binimetinib, and cobimetinib, enable downstream inhibition of the MAPK pathway, which partly abrogates the effects of constitutively active NRAS. Compared with standard chemotherapy, either dacarbazine or paclitaxel treatment, progression-free survival rates in metastatic melanoma patients treated with trametinib were improved, although in melanoma patients with the $BRAF^{V600E}$ mutation who had not received previous treatment, the objective response rate was only 48% [174].

Since relapse following targeted therapies coincides with activation of MAPK pathway, BRAF and MEK inhibitor combinations have been trialled. $BRAF^{V600\text{-mutant}}$ unresectable or metastatic melanoma patients treated with BRAF and MEK inhibitors experience enhanced overall and progress-free survival compared with patients treated with BRAF inhibitor only. The occurrence of adverse effects across the two cohorts is similar, but adverse effects occur in a non-significantly greater proportion of the combination cohort [175-177]. Notwithstanding the increased adverse effects, patients treated with BRAF and MEK inhibitors, compared with BRAF inhibitor alone, report increased health-related quality of life [177, 178]. While the overall response rate is improved by the combination therapy, the complete response rate was 10% for patients treated with BRAF and MEK inhibitors and 4% for BRAF inhibitor alone [177]; clearly there is room for improvement.

Microphthalmia-associated transcription factor (MITF) orchestrates many aspects of melanocyte and melanoma biology, including proliferation and differentiation [179]. MITF expression is heavily regulated; however, two transcription factors that modulate its

expression lie downstream of the MAPK pathway: SOX10 and BRN2 [179]. MITF expression inversely correlates with an invasive melanoma phenotype, and high MITF expression affords cells protection against ERK inhibition in $BRAF^{V600E}$ cells [180]. Expression of receptor tyrosine kinase, AXL, is inversely proportional to MITF expression, and $MITF^{low}$-AXL^{high} expression is also implicated in resistance to MAPK pathway inhibitors [180]. These molecular means of escape from targeted therapies highlight that a more diverse range of treatment options against melanomas should be sought.

Developments in immunotherapy were sparked upon the observation of infiltrating T-lymphocytes into melanoma and this was associated with the spontaneous regression of the disease [181]. As such, interleukin-2 was administered to stimulate a response against the tumour, but was toxic and often ineffective, with a durable response rate of only 4% [182]. Interferon-α2b was trialled in patients with stage II and III melanoma, and while the relapse-free survival was improved in a dose dependent manner, neither a high nor a low dose improved patient overall survival at 5 years [183]. Nevertheless, it is offered as an adjuvant therapy to melanoma patients of these stages [169].

Melanoma cells have one of the highest mutational burdens of any cancer; therefore, the potential for neoantigen expression is high. Glycoprotein 100 (gp100) is widely expressed throughout melanoma cells and a gp100 epitope is recognised by HLA-A*0201-expressing tumor-infiltrating lymphocytes from melanoma patients [184-186]. Upon antigen recognition, an effective immune response against the tumour should be mounted; however, tumour-driven immunosuppression prevents this. To combat the repression of the immune response, immune checkpoint inhibitors have been developed. Antibodies inhibiting the immunosuppressive effects of T cell antigen cytotoxic T-lymphocyte-associated protein 4 (CTLA-4) activation, ipilimumab, improved overall survival of metastatic melanoma patients compared with patients treated with gp100 injections; however ipilimumab treatment was accompanied by immune-related adverse events in

60% patients [187]. Similarly, antibodies such as nivolumab or pembrolizumab act as antagonists to programmed cell death protein 1 (PD-1), thereby de-repressing the immune response, and are efficacious in melanoma patients. Accordingly, in advanced melanoma patients without BRAF mutations, nivolumab treatment led to increased progression-free survival compared with patients treated with dacarbazine, and the objective response rate was significantly higher in those treated with nivolumab compared with those treated with dacarbazine [188]. However, 60% of patients treated with nivolumab failed to achieve an objective response. While these are promising findings, evidently many patients still lack treatments that offer meaningful tumour regression without toxicity.

Immune checkpoint inhibitors can be used alone or combined with targeted inhibitors [168]. As single therapies, the 5 year survival rates of ipiliumamab and nivolumab are 26% and 44%, respectively [189]. However, advanced melanoma patients who are treated with a combination of nivolumab and ipilimumab have increased overall and progression-free survival compared to those who are treated with either single therapy; in fact, the median survival was not reached at 5 years in the combination therapy cohort [189]. Therefore, this represents a highly promising novel treatment for melanoma patients [189]. However, stratification of patients for BRAF mutations shows that the increase in survival is most pronounced in patients with BRAF mutations, whereas those without BRAF mutation experience 3% improvement in progression-free survival when treated with the combination compared with nivolumab alone, the best performing single therapy [189].

There are several observations that indicate that there is a strong rationale to investigate combinations of targeted and immunotherapies in melanoma: resistance to BRAF inhibitors coincide with an increase in PD-L1 expression [190]. Additionally, BRAF inhibitors induce melanoma antigen presentation in $BRAF^{V600E}$ cells, which leads to improved recognition by antigen-specific lymphocytes [191].

Trametinib, in combination with one of CTLA-4, PD-1 or PD-L1 inhibitors, leads to enhanced survival than either treatment alone *in vivo* [190]. However, in mice bearing $BRAF^{V600E}$ mutant melanomas, treatment with a BRAF inhibitor reduces immune tumour infiltrate, and there is no additional survival advantage to treatment with BRAF inhibitor and anti-CTLA-4 antibodies compared to BRAF inhibitors alone [192]. Nevertheless, clinical trials with BRAF or MEK inhibitors with immune checkpoint inhibitors have begun [193]. Three trials show improved responses of combined BRAF inhibitor, MEK inhibitor and immune checkpoint inhibitors (anti PD-L1 or PD-1 antibodies) compared with BRAF or MEK inhibitor alone. However, toxicities are more frequent in patients treated with the triple inhibitor regimens compared with BRAF or MEK inhibitor alone [194]. Additionally, the long-term survival benefits of the triple therapy are yet to be observed; thus, it cannot yet be concluded whether the potentially additional survival advantage outweighs additional toxicities, or not.

Epigenetic therapies in melanoma remain relatively under explored. As single therapies, HDAC inhibitors induce G1 cell cycle arrest and reduce tumour cell growth *in vitro* and *in vivo* [195]. In combination with targeted therapies, HDAC inhibitors re-sensitise a subset of BRAF inhibitor-resistant melanomas to BRAF inhibitor, encorafenib, and can act synergistically *in vitro* and *in vivo* with encorafenib [196]. Regarding effects on immunotherapy efficacy, HDAC inhibitors lead to increased PD-1 expression in a range of melanoma cell lines and patient samples *in vitro* and *in vivo*, thereby, potentially rendering melanoma cells more susceptible to immunotherapies [197]. Indeed, combining anti-PD-1 antibodies and the HDAC inhibitor, LBH589, significantly increases murine survival and decreases tumour burden compared with the control mice, where both single therapies failed to do so [197]. HDAC inhibitors have been entered into clinical trials for advanced melanoma with mixed responses; only 2 patients from a cohort of 32 experienced stable disease following treatment with vorinostat, which was swiftly followed by relapse.

However, 39% patients treated with valproic acid achieved stable disease, although median progression-free survival was 8.9 weeks [198, 199]. Therefore, while epigenetic therapies show promise, further investigation is required to determine how they can be best utilised.

In summary, while there have been many advances in the treatment for metastatic melanoma patients, there is clearly room for improvement. A significant subset of patients do not respond to any available therapy, or combination, and side effects and relapse remain problems for many patients; resistance onset typically occurs within 7 months [200-202]. Immunotherapy yields impressive responses; however, only in a small percentage of patients, and many cases this is hampered by immune-related adverse events [187, 203-206]. Therefore, a more diverse range of treatment options is needed. Investigations into epigenetic therapies in melanoma show signs of optimism, and more work is needed to determine which patients would benefit most from this potential treatment.

1.8 BETs in melanoma

1.8.1 Rationale for BET targeting

The reliance of melanomas on different members of the BET protein family highlight the lack of functional redundancy exhibited by members of the BET protein family in melanoma. BRD2 and BRD4 mRNA expression levels are up-regulated in melanomas compared with normal melanocytes and naevi [151]. Similarly, BRD2 and BRD4 protein expression levels are increased in primary and metastatic melanoma samples compared with healthy melanocytes and naevi [151, 207]. Many metastatic melanoma cell lines show increased BRD2 and BRD4 copy number compared with healthy melanocytes [151]. Unsurprisingly, genetic perturbation of BRD2 or BRD4 leads to loss of malignant cell growth and colony formation *in vitro*, with BRD4 loss also leading to reduced tumour

progression *in vivo*, indicating the necessity of BRD4 protein expression for tumour maintenance [95, 151, 207]. BRD2 and BRD4 occupy super-enhancers found in melanoma, but not in normal human melanocytes, further supporting the notion that they promote malignant growth [152].

BRD3 may function as a tumour suppressor in nasopharyngeal carcinoma, suggesting its loss may promote cancer cell growth [57]. However, BRD3 knockdown has little effect on melanoma cell viability or melanoma survival genes *in vitro* [151, 152]. Thus, BRD3 appears not to play a role in driving melanoma.

Figure 1.1C shows BRD -2, -3, and -4 mRNA expression are elevated in patient skin cancer tissue samples. BRDT expression is testis specific and is not deregulated in skin cancer tissues (Figure 1.1C); therefore, the focus of this thesis will continue to be on BRD -2, -3, and -4. Across a range of cancer cell lines with diverse origins, BET mRNA expression levels vary, but little change is observed in skin cancer cell lines as a whole (Figure 1.1E). However, when BET mRNA expression levels are examined in individual skin cell lines, BRD -2, -3 and -4 mRNA expression levels fluctuate compared with healthy melanocyte BET expression levels (Figure 1.1F). This indicates that deregulation of BET expression may contribute to the maintenance of melanomas.

1.8.2 BET inhibition in melanoma

Given the rationale underpinning the exploration of BET BRD inhibitors in melanoma, the consequences BET BRD inhibition have been investigated, both *in vitro* and *in vivo* melanoma models. The mechanism by which BET BRD inhibitors cause a cessation in cellular proliferation, and determinants of sensitivity have been explored, and are outlined below. Additionally, the problems of toxicity and potential resistance have demanded investigations into combinatorial approaches, alternative BET protein targeting strategies and BET degraders, which are also described below.

1.8.2.1 BET BRD inhibition in melanoma

Upon treatment with various BET BRD inhibitors, melanoma continuous cells lose viability and display impaired clonogenic growth capacity [95, 151, 153, 208-210]. Interestingly, BET BRD inhibition has heterogeneous effects on cell cycle arrest *in vitro*. Patient-derived cells show a G1 cell cycle arrest, which is most pronounced in cells collected pre-relapse [95]. Continuous cell lines arrest cycling at heterogenous points, many at G1, while the most sensitive cell line arrests in G2/M; however, the point at which the cells arrest does not correlate with sensitivity to BET BRD inhibition [95, 154, 207].

Cell death mechanisms range from the programmed to the uncontrolled, and include pyroptosis, necrosis and apoptosis. Pyroptosis is an inflammatory form of apoptosis, driven by caspase 1, often driven by infectious stimuli [211]. Necrosis is an uncontrolled form of cell death, where the cellular contents spill into the extracellular environment [211]. In contrast, apoptosis is a controlled mechanism of cell death, preventing the cellular contents from entering into the extracellular environment [212]. Both arms of the apoptotic cascade, intrinsic and extrinsic, involve the activation of initiator caspases (8 and 9), and subsequent activation of executor caspases (3, 6 and 7) [213]. While the effectors within each pathway differ, their activation converges upon the cleavage of PARP [211, 214]. Many melanoma cell lines undergo apoptosis following (+)-JQ1 treatment, which, unsurprisingly, is accompanied by caspase and PARP cleavage [95]. Furthermore, pre-treatment, patient-derived cell lines show increased caspase- and BIM- dependent cell death following BET BRD inhibition; however, cells derived from patients post-relapse only show a modest induction of cell death [95], suggesting perhaps that BET BRD inhibitors may be more suitable for treatment-naive patients.

In more physiologically relevant models, BET BRD inhibitors also show efficacy. 3D human skin mimetic models treated with BET BRD inhibitors display a decrease in Ki-67 staining

[154]. Ki-67 was initially identified as a highly expressed protein throughout S, G2 or M phases of the cell cycle. Upon exit from cell cycle, entering G0 phase, Ki-67 expression drops [215]. While its expression in G1 is variable, Ki-67 is regarded as a proliferation marker [216], and its loss of expression indicates a reduction in the population of cycling cells. Additionally, *in vivo* models show that treatment with various BET BRD inhibitors decrease tumour growth, burden and metastases compared to control [95, 151].

1.8.2.2 BET BRD inhibitor mechanism in melanoma

In melanoma cell lines undergoing a G1 cell cycle arrest, up-regulation of cell cycle regulators, such, p21 or p27, is observed [95, 151, 152]. In patient-derived melanoma cells, MYC is down-regulated and p21 up-regulated upon pan-BET BRD inhibition [151, 207]. However, neither MYC over-expression nor p21 knockdown protect cells from BET BRD inhibition, suggesting that BET BRD inhibitors affect multiple, non-redundant cell signalling pathways that relate to cell cycle and viability [151]. Moreover, it suggests that the cellular response to BET BRD inhibition is not underpinned by the loss of MYC expression or p21 up-regulation.

BRD4 knockdown recapitulates the effects of BRD inhibitors on tumour cell growth *in vitro* and *in vivo*, suggesting that it is the dominant BET member in driving this cancer [151]. However, BRD2 knockdown also leads to loss of cellular proliferation [207], indicating that BRD4 is not the sole contributor of the BET protein family to maintenance of melanoma. The role of BRD3 in melanoma is currently unknown and genetic perturbation of BRD3 does not impact melanoma growth *in vitro* [151]. However, since BRD3 expression is deregulated in skin cancer patient tissues and skin cancer cell lines (Figures 1.1C and 1.1E), and has a potentially tumour suppressive function in nasopharyngeal cancer, it is possible BRD3 has an under-explored role in melanoma.

Notwithstanding the decrease in MYC expression following BET BRD inhibition in melanoma, there is a distinct lack of correlation between MYC expression and sensitivity to BET [151]. Furthermore, melanoma cell line sensitivity to BET BRD inhibitor is not dependent upon NRAS or BRAF mutational status [151, 217], nor is there any correlation between expression of the melanocyte-specific transcription factor and oncogene, MITF, and sensitivity to BET BRD inhibition [217, 218]. Moreover, cell lines harbouring a BRD4-bound super-enhancer for the gene PGC-1α, and subsequent elevated expression levels of PGC-1α are more sensitive to BET BRD inhibition. Murine models harbouring patient-derived PGC-1α high and low xenografts have recapitulated this finding [217]. However, ectopic PGC-1α expression only leads to partial rescue from anti-proliferative effects of BET BRD inhibition, suggesting other pathways also affect cell viability. Additionally, NCI-60 data using the same cell lines in a drug screen using (+)-JQ1 yielded conflicting data on which cell displayed the most sensitivity to the BET BRD inhibitor [217, 219]. Therefore, it is unlikely that PGC-1 α is a determinant of melanoma cell line sensitivity to BET BRD inhibition.

AMIGO2 is a BET-sensitive survival gene in melanoma [152]. Treatment with (+)-JQ1 leads to down-regulation of *AMIGO2* and modest down-regulation of AMIGO2 protein expression [152]. Individual knockdown of BRD2 or BRD4, but not BRD3, leads to loss of *AMIGO2* expression [152]. Loss of AMIGO2 expression leads to caspase activation, PARP cleavage, cell death, loss of capacity for colony formation and melanoma cell viability *in vitro* and *in vivo*, establishing AMIGO2 as a melanoma driver gene [152]. However, neither BET knockdown nor pharmacological BET BRD inhibition caused cell death in this study [152]. Thus, while AMIGO2 expression appears sensitive to BET inhibition, it has not been established as a determinant of cellular sensitivity to BET BRD inhibition.

Additionally, across a range of melanoma cell lines, BRD4 expression does not correlate with sensitivity to BET BRD inhibition [217], and BRD -2, and -3 - expression levels have not been correlated with sensitivity of melanoma cells to (+)-JQ1. Similarly, Figure 1.2 shows that there is no correlation between BRD -2, -3, and -4 mRNA expression levels and sensitivity of melanoma cell lines to (+)-JQ1.

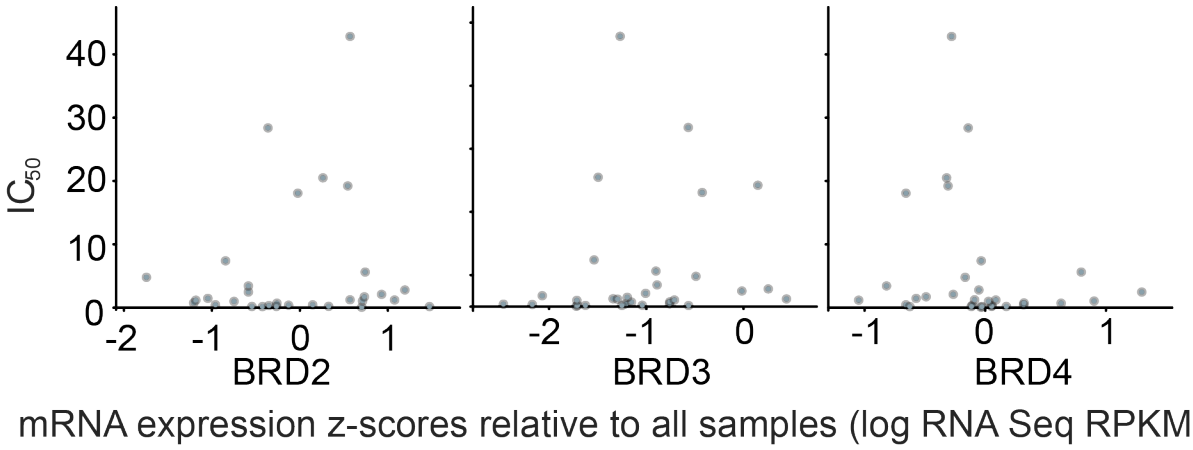


Figure 1.2*: mRNA expression levels of BRD -2, -3, and -4 do not correlate with sensitivity of melanoma cell lines to (+)-JQ1. mRNA expression from RNA-sequencing (RNA-seq) data correlated with cell viability following treatment of melanoma cell lines with (+)-JQ1.Data from cBioportal [220, 221].*

Altogether, the mechanisms underpinning the efficacy of BET BRD inhibition in melanoma, and the determinants of melanoma sensitivity to BET BRD inhibitors require further elucidation.

1.8.2.3 Combinatorial approaches

BET BRD inhibitors have been combined with a number of melanoma treatments *in vitro*, yielding mixed success. The combination of (+)-JQ1 and the BRAF-inhibitor, vemurafinib, leads to greater reduction in cellular growth and activation of apoptosis compared to either agent individually, indicating synergism between the two compounds. Analysis of cell line protein lysate shows that many components of the intrinsic apoptotic pathway are up-

regulated following treatment with the combination [222]. In addition, murine xenografts show enhanced animal survival when treated with both compounds, compared to individual treatments. RNA-sequencing (RNA-seq) of the xenograft samples reveal that a number of pro-apoptotic and cell cycle related genes are only down-regulated in tumours treated with the combination. These results suggest that the two compounds target multiple cell death pathways, which gives rise to their anti-proliferative activity [222].

The dual combination of BRAF and MEK inhibitors leads to up-regulation of receptor tyrosine kinases ERBB3 and PDGFR-β [154]. However, the triple combination of BET BRD, BRAF, and MEK inhibitors prevents ERBB3 and PDGFR-β up-regulation; thus, BET BRD inhibition prevents melanoma cell kinome rewiring following BRAF and MEK inhibitor treatment [154]. Additionally, the triple combination leads to a greater reduction of cellular proliferation *in vitro*, in human skin mimetic models and *in vivo*, compared with the dual BRAF and MEK inhibitor combination, or BET BRD inhibitors alone [154].

When a BET BRD inhibitor has been combined with an ataxia-telangiectasia and Rad3-related (ATR) inhibitor, the combination treatment leads to a greater loss of cell viability and greater induction of apoptosis *in vitro* compared with either inhibitor alone [210]. *In vivo*, apoptosis of tumour cells from patient-derived xenograft models and reduced tumour growth is observed following treatment with BET BRD and ATR inhibitors compared with the vehicle control [210]. However, data showing the effects of BET BRD or ATR inhibitors as single therapies is not show, so it is unclear how much benefit the dual combination confers compared to either inhibitor alone.

In combination with vitamin C, a lower dose of BET inhibitors is required to reduce cell proliferation and induce apoptosis *in vitro* in melanoma cells [223]. This result has been recapitulated *in vivo*; when mice are supplemented with vitamin C and treated with a sub-therapeutic dose of (+)-JQ1, reduced metastasis and xenograft growth is observed [223].

Vitamin C causes a decrease in histone H4 -K5ac and -K12ac acetylation, negatively impacting on the co-localisation between BRD4 and the remaining acetylated H4, which is exacerbated when cells were also treated with (+)-JQ1 [223].

While combinatorial strategies offer potentially increased efficacy and decreased toxicity [223], it can, at times, come at the cost of increased toxicity [154]. Additionally, the threat of resistance emergence to combinatorial approaches lingers; while dual or triple combination may offer patients relief, highly plastic tumour cells are well equipped to develop resistance to an ever-increasingly complex cocktail of inhibitors.

1.8.2.4 BET degraders in melanoma

Proteolysis-targeting chimeras (PROTACs) involve targeting proteins for degradation by E3 ubiquitin ligases [224]. The BET-BRD specific PROTAC, dBET6, displays greater anti-proliferative effects than (+)-JQ1 in a panel of 39 cell lines derived from a range of malignant origins, including a melanoma cell line [225]. Following treatment with BET degrader, ARV, melanoma cell lines exhibit a reduction in migration, colony formation, proliferation and induction of apoptosis in two vemurafenib resistant cell lines [226]. However, ARV showed poor aqueous solubility, and the anti-proliferative effects appear to be dependent upon sensitivity to vemurafenib; vemurafenib sensitive parental cell lines counterparts maintain clonogenic growth and cellular migration [226].

Similar to pharmacological inhibitors of BET protein function, potential resistance mechanisms to BET degraders should also be taken into consideration; sensitivity to BET degraders relies on intact function of E3 ligase machinery [227]. The lack of ARV solubility, combined with the dependence of PROTAC efficacy in melanoma on vemurafenib resistance, and emergence of potential resistance call for further investigation into alternative BET targeting in melanoma.

1.8.2.5 Alternative BET protein targeting in melanoma

Simultaneous targeting of both BRD modules, or targeting individual BET BRDs within a BET protein, enables more selective BET inhibition. In melanoma, treatment with an inhibitor specific to the second BRD of BRD4, N13, leads to senescence onset and reduced invasion *in vitro*, which is mediated through disruption of the binding of BRD4 to CDK6 and WNT5A promoters, consequently reducing their expression [228]. CDK6 drives melanoma cell viability, migration and *in vivo*, CDK6 knockout leads to reduced subcutaneous tumour formation [229]. WNT5A, a member of the non-canonical Wnt signalling pathway, promotes migration and invasion in melanoma [230]. Thus, down-regulation of CDK6 and WNT5A is indicative of the mechanism by which reductions in cell viability and migration are achieved. N13 shows reduced toxicity to differentiated macrophages compared with (+)-JQ1, but exhibits similar toxicity in undifferentiated macrophages [228]. Therefore, targeting the second BRD specifically represents a strategy for modulation of gene expression that may prove to have fewer adverse effects in a range of cancers.

Alternative targeting of BETs has beneficial effects in melanoma, yet there are still questions surrounding the mechanism by which BET inhibition leads to loss of malignant cell growth, and toxicity. Further investigations into alternative BET targeting strategies may lead to a greater understanding of BET protein attenuation in this context, and treatments with improved efficacy with reduced toxicity.

1.9 Summary and questions

While BET BRD inhibitors are efficacious and tolerated in some circumstances, the problems of potential resistance to BET BRD and BET-BRD-inhibitor-induced toxicity call for further investigation into the determinants of cellular response to BET BRD inhibitors, and alternative targeting strategies. An arsenal of BET-protein inhibition strategies

combined with greater knowledge of BET-protein biology could facilitate patient stratification, leading to higher treatment efficacy and fewer adverse effects.

Melanoma is an area of clinical need; only a subset of patients respond to available treatments, with the almost inevitable emergence of resistance [187, 200-206]. Therefore, advances in treatments for this malignancies are highly sought after. Melanoma has been used as a model to investigate the efficacy of BET BRD inhibition and the impact of alternative BET-targeting [95, 151, 153, 208-210, 228], yet determinants of the cellular response to BET inhibition have not been revealed. If BET BRD inhibitors are to be utilised with greatest efficacy with minimal adverse effects, the biology underpinning the cellular response requires deeper understanding. Therefore, the first aim of this thesis is to investigate the cellular response to BET BRD inhibition in melanoma, and identify putative determinants of the cellular response.

The second aim is to determine whether this response is melanoma-specific. Melanoma and prostate cancer both have been used as models for investigating alternative BET-targeting strategies [228, 231, 232], owing to concerns surrounding toxicity and resistance to traditional BET BRD inhibitors, and a need for improved treatments for these malignancies. Investigating the mode of action in another solid cancer model will provide a more thorough understanding of the cellular response to BET inhibitors. Therefore, the second aim of this thesis is to explore the impact of RT53, a novel BET BRD inhibitor, on prostate cancer cells.

Lastly, the concerns surrounding toxicity are not limited to in BET BRD inhibitors, but also relate to use of PROTACs [233]. Thus, more creativity in the strategies employed to target BET protein function is required. All BETs share an ET-domain, which represents an alternative, pan-BET therapeutic strategy that would exploit the assembly of recruited

protein complexes on BETs. The final aim of this study will be to investigate if BET ET-domain inhibition elicits beneficial phenotypic responses in melanoma *in vitro.*

Chapter 2: Materials and Methods

2.1 Materials

2.1.1 Cell lines

Cell line	Cell type	Source	Reference
501MEL	Human melanoma cell line	Professor Goding's lab	[234]
A375 metastatic cell line (A375M)	Human melanoma cell line	Professor Goding's lab	[235]
CHL1	Human melanoma cell line	Professor Goding's lab	[235, 236]
Institut Gustave Roussy-37 (IGR37)	Human melanoma cell line	Professor Goding's lab	[237]
Institut Gustave Roussy-39 (IGR39)	Human melanoma cell line	Professor Goding's lab	[237]
Lymph node carcinoma of the prostate (LNCaP)	Human prostate cancer cell line	Dr Srinivasa Rao Rao, Claire Edwards' lab	[236, 238, 239]
Prostate cancer cell line (PC3)	Human prostate cancer cell line	Yiannis Philippou, Richard Bryant's lab	[240]
SK-mel-28	Human melanoma cell line	Professor Goding's lab	[235]

Table 2.1: Parental cell lines used throughout this thesis

2.1.2 siRNAs and primers

Target	Dharmacon catalogue number
BRD2	J-004935-06
BRD2	J-004935-07
BRD2	J-004935-08
BRD2	J-004935-09
BRD3	J-004936-05
BRD3	J-004936-06
BRD3	J-004936-07
BRD3	J-004936-08
BRD4	J-004937-06
BRD4	J-004937-07
BRD4	J-004937-08
BRD4	J-004937-09
None - negative scrambled control (siNC)	D-001810-10-50

Table 2.2: siRNAs used throughout this thesis

Primer name	Sequence	Application
18S-rRNA-F	5’-GCTTAATTTGACTCAACACGGGA-3’	qPCR
18S-rRNA-R	5’-AGCTATCAATCTGTCAATCCTGTC-3’	qPCR
ADM-F	5’-CGGAGTTTCGAAAGAAGTGG-3’	qPCR
ADM-R	5’-GTAGCGCTTGACTCGGATGC-3’	qPCR
AR-FL-1-F	5’-CAGCCTATTGCGAGAGAGCTG-3’	qPCR
AR-FL-1-R	5’-GAAAGGATCTTGGGCACTTGC-3’	qPCR
AR-FL-2-F	5’-CAAATCACCCCCCAGGAAT-3’	qPCR
AR-FL-2-R	5’-ACTGGAATAATGCTGAAGAGTAGCA-3’	qPCR
AR-V7-1-F	5’-CCATCTTGTCGTCTTCGGAAATGTTA-3’	qPCR
AR-V7-1-R	5’-TTTGAATGAGGCAAGTCAGCCTTTCT-3’	qPCR
AR-V7-2-F	5’-TGCCAACCCGGAATTTTTCT-3’	qPCR
AR-V7-2-R	5’-GTCGTCTTCGGAAATGTTATGAA-3’	qPCR
ATG12-F	5’-TGTGAATCAGTCCTTTGCTCC-3’	qPCR

Primer name	Sequence	Application
ATG12-R	5’-ACCATCACTGCCAAAACACTC-3’	qPCR
ATG4B-F	5’-TGCTGTCTTCGATACGTGGA-3’	qPCR
ATG4B-R	5’-GTCGGAATCTGCAGGAAACG-3’	qPCR
BNIP3-F	5’-GCCATGTCGCAGAACGGA-3’	qPCR
BNIP3-R	5’-TAGAAACCGAGGCTGGAACG-3’	qPCR
BNIP3L-F	5’-CACACCAGCAGGGACCATAG-3’	qPCR
BNIP3L-R	5’-TGGGTGGAATGTTTTCGGGT-3’	qPCR
BRD2-F	5’-CCAGCACGGCTTCGTTTTC-3’	qPCR
BRD2-R	5’-GCAGCAGCGAAGAATCTGGA-3’	qPCR
BRD3-F	5’-AGGCCAACTGTCGCCTG-3’	qPCR
BRD3-R	5’-ACTTTCTGTCACAGCAGCGG-3’	qPCR
BRD4-dET-F	5’-GTGCAAGCCTAAAAGGAAACCTCAAGCTGAGAAAGTTGATGTGAT-3’	Cloning
BRD4-dET-R	5’-GTTTCCTTTTAGGCTTGCACTTGTCCTCTTCCTCCGACTC-3’	Cloning
BRD4-F	5’-CTGACAGCGAAGACTCCGAA-3’	qPCR
BRD4-R	5’-GGTGGTGATGATGGTGCTTCT-3’	qPCR
BRD4L-NaeIcut-F	5’-AAGCTGGGCCAGCGGCGGGAGAGCAGCCGGCCTGTGAAACCTCCA-3’	Cloning
BRD4L-NaeIcut-R	5’-ACGAGAAGCCCTTCATCTTGGAGGAGCCGGCAATCACATCAACTT-3’	Cloning
CDKN2D-F	5’-CTCAACCGCTTCGGCAAGAC-3’	qPCR
CDKN2D-R	5’-CCATCAGGCACGTTGACATCAG-3’	qPCR
CLCN7-F	5’-TTCACAGAGAAGGGCGGAC-3’	qPCR
CLCN7-R	5’-GGATCTTCACCCCGTTGAG-3’	qPCR
CTSF-F	5’-GATGGCTTCAATCTTCAAGAACT-3’	qPCR
CTSF-R	5’-CTCCATACTGAGCTGTGCCA-3’	qPCR
E2F2-F	5’-GACCCGAGGGCCAAGTTGTGCGATG-3’	qPCR
E2F2-R	5’-GCCCCAGCGAAGTGTCATACCGAGT-3’	qPCR
ETV-1-F	5’-GCAAGAAGGCTTCCTGGCTCAT-3’	qPCR

Primer name	Sequence	Application
ETV-1-R	5’-CCTTCCCGATACATTCCTGGCT-3’	qPCR
HEXIM1-F	5’-TTTATTGGGGTGCTCCGCTT-3’	qPCR
HEXIM1-R	5’-GCAATCTGGGGAGCTCAAGT-3’	qPCR
MAP1LC3B-F	5’-CCGACTTATTCGAGAGCAGCA-3’	qPCR
MAP1LC3B-R	5’-AGCTGCTTCTCACCCTTGTA-3’	qPCR
MITF-F	5’-GAAGAGCAAAACAGGGCAGAGAGCGAGTGC-3’	qPCR
MITF-R	5’-GCAAAGCAGGATCCATCAAGCCCAAGATTT-3’	qPCR
MYC-F	5’-AACGACAGCAGCTCGCCCAAGTCCT-3’	qPCR
MYC-R	5’-TTTGCCAGGAGCCTGCCTCTTTTCC-3’	qPCR
NEU1-F	5’-TGGTATGGAGCAAGGATGATG-3’	qPCR
NEU1-R	5’-CATGGCCACACACGATGAG-3’	qPCR
p53-F	5’-ATGGAGGAGCCGCAGTCAGATCCTA-3’	PCR
p53-R	5’-TCAGTCTGAGTCAGGCCCTTCTGTC-3’	PCR
PepX GFP-R	5’-CCTTGCTCACCATGGTACCAAGCTTCTCACTCGAGGATCTCTTA-3’	Cloning
PepX-GFP-F	5’-GACTCTAGCGTTTAAACTTAAGCTATGGGCAGCCCTCGTGTACCTGAT-3’	Cloning
SDHA-F	5’-GCATTTCAGAGACAGCCAT-3’	qPCR
SDHA-R	5’-TGCCCCTTGTAGTTGGT-3’	qPCR
ZMYND8-F	5’-GAAAAAGAAAATGTATGGCTGCACAGAAGC-3’	qPCR
ZMYND8-R	5’-CAGATTTTGATGACTACTTTCGCTATTTGC-3’	qPCR

Table 2.3: primers used throughout this thesis

2.1.3 Antibodies

Protein	Dilution	Species	Vendor	Catalogue Number	Application	RRID Identifier
AKT	1:1000	Rabbit	Cell Signalling Technology	9272	WB	AB_329827
Alexa Fluor 488 Donkey Anti-Rabbit	1:500	Donkey	Life Technologies	A-21206	IF	AB_2535792
Alexa Fluor 546 Donkey Anti-Mouse IgG	1:500	Donkey	Life Technologies	A10036	IF	AB_2534012
AMPK	1:1000	Mouse	Santa Cruz Biotechnology	sc-74461	WB	AB_1118940
Anti-rabbit IgG, HRP-linked Antibody	1:5000	Goat	Cell Signalling Technology	7074S	WB	AB_2099233
Beclin	1:1000	Rabbit	Cell Signalling Technology	3738	WB	AB_490837
BFP	1:5000	Rabbit	Evrogen	AB233	WB	AB_2571743
BRD2	1:1000	Rabbit	Bethyl	A302-583A	WB	AB_2034829
BRD3	1:1000	Rabbit	Bethyl	A302-368A	WB	AB_1907251
BRD4	1:2500	Rabbit	Abcam	128874	WB	AB_11145462
Caspase 3	1:1000	Rabbit	Cell Signalling Technology	9662	WB	AB_331439
Cleaved PARP	1:1000	Rabbit	Cell Signalling Technology	9541	WB	AB_331426
ERK	1:10,000	Rabbit	Cell Signalling Technology	4695S	WB	AB_390779
GAPDH	1:1000	Rabbit	Santa Cruz Biotechnology	sc-32233	WB	AB_627679

Protein	Dilution	Species	Vendor	Catalogue Number	Application	RRID Identifier
Goat Anti-Mouse IgG (H + L)-HRP Conjugate	1:5000	Goat	Biorad	1706516	WB	AB_11125547
H3K9 dimethyl	1:5000	Mouse	Abcam	Ab1220	WB	AB_449854
LC3B	1:2000	Rabbit	Cell Signalling Technology	2775	WB	AB_915950
MITF	1:2000	Rabbit	Atlas Antibodies	HPA003259	WB	AB_1079381
mTOR	1:1000	Rabbit	Cell Signalling Technology	2983	WB	AB_2105622
p-AKT	1:1000	Rabbit	Cell Signalling Technology	4056	WB	AB_331163
p-AMPK	1:500	Rabbit	Cell Signalling Technology	2531	WB	AB_330330
p-ERK	1:1000	Rabbit	Cell Signalling Technology	4377S	WB	AB_331775
p-mTOR	1:500	Mouse	Santa Cruz Biotechnology	sc-293133	WB	AB_2861149
p-P70S6K	1:1000	Rabbit	Cell Signalling Technology	9205	WB	AB_330944
p-TSC2 S1387	1:1000	Rabbit	Cell Signalling Technology	23402S	WB	AB_2798864
p-TSC2 T1462	1:1000	Rabbit	Cell Signalling Technology	3617	WB	AB_490956
p-ULK1 S555	1:1000	Rabbit	Cell Signalling Technology	5869S	WB	AB_10707365
p-ULK1 S757	1:1000	Rabbit	Cell Signalling Technology	6888	WB	AB_10829226
p62/SQSTM1	1:1000	Mouse	Cell Signalling Technology	88588	WB	AB_2800125

Protein	Dilution	Species	Vendor	Catalogue Number	Application	RRID Identifier
P70S6K	1:1000	Mouse	Santa Cruz Biotechnology	sc-8418	WB	AB_628094
Pan-H3	1:10,000	Rabbit	Abcam	Ab-176840	WB	AB_2715502
SDHA	1:1000	Mouse	Santa Cruz Biotechnology	sc-166909	WB	AB_10611174
SLC1A5	1:1000	Rabbit	Sigma	HPA035239	WB	AB_10670587
SLC3A2	1:1000	Rabbit	Sigma	HPA017980	WB	AB_2669723
TSC2	1:1000	Rabbit	Cell Signalling Technology	4308	WB	AB_10547134
Tubulin	1:100	Mouse	Abcam	Ab11308	IF	AB_297911
ULK1	1:1000	Mouse	Santa Cruz Biotechnology	sc-390904	WB	AB_2861148
YAP/TAZ	1:500	Mouse	Santa Cruz Biotechnology	sc-101199	IF	AB_1131430
ZMYND8	1:5000	Rabbit	Bethyl	A302-089A	WB	AB_1604282

Table 2.4: Antibodies used throughout this thesis

2.1.4 Buffers and reagents

Buffer	Components
0.2 M Citric acid/sodium phosphate buffer	36.85 ml citric acid buffer mixed with 63.15ml Sodium phosphate buffer, pH adjusted to 6.0
0.2% Triton-X100	0.2% Triton-X100 v/v, in PBS
4% Formaldehyde	4% formaldehyde v/v, in PBS
Annexin V binding buffer	10 mM HEPES, 140 mM NaCl, 2.5mM $CaCl_2$, pH 7.4 in distilled water
Blocking buffer	5% w/v skimmed milk powder (Marvel, cat. #3023034) in TBS-T

Buffer	Components
Cell lysis buffer	150 mM NaCl, 1 mM EDTA, 10 mM Tris-HCl pH 8.0, 0.5% NP-40, Protease inhibitor Cocktail Set III, EDTA-Free (539134, Calbiochem), 1 mM PMSF, TurboNuclease (Sigma, T4330) , 1 mM $MgCl_2$, Sodium Orthovanadate (New England Bio Labs, cat. #P0758S)
Citric acid buffer	100 mM $C_6H_8O_7.H_2O$ in distilled water
Crystal violet stain	10% methanol v/v, 1 % crystal violet powder w/v, in distilled water
DAPI solution	0.1% 1 mg/mL DAPI v/v in PBS
Freezing solution	90% FBS v/v, 10% DMSO v/v
Glycerol storage buffer	90% glycerol v/v, 10% 20 mM Tris-HCl pH 8.0 v/v
Loading buffer	NUS SDS PAGE 4x loading buffer, cat. #NP0008, with 40 mM DTT
Magnesium chloride hexahydrate solution	1M $MgCl_2.6H_2O$ in distilled water
Mowiol	2.4 g Mowiol 4-88, 6 g glycerol, 6 ml distilled H_2O, 12 ml 0.2M Tris-Cl pH 8.5
Potassium hexacyano-ferrate (II) trihydrate buffer	100 mM $K_4[Fe(CN)_6]3H_2O$ in distilled water
Potassium hexacyano-ferrate (III) buffer	100 mM $K_3[Fe(CN)_6]$ solution in distilled water
Propdium iodine staining solution	50 µg/mL RNase A, 50 µg/mL propidium iodide, 0.05% Triton X-100 in PBS
Sodium phosphate buffer	200 mM $Na_2HPO_4.2H_2O$ in distilled water
SS5 solution	5% FBS v/v, NaN_3 0.01% v/v in PBS
TAE	40 mM Tris, 20 mM glacial acetic acid, 1 mM EDTA, in distilled water
Transfer buffer	20% methanol, 25 mM Tris, 192 mM glycine in distilled water
Tris-buffered saline with Tween (TBS-T)	0.05% Tween20 v/v, 20 mM Tris, 150 mM NaCl in distilled water
X-gal solution	20 mg/ml X-gal (Sigma, cat. #10745740001) dissolved in N,N-dimethylformamide
β-galactosidase staining solution	40 mM citric acid/ sodium phosphate buffer, 5 mM $K_4[Fe(CN)_6]3H_2O$, 5 mM $K_3[Fe(CN_6)]$, 150 mM NaCl, 2 mM $MgCl_2$, and 1 mg/ml X-gal in distilled water

Table 2.5: Buffers used throughout this thesis

Reagent	Vendor	Catalogue number
10x Tango Buffer (330 mM Tris-acetate (pH 7.9 at 37 °C), 100 mM magnesium acetate, 660 mM potassium acetate, 1 mg/ml BSA)	Thermo Fisher Scientific	BY5
1 kb Plus DNA ladder	Thermo Fisher Scientific	10787018
5x loading dye	Qiagen	239901
5x MyTaq™ Reaction Buffer Red	Bioline	BIO-37112
8-well glass imaging chamber dishes	Thermo Fisher Scientific	155411PK
ABgene adhesive film	Thermo Fisher Scientific	AB0558
Agarose	Web Scientific	AGR-500
Ampicillin	Sigma	A9518
Annexin V Alexa Fluor™ 647	Thermo Fisher Scientific	A23204
Bafilomycin A	Cell Signalling Technology	54645S
BioRad Clarity™ Western ECL Substrate	Bio-Rad	1705061
Blotting paper	GE Healthcare	3030-917
Bovine serum albumin	Sigma	A3059
Bradford assay reagent	Bio-Rad	5000006
CellEvent™ Caspase 3/7 Green Detection Reagent	Invitrogen	C10723
Chloroquine	Sigma	C6628
Citric acid anhydrous ($C_6H_8O_7.H_2O$)	Acros Organics	110450000
CutSmart 2.0 Buffer	New England Bio Labs	B7204S
DAPI (1 mg/ml)	Thermo Fisher Scientific	62248
Dimethyl sulfoxide (DMSO)	Sigma	D8418
Dithiothreitol (DTT)	Sigma	43819
Dulbecco’s Modified Eagle Medium (DMEM)	Gibco	31966021
Ethanol	Merck	32221
Ethylendiaminetetraacetic acid (EDTA)	Sigma	EDS
Fetal bovine serum (FBS)	Biosera	FB-1001/500

Reagent	Vendor	Catalogue number
FuGENE 6	Promega	E2311
Gateway™ LR Clonase Mastermix	Thermo Fisher Scientific	11791020
Geneticin	Thermo Fisher Scientific	10131035
Gibson Assembly Mastermix	New England Bio Labs	E5520S
HindIII-HF	New England Bio Labs	R3104S
LightCycler 480 Multiwell Plate 384, white	Roche	04729749001
LightCycler480 SYBR Green 1 Master, 2x concentration	Roche	04887352001
Lipofectamine RNAiMAX	Invitrogen	13778-150
Magnesium chloride hexahydrate ($MgCl_2.6H_2O$)	Sigma	M2670
MES SDS Running Buffer	Invitrogen	NP0002
Methanol	Honeywell	32213
MyTaq™ polymerase	Bioline	21105
N,N-dimethylformamide	Sigma	D4551
NaeI	New England Bio Labs	R0190S
NP-40	Thermo Fisher Scientific	85124
NUS SDS PAGE 4x loading buffer	Invitrogen	NP0008
OptiMem	Gibco	31985062
PageRuler™ Plus Prestained Protein Ladder 10 to 250 kDa,	Thermo Fisher Scientific	26620
Penicillin Streptomycin	Thermo Fisher Scientific	15070063
peqGREEN	peqLab	732-2960
Phenylmethanesulfonyl fluoride (PMSF)	Sigma	78830
Polylysine covered microscope slides	Fisher Scientific	10219280
Ponceau stain	Sigma	P7170
Potassium hexacyano-ferrate (II) trihydrate/ Potassium ferrocyanide trihydrate ($K_4[Fe(CN)_6]3H_2O$)	Sigma	P3289

Reagent	Vendor	Catalogue number
Potassium hexacyanoferrate (III)/Potassium ferricyanide ($K_3[Fe(CN_6)]$)	Sigma	702587
Propidium Iodide	Thermo Fisher Scientific	P3566
Protease inhibitor Cocktail Set III, EDTA-Free	Calbiochem	539134
Puromycin	Thermo Fisher Scientific	A1113803
PVDF membrane	Sigma	GE10600023
RNAse A	Thermo Fisher Scientific	EN0531
RNAse-free water	Invitrogen	AM9932
Roswell Park Memorial Institute (RPMI) 1640 media	Gibco	42401018
S.O.C. medium	Thermo Fisher Scientific	15544034
SDS PAGE NuPAGE Novex Bis-Tris Protein Gel	Invitrogen	WG1403BOX
Skimmed milk powder	Marvel	3023034
Sodium chloride (NaCl)	SLS	CHE3316
Sodium Orthovanadate	New England Bio Labs	P0758S
Sodium phosphate (monobasic dihydrate) ($Na_2HPO_4.2H_2O$)	Acros Organics	271750000
SYTOX® AADvanced™	Invitrogen	S10349
Triton X-100	Sigma	T9284
Trypsin-EDTA	Thermo Fisher Scientific	25200056
X-gal	Sigma	10745740001
X-ray film	Fujifilm	47410 19289

Table 2.6: Reagents used in this thesis

2.1.5 Commercially available kits

Kit name	Vendor	Catalogue number
Cell Titer 96® Non-Radiactive Cell Proliferation Assay	Promega	G4000
CellEvent™ Caspase-3/7 Green Flow Cytometry Assay Kit	Invitrogen	C10427
Gel Purification Kit	Qiagen	28704
Herculase II Fusion DNA polymerase Kit	Agilent	600677
iScript™ cDNA Synthesis Kit	Bio-Rad	1708891
Mini-Prep Kit	Qiagen	27106
MycoAlert Detection Kit	Lonza	LT07-118
RNeasy Mini Kit (250)	Qiagen	74106

Table 2.7: Commercially available kits used throughout this thesis

2.1.6 Pharmacological BET inhibitors

Inhibitor	Description	Synthesis
(+)-JQ1	BET BRD inhibitor	As described [71]
(-)-JQ1	Negative stereoisomer of (+)-JQ1	As described [71]
RT20	BET BRD inhibitor	As described [72]
RT53	Novel, unpublished epigenetic inhibitor	Unpublished

Table 2.8: Pharmacological BET inhibitors used throughout this thesis

2.2 Methods

2.2.1 Cell biology

2.2.1.1 Cell culture conditions

Unless stated otherwise, cells were cultured in Roswell Park Memorial Institute (RPMI) 1640 media (Thermo Fisher Scientific, cat. #11875093) supplemented with 10% fetal bovine serum (FBS) (v/v, Biosera, cat. #FB-1001/500), antibiotics (1% Pencillin Streptomycin (Thermo Fisher Scientific, cat. #15070063) in a humidified incubator at 37 °C, 10% CO_2. The cells were grown in T-75 flasks (Corning, cat. #CLS430641U-100EA), unless stated otherwise. Where cells were treated in experiments, media containing 5% FBS, 1% antibiotics was used, unless stated otherwise. Cells were tested once per month for mycoplasma using MycoAlert Plasma Detection kit (Lonza, cat. #LT07-118) and were only used in experiments if mycoplasma negative. Cell lines were authenticated using short tandem repeat profiling.

Cells were passaged to ensure cells grew in a monolayer that did not exceed 90% density. When cells were passaged, cells were washed with 5 ml autoclaved phosphate-buffered saline (PBS), which was aspirated, then cells were trypsinised using 3 ml 0.25% trypsin-EDTA (Thermo Fisher Scientific, cat. #25200056). Cells detached in an incubator, then trypsin was neutralised by the addition of 4 ml media. The cell suspension was transferred to a falcon tube, and cells were centrifuged for 4 minutes (min) at 1500 g. The cell pellet was resuspended in media, and an appropriate proportion of cells, between 1:3 and 1:20, were then transferred to a fresh flask. For storage and freezing of cells, following centrifugation, cells were resuspended in 1 ml freezing solution, and aliquoted into cryo-tubes. Cryo-tubes were then placed in a Mr Frosty freezing container (Thermo Fisher Scientific, cat. #5100-0001), and were placed in the -80 °C freezer. For long term storage,

cells were then transferred to a liquid nitrogen tank. To retrieve frozen cells, cryo-tubes were placed in a 37 °C bead bath to defrost. Once cells had defrosted, they were transferred to a fresh flask for growth. Cells were passaged at least once before they were used in an experiment.

2.2.1.2 Stable cell line generation

501mel cells were cultured in RPMI media with 10% FBS, 1% PenStrep at 37 °C, at 10% CO_2. The cells were seeded at 50% confluency, in 6 well plates, with each well containing 2 ml RPMI media. 24 h later, cells were transfected using 3 µL FuGENE6 (Promega, cat #E2311), according to manufacturer's instructions, with 1.8 µg DNA of pPB-hCMV1-cHApA-insert (PiggyBac plasmid with one of the following inserts: PepX-BFP-NLS, KRR-BFP-NLS, LIL-BFP-NLS, or BFP-NLS. Figure 2.1A), 0.1 µg DNA of transactivator-ires-neo plasmid (Figure 2.1B), and 0.1 µg DNA of transposase plasmid (Figure 2.1C). Plasmids were passed to me by a postdoctoral scientist within our lab group, and plasmid maps are shown below. Media was changed 24 h after transfection, and antibiotic selection began a further 24 h later. Selection took 2-3 weeks, at which point all untransfected control cells were dead, after which positive clones were allowed to grow in RPMI media with 10% FBS and 1% PenStrep, 1% Geneticin (Thermo Fisher Scientific, cat. #0131027) and 1 µg/ml puromycin in a 10 cm dish, from which frozen stocks were prepared. Resulting cell lines shown in Table 2.9. Throughout experiments, the resulting cells were treated using RPMI medium, supplemented with 10% FBS, 1% PenStrep, 1% Geneticin and 1 µg/ml puromycin with the indicated concentrations of doxycycyline.

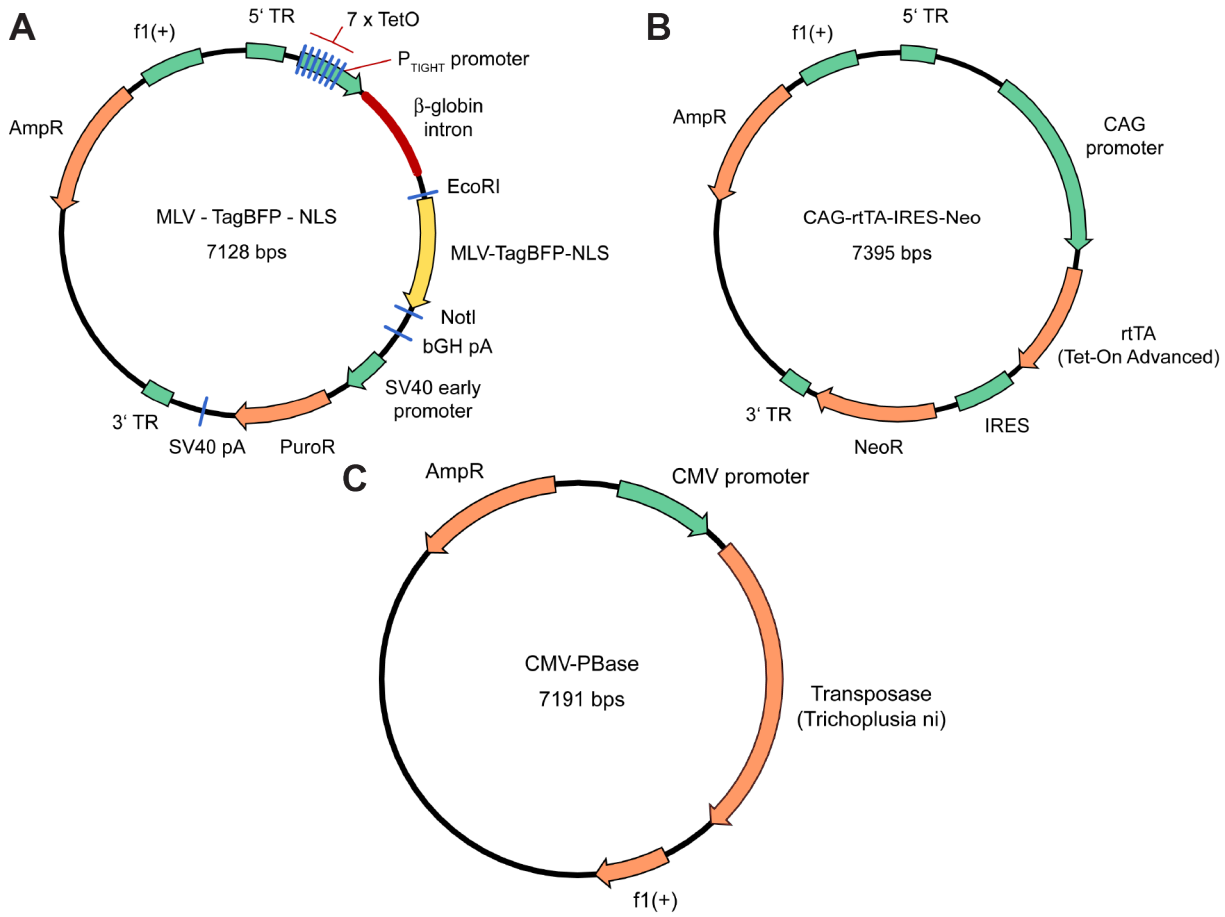


***Figure 2.1**: Plasmid maps of plasmids used in Tet-on piggybac system. (**A**) pPB-hCMV1-cHApA-insert plasmid. Insert in this plasmid map is labelled as "MLV-TagBFP-NLS". (**B**) Transactivator-ires-neo plasmid. (**C**) Transposase plasmid.*

Cell line	**Cell type**	**Source**
501MEL-KRR	Modified human melanoma cell line	Self-generated
501MEL-LIL	Modified human melanoma cell line	Self-generated
501MEL-NLS	Modified human melanoma cell line	Self-generated
501MEL-PepX	Modified human melanoma cell line	Self-generated

Table 2.9: Piggybac cell lines used throughout Chapter 5 of this thesis

2.2.1.3 siRNA transfection

30,000 cells were seeded in 6 well plates, ensured to be 60-80% confluent at the time of transfection (24 h after seeding). Forward siRNA transfection was carried out using lipofectamine RNAiMAX 2013 (Invitrogen by Life Technologies, cat. #13778-150) and 40 pmol of pooled siRNA per well (according to the manufacturer's protocol) or the negative control (details can be found in Table 2.18). Pooled siRNA targeting one of BRD2, BRD3 or BRD4 consisted of equal quantities of each of the four single siRNAs that targeted the same protein (Table 2.3). For example, pooled siRNA against BRD2, consisted of equal amounts of four single siRNAs that each target BRD2, cat. # J-004935-06, -07, -08, -09, Dharmcacon. "siBETs" siRNA consisted of equal quantities of each of the pooled siRNAs that each target one of BRD2, BRD3 or BRD4. Briefly, 24 h after seeding, 9 µL of lipofectamine was diluted in 150 µL OptiMem (Thermo Fisher Scientific, cat. #31985062) and incubated at room temperature for 5 min. In a separate microcentrifuge tube, 4 µL siRNA is diluted in 150 µL OptiMem. The diluted lipofectamine and siRNA are combined and incubated together for 5 min and then added to the cells in a drop-wise fashion. Cell media was changed 4 h after transfection, and cells were then incubated at 37 °C for a further 48 h, after which, plates were washed with PBS and stored at 80 °C until RNA was extracted or cells were lysed for western blotting.

2.2.1.4 Flow cytometry analysis of cell cycle

For melanoma cells, 15,000 cells were seeded in 3 ml media in 6 well plate, if treated for 72 h. If cells were treated for 48 h, 30,000 cells were seeded in 6 well plate in 3 ml media. For LNCaP cells, 50,000 cells were seeded. Doxycycline was refreshed every 48 h if cells were not already harvested. Following treatment, cells were washed with ice cold PBS and trypsinised using 135 µL 0.25% trypsin-EDTA (Thermo Fisher Scientific, cat. #25200056). Trypsin was neutralised upon addition of SS5 solution. Cells were centrifuged for 2 min at

1800 g at 4 °C. Cells were resuspended in PBS, and fixed with 100% ethanol for at least 1 h on ice. Fixed cells were centrifuged for 2 min at 1800 g at 4 °C and incubated with a propidium iodide (PI) staining solution for 30 min at 37 °C, protected from light. Cells were washed with PBS, and centrifuged for 2 min at 1800 g at 4 °C and resuspended in 400 µL PBS. DNA content was analysed with a FACS Canto Flow Cytometer (BD Bioscience).

2.2.1.5 Flow cytometry analysis of caspase 3/7 activation

15,000 cells were seeded in 3 ml medium in a 6 well plate, if treated for 72 h. If cells were treated for 48 h, 30,000 cells were seeded in 6 well plate in 3 ml media. Doxycycline was refreshed every 48 h if cells were not already harvested. Following treatment, cells were washed with PBS, PBS was harvested, and cells were trypsinised using 135 µL 0.25% trypsin-EDTA (Thermo Fisher Scientific, cat. #25200056). Trypsin was neutralised upon addition of cell culture media. Cells were centrifuged at 80 g for 4 min, resuspended in 500 µL PBS and transferred to Eppendorf tubes. 2 µL of CellEvent™ Caspase 3/7 Green Detection Reagent (from CellEvent™ Caspase-3/7 Green Flow Cytometry Assay Kit, Invitrogen, cat. #C10427) was added to 1 ml sample. Samples were incubated for 30 min at 37 °C, protected from light. During the final 5 min of staining, 1 µL of 1 mM SYTOX® AADvanced™ was added to the appropriate samples. Cells were analysed with a FACS Canto Flow Cytometer (BD Bioscience), using 488 nm excitation and collecting fluorescence emission using a 530/30 bandpass filter for CellEvent™ Caspase 3/7 Green Detection Reagent and a 690/50 BP filter for SYTOX® AADvanced™ dead cell stain.

2.2.1.6 Flow cytometry analysis of annexin V staining

15,000 cells were seeded in 3 ml media in a 6 well plate, if treated for 72 h. If cells were treated for 48 h, 30,000 cells were seeded in 6 well plate in 3 ml media. Doxycycline was refreshed every 48 h if cells were not already harvested. Following treatment, supernatant from cells was harvested. Cells were washed with 1 ml PBS, which was harvested after

washing, and trypsinised using 200 µL 0.25% trypsin-EDTA (Thermo Fisher Scientific, cat. #25200056). Trypsin was neutralised using 1 ml media. Cells in trypsin and media were collected and centrifuged at 600 g for 3 min. Medium was aspirated and cells were resuspended in 1 ml annexin V binding buffer (Table 2.6). Cells were centrifuged at 600 g for 3 min and resuspended in 100 µL annexin V binding buffer (Table 2.6). 0.5 µL of annexin V Alexa Fluor™ 647 (Thermo Fisher Scientific, cat. #A23204) was added to each sample. Samples were incubated at 4 °C for 15 min. 400 µL annexin V binding buffer (Table 2.6) was added to each sample, before cells were analysed with a FACS Canto Flow Cytometer (BD Bioscience).

2.2.1.7 Flow cytometry analysis

During all flow cytometry experiments, approximately 10,000 cells were used for each analysis. Briefly, live, single cells were gated using forward (FSC) and side scatter (SSC), before channels were selected for analysis. PE channel was selected for PI staining. APC channel was selected for CellEvent™ Caspase3/7 Green Detection Reagent, and PE for SYTOX® AADvanced™ dead cell stain. Flow cytometric analyses were performed with FlowJo software.

2.2.1.8 Immunofluorescence

In the case of 501mel and A375M, 30,000 cells were seeded in 3 ml medium in 6 well plate containing sterilised coverslips (coverslips were sterilised using UV irradiation). Cells were treated with 1 µM DMSO, (+)-JQ1 or (-)-JQ1 for 24 or 48 h.

In the case of LNCaP cells, 50,000 cells were seeded in 3 ml media in 6 well plate containing sterilised coverslips (coverslips were sterilised using UV irradiation). Cells were treated with 1 µM RT20 or RT53, or 0.1% DMSO as a negative control, for 48 h.

Following treatment, cells were fixed using 1 ml 4% formaldehyde for 20 min. Cells were washed with PBS for 3 min, or overnight in 4 °C. Coverslips were then washed 3 times in PBS for 3 min. Cells were permeablised using 1 ml 0.2% Triton-X100. Coverslips were incubated in 50 µL primary antibody in PBS containing 5% bovine serum albumin (BSA) for 20 min on parafilm. Antibodies details listed in Table 5. Coverslips were washed 3 times in PBS for 3 min. Coverslips were incubated in 50 µL secondary antibodies in PBS containing 5% BSA and in 0.1% DAPI v/v (Thermo Fisher Scientific, cat. #62248) for 20 min on parafilm. If cells were stained with phalloidin, coverslips were incubated on parafilm at room temperature for 15 min with 50 µL of 2% phalloidin v/v (Thermo Fisher Scientific, cat. #A12379) in PBS. Coverslips were washed 4 times in PBS for 3 min. Coverslips were mounted on polylysine covered microscope slides (Thermo Fisher Scientific, J2800AMNZ, cat. #10219280) using 8.6 µL Mowiol. Cells were imaged using a Zeiss LSM 710 scan-head (Zeiss GmbH, Jena, Germany) coupled to an inverted Zeiss Axio Observer Z1 microscope equipped with a 20x and high-numerical-aperture (N. A. 1.40) 63x oil immersion objective (Zeiss GmbH, Jena, Germany). The following lasers were used: 405nm excitation laser and a 410-488nm emission filter were used to detect DAPI fluorescence. A 488 nm excitation laser and a 494-542 nm emission filter were used to detect green fluorescence. A 543 nm excitation laser and a 549-679 nm emission filter were used to detect red fluorescence. Images were acquired using ZEN 2011 software (Carl Zeiss, Germany).

2.2.1.9 β-galactosidase staining

Method adapted from a previously published report [241]. 30,000 cells were seeded in a 6 well plate in 3 ml media. Cells were treated for 48 h. After treatment, cells were washed twice with 1 ml PBS per well for 30 seconds. Then cells were fixed using 2 ml 4% formaldehyde per well for 10 min. Formaldehyde was removed and cells were washed twice with 1 ml PBS per well for 30 seconds. 1 ml fresh β-galactosidase staining solution

(40 mM citric acid/ Na phosphate buffer (36.85 ml 100 mM $C_6H_8O_7.H_2O$ solution in distilled water mixed with 63.15ml 200mM $NaH_2PO_4.H_2O$) , 5 mM $K_4[Fe(CN)_6]3H_2O$, 5 mM $K_3[Fe(CN_6)]$, 150 mM NaCl, 2 mM $MgCl_2$, and 1 mg/ml X-gal dissolved in N,N-dimethylformamide (Sigma, cat. #10745740001) in distilled water) was added to each well. Plates were sealed with parafilm, covered with aluminium foil and incubated overnight at 37 °C. After the incubation, cells were washed twice with 1 ml PBS per well for 30 seconds, once with 1 ml per well methanol for 30 seconds, then a final wash with 1 ml PBS per well for 30 seconds. Cells were kept at room temperature in PBS until imaged using an Operetta microscope. Analysis was carried out using Operetta software.

2.2.1.10 Crystal violet cell viability assay

In the case of 501mel and A375M cells, 1000 cells were seeded per well in 1 ml media, in 24 well plates. 24 h after seeding, cells were treated with different doses (0, 10, 25, 50, 75, 100, 200, 300, 400, 500, 750, 1000 nM) of (+)-JQ1 and (-)-JQ1 for 1 week.

For PepX, NLS, KRR and LIL cell line treatments, 1000 cells were seeded per well in 24 well plates in 1 ml media. 24 h after seeding, cells were treated with doxycycline of the indicated concentration for 48 or 72 h. Doxycycline was refreshed every 48 h if cells were not already harvested.

For LNCaP and PC3 cells, 10000 cells were seeded per well in 24 well plates in 1 ml media. 24 h after seeding, cells were treated with 0, 0.5 and 1 μM RT20 and RT53 for 12 days in 10% FBS, 1% PenStrep, RPMI media. DMSO at 0.05% and 0.1% was used as negative controls.

After treatment, cells were washed with PBS and fixed with 500 μL 4% formaldehyde, washed twice with 500 μL PBS, stained using 500 μL crystal violet for 10 min, then washed with water and left to dry at room temperature. There were 3 biological replicates

per cell line, and within each biological replicate there were technical duplicates. EC_{50} values were calculated using nonlinear sigmoidal curve fit (DoseResp) in Origin software. Error bars represent standard deviation.

2.2.1.11 MTT assay

5000 cells were seeded per well. Cells were treated with varying concentrations (as indicated in figures) of RT20, RT53, (+)-JQ1, (-)-JQ1 and doxycycline ± 10 μM chloroquine (CQ). 501mel, A375M, CHL1, IGR37 and IGR39 cells were treated for 48 h. PepX cells were treated for 72 h, although doxycycline was refreshed after 48 h. LNCaP and PC3 cells were treated with 48 h in Figure 4.1, but LNCaP cells were treated for 96 h in Figures 4.8A-4.8B. Following treatment, cellular proliferation was measured using Cell Titer 96® Non-Radioactive Cell Proliferation Assay (Promega, cat. #G4000) according to the manufacturers' instructions. Briefly, 15 μL dye solution was added to cells using a multi-channel pipette, and the cells were incubated in the tissue culture incubator for 3 h. 100 μL stop solution was added to cells using a multi-channel pipette, and cells were incubated for at least 1 h in the tissue culture incubator. The coloured formazan product was re-suspended in the wells using a multi-channel pipette before absorbance at 560 nm was recorded using a Promega GloMax 96 well plate reader.

2.2.1.12 Clonogenicity assay

15,000 cells were seeded. 24 h later cells were treated. 501mel and A375M cells were treated with DMSO, (-)-JQ1 and (+)-JQ1 for 48 h. PepX cells were treated with DMSO and doxycycline for 72 h, although doxycycline was refreshed after 48 h. Following treatment, media was aspirated, cells were washed with PBS and trypsonised using 135 μL trypsin. Trypsin was neutralised with 1 ml medium, and cells were centrifuged for 4 min at 80 g. 1000 cells from each sample were seeded in 3 ml fresh medium in a 6 well plate. After 1

week, colonies were stained using crystal violet (described above), the plates were scanned and colonies were counted using ImageJ software.

2.2.1.13 RNA extraction

RNA was extracted (using RNeasy Mini Kit (250) (Qiagen, cat. #74106), extracted RNA was quantified using the Nanodrop™ (Thermo Fisher Scientific) and stored at -80 °C.

2.2.1.14 cDNA synthesis

500 ng of RNA was converted into cDNA using iScript™ cDNA Synthesis Kit (BioRad, Cat#1708891), according to the manufacturers' instructions, using a reaction volume of 20 µL, as detailed in Table 2.10. Conditions of the cDNA reactions are detailed in Table 2.11.

Component	**Quantity**
RNA	500 ng
5x iScript mastermix	4 µL
iScript Reverse Transcriptase	1 µL
H_2O	Up to 20 µL

Table 2.10: Components of cDNA synthesis reactions

Temperature (°C)	**Time**	**Purpose**	**Cycles**
25	5 min	Annealing	1
42	30 min	Extension	1
85	5 seconds	Melting	1
4	Continuous	Hold	1

Table 2.11: cDNA synthesis reaction conditions

2.2.1.15 Quantitative polymerase chain reaction (qPCR)

Prior to use in qPCR reactions, cDNA was adjusted from the cDNA synthesis reaction volume of 20 µL to 300 µL. qPCR reaction mix was assembled as detailed in Table 2.12

and pipetted into each well of a 384 well plate (LightCycler 480 Multiwell Plate 384, white, cat. #04729749001). 4 technical replicates were assigned to each sample. qPCR reaction was carried out using a Lightcycler® 480 II qPCR machine (Roche). Details of qPCR reaction conditions are described in Table 2.13. Annealing temperature depended upon primers used. Quantification of gene expression was carried out by first calculating the average expression value for each sample from the 4 technical replicates. ΔCT for each samples was calculated using the following formula: ΔCT = gene of interest - housekeeping gene. The ΔCT values for each biological replicate of each gene were averaged to give one ΔCT value for each gene (which comprised data from 3 biological replicates, each of which consisted of 4 technical replicates). ΔΔCT for each sample was calculated using the following formula: $\Delta\Delta CT = \Delta CT^{\text{treated sample}} - \Delta CT^{\text{control sample}}$. The relative fold change of gene expression in treated samples compared with control sample is $2^{-\Delta\Delta CT}$. Mean expression values are displayed relative to 18S rRNA expression, errors are standard deviation.

Component	**Quantity**
cDNA	3 µL (5 ng)
Primers (diluted to 10 µM)	2 µL
LightCycler480 SYBR Green 1 Master, 2x concentration, Mastermix (Roche, cat. #04 887 352 001)	5 µL

Table 2.12: Components of cDNA synthesis reactions

Temperature (°C)	Time	Ramp Rate (°C/ second)	Purpose	Cycles
50	2 min	4.4	Warming	1
95	2 min	4.4	Melting	1
95	15 seconds	4.4	Melting	55 cycles
55-65	30 seconds	2.2	Annealing	
72	5 seconds	2.2	Extension	
95	Continuous	-	Melting	1

Table 2.13: qPCR conditions

2.2.1.16 Sample preparation prior to RNA-sequencing

Samples were treated according to Table 2.14. Following treatment, media was aspirated, the plates were washed with PBS and stored at -80 °C until RNA was extracted. RNA was extracted as earlier described. Prior to submission to Wellcome Trust Centre for Human Genomics (WTCHG) for sequencing, RNA integrity was determined using Bioanalyser (Agilent Technologies). All samples had a RIN value above 8, which rendered them of sufficient quality for RNA-seq. A total of 1 µg RNA in 30 µL per samples was submitted for RNA-seq. RNA was diluted in RNAse-free water (Invitrogen cat. #AM9932). Following submission, samples were subject to sequencing using HiSeq4000 (Illumina) at the WTCHG, Oxford.

Cell line	Treatment	Concentration	Duration (h)	Negative control	Number of biological replicates for each sample
501mel	(+)-JQ1	500 nM	24	(-)-JQ1	3
501mel	siBRD2	40 pmol	48	Negative control siRNA	3
501mel	siBRD3	40 pmol	48	Negative control siRNA	3
501mel	siBRD4	40 pmol	48	Negative control siRNA	3
501mel	siBETs	40 pmol	48	Negative control siRNA	3
A375M	(+)-JQ1	500 nM	24	(-)-JQ1	3
A375M	siBRD2	40 pmol	48	Negative control siRNA	3
A375M	siBRD3	40 pmol	48	Negative control siRNA	3
A375M	siBRD4	40 pmol	48	Negative control siRNA	3
A375M	siBETs	40 pmol	48	Negative control siRNA	3
501mel-PepX	Doxycycline	50 nM	48	DMSO	4
501mel-NLS	Doxycycline	30 nM	48	DMSO	4
501mel-KRR	Doxycycline	8 nM	48	DMSO	4
501mel-LIL	Doxycycline	60 nM	48	DMSO	4

Table 2.14: Samples submitted for RNA-seq

2.2.1.17 RNA-sequencing data analysis

Each sample contained multiple biological replicates (Table 2.14), which were stitched together using UNIX to generate a single forward and a single reverse fastq file for each sample. Quality control was carried out on raw fastq files using FASTQC (version 0.11.7), IGV (version 2.3.55) and Seqmonk (version 1.31.1). Raw fastq files were mapped using RNASTAR (version 2.5.3a) to human genome build hg19 (GRCh37). The resulting bam files from RNASTAR were used to generate a raw data counts table using featureCounts

within Subread (version 1.4.5 [242]). Resulting raw data counts were used as input for differential gene expression analysis using DESeq2 (version 1.8.2 [243]). Reads for each sample were first filtered for genes whose expression was <3 counts per million (owing to 3 biological replicates per sample) prior to generation of DESeq2 object. Gene Set Enrichment Analyses were carried out using Bioconductor package fgsea [244].

2.2.1.18 p53 mutation screen

Cells were washed with 5 ml PBS, which was aspirated, then cells were trypsinised using 3 ml 0.25% trypsin-EDTA (Thermo Fisher Scientific, cat. #25200056). Cells detached in an incubator, then trypsin was neutralised by the addition of 4 ml media. The cell suspension was transferred to a falcon tube, and cells were centrifuged for 4 min at 80 g. The cell pellet was resuspended in media, as some cells were transferred to a fresh flask for further growth. The remaining cells were transferred to a microcentrifuge tube and centrifuged again for 4 min at 80 g. Cells were resuspended in PBS to wash cells, then centrifuged for a further 4 min at 80 g. The resulting cell pellet was frozen at -80 °C until required for RNA extraction. RNA was extracted (method detailed above), from which cDNA was synthesised (method detailed above). cDNA was used as the DNA template in polymerase chain reaction (PCR), the components of which are detailed in Table 2.15 using Herculase Fusion DNA polymerase kit (Agilent, cat. #600677), using primers p53-F and p53-R in Table 2.4. Conditions used in the PCR are described in Table 2.16. PCR products were mixed with 12 µL loading dye (Qiagen, cat. #239901). 30 µL of from each sample was run in 3 consecutive wells and run on a 1% agarose gel 120V for 1 h alongside 1 kb Plus DNA ladder (Table 2.9, Thermo Fisher Scientific, cat. #10787018). Fragments from the same sample were purified together using Qiagen kit to ensure maximum DNA yield. Samples were submitted to Eurofins for sequencing with p53-F and p53-R primers. Sequences were aligned with the p53 reference sequence (National Center for Biotechnology Information (NCBI) accession number NM_000546.5) using SeqManPro (DNASTAR).

Component	Quantity
DNA	1 µg
Primers (diluted to 10 µM)	7.5 µL
Herculase II Fusion DNA Polymerase	3 µL
5x Herculase Reaction Buffer	15 µL
dNTPs (100 mM; 25 mM per dNTP)	3 µL
H_2O	Up to 60 µL

Table 2.15: Components of PCR reactions

Temperature (°C)	Duration	Step	Cycles
98	2 min	Melting	1
98	15 seconds	Melting	25
55	15 seconds	Annealing	
72	1 min and 15 seconds	Extension	
15	Continuous	Hold	1

Table 2.16: Details of PCR reaction conditions

2.2.2 Molecular Biology

2.2.2.1 Agarose gel electrophoresis

DNA fragments were resolved on agarose gels. Agarose (Web Scientific, cat. #AGR-500) was dissolved in TAE by heating in the microwave until homogenous and was poured into a tray to cast the gel. Gels were between 1-2% agarose w/v, depending on the fragment size of DNA in question, and contained 2 µL peqGREEN (peqLab, cat. #732-2960) for every 25 ml TAE. Once solidified, the agarose gel was submerged in TAE, and samples were loaded into wells. Samples were mixed as detailed in Table 2.17, and were run alongside 1kb Plus DNA ladder (Thermo Fisher Scientific, cat. #10787018), Table 2.18, to indicate size of fragments. Electrophoresis took place at 100V for approximately 30 min. The DNA fragments were visualised using ultraviolet light, emitted from a UVIdoc (UVItec).

Component	Volume (µL)
DNA	5
5x loading dye (Qiagen, cat. #239901)	4
H_2O	Up to 20

Table 2.17: Mixing of samples prior to loading on agarose gel

Component	Volume (µL)
1kb Plus DNA ladder (Thermo Fisher Scientific, cat. #10787018)	2
5x loading dye (Qiagen, cat. #239901)	4
H_2O	14

Table 2.18: Mixing components of 1 kb Plus DNA ladder prior to loading on agarose gel

2.2.2.2 Bacterial Transformation

Competent MACH1 *E.coli* bacteria were stored in -80 °C until required, at which point they were defrosted on ice. Cloning products and bacteria were mixed and incubated on ice for 20 min. Bacteria were then subject to heat shock: incubation at 42 °C for 1 min, following by incubation on ice for 1 min. Following heat shock, 200 µL S.O.C. medium (Thermo Fisher Scientific, cat. #15544034) was added to bacteria, after which cells were incubated at 37 °C for 1 h. During incubation, 10 cm Luria-Broth (LB) agar plates plates were cast from autoclaved LB medium with 100 µg/ml ampicillin and were allowed to cool to room temperature and solidify prior to plating of bacteria. 75-300 µL bacteria were then plated using a sterile L-shaped spreader on each plate and were incubated at 37 °C overnight to allow colonies to form.

2.2.2.3 Screening bacterial colonies using PCR

Reaction mix was assembled according to Table 2.19. Single colonies were picked using a sterile loop, and bacteria were mixed with the reaction mix, then immediately used to inoculate LB containing antibiotics in a 96 well block. The 96 well block was sealed with

ABgene adhesive film (Thermo Fisher Scientific, AB0558) and the PCR reaction was run according to conditions in Table 2.20.

Component	Volume (µL)
Primers (diluted to 10 µM)	1
5x MyTaq™ Reaction Buffer Red (Bioline, cat. # BIO-37112)	4
MyTaq™ polymerase (Bioline, cat. # 21105)	0.1
H_2O	15

Table 2.19: Components of colony PCR reaction.

Step	Temperature (°C)	Duration	Cycles
Melting	98	2 min	1
Melting	98	15 seconds	30
Annealing	50	15 seconds	
Extension	72	1 -3 min	
Hold	15	Continuous	1

Table 2.20: Details of colony PCR reaction conditions

2.2.2.4 Plasmid Purification

Bacteria were inoculated into 20 ml LB medium and grown overnight at 37 °C in a shaking incubator at 225 rpm. The next day, bacteria were centrifuged at 5000 g for 10 min. Supernatant was discarded, and plasmids were purified from bacteria using a Mini-Prep kit (Qiagen, cat. #27106). Plasmids were eluted in deionised water, and concentration was determined using Nanodrop™ (Thermo Fisher Scientific).

2.2.2.5 Glycerol stock preparation

Bacteria were inoculated and grown overnight at 37 °C in a shaking incubator at 225 rpm in 20 ml LB medium containing antibiotics. The following day, 1 ml of bacteria was added to 330 µL 60% glycerol in cryo-tubes, and frozen at -80 °C.

2.2.3 Protein biology

2.2.3.1 Whole cell lysate extraction

Cells were lysed on ice in 200 µL lysis buffer (150 mM NaCl, 1 mM EDTA, 10 mM Tris-HCl pH 8.0, 0.5% NP-40, Protease inhibitor Cocktail Set III, EDTA-Free (Calbiochem, 539134), 1 mM PMSF, TurboNuclease (Sigma, cat. #T4330) , 1 mM $MgCl_2$, Sodium Orthovanadate (New England BioLabs Inc., cat. #P0758S)). Cells were detached using a cell scraper and were transferred into microcentrifuge tubes and rotated for 30 min at 4 °C. Supernatant was then spun at 21,130g for 20 min at 4 °C, then transferred into new microcentrifuge tubes on ice. A Bradford assay (using Bradford assay reagent, BioRad, cat. #5000006) was then carried out to determine protein concentration on a 96 well plate and a Tecan plate reader measured the light absorbance to give the results. Samples were mixed with loading buffer (NUS SDS PAGE 4x loading buffer, cat. #NP0008, with 40 mM DTT added), and boiled at 95 °C for 3 min. Lysates were stored at -20 °C.

2.2.3.2 Immunoblotting

Proteins were separated on a 4-12% gradient gel (Invitrogen, cat.# WG1403BOX) in a tank containing MES SDS Running Buffer (Invitrogen, cat. #NP0002). Samples of equivalent protein concentration were loaded with 1 µL of protein marker (Thermo Fisher Scientific, PageRuler™ Plus Prestained Protein Ladder 10 to 250 kDa, cat. #26620), and each was run for 1 h at 170 V. Wet transfer was used to transfer proteins onto PVDF membranes (Sigma Aldrich, cat. #GE10600023) at 50 V for 2 h in transfer buffer, whilst the gel and PVDF membrane were sandwiched between blotting paper (GE Healthcare, cat. #3030-917).

Membranes were incubated in Ponceau stain (Sigma, cat.# P7170) for 5 min to ensure the transfer was even. Ponceau was washed from membranes by washing for 5 min in TBS-T.

The membranes were incubated in a blocking buffer for 30 min at room temperature. Each membrane was then washed in trie-buffered saline (TBS-T) three times, each wash lasting 5 min at room temperature. Primary antibody (antibody information and concentrations are detailed in Table 2.5) in TBS-T containing 5% BSA and membranes were incubated overnight at 4 °C.

The membranes were then washed in TBS-T three more times, each for 5 min, before incubation in a secondary antibody (Table 2.5) for 3 h in blocking buffer at room temperature. The membranes were then washed six times, each wash for 5 min, in TBS-T at room temperature, before they were incubated in ECL (BioRad Clarity™ Western ECL Substrate, 500 ml cat. #1705061), for 1 min, prior to developing using x-ray film (Fujifilm, cat.# 47410 19289). Protein sizes on immunoblot are indicated in kilodaltons (kDa).

2.2.4 Statistical analyses

2.2.4.1 ChIP-sequencing (ChIP-seq) data analysis

Previously published ChIP-seq data, GEO# GSE55064 [34], was downloaded. BigWig files from samples GSM1328969, GSM1328970, GSM1328971, GSM1328972, GSM1328973, GSM1328974, GSM1328975, GSM1328976, GSM1328977, GSM1328982, and GSM1328983 were uploaded to, and visualised using, the UCSC Genome Browser.

2.2.4.2 Statistical analysis

Statistical analysis was performed using unpaired Student's t-test. Mean values are shown, and error bars represent standard deviation when multiple biological replicates were used. Graphs are generated using Origin software. P values represented as * = $p < 0.05$, ** = $p < 0.01$, *** = $p < 0.001$, unless stated otherwise.

Chapter 3: Mechanism of inhibition following BRD inhibition in melanoma

3.1 Introduction

BET BRD inhibition often leads to the regression of melanoma *in vivo* and the loss of cellular proliferation *in vitro* [95, 151, 153, 208-210]; however, the mechanism behind this remains to be elucidated in many solid tumours. In AML [92, 98] and neuroblastomas harbouring MYCN translocations [94], MYC down-regulation as a result of BET inhibition is the key to therapeutic success, with over-expression of MYC affording protection against BET BRD inhibition in the context of AML [92, 98]. However, this is not the case in many malignancies, including melanoma, nor does MYC expression correlate with sensitivity to (+)-JQ1 in this context [151, 217].

In a subset of melanoma cell lines, pharmacological BET BRD inhibition leads to loss of cell viability through the down-regulation of the expression of the survival gene, AMIGO2 [152]. AMIGO2 is up-regulated in melanomas in comparison with melanocytes [152], and following AMIGO2 knockout or BET inhibition [95, 152], melanoma cells undergo apoptosis, leading to reduced tumour growth *in vivo* [95, 152]. However, there are many melanoma cell lines that do not express elevated levels of *AMIGO2* mRNA [152], suggesting in these contexts it is unlikely that BET BRD inhibition would result in loss of cell viability via a further reduction in *AMIGO2* expression. Therefore, it is difficult to argue that a universal mechanism underlying BET BRD efficacy for melanomas has been identified; thus, the mechanism underpinning loss of proliferation following treatment with a BET BRD inhibitor still lacks clarity.

Melanoma represents an area of clinical need as one of the few malignancies with a rising incidence [165]. While immunotherapies have increased the proportion of patients that

show an initial response to a treatment, this treatment regimens is not always well tolerated and many patients develop resistance and an incurable disease [187, 203, 246]. The combination of unmet clinical need and responsiveness to BET BRD inhibitors without a clear understanding as to how loss of cellular proliferation is achieved serves as a rationale for which to study the effects of BET protein attenuation in melanoma.

Many key melanoma genes have already been screened as potential determinants of sensitivity to BET BRD inhibitors. MITF is a key transcription factor involved in the expression of melanocyte-specific genes, as well as genes involved in an array of cellular processes including survival, lysosomal biogenesis, metabolism, senescence, proliferation and differentiation [179]. The expression level of MITF in melanoma is associated with different cellular phenotypes; high MITF expression is associated with differentiation, cells with intermediate MITF expression are highly proliferative owing to reduced p27 and p21 expression, and low MITF expression correlates coincides with an invasive phenotype [179, 247, 248]. While MITF plays an important role in coordinating many biological processes in the context of melanoma, its expression was found not to be a determinant of sensitivity [217].

NRAS, a GTPase that activates MAPK signalling, is significantly mutated in melanoma [249, 250]. In NRAS mutant melanomas, high BRD4 expression correlates with poorer patient survival and higher sensitivity to (+)-JQ1 *in vitro* in comparison NRAS mutant melanomas with low BRD4 expression [251]. However, as NRAS mutant cases account for 26% of melanomas [252], this provides a rationale for targeting BETs only in some melanomas, the cause of sensitivity across the majority of cases is yet to be identified. Moreover, neither the mutation status of NRAS nor BRAF, another member of the MAPK signalling pathway, bear correlation with melanoma cell line sensitivity to BET BRD inhibition, despite the oncogenic influences of mutations in these proteins [151, 217, 249]. Thus, the common denominator for sensitivity to BET BRD inhibition in the context of

melanoma remains to be identified. In addition, the points at which cell cycle arrest take place are inconsistent between cell lines, hinting at non-uniform mechanisms for loss of cellular proliferation in response to BET BRD inhibition [95, 154, 207].

It is clear that across multiple cancer models, including melanoma, there is a transcriptional response following BET BRD inhibition [92, 94, 95, 152], which could provide pointers concerning the cellular response and the molecular triggers involved. Therefore, the aim of this chapter is to elucidate the phenotype that is elicited following BET BRD inhibition, and the mechanism as to how this phenotype is achieved, with the aim of identifying the determinant(s) of the cellular response of melanoma cell lines to BET BRD inhibition.

3.2 Results

3.2.1 Melanoma cell lines display different sensitivities to BET BRD inhibition

Melanoma cell lines display differing levels of sensitivity to BET BRD inhibition, and the reason for this is so far unknown. In neuroblastoma, MYC expression correlates with sensitivity to BET BRD inhibition; however, this is not the case in melanoma [94, 217]. In fact, neither MITF expression levels, nor BRAF nor NRAS mutation statuses correlate with sensitivity to BET BRD inhibition [94, 151, 217]. There are indications that PGC-1α expression in melanoma cell lines may correlate with sensitivity to (+)-JQ1; however, NCI-60 findings contravene these data (+)-JQ1 [217, 219].

Previous studies have shown that melanoma cell lines display an array of sensitivities to BET BRD inhibition, and BET BRD inhibition leads to the slowing of tumour growth *in vivo* [95, 151]. Here, cell lines with a range of PTEN and p53 mutation statuses, and MITF expression levels have been examined; PTEN mutation, or loss, drives PI3K/AKT pathway activation [167]. Function of the transcription factor and tumour suppressor, p53, influences the cellular response of leukaemia cells to BET BRD inhibitors [253]. Therefore, p53 mutation status may affect the melanoma cellular response to BET BRD inhibition. Lastly, extreme high or low MITF can drive resistance to MAPK pathway inhibitors, and MITF expression level is intimately linked to melanoma proliferation and differentiation [179, 180]. Assessing the response of cell lines to BET BRD inhibitors that harbour a range of mutations and constitutively activated pathways may provide clues as to how BET BRD inhibition leads to loss of cell viability, and what underpins sensitivity to BET BRD inhibition in melanoma.

Figure 3.1A shows that members of the BET protein family are expressed across BRAF-mutant, NRAS-WT melanoma cell lines with a range of PTEN and p53 mutation statuses,

and MITF expression levels (Figure 3.1A, Table 3.1). This reinforces the notion that there is, indeed, a rationale for targeting these proteins in this malignancy model, independent of genetic background and MITF expression. SDHA was used as a loading control because its expression is unaffected by BET BRD inhibition in melanoma according to previously published data [152]. Several isoforms of BRD4 exist, which are categorised as BRD4-long (BRD4L) or BRD4-short (BRD4S) (Figure 1.1A). The expression of a CTM, which enables interactions with P-TEF-b [37], distinguishes BRD4L from BRD4S (Figure 1.1A). A non-specific band is visible between the two BRD4 isoforms (Figure 3.1A), which is unaffected by siRNA (Figures 3.4A-3.4B) and has been previously observed [68].

Pharmacological inhibition of BET BRDs has been conducted using different ranges of BET BRD inhibitor concentrations, different durations, and different measures of cellular proliferation (Figure 3.1B); therefore, different EC_{50} values are available for each cell line.

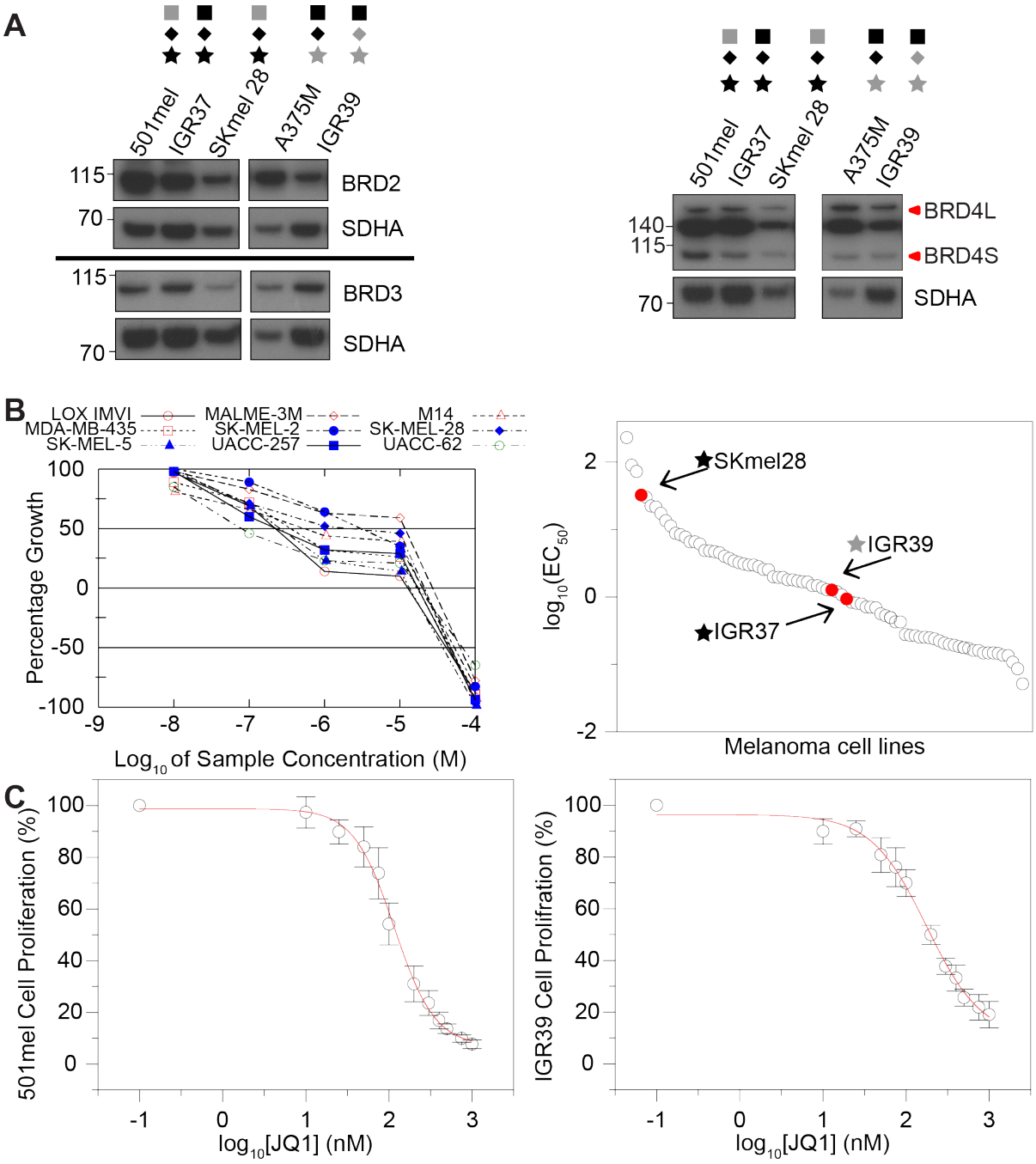


***Figure 3.1**: Melanoma cell lines express BETs and display different sensitivities to BET BRD inhibition. (**A**) Immunoblot showing BRD2,3 and 4 expression in melanoma cell lines under basal conditions. BRD4L and BRD4S are indicated by red arrows. MITF expression = high (black star), low (grey star), PTEN expression = present (black diamond), absent (grey diamond), p53 expressed = at least one copy of WT p53 (black square), only mutant p53 (grey square). (**B**) Melanoma cell viability data from NCI-60 after treatment with (+)-JQ1 for 48 h [219] (left) and EC_{50} values calculated after treatment for 72 h with (+)-JQ1 in*

*melanoma cell lines, which are shown ordered by sensitivity [94] (right). Highlighted cell lines in the right panel are included in Table 3.1. Stars in right panel denote cell line MITF expression level: $MITF^{high}$ (black), $MITF^{low}$ (grey). (**C**) BET BRD inhibition leads to a reduction in cellular proliferation in 501mel and IGR39 cells. Cells were treated with concentrations of (+)-JQ1 up to 1 μM for 1 week, at which point cells were stained with crystal violet. Plates were scanned and cell proliferation at each concentration was calculated, normalised to (-)-JQ1, the negative control. EC_{50}= 115.8 nM ±7.5 nM (501mel, left), EC_{50}= 176.8 nM ±19.6 nM (IGR39, right). Error bars represent standard deviation. N = 3 biological replicates.*

Given the heterogeneity of EC_{50} values and methodologies by which they were obtained between previously published studies (Figure 3.1B), screening a panel of genetically diverse melanoma cell lines (Figure 3.1A, Table 3.1) enabled the ranking of cell lines by loss of proliferation in response to BET BRD inhibition and enabled selection of cell lines with which more extensive work into this loss of proliferation could be carried out. Briefly, cells were treated with concentrations of (-)-JQ1 and (+)-JQ1 up to 1 μM for 1 week, at which point cells were stained with crystal violet. (-)-JQ1 was used in this experiment as the negative control as it is the negative stereoisomer of (+)-JQ1 and as such does not bind to the BRD binding pocket. The resulting values were used to generate a growth curve and EC_{50} value for each cell line. Figure 3.1C shows examples of these growth curves, and EC_{50} values are displayed in Table 3.1.

As well as EC_{50} values, elucidation of mutation status of key melanoma genes were necessary for the investigation into the phenotype resulting from BET BRD inhibition. The data in Table 3.1 agree with a published study showing there is no correlation between NRAS mutation status and melanoma cell line sensitivity [151]. While it appears as though cells with low MITF expression may be less sensitive to (+)-JQ1 (Table 3.1), only five cell lines were used in this study. Thus, more work using a wider panel of cell lines, should be

used to confirm this observation. Additionally, Figure 3.1B shows that published data suggest MITF is not a determinant for sensitivity [217]. Therefore, another determinant of phenotype following BET BRD inhibition is sought after.

p53 is a transcription factor and well known tumour suppressor and is involved in many cellular processes including cell cycling, autophagy, senescence induction and apoptosis, integrating signals from many stimuli and mechanisms [254-258]. Approximately half of cancers harbour a p53 mutation and ~95% of these mutations appear within its sequence-specific DNA binding domain [255, 259]. As mentioned previously, p53 function influences the phenotype adopted by leukaemia cells following BET BRD inhibition, with increased p53 activity leading to greater apoptotic caspase activation and cell death [253]. p53 is deemed a significantly mutated gene in melanoma, and is mutated in approximately 20% of patients [249, 260]. Harbouring a p53 mutation in the DNA binding domain can sometimes confer benefit to overall survival a from stage IV melanoma diagnosis, indicating p53 mutations could have clinically relevant effects on cellular biology in this malignancy [260, 261]. One possible explanation as to why melanoma cell lines exhibit heterogeneous responses to (+)-JQ1 treatments may be differences in p53 functionality. It is possible that cell lines harbour mutations in the p53 gene, which may result in its inactivation or limited function. Thus, p53 transcripts were sequenced and the mutation status of p53 was added to Table 3.1, and were confirmed by literature where previously known. Following this, 501mel and A375M were selected as the most appropriate cell lines to continue investigations into impact of p53 mutation on cellular response to (+)-JQ1. While 501mel is MITF-high and A375M is MITF-low in terms of protein expression and differ in p53 mutation status, this was the minimum number of variables between two cell lines with differing p53 mutation statuses with different sensitivities to (+)-JQ1 from this panel. Both express mutant BRAF and WT NRAS, and 501mel expresses mutant p53

while A375M is WT, whilst displaying different levels of sensitivity to BET BRD inhibition (Table 3.1).

Cell line	MITF expression	BRAF mutation status	NRAS mutation status	PTEN expression	p53 mutation status	Estimated EC_{50} (nM)
IGR37	High [262-264]	V600E [263, 264]	WT [265, 266]	Expressed [265]	Heterozygous WT with stop at 238 [267]	50.8 ±3.2
SK-mel-28	High [262, 264]	V600E [151, 268]	WT [151]	Expressed, T167A [262]	P72R, R273H [269], L145R [262, 268]	110.1 ±14.4
501mel	High [264]	V600E [270]	WT [151]	Expressed, WT [271]	C275W (Figure 3.2A)	115.8 ±7.5
IGR39	Low [263, 264]	V600E [263, 264, 272]	WT [272]	Homozygous deletion [273]	Heterozygous WT with stop at 238 [267]	176.8 ±19.6
A375M	Low [264]	V600E [274]	WT [275, 276]	Expressed [277]	WT [267] (Figure 3.2A)	303.4 ±23.4

Table 3.1: Key melanoma gene expression and mutation status and estimated summary of EC_{50} values for melanoma cell lines after treating with (+)-JQ1 for 1 week. Cells were treated with 0, 10, 25, 50, 75, 100, 200, 300, 400, 500, 750, 1000 nM (-)-JQ1 or (+)-JQ1 for 1 week, in media supplemented with 10% FBS. (-)-JQ1 was used as the negative control. Following treatment cells were stained with crystal violet to assess cell viability. Mean EC_{50} values shown, ± standard deviation. N = 3 biological replicates.

3.2.2 p53 mutation correlates with loss of p21 up-regulation in melanoma cells

Table 3.1 shows the mutation status of p53 in melanoma cell lines. DNA was extracted from 501mel cells and subject to Sanger Sequencing to confirm the C275W mutation carried by 501mel (Figure 3.2A). C275 lies within the DNA-binding domain of p53; therefore, mutations at this locus may alter the binding of p53 to genomic loci [255]. C275 interacts with the residue R273 [278]. R273 is vital in mediating contact between p53 and DNA, and is a hotspot mutation site [279]; thus, disruption of the C275-R273 interactions may result in erroneous DNA contact. Moreover, the mutation of a nearby cysteine residue,

C277, to phenylalanine, may prevent sequence-specific DNA-binding owing to the introduction of a large hydrophobic group [280]. Tryptophan also has a large, hydrophobic side chain; therefore, it is possible this C275W mutation affects the DNA binding functionality of p53, potentially through disruption of sequence-specific DNA-binding. This mutation has been observed in melanoma patients [249], so it is possible it may contribute to driving malignancy. To examine the effects of the C275W mutation, the mutation was modelled *in silico*. Figure 3.2B shows the crystal structures of WT p53 and the C275W mutant p53. The cysteine residue appears to lie in close proximity with other residues, interacting with residues close in physical space to form the secondary or tertiary structure (Figures 3.2B-3.2C), which could plausibly be disrupted by the C275W mutation.

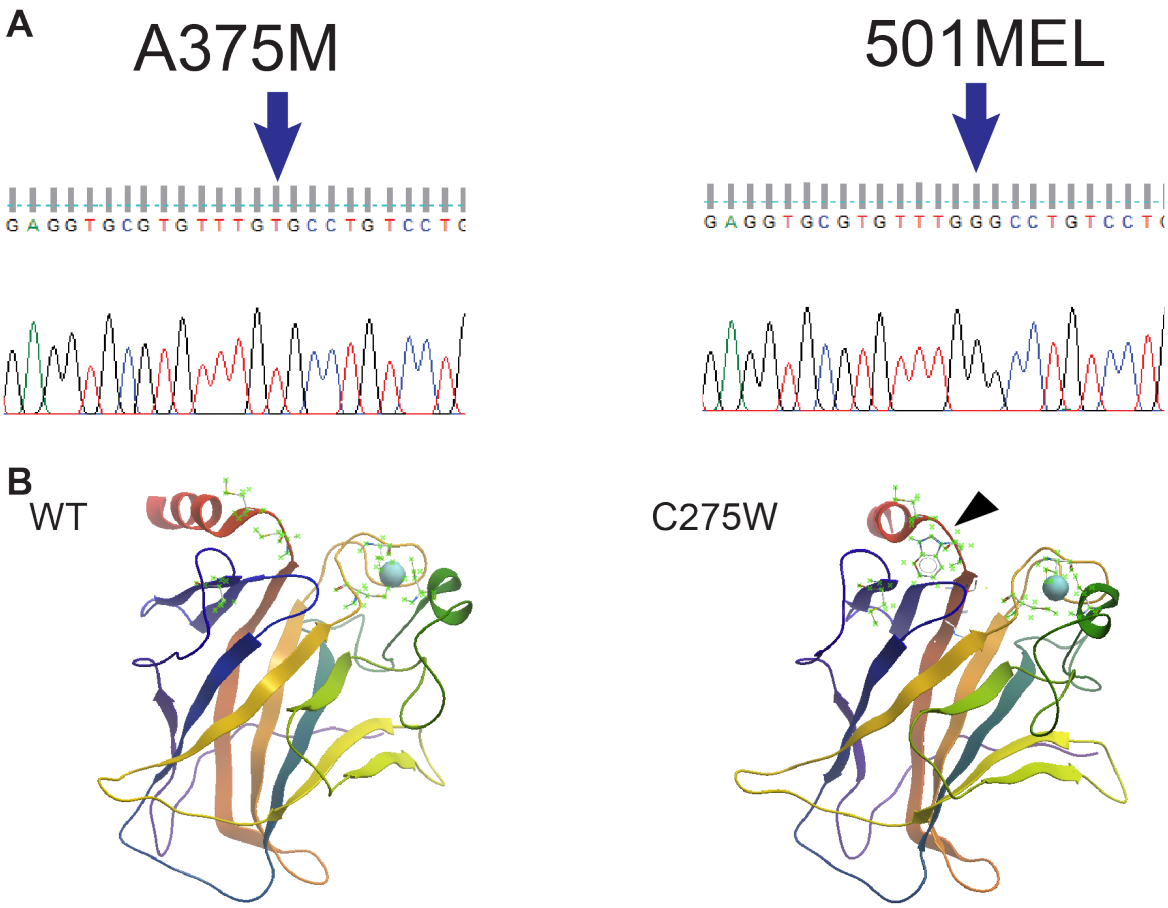

A
A375M
501MEL
B
WT
C275W
C
C277
C275
D291
R273
D
501mel
- + JQ1
25
GAPDH
E
A375M
- + JQ1
25
p21
GAPDH
F
p21 expression normalised to GAPDH
2.5
2.0
1.5
1.0
0.5
0.0
*
(-)JQ1
(+)-JQ1

***Figure 3.2**: p53 mutation status correlates with p21 up-regulation following BET BRD inhibition in melanoma cell lines. (**A**) Sequencing results showing p53 genotype of A375M and 501mel cells. A375M cells express WT p53 and 501MEL expresses mutant p53. Arrows show site of mutation in 501mel and WT base in A375M. (**B**) In silico p53 crystal structures (PDB ID = 4MZI, [281]). Cysteine residues are visible. C275W mutation leads to a tryptophan in place of a cysteine residue within the DNA binding domain. Tryptophan residue indicated by black arrow. (**C**) Residues forming secondary structure with C275 labelled in p53. Image created using Mol*, (PDB ID = 4MZI, [281]), RCSB PDB. (**D**) Immunoblot showing p21 expression in 501mel cells following 48 h of treatment with 1 μM (-)-JQ1 (negative control) and (+)-JQ1. The two visible bands are non-specific (Figure 7.1). (**E**) Immunoblot showing p21 expression in A375M following 48 h of treatment with 1 μM (-)-JQ1 (negative control) and (+)-JQ1. (**F**) Quantification of p21 expression normalised to GAPDH expression in A375M cells following 48 h of treatment with 1 μM (-)-JQ1 (negative control) and (+)-JQ1. Mean protein expression shown ± standard deviation. Statistical significance was determined using a two-tailed Students t-test. * = p <0.05*

To determine whether the C275W mutation affects p53 function *in vitro*, A375M and 501mel cells were treated with (+)-JQ1 and the expression of p21, a known regulator of the cell cycle and downstream target of p53 [254, 282, 283], was observed. GAPDH is used as a loading control as it has been used in solid malignancy models, including melanoma, owing to its constant expression level despite BET inhibition [147, 152]. While p21 expression does not increase following (+)-JQ1 treatment in 501mel (Figure 3.2D), Figures 3.2E and 3.2F show that p21 expression significantly increases in response to (+)-JQ1 treatment in A375M in comparison to (-)-JQ1. In the case of 501mel, there is no p21 band, which is clear when A375M and 501mel samples are side by side on the same gel during immunoblotting (Figure 7.1). (-)-JQ1, the negative stereoisomer of (+)-JQ1 is used

in these experiments as a negative control. This shows that 501mel cells do not up-regulate p21 expression following BET BRD inhibition.

To further investigate the cellular response to (+)-JQ1, an RNA-seq experiment was carried out. Prior to subjecting samples to RNA-seq, dose and duration of treatment were varied within the scope of previously published studies [95, 151, 152, 284] to identify optimal conditions for sample treatment. No RNA-seq data is currently available for A375M cells following BET BRD inhibition; therefore, suitability of treatment conditions was judged based upon 501mel expression data. Previously published data show that expression of *MYC* significantly decreases, and *ADM1* expression significantly increases following BET BRD inhibition in 501mel cells [152]; therefore, the expression changes of these genes were used to determine appropriate treatment conditions prior to RNA-seq. In these qPCR experiments, 18S rRNA was used for normalisation when quantifying gene transcripts, a widely used internal control [285]. The data shown in Figure 3.3A show that in 501mel cells following 24 h treatment with 500 nM (+)-JQ1, *MYC* significantly decreases in expression and *ADM1* significantly increases in expression, which emulates previously published data [152]. Therefore, 501mel and A375M cells were subject to 24 h treatment with 500 nM (+)-JQ1 before RNA was extracted and subject to RNA-seq. (-)-JQ1 was used as a negative control in the RNA-seq experiment.

Computational RNA-seq analysis was carried out. Briefly, first transcript reads were mapped to a reference assembly genome. The mapped reads were used to generate a table of normalised fragments per kilobase per million mapped reads (FPKM) counts for each gene. The normalised counts were then used to carry out differential gene expression analysis to generate a table of log2fold changes (LFCs) and p values for each gene using DESeq2 [243]. The LFCs and adjusted p values were subsequently used in Gene Set Enrichment Analysis (GSEA).

The computational analysis package, DESeq2, works on the assumption that the majority of genes do not change following cellular treatments [243]. Therefore, this analysis method has the limitation of not being able to accurately detect global gene down- or -upregulation. To address this issue, a spike-in method, wherein known quantities of RNA from a different organism are added to the sample prior to sequencing, will enable absolute quantification of transcripts and detection of changes in global gene expression [286]. To follow up RNA-seq findings and validate individual genes are affected by a given treatment, qPCR can be used to detect changes in mRNA expression. In the case of protein-coding genes, a western blot can be used to validate that the protein level is also affected by a given treatment.

The p21 protein is encoded by the gene, CDKN1A [287]. FPKM values were analysed for *CDKN1A* mRNA in 501mel and A375M cells examining the normalised counts of *CDKN1A* transcripts in each replicate, (see Chapter 7.3.1). Figure 3.3B shows that (+)-JQ1 treatment induces an increase in *CDKN1*A mRNA expression in A375M cells but not in 501mel cells. Since p21 is the protein product of the *CDKN1A* mRNA transcript, this is reminiscent of the immunoblot findings in Figures 3.2C and 3.2D, and indicates that 501mel cells fail to up-regulate both the mRNA and protein of p21 following BET BRD inhibition. This suggests that the p53 mutation confers some loss of function with regards to its role as a transcription factor, and may play a role in the cellular response to BET BRD inhibition.

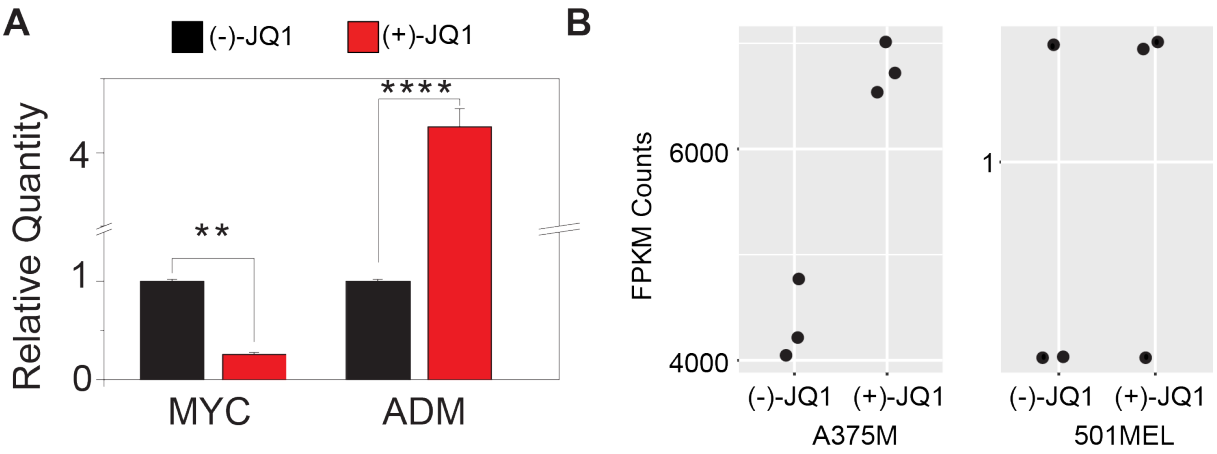


***Figure 3.3**: (+)-JQ1 treatment in 501mel induces changes in gene expression reminiscent of published data and CDKN1A expression does not vary in 501mel cells following (+)-JQ1 treatment. (**A**) qPCR results from 501mel cells that have been subject to RNA-seq following 24 h treatment with 500nM (-)-JQ1 or (+)-JQ1. Black (-)-JQ1, red (+)-JQ1. N = 3 biological replicates. Mean expression shown ± standard deviation. Statistical significance was determined using a two-tailed Students t-test.* = p <0.05, ** = p <0.01, *** = p < 0.001, **** = p < 0.0001. (**B**) Normalised fragments per kilobase per million mapped reads (FPKM) of CDKN1A following RNA-seq in A375M and 501mel cells. Counts in each biological replicate of each cell line is represented by a black dot. Cells were treated with 500 nM (+)-JQ1 for 24 h before RNA was extracted and subject to sequencing. (-)-JQ1 was used as a negative control. N = 3 biological replicates per condition, per cell line.*

In addition, 501mel and A375M cells were treated with siRNA targeting an individual BET, or with pooled siRNA targeting BRD -2, -3, and -4 concomitantly (siBETs) for 48 h, prior to RNA-seq. While BET protein family members exhibit functional redundancy, the embryonic lethal single Brd2 or Brd4 murine knockouts indicate that BETs have partially unique functions [42, 46-48]. Thus, the roles of individual BET family members in melanoma were dissected.

Immunoblotting was carried out to determine optimal conditions for siRNA transfection that would yield the greatest loss of target protein expression. Transfection of 501mel (Figure 3.4A) and A375M (Figure 3.4B) with 40 pmol siRNA induced the most effective loss of target protein expression, except for loss of BRD2 expression following transfection with siBETs. SDHA was used as a loading control because its expression remains largely unaffected following BET BRD inhibition in melanoma [152]. Negative controls used were scrambled negative control siRNA (siNC), and samples that did not undergo any treatment (NT). To confirm that these transfection conditions were suitable, the expression levels of *BRD2*, *BRD3*, and *BRD4* were examined following transfection. *MITF*, *ZMYND8* and *MYC* expression was also observed to determine whether previous data could be recapitulated; MITF was included as a key melanoma gene that remained constant despite BET perturbation via RNA-interference in MITF-high cells [288], ZMYND8 was shown by our lab to lie downstream of BRD2 in 501mel (data not shown), and MYC has been shown to decrease in expression following BRD4 perturbation in AML and neuroblastoma [94, 98]. Figure 3.4C shows that BET family member expression levels were reduced following knockdown in both cell lines. In 501mel cells, the MITF-high cell line, *MITF* remained constant despite BET knockdowns, *ZMYND8* decreased in expression following BRD2 or siBETs knockdown, and *MYC* expression decreased following BRD4 or siBETs knockdown. Although knockdown of BRD3 affected BRD2 expression in A375M cells, the data from 501mel cells recapitulated published findings and previous work within our group, and all changes in gene expression mimic those induced by BET BRD inhibition [152]. Thus, 501mel and A375M cells were transfected with 40 pmol siRNA, and 48 h post transfection cells were harvested prior to RNA extraction and samples were subject to RNA-seq. The results of the RNA-seq experiments will be discussed throughout this chapter.

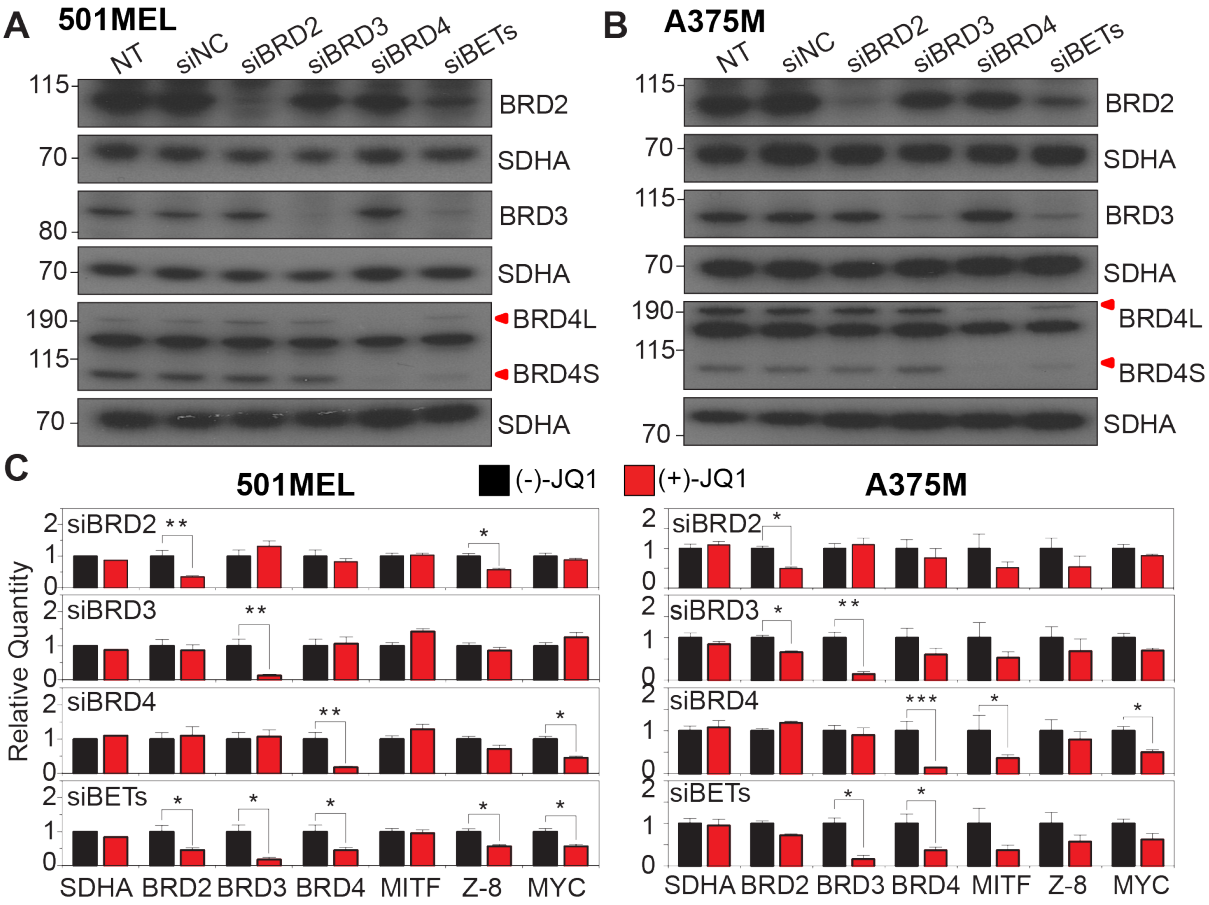


***Figure 3.4**: BET protein knockdown in 501mel and A375M cells. (**A**) Immunoblot showing down-regulated of BETs following 40 pmol siRNA transfection for 48 h in 501mel cells. Scrambled negative control (siNC) was used as a negative control, as well as cells that had not undergone any treatment (NT). N = 3 biological replicates. (**B**) Immunoblot showing down-regulated of BETs following 40 pmol siRNA transfection for 48 h in A375M cells. Scrambled negative control (siNC) was used as a negative control, as well as cells that had not undergone any treatment (NT). N = 3 biological replicates. (**C**) BET knockdowns and effects on MITF, ZMYND8 and MYC in 501mel samples (left) and A375M samples (right) subject to RNA-seq. Black bars represent expression in cells transfected with non-targeted RNA, the negative control (siNC). Red bars are expression levels in sample treated with indicated siRNA. ZMYND8 has been abbreviated to Z-8. N = 3 biological replicates. Mean expression shown ± standard deviation. Statistical significance*

was determined using a two-tailed Students t-test. = p <0.05, ** = p <0.01, *** = p < 0.001, **** = p < 0.0001.*

3.2.3 BET BRD inhibition causes a p53-dependent G1 cell cycle arrest

Inhibition of BET BRDs by (+)-JQ1 leads to changes in transcription programs relating to cell cycle arrest in melanoma [95, 151]. The cell cycle comprises four phases, G1, S, G2, and mitosis (M) and its progression is driven by cyclin dependent kinases (CDKs) [289]. The function of these kinases is largely governed by cyclins, the expression of which is heavily regulated [289]. Cell cycle progression is inhibited by cyclin-dependent kinase (CDK) inhibitors such as p21 (CDKN1A), p15 (CDKN2B), p16 (CDKN2A) and p27(CDKN1B) [290], many of which are downstream targets of tumour suppressors, such as p53. Inhibitors of cell cycle stop cells entering cell cycle in the first instance, or progressing through checkpoints such as G1-S and G2-M checkpoints, which are both regulated by p21 [254].

An RNA-seq experiment was carried out, as detailed in Chapter 3.2.2. Figure 3.5 shows that in each cell line, the effects of (+)-JQ1 on global gene expression were similar: in A375M cells 647 genes were down-regulated and 185 genes were up-regulated, and in 501mel cells 592 genes were down-regulated and 213 genes were up-regulated.

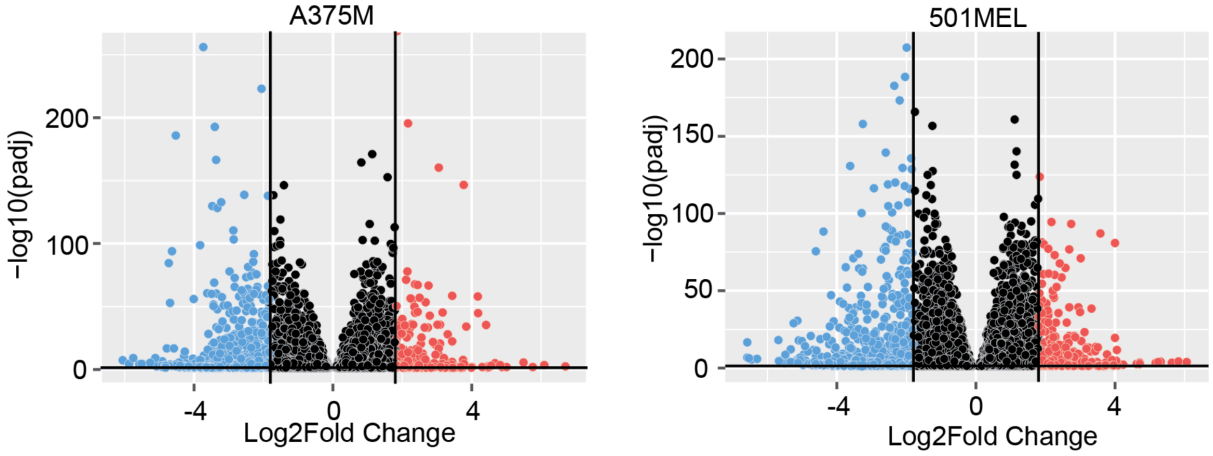


***Figure 3.5**: (+)-JQ1 induces global changes in gene expression in A375M and 501mel cells. Changes in gene expression induced by 500 nM 24 h treatment with (+)-JQ1 compared with (-)-JQ1 (negative control) represented in volcano plots A375M (left) 501mel (right). Blue dots represent genes with a LFC ≤ -1.8 and an adjusted p value of ≤ 0.05, pink dots represent genes with a LFC ≥ 1.8 and an adjusted p value of ≤ 0.05. Blue and pink genes are deemed down- and up-regulated, respectively, as previously specified [152]. Vertical black lines indicate 1.8 LFCs. Horizontal black line indicates an adjusted p value ≤ 0.05.*

To ascertain which BET protein mediates the transcriptional effects of (+)-JQ1 in each cell line, the LFCs of changes in gene expression following (+)-JQ1 treatment (compared with (-)-JQ1 treatment) were correlated with LFCs in gene expression induced following genetic BET protein inhibition (compared with cells transfected with negative control siRNA (siNC)) in scatter plots. Genes with significant (adjusted p value ≤ 0.05) LFCs following both treatments were highlighted in red. Genes with significant (adjusted p value ≤ 0.05) LFCs following the treatment shown on the x or y axis were highlighted in orange or blue, respectively. Genes with non-significant (adjusted p value > 0.05) LFCs following both treatments were represented by a grey dot. The correlation between genes that are significantly differentially regulated by both treatments is shown by the linear regression line and is indicated by the R^2 values shown.

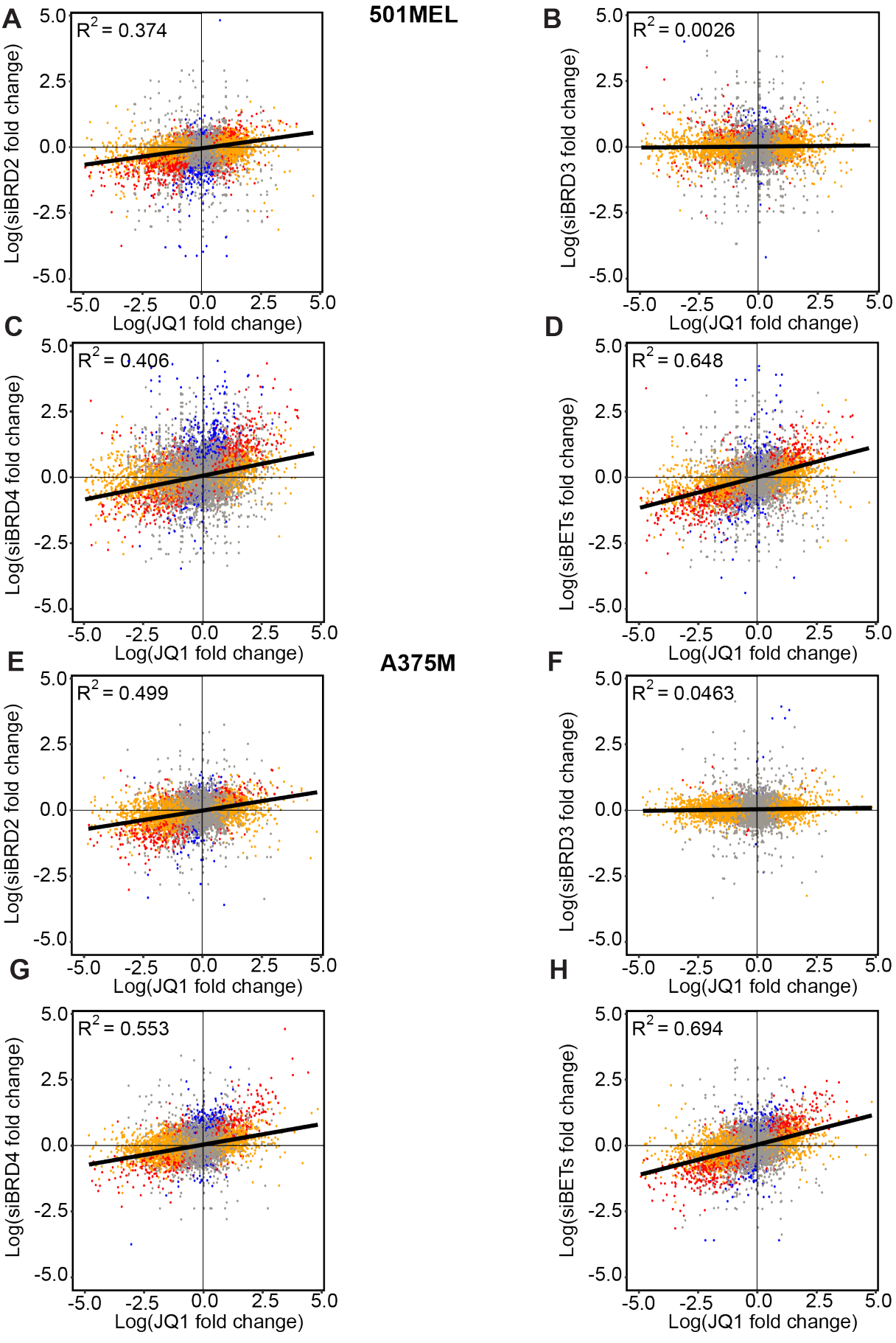

501MEL
A
R^2 = 0.374
Log(siBRD2 fold change)
B
R^2 = 0.0026
Log(siBRD3 fold change)
C
R^2 = 0.406
Log(siBRD4 fold change)
D
R^2 = 0.648
Log(siBETs fold change)
Log(JQ1 fold change)
A375M
E
R^2 = 0.499
Log(siBRD2 fold change)
F
R^2 = 0.0463
Log(siBRD3 fold change)
G
R^2 = 0.553
Log(siBRD4 fold change)
H
R^2 = 0.694
Log(siBETs fold change)
Log(JQ1 fold change)
5.0
2.5
0.0
-2.5
-5.0

***Figure 3.6**: (+)-JQ1 induces BET-dependent changes in gene expression. Scatter plots depicting the correlation between LFCs in expression induced by (+)-JQ1 (compared with (-)-JQ1) compared with LFCs in expression induced by siBRD2 (compared with siNC) (**A**), siBRD3 (compared with siNC) (**B**) or siBRD4 (compared with siNC) (**C**), siBETs (compared with siNC) (**D**) in 501mel cells. Scatter plots depicting the correlation between LFCs in expression induced by (+)-JQ1 (compared with (-)-JQ1) compared with LFCs in expression induced by siBRD2 (compared with siNC) (**E**), siBRD3 (compared with siNC) (**F**) or siBRD4 (compared with siNC) (**G**), siBETs (compared with siNC) (**H**) in A375M cells. Genes are depicted as dots. The colour of the dot signifies the significance of the LFC: if LFC adjusted p value ≤ 0.05 for both treatments, the dot is red, if LFC adjusted p value ≤ 0.05 for treatment on the x axis, the dot is orange, if LFC adjusted p value ≤ 0.05 for treatment on the y axis, the dot is blue, if LFC adjusted p value > 0.05 for both treatments, the dot is grey. Linear regression line shows the correlation between genes that are significantly differentially regulated by both treatments. R^2 values shown.*

The correlations in 501mel cells between LFCs in gene expression when cells are treated with (+)-JQ1 compared with siRNA-mediated BRD2 knockdown (siBRD2), siRNA-mediated BRD3 knockdown (siBRD3) and siRNA-mediated BRD4 knockdown (siBRD4) and pan-BET knockdown (siBETs) are shown in Figures 3.6A, 3.6B, 3.6C and 3.6D respectively. There are similar extents of correlation between the genes affected by (+)-JQ1 and siBRD2, and (+)-JQ1 and siBRD4 as indicated by the R^2 values (Figures 3.6A and 3.6C). Significant changes in gene expression following siRNA-mediated knockdown of BRD3 show the least correlation with significant changes in gene expression following (+)-JQ1 treatment, as indicated by the R^2 value (Figure 3.6B), which, together with Figures 3.6A and 3.6C suggest that inhibition of BRD2 and BRD4 likely account for the effects of (+)-JQ1 on transcription. Intriguingly, in 501mel cells BRD2 knockdown significantly down-regulated some genes that (+)-JQ1 did not significantly affect (Figure 3.6A), and BRD4

knockdown up-regulated some genes that (+)-JQ1 did not significantly affect (Figure 3.C), suggesting BETs have non-redundant roles.

The correlations in A375M cells between LFCs in gene expression when cells are treated with (+)-JQ1 compared with siRNA-mediated BRD2 knockdown (siBRD2), siRNA-mediated BRD3 knockdown (siBRD3) and siRNA-mediated BRD4 knockdown (siBRD4) and pan-BET knockdown (siBETs) are shown in Figures 3.6E, 3.6F, 3.6G and 3.6H respectively. Seemingly, the lack of correlation between those genes significantly affected by BRD3 knockdown and genes significantly affected by (+)-JQ1 is conserved across both 501mel and A375M melanoma cell lines (Figures 3.6B and 3.6F). Moreover, similar levels of correlation between the genes affected by (+)-JQ1 and siBRD2, and (+)-JQ1 and siBRD4, as indicated by the R^2 values (Figures 3.6E and 3.6G), are also observed in A375M cells. Unsurprisingly, significant changes in gene expression following pan-BET siRNA-mediated knockdown (siBETs) showed the greatest correlation with genes that were significantly differentially expressed following (+)-JQ1 treatment in both cell lines (Figures 3.6D and 3.6H), indicating that (+)-JQ1 acts via BETs. Overall the data presented in Figure 3.6 show that in both 501mel and A375M cell lines, the inhibitory effects of (+)-JQ1 are likely mediated by BRD2 and BRD4 attenuation, and BETs potentially have non-overlapping roles in melanoma.

The RNA-seq data was examined to discern if transcriptional events underpin cell cycle arrest. Figure 3.7A demonstrates that there is a down-regulation of E2F targets and MYC targets by (+)-JQ1 treatment in A375M cells compared with (-)-JQ1 treatment. In the G1 phase of the cell cycle, the phosphorylation of retinoblastoma (Rb) protein enables the release of E2F, which then initiates the transcription of S phase genes in readiness for DNA synthesis and the G1-S phase transition [291]. MYC promotes cell cycle progression through simultaneous stimulation of E2F, cyclin D and cyclin E expression and inhibiting the transcription of cell cycle inhibitors such as p15, p21 and p27 [292]. In a diverse range

of malignancies [26, 76, 78, 88, 94, 114, 138], including melanoma [151], down-regulation of MYC coincided with loss of cellular growth. Therefore, the down-regulation of E2F and MYC target genes, as seen in Figure 3.7A, and p21 up-regulation (Figures 3.2E-3.2F) are indications of a cell cycle arrest. To reinforce this finding, the RNA-seq data collected following siRNA-mediated knockdown of all BETs was analysed. Following simultaneous siRNA-mediated knockdown of BRD -2, -3, and -4, E2F, MYC targets and G2M checkpoint genes were down-regulated in A375M cells (Figure 3.7B). This suggests that attenuation of BET function in A375M cells leads to changes in transcriptional programs that promote the progression of cell cycling, and thus, agrees with the data presented in Figure 3.7A. To unpick further the intricacies of BET protein family function, the RNA-seq data collected following siRNA-mediated knockdown of individual BETs was analysed. Following BRD4 knockdown, MYC target genes are also down-regulated (Figure 3.7C), suggesting BRD4 is involved in orchestrating the transcriptional events that lead to cell cycle arrest.

To test whether a cell cycle arrest took place in this cell line following (+)-JQ1 treatment, cells were stained with PI and analysed via flow cytometry. (-)-JQ1, the negative stereoisomer to (+)-JQ1, was used as a negative control. Figure 3.7D shows that there is an increase in the population of cells in G1 phase of cell cycle following (+)-JQ1 treatment. The quantification from 3 biological replicates of this experiment is shown in Figure 3.7E; there is a significant accumulation of cells G1 cell cycle; however, the lack of significant decrease in the S phase cell population suggests that a cell cycle arrest is not achieved.

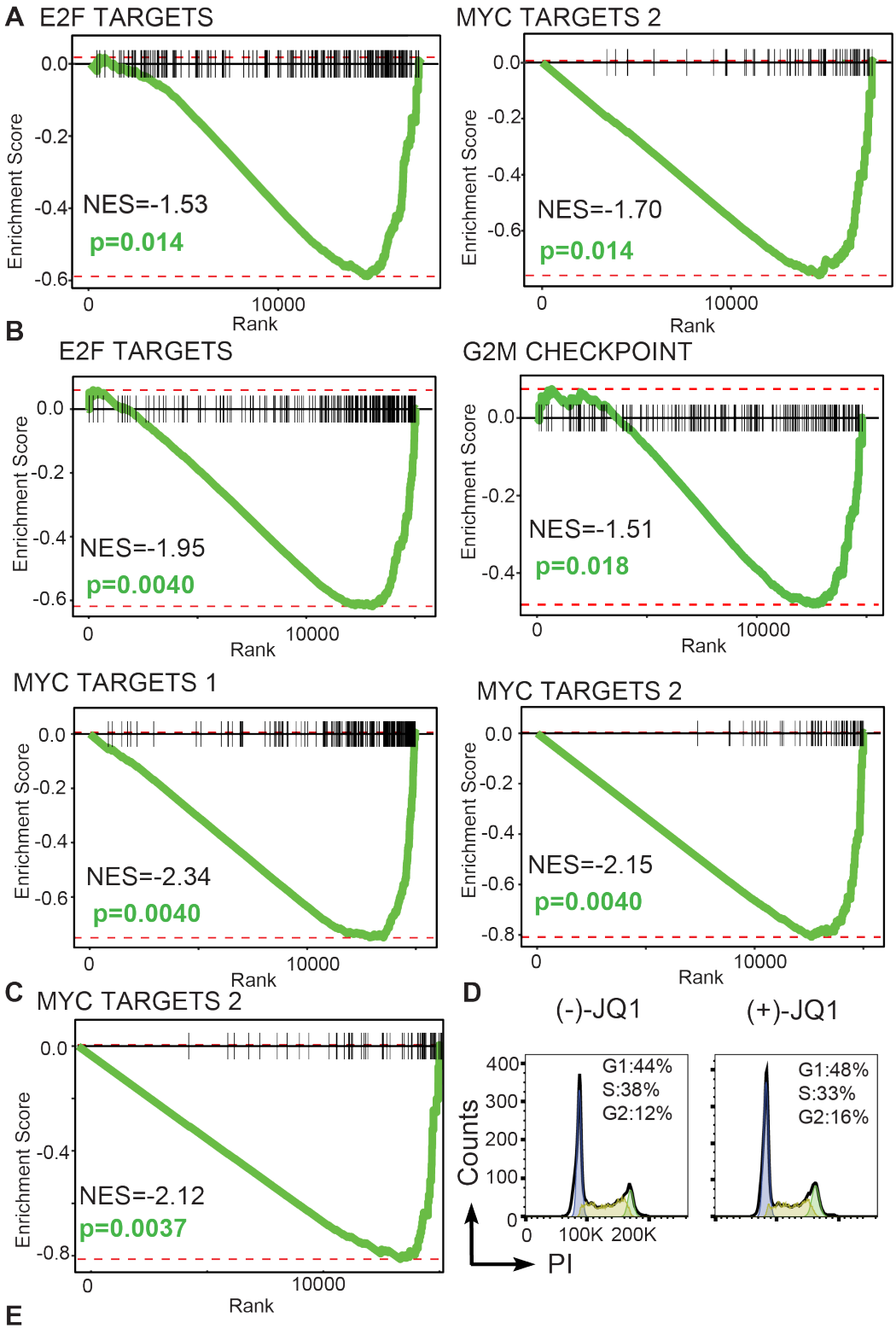

A
E2F TARGETS
Enrichment Score
NES=-1.53
p=0.014
Rank
MYC TARGETS 2
NES=-1.70
p=0.014
B
E2F TARGETS
NES=-1.95
p=0.0040
G2M CHECKPOINT
NES=-1.51
p=0.018
MYC TARGETS 1
NES=-2.34
p=0.0040
MYC TARGETS 2
NES=-2.15
p=0.0040
C
MYC TARGETS 2
NES=-2.12
p=0.0037
D
(-)-JQ1
(+)-JQ1
G1:44%
S:38%
G2:12%
G1:48%
S:33%
G2:16%
Counts
PI
E
JQ1-(-)
JQ1-(+)
Cell population (%)
G1
S
G2
Cell cycle phase
ns

***Figure 3.7**: (+)-JQ1 causes an accumulation of A375M cells in G1 phase of the cell cycle and this could be underpinned by changes in cell cycle-related gene expression. (**A**) GSEA showing down-regulation of cell cycle related gene sets ("HALLMARK_E2F_TARGETS", left, "HALLMARK_MYC_TARGETS_V2", right) following 500 nM (+)-JQ1 compared with (-)-JQ1 treatment for 24 h in A375M cells. (**B**) GSEA showing down-regulation of cell cycle related gene sets ("HALLMARK_E2F_TARGETS", upper left, "HALLMARK_G2M_CHECKPOINT", upper right, "HALLMARK_MYC_TARGETS_V1", lower left,"HALLMARK_MYC_TARGETS_V2", lower right) compared with negative control siRNA, following siRNA-mediated knockdown of BRD2, BRD3 and BRD4 (through "siBETs") for 48 h in A375M cells. (**C**) GSEA showing down-regulation of MYC targets hallmark gene set ("HALLMARK_MYC_TARGETS_V2") compared with negative control siRNA, following siRNA-mediated knockdown of BRD4 for 48 h in A375M cells. In (**A-C**), computational analysis was carried out using DESeq2 [243] to identify differentially expressed genes, which were used for GSEA analysis in R [244]. NES = normalised enrichment score. P value represents adjusted p value. (**D**) Flow cytometry PI staining profile showing cell cycling in A375M cells following treatment for 24 h with 500 nM (-)-JQ1 or (+)-JQ1. The purple peak represents cells in G1 phase, yellow represents those in S phase and green represents those in G2/M phase. (**E**) Percentage of cell population in each stage of cell cycle in A375M after 24 h of treatment with 500 nM (-)-JQ1 or (+)-JQ1. Mean cell population shown ± standard deviation. Statistical significance was determined using a two-tailed Students t-test.*

The same experiments were carried out in 501mel cells to determine if the p53 mutation would correlate with a cell cycle arrest following BET BRD inhibition. GSEA revealed that G2M checkpoint genes and E2F and MYC target gene sets are down-regulated by (+)-JQ1 treatment compared with (-)-JQ1 treatment (Figure 3.8A). These findings were recapitulated when all BETs were knocked down via siRNA (Figure 3.8B). However, upon knockdown of individual BETs, compared with the negative control siRNA, knockdown of BRD2 led to the up-regulation of MYC target genes in 501mel (Figure 3.8C (left)), which is contrary to the actions of BRD4 knockdown (Figure 3.8C right). Since pan-BET inhibition leads to down-regulation of this gene set, whether through pharmacological (Figure 3.8A) or genetic inhibition (Figure 3.8B), this suggests that the cell cycle arrest phenotype following (+)-JQ1 treatment is dominated by BRD4 in this cell line. This suggests that BRD2 has unexplored functions, especially as in 501mel cells, BRD2 appears to regulate tumour suppressor HEXIM1 expression (Figure 7.2) [293]. To confirm whether a G1 arrest takes place in 501mel cells, cells were treated with 500 nM (+)-JQ1, or (-)-JQ1 as a negative control, for 24 h. This led to a cell cycle arrest via accumulation of cells in G1 arrest and concomitant decrease in cells in S phase (Figure 3.8D), and the findings from 3 biological replicates are quantified in Figure 3.8E. This is perhaps surprising owing to its p53 mutation status and the lack of p21 up-regulation following BET BRD inhibition (Figures 3.2D-3.3B).

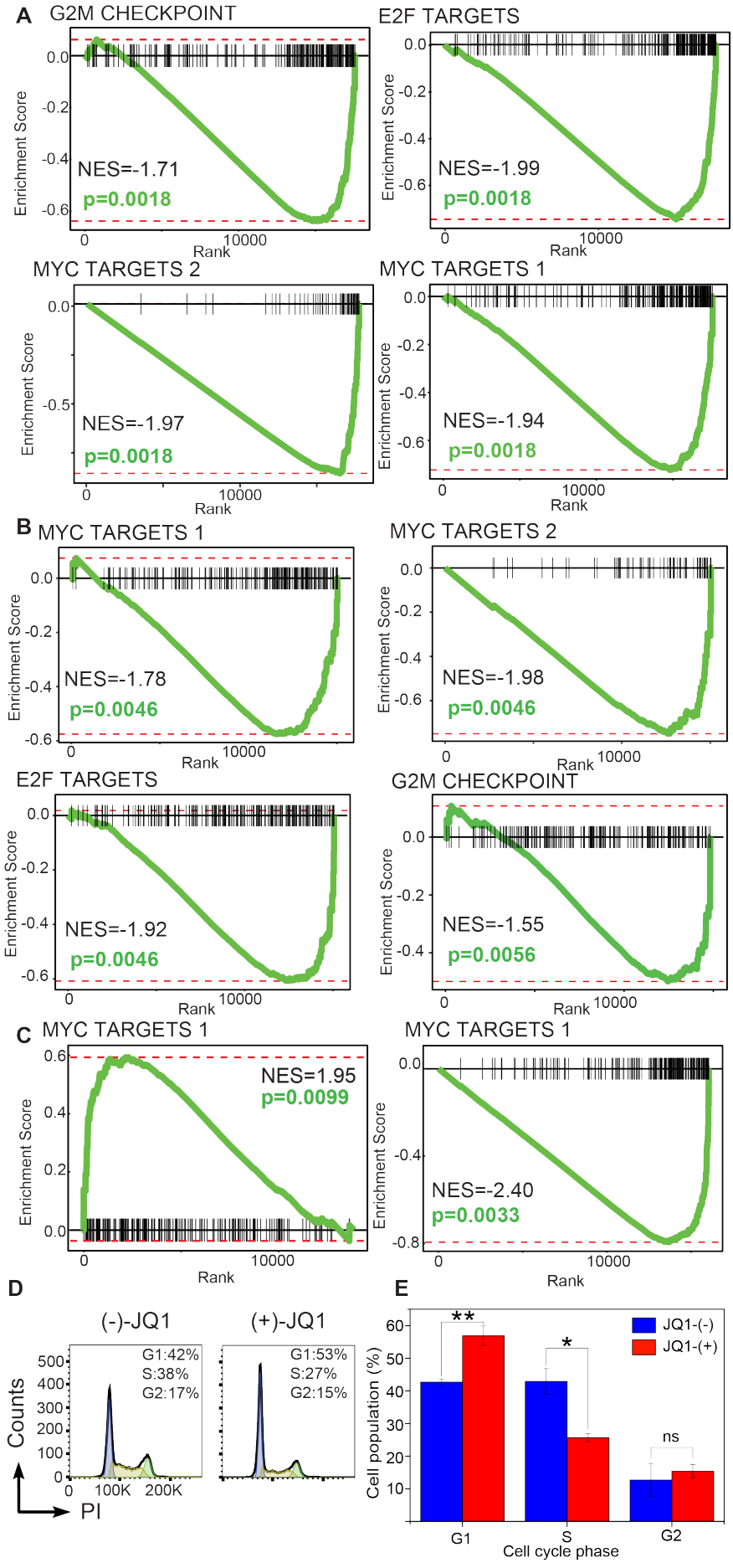

A
G2M CHECKPOINT
NES=-1.71
p=0.0018
E2F TARGETS
NES=-1.99
p=0.0018
MYC TARGETS 2
NES=-1.97
p=0.0018
MYC TARGETS 1
NES=-1.94
p=0.0018
B
MYC TARGETS 1
NES=-1.78
p=0.0046
MYC TARGETS 2
NES=-1.98
p=0.0046
E2F TARGETS
NES=-1.92
p=0.0046
G2M CHECKPOINT
NES=-1.55
p=0.0056
C
MYC TARGETS 1
NES=1.95
p=0.0099
MYC TARGETS 1
NES=-2.40
p=0.0033
Enrichment Score
Rank
D
(-)-JQ1
(+)-JQ1
G1:42%
S:38%
G2:17%
G1:53%
S:27%
G2:15%
Counts
PI
E
JQ1-(-)
JQ1-(+)
Cell population (%)
G1
S
G2
Cell cycle phase
ns

***Figure 3.8**: BET BRD inhibition causes G1 cell cycle arrest in 501mel cells. (**A**) GSEA showing down-regulation of cell cycle related gene sets ("HALLMARK_G2M_CHECKPOINT", upper left, "HALLMARK_E2F_TARGETS", upper right, "HALLMARK_MYC_TARGETS_V2", lower left,"HALLMARK_MYC_TARGETS_V1", lower right) following 500 nM (+)-JQ1 compared with (-)-JQ1 treatment for 24 h in 501mel cells. (**B**) GSEA showing down-regulation of cell cycle related gene sets ("HALLMARK_MYC_TARGETS_V1" , upper left, "HALLMARK_MYC_TARGETS_V2", upper right, "HALLMARK_E2F_TARGETS", lower left, "HALLMARK_G2M_CHECKPOINT", lower right) compared with negative control siRNA, following siRNA-mediated knockdown of BRD2, BRD3 and BRD4 (through "siBETs") for 48 h in 501mel cells. (**C**) GSEA showing down-regulation of MYC targets hallmark gene set ("HALLMARK_MYC_TARGETS_V1") compared with negative control siRNA, following siRNA-mediated knockdown of BRD2 (left) or BRD4 (right) for 48 h in 501mel cells. In (**A-C**), computational analysis was carried out using DESeq2 [243] to identify differentially expressed genes, which were used for GSEA analysis in R [244]. NES = normalised enrichment score. P value represents adjusted p value. (**D**) Flow cytometry PI staining profile showing cell cycling in 501mel cells following treatment for 24 h with 500 nM (-)-JQ1 or (+)-JQ1. The purple peak represents cells in G1 phase, yellow represents those in S phase and green represents those in G2/M phase. (**E**) Percentage of cell population in each stage of cell cycle in 501mel after 24 h of treatment with (-)-JQ1 or (+)-JQ1. Mean cell population shown ± standard deviation. Statistical significance was determined using a two-tailed Students t-test. ns = non-significant difference,* = p <0.05, ** = p <0.01.*

A375M cells harbour WT p53 and 501mel cells harbour mutant p53 (Table 3.1, Figure 3.2A); however, both cell lines respond to (+)-JQ1 treatment with regard to cell cycling. This suggests that these responses to (+)-JQ1 are p53-independent. To investigate the involvement of p53 in cell cycle perturbation following BET attenuation, analysis of RNA-seq data was carried out, which shows that neither cell line up-regulated expression of the p53 pathway following (+)-JQ1 treatment (Figure 3.9). This suggests that even in A375M cells, the p53 WT cell line, cell cycle may be controlled in a p53-independent (Figure 3.9), but p21-dependent (Figures 3.2E-3.2F, 3.3B) manner.

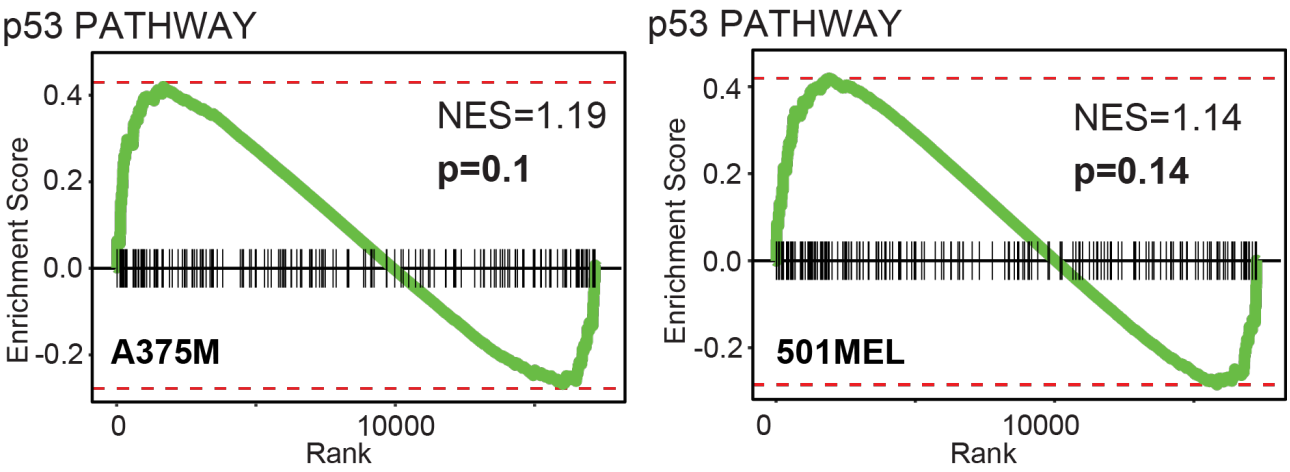


***Figure 3.9**: p53 Pathway is not up-regulated in either A375M or 501mel cells following (+)-JQ1 treatment. GSEA showing no changes in the p53 pathway gene set ("HALLMARK_P53_PATHWAY") following 500 nM (+)-JQ1 compared with (-)-JQ1 treatment for 24 h in A375M cells (left) and 501mel cells (right). Computational analysis was carried out using DESeq2 [243] to identify differentially expressed genes, which were used for GSEA analysis in R [244]. NES = normalised enrichment score. P value represents adjusted p value.*

While it's not clear exactly how the interplay between BETs yields loss of cellular proliferation in 501mel, the p53 mutant cell line, these results show that BET proteins may

have distinct roles in melanoma. It remains to be seen why a significant G1 cell cycle arrest occurred in 501mel cells, despite compromised p53 functionality and lack of 21 up-regulation, when arguably, an arrest did not occur in the A375M cells, which harbour WT p53, but do up-regulate p21 expression in response to (+)-JQ1 (Figures 3.2E-3.2F). This discrepancy between 501mel and A375M cell cycle arrests is in line with sensitivity data; A375M cells are less sensitive to (+)-JQ1 than 501mel cells (Table 3.1); therefore, it seems plausible that (+)-JQ1 has a more significant effect on 501mel cell cycling. The data presented in Figure 3.9 also undermine the importance of the p53 mutation harboured by 501mel cells, as A375M cells do not up-regulate the p53 pathway following (+)-JQ1 despite harbouring WT p53 and up-regulating p21 following BET BRD inhibition. This suggests that accumulation of cells in G1 phase is induced in a p53-independent manner regardless of the p53 mutation status. Additionally, despite a change in cellular morphology, transcription factors and drivers of cell cycle [294], YAP/TAZ, were not displaced from the nucleus following (+)-JQ1 treatment (Figure 7.3), despite the role of the actin cytoskeleton in their sub-cellular localisation in melanoma [295]. Together, these results indicate there could be p53-independent transcriptional basis to the loss of cellular proliferation, and suggest that cell cycle arrest in melanoma cell lines following BET BRD inhibition is p53-independent.

3.2.4 BET BRD inhibition leads to p53-independent activation of autophagy in melanoma cell lines

I have shown that BET BRD inhibition leads to changes in cell cycle gene expression in a potentially p53-independent manner in 501mel and A375M melanoma cell lines. To discover more about the phenotype elicited following BET BRD inhibition in each cell line, the RNA-seq data was further examined. Macroautophagy (referred to as autophagy hereafter) primarily serves as a mechanism through which cells can combat a nutrient

deficit [296]. It involves the degradation and recycling of macromolecules and structures within the cell in order to increase the supply of available amino acids and lipids [296]. Solute channels within the cell membrane control the influx and efflux of amino acids [297, 298]. If amino acid levels drop, mTOR phosphorylation within the mTORC1 complex decreases, which in turn leads to up-regulation of autophagic flux. Substrates are loaded into phagosomes from the cytoplasm and, upon fusion to the acidic lysosomes, cargos, including the substrate LC3BII, are degraded in the autophagolysosome [296, 299].

Autophagy is linked to several phenotypes including cell cycle arrest; therefore, it is possible that investigating the up-regulation of autophagy may shed light on how cell cycle arrest is achieved [300]. First, the RNA-seq data was analysed, specifically checking for autophagy-related gene ontologies. Figure 3.10A shows that in 501mel cells, cells respond to (+)-JQ1 by up-regulating autophagy-related transcriptional gene sets. RNA-seq data was analysed following siRNA-mediated knockdown of BETs, which showed that the autophagosome organisation gene ontology was also up-regulated in this scenario, suggesting that BET perturbation in 501mel cells, whether through pharmacological or genetic means, led to the expression of autophagy-related genes (Figure 3.10B). To identify which BET protein may regulate this increase in autophagy gene expression, RNA-seq data was analysed following individual knockdown of BET family members. Figure 3.10C shows that following BRD4 knockdown, there was significant up-regulation of genes involved in autophagosome organisation. Thus, BRD4 inhibition may promote the expression of autophagy-related genes.

To validate these RNA-seq findings, 501mel cells were treated with (+)-JQ1 for 24 h. Cells were treated with (-)-JQ1 as a negative control. Following this, RNA was extracted and was converted into cDNA. In these qPCR experiments 18S rRNA was used for normalisation [285]. The genes examined in this experiment were selected because they are known to be involved in autophagy [282, 284-293]. Figure 3.10D shows that there was

up-regulation of NEU1, a catabolic enzyme involved in autophagy [301], and down-regulation of CLCN7, a channel involved in lysosome acidification [302, 303]. While not statistically significant, the direction of change in expression of *MAPLC3B*, *ATG12*, *BNIP3* and *BNIPL3* observed in Figure 3.10D reflect the RNA-seq findings in Figure 3.10A, although increase in CTSF and ATG4B were also expected (see Chapter 7.3.1). The changes in expression of NEU1 and CLCN7 are indicative of conflicting effects of (+)-JQ1 on autophagy, with the former indicating up-regulation and the latter indicative of down-regulation [301-303]. These data do not provide a clear picture about how (+)-JQ1 affects autophagy; therefore, another autophagy marker must be examined.

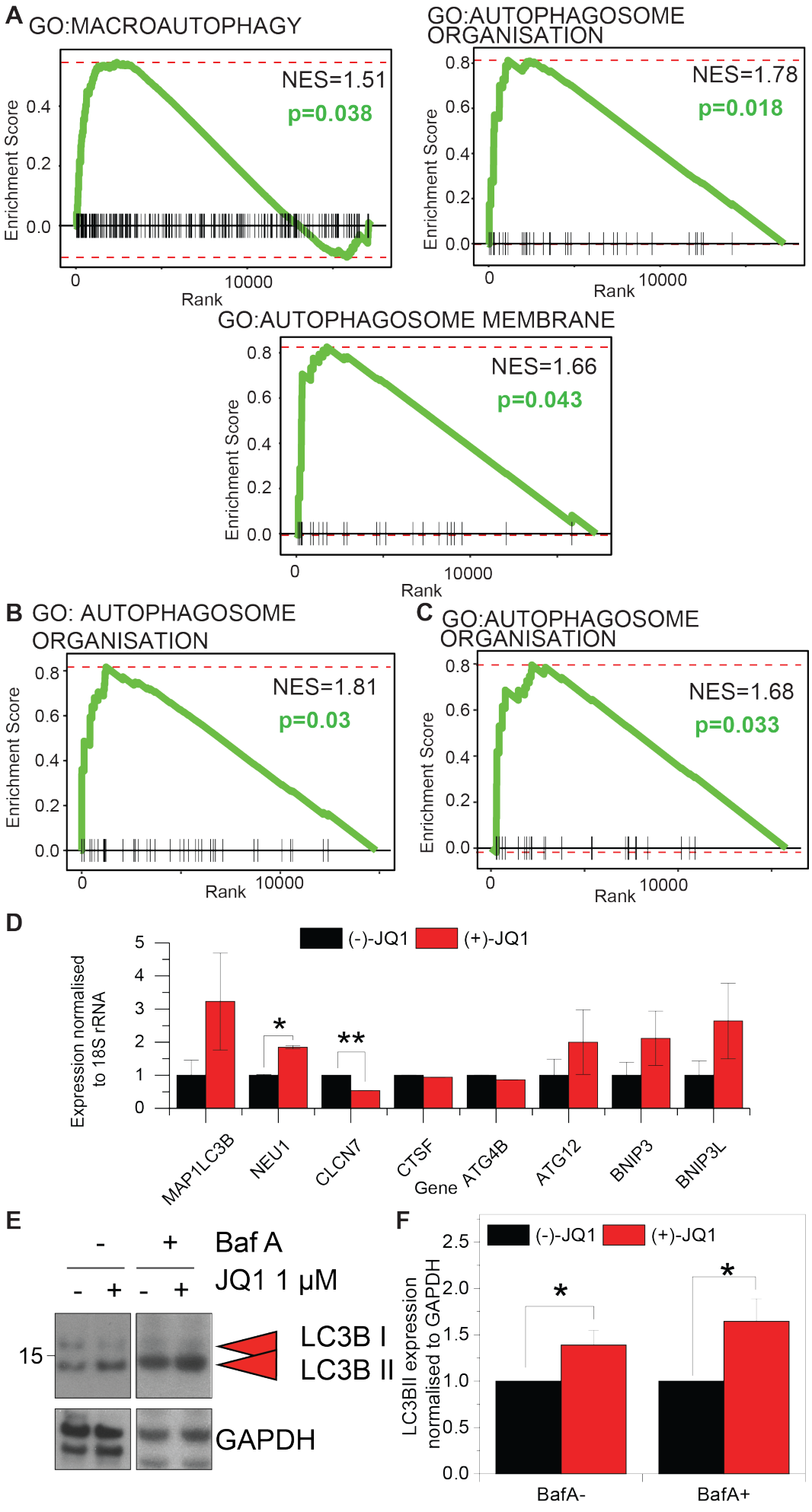

A
GO:MACROAUTOPHAGY
NES=1.51
p=0.038
GO:AUTOPHAGOSOME ORGANISATION
NES=1.78
p=0.018
GO:AUTOPHAGOSOME MEMBRANE
NES=1.66
p=0.043
Enrichment Score
Rank
B
GO: AUTOPHAGOSOME ORGANISATION
NES=1.81
p=0.03
C
GO:AUTOPHAGOSOME ORGANISATION
NES=1.68
p=0.033
D
(-)-JQ1
(+)-JQ1
Expression normalised to 18S rRNA
MAP1LC3B
NEU1
CLCN7
CTSF
ATG4B
ATG12
BNIP3
BNIP3L
Gene
E
Baf A
JQ1 1 μM
LC3B I
LC3B II
GAPDH
15
F
LC3BII expression normalised to GAPDH
BafA-
BafA+

***Figure 3.10**: BET BRD inhibition leads to autophagy up-regulation in 501mel cells. (**A**) GSEA plot of autophagy-related gene ontologies, following treatment with 500 nM (+)-JQ1 in 501mel cells compared with (-)-JQ1. (**B**) GSEA plot of the autophagosome organisation gene ontology (GO) following siRNA-mediated knockdown of BRD2, BRD3 and BRD4 (using "siBETs") in 501mel cells compared with negative control siRNA (siNC). **C**) GSEA plot of the autophagosome gene ontology (GO), following siRNA-mediated knockdown of BRD4 in 501mel cells compared with negative control siRNA (siNC). In (**A-C**), computational analysis was carried out using DESeq2 [243] to identify differentially expressed genes, which were used for GSEA analysis in R [244]. NES = normalised enrichment score. P value represents adjusted p value. (**D**) Quantification of mRNA expression by qPCR of autophagy-related genes in 501mel cells following 24 h of treatment with 1 μM (-)-JQ1 or (+)-JQ1. N = 3 biological replicates. Mean RNA expression shown ± standard deviation. Statistical significance was determined using a two-tailed Students t-test. * = $p < 0.05$, ** = $p < 0.01$. (**E**) Immunoblot showing LC3BII expression in 501mel cells following 24 h of treatment of 1 μM (-)-JQ1 or (+)-JQ1, and 3 h of treatment with 10 nM Bafilomycin A (BafA). N = 3 biological replicates. (**F**) Quantification of LC3BII staining normalised to GAPDH expression in 501mel cells following 24 h of treatment of 1 μM (-)-JQ1 or (+)-JQ1, and 3 h of treatment with 10 nM BafA. N = 3 biological replicates. Mean protein expression shown ± standard deviation. Statistical significance was determined using a two-tailed Students t-test. * = $p < 0.05$.*

Accordingly, immunoblots were carried out to detect the expression of LC3BII. GAPDH is used as a loading control in immunoblots and is widely used as such when investigating BET protein inhibition [34, 94, 152]. During autophagosome formation, LC3BI is incorporated into the autophagosome membrane through conjugation of LC3BI to phosphatidylethanolamine (PE) by ATG4B and ATG7 [299]. Conjugation of LC3BI during autophagosome membrane elongation is also referred to as LC3BI lipidation, the product

of which is lipidated LC3BI, which is referred to as LC3BII [299]. Increased expression of LC3BII is indicative of autophagosome accumulation, which can represent either inhibition or activation of autophagy [299]. LC3BI and LC3BII, can be observed on an immunoblot as two distinct bands; LC3BII is faster migrating band compared with LC3BI [304]. Therefore, LC3BII is frequently used as a marker of autophagic flux [68, 304, 305] , and as such has been used in the experiments presented here. Figure 3.10E shows that LC3BII expression levels are significantly increased following (+)-JQ1 treatment with or without treatment with bafilomycin A (BafA) (quantified in Figure 3.10F). BafA binds to the pore-forming domain of the ATPase that maintains acidity of the lysosomes [306]; thus, inhibiting autophagy through preventing fusion of lysosomes to autophagosomes and the acidic degradation of autophagosomal contents [304, 305]. (+)-JQ1 treatment alone increased expression of LC3BII (Figure 3.10E), and signals an increase in the number of autophagosomes within cells [304, 305]. However, it remains unclear whether this increase in autophagosomes is due to the up-regulation of autophagy, or the inhibition of degradation of autophagosomal cargo, resulting in the accumulation of autophagosomes awaiting degradation. Therefore, the addition of BafA to cells concomitantly with (+)-JQ1 is necessary and allows the observation of the accumulation of the LC3BII that results from the inhibition of autophagy. Given that the expression of LC3BII is greater in cells that have been exposed to both BafA and (+)-JQ1, compared with cells treated with (-)-JQ1 and BafA, it suggests that (+)-JQ1 leads to an up-regulation of autophagy.

I next determined whether A375M cells also underwent autophagy activation following treatment with (+)-JQ1. Given that p53, WT or mutant, can have context-dependent effects on autophagy regulation [307, 308], it was unclear whether to expect autophagy activation in the A375M cell line following BET BRD inhibition. RNA-seq data following (+)-JQ1 treatment was analysed and showed an up-regulation of mTORC1 signalling (Figure 3.11A). Under starvation conditions, a reduction in mTORC1 signalling leads to a decrease

in translation and an increase in autophagy [309, 310]; thus, Figure 3.11A suggests that BET BRD perturbation down-regulates autophagy in A375M cells. To validate this change in mTOR signalling induced by (+)-JQ1, immunoblotting was performed. Figure 3.11B shows that (+)-JQ1 causes loss of phospho-mTOR (p-mTOR) expression, which is contrary to the RNA-seq indications, as up-regulation of mTORC1 signalling translates to an increase in mTOR phosphorylation. RNA-seq data suggest a down-regulation of autophagy, whereas loss of p-mTOR suggests activation of autophagy [309]; these conflicting data demand further investigation in to the effect of (+)-JQ1 on autophagy.

Next the expression of autophagy genes was examined (Figure 3.11C). Therefore, first the effects of (+)-JQ1 on genes related to autophagy was determined using qPCR, using the same methodology as the experiments carried out in 501mel. Figure 3.11C shows that there was up-regulation of NEU1, ATG4B, BNIP3, BNIP3L, and down-regulation of CTSF. Up-regulation of NEU1, ATG4B, BNIP3 and BNIP3L expression suggests autophagy is up-regulated [284, 286-288, 290, 291]. The down-regulation of CTSF expression in Figure 3.11C indicates that autophagy is down-regulated, in agreement with Figure 3.11A. Therefore, further clarity is needed as to how BET BRD inhibition affects autophagy in A375M cells. LC3BII expression, a marker of autophagic flux was examined. Immunoblots were carried out in the same manner as those carried out in 501mel. Figure 3.11D shows that LC3BII is up-regulated following (+)-JQ1 treatment, in the absence and presence of autophagy inhibitor, BafA, and the quantification of 3 biological replicates shows that this is a significant effect (Figure 3.11E).

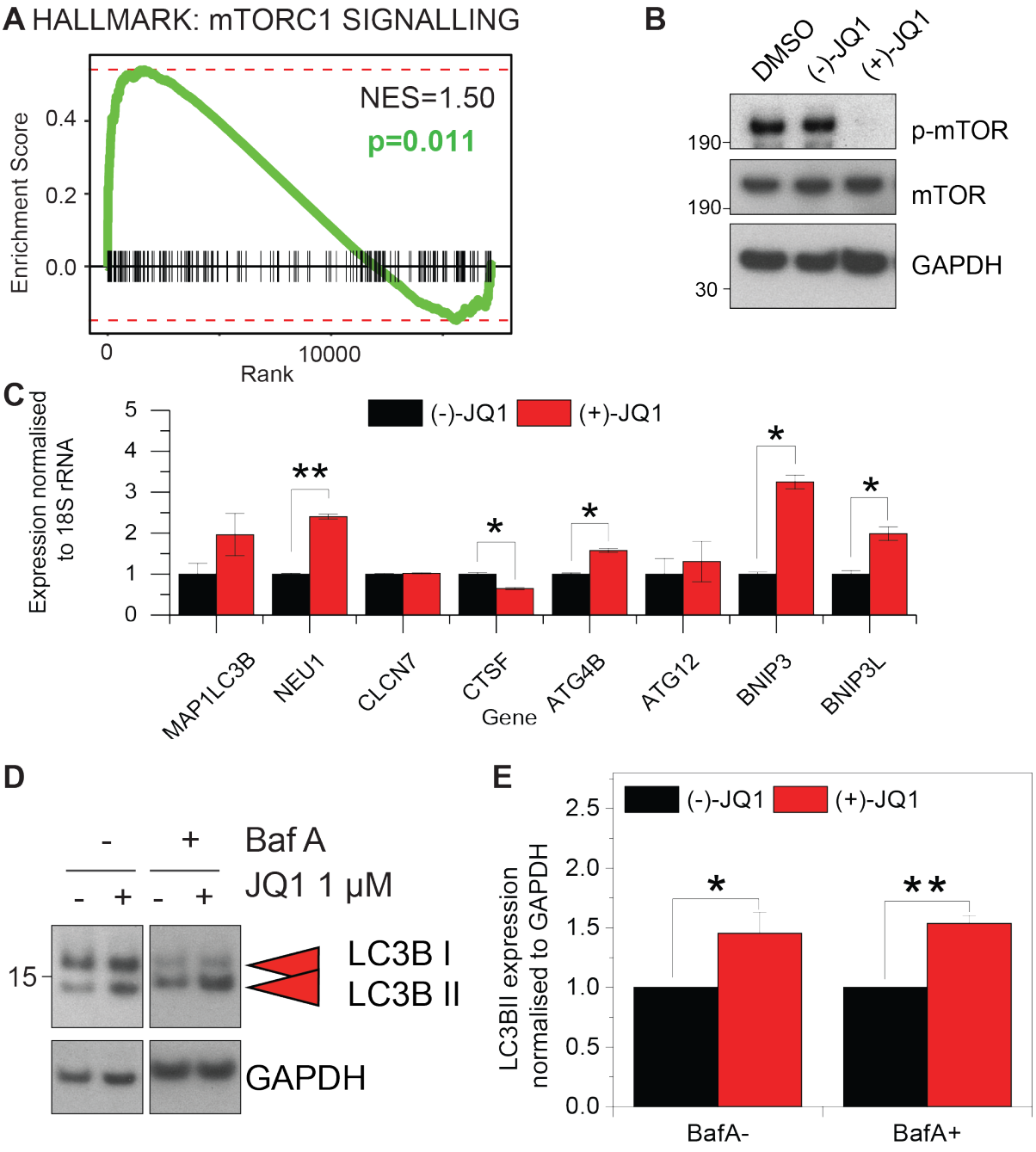


***Figure 3.11**: BET BRD inhibition induces autophagy in A375M cells. (**A**) GSEA plot of the mTORC1 signalling hallmark, following treatment with 500 nM (+)-JQ1 in A375M cells compared with (-)-JQ1. Computational analysis was carried out using DESeq2 [243] to identify differentially expressed genes, which were used for GSEA analysis in R [244]. NES = normalised enrichment score. P value represents adjusted p value. (**B**) Immunoblot showing p-mTOR and mTOR expression in A375M cells following 24 h of treatment of DMSO or 1 μM (-)-JQ1 or (+)-JQ1. N = 3 biological replicates. (**C**) Quantification of mRNA expression by qPCR of autophagy-related genes in A375M cells following 24 h of*

*treatment with 1 μM (-)-JQ1 or (+)-JQ1. N = 3 biological replicates. Mean RNA expression shown ± standard deviation. Statistical significance was determined using a two-tailed Students t-test. * = p < 0.05, ** = p < 0.01. (**D**) Immunoblot showing LC3BII expression in A375M cells following 24 h of treatment of 1 μM (-)-JQ1 or (+)-JQ1, ± 3 h of treatment with 10 nM BafA. N = 3 biological replicates. (**E**) Quantification of LC3BII staining normalised to GAPDH expression in A375M cells following 24 h of treatment of 1 μM (-)-JQ1 or (+)-JQ1, ± 3 h of treatment with 10 nM BafA. N = 3 biological replicates. Mean protein expression shown ± standard deviation. Statistical significance was determined using a two-tailed Students t-test. * = p < 0.05, ** = p < 0.01.*

Therefore, Figures 3.10-3.11 show that both 501mel and A375M melanoma cell lines up-regulate autophagy in response to pharmacological BET BRD inhibition, and this may have a transcriptional basis. Interestingly, the only gene differentially regulated in both cell lines from the up-regulated autophagy gene sets in Figures 3.10A and 3.11A was SQSTM1, which is selectively degraded by autophagy and is part of the cargo loaded into autophagosomes for degradation upon fusion with a lysosome [305]; therefore, different subsets of autophagy-related genes are up-regulated following BET BRD inhibition in 501mel and A375M cells. p53 mutation status appeared to have no effect upon autophagy up-regulation; however, given that only two cell lines have been used in this study, and no further experiments into the role of p53-dependent autophagy regulation have been carried out, it remains possible that p53 regulates autophagy genes in a way that is unperturbed by the C275W mutation in 501mel.

3.2.5 p53 mutation status correlates with cell fate and role of autophagy in melanoma cell lines following BET BRD inhibition

Thus far, the presented data describe how 501mel and A375M melanoma cell lines respond to BET BRD inhibition through loss of cellular proliferation, accumulation of cells

in G1 phase of cell cycle and activation of autophagy, all independent of p53 mutation status. To gain more insight into how the cell cycle arrest occurs, I carried out investigations into two potential causes: cell death, and cellular senescence.

Autophagy, apoptosis and senescence are very closely linked cellular processes. Activation of senescence is seldom separable from autophagic perturbation; autophagic flux increases in senescent cells [311]. While the link between them is far from clear, and seemingly context-dependent, there is much evidence in favour of relationship between the two cellular phenomena. Autophagy can be pro-senescence, by increasing the available pool of amino acids needed for the senescence associated secretory phenotype, or autophagy can be anti-senescent, by leading to the degradation of damaged organelles, which would, if left within the cell, lead to the activation of senescence [312]. Conflicting findings suggest that the relationship between autophagy and senescence can be activatory or inhibitory depending on the context [311-313]. Similar can be said for the complex relationship between autophagy and apoptosis. Cells can switch between apoptotic and autophagic phenotypes, and one can inhibit or activate the other in a context-dependent manner, yet can also accompany each other without a functional connection [314, 315]. Apoptosis and autophagy can be activated by the same stimuli and signalling pathway components can be shared between the two cellular processes [314, 315].

Senescence is defined as an irreversible cell cycle arrest in response to cellular stress while cells remain metabolically active [311]. In normal tissues, senescence occurs when telomeres reach a critical length to prevent the propagation of potentially damaged DNA, which is referred to as replicative senescence [316]. Senescence can be induced in telomere-independent circumstances such as through oncogene expression (oncogene induced senescence (OIS)), loss of tumour suppressor expression or through cellular stress [317]. Hallmarks of activation of senescence include the expression of β-

galactosidase, heterochromatin foci, up-regulation of G1 cell cycle arrest associated markers such as p21 and p16, and activation of the senescence associated secretory phenotype [317]. In the context of melanomagenesis, autophagy induction can precede OIS to prevent tumourigenesis following BRAF oncogene activation [318, 319].

To shed more light on the phenotype elicited by BET BRD inhibition in melanoma cells, RNA-seq data was first examined. There is evidence to suggest that some melanoma cell lines undergo apoptosis when treated with BET BRD inhibitors [95]. Figure 3.12A shows that following BET BRD inhibition, the apoptotic hallmark gene set is up-regulated in A375M cells, suggesting that apoptosis may be induced and underpinned by transcriptional events. Figure 3.12B sheds more light on this; following siRNA-mediated knockdown of BRD2, the apoptotic hallmark is also up-regulated, which indicates that perhaps BRD2 perturbation specifically may lead to transcription-driven apoptosis. With these indicators that apoptosis may occur, activation of the apoptotic pathway was investigated. Caspase 3/7 activation and PARP cleavage are indicative of activation of the intrinsic apoptotic pathway [211, 213, 214]. Briefly, to detect caspase activation, cells were stained with a fluorescent reagent that binds to the cleaved caspase at the cleavage site. The samples were also stained with a dye specific for dead cells. The cell staining was subsequently analysed using flow cytometry. During flow cytometry analysis, cells were divided into four categories: negative for both stains (lower left quadrant), positive for dead cell stain only (upper left quadrant), positive for caspase activation (lower right quadrant) and cells positive for both caspase activation and dead cell stain (upper right quadrant). The lower and upper right panels were assigned as populations of cells which display caspase activation. Figures 3.12C-3.12D show that caspase 3/7 activation is significantly increased by (+)-JQ1, by approximately 3-fold in comparison with (-)-JQ1. Immunoblots were used to investigate PARP cleavage and SDHA was used as a loading control.

Figures 3.12E-3.12F show there is a significant increase in PARP cleavage when cells are treated with (+)-JQ1.

To ascertain whether or not cells die, as well as activate apoptotic signalling, cells were stained with annexin V. Annexin V stains cells with phosphatidylserine (PS) on the outer phospholipid bilayer membrane leaflet [320, 321], and positively stained cells can be detected using flow cytometry. Under normal conditions, PS is found only on the inner leaflet of the cell membrane; however, cell death signalling cascades converge on the loss of cell membrane integrity, during which PS is translocated to the outer leaflet [320, 322, 323]. The cellular population positive for annexin V was quantified using flow cytometry (Figure 3.12G). Figure 3.12H shows that there is an increase in annexin V staining in A375M cells after 48 h of treatment with (+)-JQ1, which was exacerbated after 72 h, resulting in an approximately 5-fold increase in cell death compared with (-)-JQ1, suggesting BET BRD leads to cell death in a time-dependent manner.

To show orthogonally that cells died following (+)-JQ1 treatment, a clonogenicity assay was carried out. Briefly, cells were treated for 48 h with the indicated compound, after which cells were re-plated as single cells (200 cells/well) in normal medium. Over the course of 1 week, single cells grew and divided formed colonies, which were then stained with crystal violet and quantified. DMSO and (-)-JQ1 were negative controls and staurosporine was the positive control [324]. Figure 3.12I-3.12J show that significantly fewer colonies formed following BET BRD inhibition, despite the week in normal medium to recover from the treatment. To confirm that A375M cells were not undergoing cellular senescence, β-galactosidase staining was carried out on A375M cells (Figure 7.4). This provides further evidence that A375M cells die when treated with a BET BRD inhibitor and the effects of (+)-JQ1.

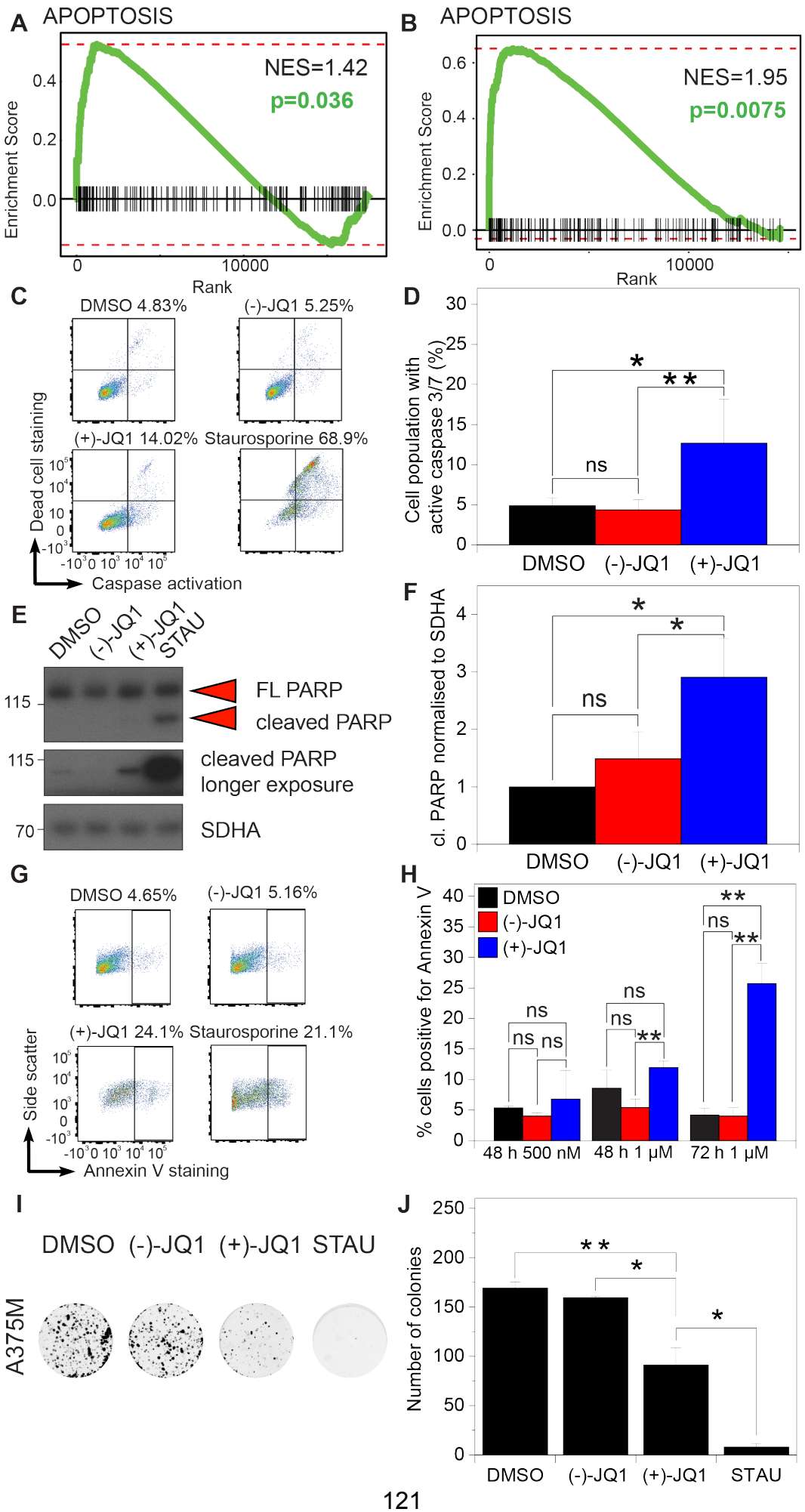

A
APOPTOSIS
NES=1.42
p=0.036
Enrichment Score
Rank
B
APOPTOSIS
NES=1.95
p=0.0075
C
DMSO 4.83%
(-)-JQ1 5.25%
(+)-JQ1 14.02%
Staurosporine 68.9%
Dead cell staining
Caspase activation
D
Cell population with active caspase 3/7 (%)
ns
DMSO
(-)-JQ1
(+)-JQ1
E
DMSO
(-)-JQ1
(+)-JQ1
STAU
115
FL PARP
cleaved PARP
115
cleaved PARP
longer exposure
70
SDHA
F
cl. PARP normalised to SDHA
G
DMSO 4.65%
(-)-JQ1 5.16%
(+)-JQ1 24.1%
Staurosporine 21.1%
Side scatter
Annexin V staining
H
% cells positive for Annexin V
DMSO
(-)-JQ1
(+)-JQ1
48 h 500 nM
48 h 1 µM
72 h 1 µM
I
DMSO
(-)-JQ1
(+)-JQ1
STAU
A375M
J
Number of colonies

***Figure 3.12**: BET BRD inhibition induces apoptosis in A375M cells. (**A**) GSEA plot shows apoptosis hallmark ("HALLMARK_APOPTOSIS") is up-regulated in A375M cells following (+)-JQ1 treatment compared with (-)-JQ1 following treatment of 500 nM for 24 h. (**B**) GSEA plot shows up-regulation of apoptotic hallmark ("HALLMARK_APOPTOSIS") following siRNA mediated knockdown of BRD2 for A375M cells compared with negative control siRNA transfection for 48 h. In (**A-B**), computational analysis was carried out using DESeq2 [243] to identify differentially expressed genes, which were used for GSEA analysis in R [244]. NES = normalised enrichment score. P value represents adjusted p value. (**C**) Cell staining showing caspase 3/7 activation in A375M cells following treatment with 0.1% v/v DMSO, 0.1% v/v staurosporine, 1 μM (-)-JQ1 or (+)-JQ1 for 48 h. (**D**) Quantification of caspase 3/7 activation in A375M cells following treatment with 1 μM (+)-JQ1 for 48 h. Negative controls are 0.1% v/v DMSO and 1 μM (-)-JQ1, the solvent for JQ1 and the inactive stereoisomer of (+)-JQ1 that does not display binding to the BET BRD pocket. N = 3 biological replicates. Mean percentage of cells stained positive for active caspases 3/7 shown ± standard deviation. Statistical significance was determined using a two-tailed Students t-test. ns = non-significant difference, * = p <0.05, ** = p < 0.01. (**E**) Immunoblot showing PARP cleavage following 1 μM (+)-JQ1 treatment for 48 h in A375M cells. Negative controls were 0.1% v/v DMSO, 1 μM (-)-JQ1 and positive control was 0.1% v/v staurosporine. N = 3 biological replicates. (**F**) Quantification of PARP cleavage normalised to SDHA expression in A375M cells following 48 h of 1 μM treatment of (+)-JQ1. N = 3 biological replicates. Negative controls were 1 μM (-)-JQ1 and 0.1% v/v DMSO. Mean quantification of cleaved PARP shown ± standard deviation. Statistical significance was determined using a two-tailed Students t-test. ns = non-significant difference, * = p < 0.05. (**G**) Annexin V staining in A375M cells. A375M cells die following treatment with 1 μM (+)-JQ1 for 72 h. Annexin-V-positive cell population highlighted in box at the right of each sample. Negative controls were 0.1% v/v DMSO, 1 μM (-)-JQ1 and positive control was*

*0.1% v/v staurosporine. (**H**) Quantification of annexin V staining in A375M cells following 1 μM (+)-JQ1 treatment for 24, 48 and 72 h. N = 3 per time point. Controls are 0.1% v/v DMSO, the solvent in which (-)-JQ1 and (+)-JQ1 are dissolved, and 1 μM (-)-JQ1. N = 3 biological replicates. Mean percentage of cells stained positive for annexin V shown ± standard deviation. Statistical significance was determined using a two -tailed Students t-test. ns = non-significant difference, * = p < 0.05, ** = p < 0.01. (**I**) A375M cells colonies formed following treatment with 1 μM (+)-JQ1 for 48 h. Negative controls were 0.1% v/v DMSO, 1 μM (-)-JQ1 and positive control was 0.1% v/v staurosporine. Cells were treated with the indicated compound for 48 h then subsequently re-plated and grew for 1 week in normal media before staining with crystal violet. (**J**) Quantification of A375M colony formation following treatment for 48 h with 1 μM (+)-JQ1, and a subsequent re-plating and growth for 1 week in normal media. Negative controls were 0.1% v/v DMSO, 1 μM (-)-JQ1 and positive control was 0.1% v/v staurosporine. Cells were treated with the indicated compound for 48 h then subsequently re-plated and grew for 1 week in normal media before staining with crystal violet. Plates were scanned and colonies were quantified using ImageJ software. N = 3 biological replicates. Mean colony number shown ±standard deviation. Statistical significance was determined using a two-tailed Students t-test. * = p < 0.05, ** = p < 0.01.*

To determine whether 501mel cells share the same fate as A375M cells following (+)-JQ1 treatment, RNA-seq data was analysed when 501mel cells were treated with (+)-JQ1. Figure 3.13A shows that the apoptotic signature is not up-regulated by BET BRD inhibition. To confirm that cells did not die, cell death signalling was examined. Throughout these experiments examining apoptotic signalling, DMSO and (-)-JQ1 were used as a negative controls and staurosporine was used as a positive control as a known inducer of cell death [324]. Beginning with caspase 3/7 activation, Figures 3.13B-18C show that (+)-JQ1 treatment did not have a significant effect on caspase 3/7 activation. In agreement with this

Figures 3.13D-3.13E show that PARP cleavage was unaffected by (+)-JQ1 treatment. Cell death mechanisms lead to the loss of cell membrane phospholipid asymmetry, resulting in PS presence on the outer leaflet of the cell membrane, which can be detected by staining with annexin V [320, 321]. While cells staining positive for this dye do not shed light on the way in which cells have died, it does indicate that cells are, indeed, dying as opposed to entering states of senescence or quiescence. As such, annexin V staining provides further details about the phenotype cells adopt. Annexin V staining was carried out under three different conditions, and Figure 3.13F-3.13G show that BET BRD inhibition does not have an effect on 501mel cell death in either a time-, or dose-dependent manner.

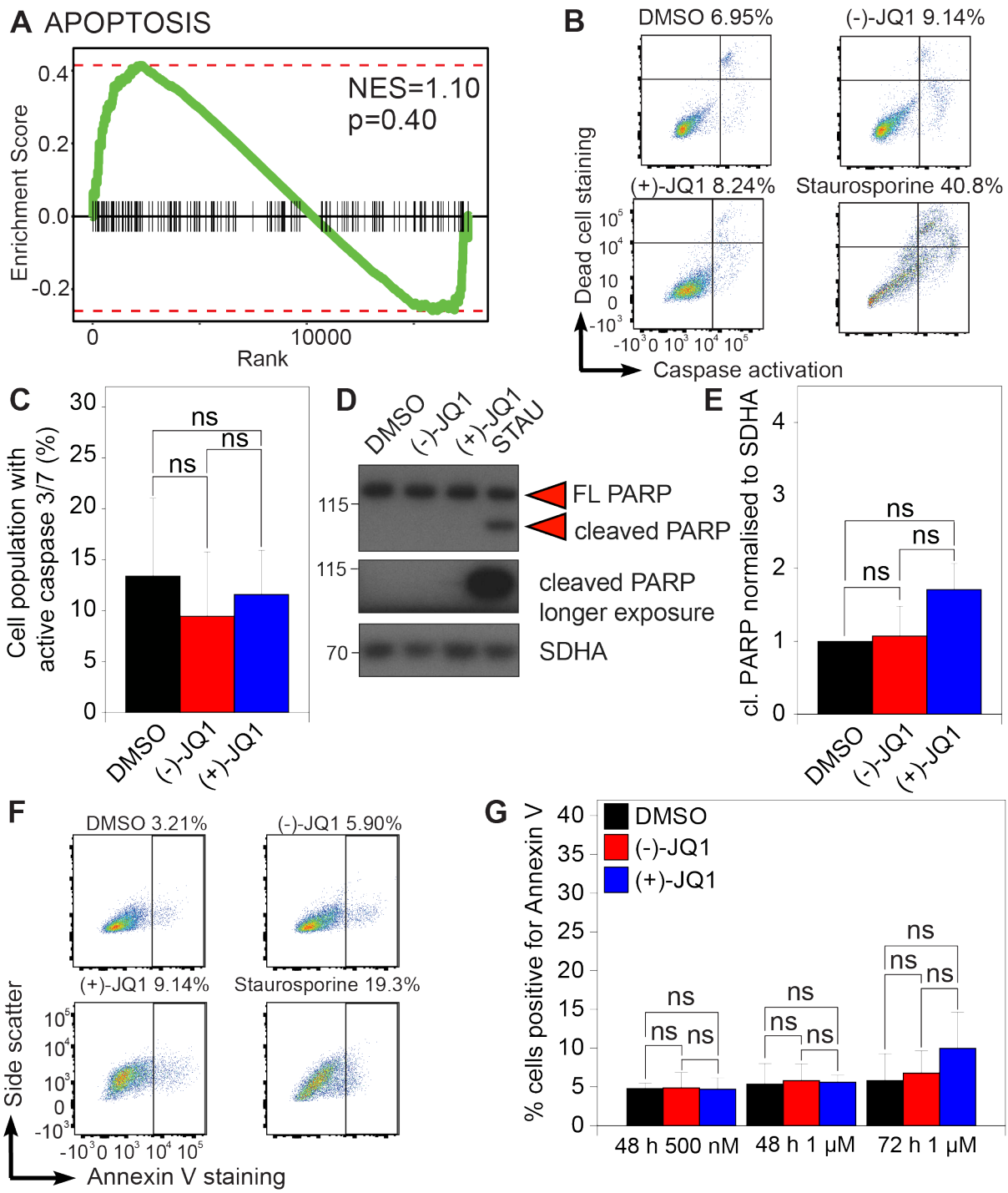

A APOPTOSIS
NES=1.10
p=0.40
Enrichment Score
Rank
B
DMSO 6.95%
(-)-JQ1 9.14%
(+)-JQ1 8.24%
Staurosporine 40.8%
Dead cell staining
Caspase activation
C
Cell population with active caspase 3/7 (%)
ns
DMSO
(-)-JQ1
(+)-JQ1
D
DMSO
(-)-JQ1
(+)-JQ1
STAU
115
70
FL PARP
cleaved PARP
cleaved PARP longer exposure
SDHA
E
cl. PARP normalised to SDHA
F
DMSO 3.21%
(-)-JQ1 5.90%
(+)-JQ1 9.14%
Staurosporine 19.3%
Side scatter
Annexin V staining
G
% cells positive for Annexin V
DMSO
(-)-JQ1
(+)-JQ1
48 h 500 nM
48 h 1 µM
72 h 1 µM
H
DMSO
(-)-JQ1
(+)-JQ1
STAU
I
Number of colonies
*
ns
J
(-)-JQ1
(+)-JQ1
K
% cells positive for β-gal
*

***Figure 3.13**: 501mel cells undergo senescence in response to BET BRD inhibition. (**A**) Apoptosis hallmark is not significantly changed in 501mel cells following (+)-JQ1 treatment compared with (-)-JQ1. Cells were treated for 24 h with 500 n M (-)-JQ1 or (+)-JQ1. RNA was extracted and submitted for RNA-seq. Computational analysis was carried out using DESeq2 [243] to identify differentially expressed genes, which were used for GSEA analysis in R [244]. NES = normalised enrichment score. P value represents adjusted p value. (**B**) Cell staining showing lack of caspase 3/7 activation in 501mel cells following treatment with 0.1% v/v DMSO, 0.1% v/v staurosporine, or 1 μM (-)-JQ1 or (+)-JQ1 for 48 h. DMSO and (-)-JQ1 were negative controls, and staurosporine is the positive control. (**C**) Quantification of caspase 3/7 activation in 501mel cells following treatment with 0.1% v/v DMSO, 1 μM (-)-JQ1 or (+)-JQ1 for 48 h. N = 3 biological replicates. Mean percentage of cells stained positive for active caspases 3/7 shown ± standard deviation. Statistical significance was determined using a two-tailed Students t-test. ns = non-significant difference. (**D**) Immunoblot showing PARP cleavage following 1 μM (+)-JQ1 treatment for 48 h in 501mel cells. Negative controls were 0.1% v/v DMSO, 1 μM (-)-JQ1, and positive control was 0.1% v/v staurosporine. SDHA was used as a loading control [152]. N = 3 biological replicates. (**E**) Quantification of PARP cleavage normalised to SDHA expression in 501mel cells following 48 h of 1 μM treatment of (+)-JQ1. Negative controls were 0.1% v/v DMSO and 1 μM (-)-JQ1. N = 3 biological replicates. Mean quantification of cleaved PARP shown ± standard deviation. Statistical significance was determined using a two-tailed Students t-test. ns = non-significant difference. (**F**) Annexin V staining in 501mel cells. 501mel cells do not die following treatment with 1 μM (+)-JQ1 for 72 h. Annexin-V-positive cell population highlighted in box at the right of each sample. 0.1% v/v Staurosporine is positive control, a known inducer of cell death. 0.1% v/v DMSO and 1 μM (-)-JQ1 are negative controls. (**G**) Quantification of annexin V staining in 501mel cells following DMSO, 1 μM (-)-JQ1 or (+)-JQ1 treatment for 24, 48 and 72 h. N = 3 biological*

*replicates per time point. Controls are 0.01% v/v DMSO and 1 μM (-)-JQ1. Mean percentage of cells stained positive for annexin V shown ± standard deviation. Statistical significance was determined using a two-tailed Students t-test. ns = non-significant difference. (**H**) 501mel cell colonies formed following treatment with 1 μM (+)-JQ1 for 48 h. Negative controls were 0.01% v/v DMSO, 1 μM (-)-JQ1 and positive control was 0.01% v/v staurosporine. Cells were treated with the indicated compound for 48 h then subsequently re-plated and grew for 1 week in normal media before staining with crystal violet. (**I**) Quantification of 501mel colony formation following treatment for 48 h with 1 μM (+)-JQ1, and a subsequent re-plating and growth for 1 week in normal media. Negative controls were 0.01% v/v DMSO, 1 μM (-)-JQ1 and positive control was 0.01% v/v staurosporine. Cells were treated with the indicated compound for 48 h then subsequently re-plated and grew for 1 week in normal media before staining with crystal violet. Plates were scanned and colonies were quantified using ImageJ software. N = 3 biological replicates. Mean colony number shown ± standard deviation. Statistical significance was determined using a two-tailed Students t-test. ns = p > 0.05, * = p < 0.05. (**J**) β-galactosidase staining in 501mel cells following treatment with 1 μM (-)-JQ1 or (+)-JQ1 for 48 h. (**K**) Quantification of β-galactosidase staining in 501mel cells after 48 h of treatment with 0.01% v/v DMSO, 1 μM (-)-JQ1 or (+)-JQ1. N = 3 biological replicates. Mean percentage of cells stained positive for β-galactosidase shown ± standard deviation. Statistical significance was determined using a two-tailed Students t-test. * = p < 0.05.*

If 501mel cells do not die following (+)-JQ1 treatment, it is possible that they enter a state of cellular senescence instead. To examine markers of senescence, the colony formation capacity of 501mel cells was tested to ascertain whether cells recover from treatment with BET BRD inhibitor. Cells were treated with (+)-JQ1 for 48 h, then re-plated as single cells, which grew into colonies over the course of 1 week in normal medium. Thus, throughout the week of growth, (+)-JQ1 was withdrawn. DMSO and (-)-JQ1 were used as negative

controls. Staurosporine was used as a positive control [324]. Figure 3.13H shows representative wells displaying colony formation following (+)-JQ1 or control treatment and 1 week of growth. (+)-JQ1 significantly reduces colony formation (Figure 3.13I) and induces an irreversible cell cycle arrest, which is indicative of senescence or cell death. However, some cells still form colonies; therefore, it is possible that colony formation capacity or cells' ability to adhere to the plate following re-plating is perturbed rather than induction of permanent cell cycle arrest. Therefore, cells were further examined for β-galactosidase expression, another indicator of senescence [317, 318]. 501mel cells were treated with (+)-JQ1 and the negative controls used in this experiment, DMSO and (-)-JQ1, and were stained for β-galactosidase expression. 501mel cells showed a significant increase in β-galactosidase staining following BET BRD inhibition (Figure 3.13J-3.13K). Altogether Figure 3.13 shows that 501mel cells undergo senescence following pharmacological BET BRD inhibition rather than cell death.

Altogether, the data presented in Figure 3.12 show that A375M cells undergo apoptosis following BET BRD inhibition. A375M cells showed increased caspase 3/7 activation and PARP cleavage, which are indicative of activation of the intrinsic apoptotic pathway [211, 213, 214], and increased annexin V staining, which is indicative of cell death [321]. 501mel cells instead undergo senescence, as indicated by a lack of increase in annexin V staining, but a significant increase in β-galactosidase staining following BET BRD inhibition (Figure 3.13). A375M cells express WT p53, and 501mel cells express mutant p53; thus, p53 mutation status correlates with the mechanism by which cells stop proliferating in response to (+)-JQ1. It is also intriguing to speculate about the origins of the apoptotic signalling in A375M. Both 501mel and A375M cells express BRD2; however, pan-BET inhibition and siRNA-mediated knockdown of BRD2 only induced the up-regulation of the apoptotic gene set in A375M cells. It would be interesting to determine whether

knockdown of BRD2 alone leads to apoptosis, and to validate differentially regulated genes that contribute to this.

In the context of melanoma, an increased basal level of autophagy can lead to the activation of senescence, which prevents tumourigenesis, and reduced autophagic signalling led to bypass of senescence [319]. A375M and 501mel cells exhibit decreases in cellular viability following treatment with (+)-JQ1 (Table 3.1) and increase in autophagic signalling after 24 h (Figures 3.10-3.11). Since BET BRD inhibition leads to induction of apoptosis in A375M (Figure 3.12) and senescence in 501mel cells (Figure 3.13) and there are documented links between senescence induction, apoptosis and autophagy [314, 315, 319], it is possible that blockade of autophagy could affect the senescent and apoptotic phenotypes.

To test this hypothesis, cells were treated with (+)-JQ1 and chloroquine (CQ) in order to determine whether blockade of autophagy would rescue cells from loss of proliferation. CQ is a treatment for malaria, and has been shown to inhibit autophagy [305]. IGR37 and IGR39 were included in this study to determine if MITF expression determined whether concomitant autophagy inhibition led to rescue of cellular proliferation. IGR37 and IGR39 are derived from the same patient; IGR37 is the metastatic counterpart to IGR39 and as such they are lineage-related but differ in MITF expression [237, 325]. CHL1 was included in this experiment as a MITF-low, BRAF-WT [268, 326-329], NRAS-WT [217], p53 mutant cell line [268, 329, 330] to investigate whether p53 mutation correlates with cellular response to BET BRD inhibition.

Using an MTT assay, Figure 3.14A shows that as the concentration of (+)-JQ1 with which cells are treated increases, the cellular viability decreases, as expected. Upon concomitant treatment with CQ, the cellular proliferation is somewhat rescued in 501mel cells (Figure 3.14A), This indicates that autophagy inhibition could bypass senescence in 501mel cells.

CQ treatment in tandem with 10 μM (+)-JQ1 does not rescue proliferation; it is possible that at 10 μM (+)-JQ1 the effects of BET BRD inhibition are so severe that autophagy inhibition is unable to compensate for the anti-proliferative effects of (+)-JQ1. There is no effect of concomitant BET BRD inhibition and autophagy inhibition on A375M, IGR37, and IG39 cellular proliferation (Figure 3.14A); therefore, induction of apoptosis by BET BRD inhibition cannot be circumvented by A375M cells through inhibition of autophagy. In terms of protein expression, IGR37 is $MITF^{high}$ while IGR39 is $MITF^{low}$ (Table 3.1, [263, 264]). Neither of these cell lines recovered from loss of cellular proliferation following concomitant BET BRD and autophagy inhibition; therefore, it is unlikely that MITF expression is the determinant of cell fate following BET BRD inhibition. CHL1 cells showed modest but statistically insignificant recovery from the effects of (+)-JQ1 treatment upon concomitant autophagy inhibition (see Chapter 7.3.1).

The H193R mutation found in CHL1 cells lies within the DNA-binding domain of p53 [255]. The H193R mutation may affect the binding of residue 193 to R273; when the arginine residue at positive 273 is mutated to a histidine, the bond between this histidine and the H193 is stronger than the bond between R273 and H193 [278]. Therefore, it may be possible that a H193R mutation also alters the strength of the bond between the residue at position 193 and R273. The R273 residue mediates contact of p53 to DNA [279]; therefore, corruption of its normal binding behaviour by a residue with which it interacts may result in disruption of p53-DNA binding, and by extension, p53 function. This mutation is found in solid cancers [331, 332], and in Li-Fraumeni Syndrome [333], suggesting this mutation prevents p53 function and drives oncogenesis.

The data presented here suggest that the p53 mutation correlates with the induction of autophagy-dependent senescence following BET BRD inhibition, and the attenuation of autophagy leads to the rescue of proliferation. BafA and CQ were used as orthogonal inhibitors of autophagy; however, both have off-target effects, suggesting that this finding

should be reinforced with an experiment involving concomitant genetic inhibition of the autophagic pathway [334].

Switching between senescence and apoptosis has been observed upon the onset of autophagy inhibition [335]. To investigate whether this occurred in either A375M or 501mel cells, annexin V staining was carried out to confirm whether 501mel or A375M displayed changes in cell death following concomitant inhibition of BET BRDs and autophagy. Figures 3.14B-3.14C show that the annexin-V-positive cell population does not change in A375M or 501mel cells when treated with (+)-JQ1 and CQ, when compared to (+)-JQ1 alone. Therefore, simultaneous blockade of autophagy and targeting with (+)-JQ1 does not lead to cell death in 501mel cells, as expected. While cell proliferation may not alter in A375M cells, perhaps there is a shift in cell fate from autophagy-independent caspase activation and cell death to senescence. This is possible as the relationship between senescence, apoptosis and autophagy is unclear and the three processes are much intertwined; however, blocking autophagy does not lead to a change in cellular fate in A375M.

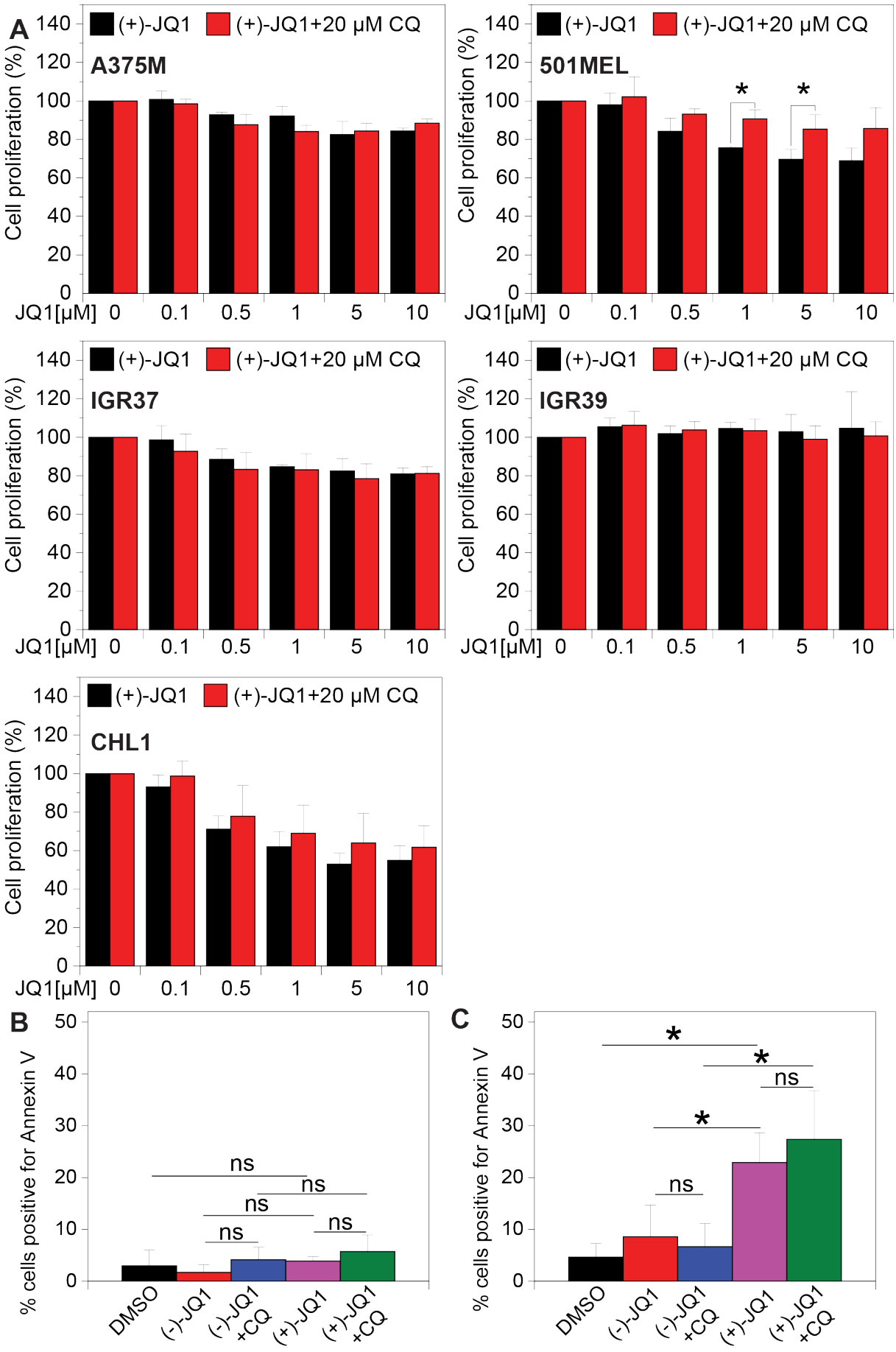

A
A375M
501MEL
IGR37
IGR39
CHL1
(+)-JQ1
(+)-JQ1+20 μM CQ
Cell proliferation (%)
JQ1[μM] 0 0.1 0.5 1 5 10
B
C
% cells positive for Annexin V
DMSO
(-)-JQ1
(-)-JQ1 +CQ
(+)-JQ1
(+)-JQ1 +CQ
ns
*

***Figure 3.14**: 501mel cellular proliferation is rescued following concomitant BET BRD and autophagy inhibition. (**A**) Cells were treated with indicated concentrations of (+)-JQ1 for 48 h, with (red bars) and without (black bars) 20 μM CQ. Cellular proliferation measured using MTT assay, with values normalised to proliferation observed when cells were treated without any treatment (black 0 μM bar) or with 20 μM CQ alone (0 μM red bar). N = 3 biological replicates. Mean cellular proliferation shown ± standard deviation. Statistical significance was determined using a two-tailed Students t-test. * = $p < 0.05$. Quantification of annexin V staining of cells following treatment with 1 μM (-)-JQ1 or (+)-JQ1 ± 10 μM CQ in 501mel cells (**B**) or A375M cells (**C**). Cells staining positive for annexin V are dead/dying cells. To control for effects of CQ, cells were treated with (-)-JQ1 (negative control of (+)-JQ1) with 10 μM CQ, and were compared with treatment with (-)-JQ1 alone. 0.01% v/v DMSO was also included as a negative control. N = 3 biological replicates. Mean percentage of cells stained positive for annexin V shown ± standard deviation. Statistical significance was determined using a two-tailed Students t-test. ns = non-significant difference.*

3.3 Discussion

In this chapter I have shown that melanoma cell lines exhibit divergent cellular fates following pharmacological BET BRD inhibition. While A375M cells undergo autophagy-independent apoptosis following (+)-JQ1 treatment, 501mel cells undergo senescence in an autophagy-dependent manner. However, it is intriguing that the more sensitive cell line, 501mel, underwent senescence rather than apoptosis, and the more resistant cell line, A375M, underwent apoptosis. It was interesting to note that 501mel cells underwent senescence following (+)-JQ1 treatment, as previously published work shows that treatment with 10 μM (+)-JQ1 led to *AMIGO2* mRNA down-regulation in this cell line [152]. Upon down-regulation of *AMIGO2* expression, 501mel cells exhibited caspase activation, PARP cleavage and cell death, establishing that 501mel cells underwent apoptosis following *AMIGO2* down-regulation, which is a result of BET BRD inhibition [152]. However, induction of apoptosis directly following (+)-JQ1 treatment was not shown [152]. Additionally, lentiviral knockout of *AMIGO2* led to drastic down-regulation of AMIGO2 protein expression, whereas (+)-JQ1 only induced modest down-regulation of AMIGO2; therefore, it is possible that this apoptosis is AMIGO2-dependent, but the direct link between (+)-JQ1 and AMIGO2-dependent apoptosis has yet to be shown [152].

Patients with melanomas harbouring p53 mutations have an increased overall survival from stage IV diagnosis compared with patients harbouring WT counterparts [260]. It is possible to speculate that p53 mutations *in vitro* may confer greater sensitivity to BET BRD inhibition; however, insufficient cell lines have been included in this study to confirm this. In this study, MITF expression appears to correlate with sensitivity; however, given that neither IGR37 nor IGR39 cellular proliferation is rescued following concomitant BET BRD and autophagy inhibition, it suggests that MITF expression does not determine whether the phenotype adopted by cells following BET BRD inhibition is autophagy-dependent or

not. As MITF does not correlate with sensitivity to BET BRD inhibition [94], the data shown in Table 3.1 should be expanded to include more melanoma cell lines before concluding that MITF signals sensitivity to BET BRD inhibition (Figure 3.1B). CHL1 proliferation was modestly, if statistically insignificantly, rescued following concomitant treatment with (+)-JQ1 and CQ (Chapter 7.3.1). While similar to 501mel cells, in that CHL1 cells harbour a p53 mutation [268], CHL1 cells are also BRAF WT [268, 326-329], whereas 501mel cells harbour mutant BRAF [270]. Therefore, this indicates that perhaps p53 mutation status correlates with cellular response to (+)-JQ1 irrespective of BRAF mutation status. Cell lines included in this study showed no variation in BRAF or NRAS genotypes; therefore, it is impossible to draw a conclusion about whether these factors correlate with sensitivity to BET BRD inhibition or not from the data in this thesis.

p53 mutations can be oncogenic gain of function, or can be loss of function and can have varying effects on p53 function [336]. p53 function doesn't always correlate with mutation; WT p53 and mutant p53 can exhibit very few differences in target gene expression [337]. Additionally, WT p53 doesn't guarantee p53 functionality [267]. PTMs of p53 may prevent normal functionality, for example, p53 is highly phosphorylated in melanoma cell lines compared with normal cell lines, which may inhibit p53 function [338]. Therefore, a greater surveillance of p53 function and transcriptional activity, rather than just mutation status, is required to understand fully the impact of p53 on the cellular response to BET BRD inhibition. However, the data presented in this chapter suggest that the cellular response to BET BRD inhibition correlates with p53 mutation status in melanoma; 501mel cells express mutant p53 and undergo autophagy dependent senescence, A375M cells express WT p53 and undergo apoptosis.

CDK4/6 inhibition leads to cell cycle arrest and activation of autophagy-dependent senescence induction in 1205Lu melanoma cells [339]. Crucially, while it has been suggested that p53 initiates cell cycle arrest during senescence [313], the 1205Lu cells did

not rely on p53 or p21 signalling for senescence induction [339]. Thus, it remains possible that, despite seemingly compromised p53 function and p21 expression, senescence is induced in p53 mutant melanoma cells. In a p53 WT colorectal cancer cell, HCT116, (+)-JQ1 treatment was shown to induce G1 cell cycle arrest and dramatic β-galactosidase staining. Despite a lack of evidence surrounding the reversibility of the effects of (+)-JQ1 on cell cycling, it was concluded that cells enter a state of senescence [340]. This suggests that p53 mutation status may not correlate with the adopted phenotype universally throughout solid cancers, but it remains possible this is the case in melanoma.

WT p53 melanoma cells can be resistant to apoptosis, even when WT p53 is over expressed in WT p53 cells [341]. However, the data presented here showed differential apoptotic gene up-regulation following (+)-JQ1 treatment, correlating with p53 mutation status (Figures 3.12A and 3.13A). A375M expresses WT p53 and high levels of MDM2, an inhibitor of p53 [267]. In this study, A375M cells still undergo apoptosis following BET BRD inhibition, so high MDM2 expression does not always equate to an inability of p53 to induce apoptosis. To determine if cells are dependent upon p53 function for apoptosis induction, treatment with an MDM2 inhibitor followed by a caspase activation assay could be used, with a greater induction of caspase activation expected as the outcome. Conversely, p53 mutations do not guarantee a total loss of p53 function and mutant p53 can retain the ability to regulate the expression of a subset of its target genes [342, 343]. In colorectal cancer cells, even the R273 hotspot mutation did not guarantee complete loss of p53 function [120, 344]. HT29 cells, which harbour a p53 R273H mutation [120, 344], display an increase in p21 RNA expression following JQ1-(+) treatment [340]. Thus, despite the seeming inability of p53 to up-regulate p21 protein expression levels, the impact of the C275W p53 mutation harboured by 501mel cells remains unclear.

There is more work that could be done to reinforce the notion that p53 mutation status determines cell fate following (+)-JQ1 treatment: firstly, only two cell lines were examined

in depth in this study. If more melanoma cell lines could be screened for either an apoptotic or senescent phenotype following (+)-JQ1, I would hypothesise that those harbouring p53 mutations, such as SK-Mel-28 [262, 268, 269], would undergo autophagy-dependent senescence, and those expressing WT p53 would undergo autophagy-independent apoptosis. Secondly, p53 expression could have been altered in A375M or 501mel cells in an attempt to carry out isogenic experiments to show the importance of the p53 mutation status on cellular response to BET BRD inhibition. I would attempt to introduce WT p53 into a p53 mutant cell line, and introduce mutant p53 into a WT p53 cell line, validate expression, and then test for apoptosis and senescence in response to (+)-JQ1. Finally, WT p53 expression does not necessarily confer functional p53 expression, which should be taken into account in the investigation into the role of p53 as a fate determinant [337]. Therefore, rather than being governed by p53 mutation status alone, perhaps cell fate may be determined in melanoma by p53 function, which could be affected by mutation status, but also additional factors such as PTMs and sub-cellular localisation [337, 345].

The role of autophagy seems to be inconsistent across melanoma cell lines following BET BRD inhibition. RNA-seq, qPCR and WB findings would suggest that both 501mel and A375M cell lines show activation of autophagy *in vitro* via transcriptional activation which culminates in LC3BII cleavage, indicative of autophagy activation (Figure 3.10-3.11). SQSTM1 was the only gene differentially regulated in both cell lines from the up-regulated gene sets in Figure 3.10A and 3.11A. This suggests that perhaps BET occupation of chromatin differs between cell lines, or perhaps autophagy is up-regulated through different mechanisms. The up-regulation of autophagy by (+)-JQ1 is an interesting notion, given that BETs are perceived as transcription activators, and thus, their displacement from chromatin would result in gene down-regulation. However, BET BRD inhibition up-regulates autophagy gene expression in pancreatic cancer [68]. Given that pan-BET

inhibition leads to autophagy gene up-regulation in 501mel and A375M cells (Figure 3.10-3.11), it is possible that BETs have a repressive role in regulating gene expression, an under-explored aspect of BET protein function.

In 501mel cells autophagy serves as the mechanism by which BET BRD inhibition induces senescence (Figure 3.14A), whereas in A375M cells this cellular process appears to be a bystander phenotype, in that its activation or perturbation does not seem to affect proliferation (Figure 3.14A), or apoptosis (Figure 3.14C). OIS is underpinned by autophagy in melanomagenesis, which is bypassed upon inhibition of autophagy [318, 319]. Interestingly, this work was carried out in cells closely related to A375M, A375 cells, which underwent senescence following up-regulation of autophagy, induced through treatment with rapamycin and over-expression of ATG5 [318]. In another study, loss of MAPK signalling induced by an aurora kinase inhibitor led to caspase activation, PARP cleavage, apoptosis and autophagy up-regulation in A375 cells [346]. However, inhibition of autophagy using CQ led to increased apoptosis; therefore, in this context autophagy was a cytoprotective response [346]. It is interesting to note that A375 cells can undergo either senescence or apoptosis upon autophagy activation [318, 346]. Therefore, perhaps the context in which autophagy is induced determines the cellular response. While the differing roles of autophagy in 501mel and A375M following (+)-JQ1 treatment could be due to p53 mutation status, it remains unclear how the p53 mutation governs the role of autophagy in response to BET BRD inhibition. Cytosolic p53 represses autophagy [257], and p53 mutants that reside in the cytoplasm to a greater extent than WT p53 have a greater repressive effect on autophagy [345]. It is unknown how the C275W mutation affects p53 sub-cellular localisation; however, this may shed light on how it may regulate autophagy.

Autophagy activation may play a role *in vivo*. Autophagy stimulates the release of immunogens HMGB1, ATP and calreticulin that stimulate clearing of cancer cells by immune cells [347, 348]. This suggests perhaps *in vivo* 501mel- and A375M-like tumours

would regress as a result of subsequent immunogenic stimulation and immune clearing, in addition to tumour loss due to the BET BRD inhibitor-induced senescence and apoptosis. There is evidence in non-small cell lung cancer that combination of (+)-JQ1 and immune checkpoint inhibitor anti PD-1 treatment leads to greater tumour regression and immune cell stimulation compared with (+)-JQ1 alone [349]. Additionally, in prostate cancer (+)-JQ1 up-regulated gene expression of proteins involved in the antigen presentation pathway, and the combination of (+)-JQ1 with immune checkpoint inhibitor anti-CTLA4 therapy led to significantly increased murine survival when compared with (+)-JQ1 treatment alone [350]. Given the promise of immunotherapy in melanoma, this could be a therapeutic strategy worth exploring in future.

BET family members have a common domain architecture, with the CTM as an exception, only expressed by BRD4 and BRDT. This domain is responsible for the recruitment of PTEF-b [37]. The transcriptional data presented in this chapter suggest that inhibition of cell cycle progression (Figures 3.6-3.8) and activation of apoptosis (Figure 3.12) arise following transcriptional modulation. These findings are in line with previously published data showing BET BRD inhibition leads to down-regulation of cell-cycle-related gene sets in melanoma [151]. Given that BETs regulate each other's expression and complex formation, it is difficult to tease apart individual functions. Having attempted to do this by knocking down individual BETs and analysing the transcriptomes from these samples, it seems as though BETs have non-redundant roles in melanoma (Figure 3.6). Figure 3.6 indicates that the inhibitory effects of (+)-JQ1 are propagated through both BRD2 and BRD4 to similar extents in both 501mel and A375M.

The data I have presented show that the knockdown of BRD4 leads to the down-regulation of cell cycle related gene sets in A375M (Figure 3.7), yet BRD2 appears to be responsible for driving apoptotic gene expression (Figure 3.12B). While BRD3 inhibition led to the reduction of cell growth in a panel of 342 cancer cell lines [36], BRD3 appears to have little

input in 501mel or A375M cells, nor does it mediate the effect of (+)-JQ1 (Figure 3.6), and in 501mel, knockdown of BRD2 appears to have opposing effects on cell cycle regulated gene sets compared with BRD4 knockdown (Figure 3.8C). In terms of cell cycle arrest, it could be argued that BRD4 attenuation dominates the phenotype in 501mel, as BRD2 inhibition leads to up-regulation of cell cycle related genes, contrary to the action of BRD4, yet cell cycle arrest is induced nonetheless. However, Figures 3.8C and 7.2 show that there may be further uncovered functions of BRD2. Overall, these findings suggest that BRD2 may have an unexplored role in driving malignancy, and that the pan-BET transcriptional phenotype in these cell lines is not driven by BRD4 alone. Despite the role of BRD4 in promoting PTEF-b-dependent transcription [37], and a range of cancers [90, 92, 100], the data in this thesis indicate that perhaps less of an emphasis should be placed on efforts to target BRD4 specifically, rather alternative targeting methods that simultaneously attenuate all members of the BET protein family should be sought.

While the exact mechanism by which the BETs work in concert remains to be clarified, the data I have presented show that BETs may have distinct roles in melanoma, and suggests that the transcriptional and phenotypic output of pan-BET inhibition is a summation of their intertwined molecular functions. This indicates that inhibitors targeting individual BETs may not elicit the desired anti-proliferative effects. Rather, efforts of more precise targeting of BETs should be focussed on targeting of individual shared domains. Collectively, the data in this chapter demonstrate that melanoma cell lines exhibit different cellular responses following BET BRD inhibition, potentially due to p53 mutations. BET BRD inhibition leads to autophagy up-regulation in two melanoma cell lines, the consequences of which correlate with p53 mutation status, but the determinants of the cellular response to BET BRD inhibition remain to be defined.

Chapter 4: Mechanism of action induced by novel BET BRD inhibitor in prostate cancer

4.1 Introduction

BET BRD inhibition is a promising therapeutic strategy for preventing the progression of many malignancies. However, the mechanism by which BET BRD inhibition causes a loss of tumour growth requires further elucidation in many malignancies. In Chapter 3, I provided more clarity on the melanoma cellular response to BET BRD inhibition. In addition to melanoma, prostate cancer is another example of solid malignancy which represents an area of need, to which BET BRD inhibition could offer a solution.

Prostate cancer is the second most common cancer in men and, therefore, represents a significant clinical challenge [165]. The reliance of prostate malignancies upon the androgen receptor (AR) signalling cascade for tumour growth and progression has been exposed as an exploitable vulnerability [351, 352]. Since androgen deprivation therapies block the testosterone receptor and reduce AR signalling, this treatment strategy often shows initial success and current strategies for tackling this malignancy centre around hormonal therapies [353, 354]. However, patients with advanced malignancy almost inevitably progress to incurable castration resistant prostate cancer, whereupon AR is over-expressed [353]. Additionally, AR-V7, a splicing variant of AR that lacks the ligand-binding domain, can carry out transcriptional activity without hormonal stimulation and regardless of androgen-deprivation therapies [355-357]. Together, over-expression of AR and the expression of the AR-V7 variant render many prostate malignancies resistant to androgen deprivation therapies.

This mechanism of resistance to androgen deprivation therapies exposes a different vulnerability of these tumours. AR over-expression promotes chromatin decompaction,

which in turn enables gene expression and AR binding to chromatin [358]. AR over-expression also leads to BRD2 and BRD4 over-expression, further exacerbating the aberrant over-expression of AR target genes, which indicates a reliance on BET protein function [358]. Accordingly, expression of the AR variant, AR-V7, drops following BET BRD inhibition, and is accompanied by loss of viability *in vitro* and in murine models [34, 147]. Indeed, high levels of BRD4 expression in patients correlate with a worse survival rate, suggesting BETs contribute to driving malignancy [147]. Conversely, cell lines that are negative for AR signalling appear to be resistant to BET inhibition [34]. However, AR mRNA expression does not directly translate to sensitivity of prostate cancer cell lines to BET BRD inhibition [34, 146, 147, 358]. Thus, AR protein correlates with sensitivity but mRNA does not.

In vitro data demonstrate that AR lies upstream of BET function, and BET inhibition leads to the down-regulation of AR target genes *in vitro* and *in vivo*, including MYC and the oncogenic fusion TMPRSS2-ERG [34, 147]. Nevertheless, MYC expression does not correlate with (+)-JQ1 sensitivity and there are discrepancies surrounding the sufficiency of siRNA-mediated MYC knockdown to recapitulate loss of cell viability, indicating BET BRD inhibition acts through MYC-dependent and MYC-independent means [34, 146, 147]. Accordingly, MYC over-expression does not protect prostate cancer cells [34]

While the mechanism by which BET inhibition leads to a loss of cell viability appears to have been partially elucidated in prostate cancer, the problem of toxicity persists. Multiple clinical trials have recorded adverse effects following treatment with BET BRD inhibitors [91, 161, 359]; therefore, a strategy to avoid toxicity whilst still targeting the BET proteins is highly sought after. An investigation into the emergence of resistance mechanisms showed that BET inhibition as a monotherapy may lead to BET-independent AR gene expression, suggesting BET inhibitors may lead to more durable tumour regression if used as part of a combinatorial regimens [360].

In an attempt to reduce toxicity whilst still targeting BET BRDs, a novel inhibitor template, which aims to exploit targeted delivery to prostate cancer cells, was developed (the final compound will be referred to as RT53). This novel compound was built on the previously disclosed benzo-diazepine chemotype I-BET762 [72], which is referred to as RT20 throughout this thesis. To ensure this targeting is best utilised in future, a thorough understanding of its biological effects and the mechanism of loss of cell viability is needed. Therefore, as part of a wider collaboration, I have investigated the mechanism by which this novel BET BRD inhibitor (RT53) acts upon prostate cancer cells *in vitro*. In addition, the data presented in Chapter 3 show that BET BRD inhibition leads to autophagy up-regulation in two melanoma cells lines. This chapter will also serve to determine whether autophagy up-regulation in response to BET BRD is melanoma-specific, or perhaps whether this could be a response shared by other solid cancers. In doing so, I will provide rationale for a novel combinatorial treatment strategy for prostate cancer.

4.2 Results

4.2.1 Novel BET BRD inhibitor leads to enhanced loss of cellular proliferation *in vitro* in prostate cancer cells

To establish a mechanism for loss of cellular proliferation, it was first necessary to establish cells were, indeed, arresting growth *in vitro*. In these initial investigations, two cell lines were used, PC3 and LNCaP. Published data demonstrate that PC3 cells do not utilise AR signalling, unlike LNCaP cells [34], rendering the former resistant to BET BRD inhibition and the latter sensitive. Therefore, it was expected LNCaP cells would exhibit higher sensitivity to RT53, compared to PC3. RT20 is used as a positive control, as it is already known to reduce malignancy growth in a range of models through BET BRD inhibition [34, 146].

In addition to AR signalling, p53 genotyping may affect the sensitivity of cells to BET BRD inhibition, or the phenotype adopted following treatment with BET BRD inhibitor. p53 mutation status correlates with the phenotype adopted by melanoma cells following BET BRD inhibition (Figures 3.13-3.14), and since high p53 expression correlates with poor clinical outcome and p53 is mutated in over 20% prostate cancers [361, 362], it remains possible that p53 may have an effect in prostate cancer. The expression status of p53 was examined, and Figure 4.1A shows that LNCaP cells express WT p53, and PC3 cells express mutant p53. This may relate to their sensitivity or cellular response to RT53.

To examine sensitivity to RT53, briefly, cells were treated with 0, 0.5 or 1 μM RT20 or RT53 for 12 days, after which they were stained using crystal violet. Figures 4.1C and 4.1D shows that the viability of PC3 cells was not significantly affected by RT20; however, there was a significant loss in cell viability after treatment with 1 μM RT53. The same observation was made when this experiment was carried out using LNCaP cells (Figure

4.1E-4.1F). However, there are limitations associated with crystal violet assays. Staining cells using crystal violet staining relies upon proliferating cells adherence to the plastic well withstanding the fixation step and many washing steps. LNCaP cells detach notoriously easily from plastic wells, and the many washing steps in crystal violet staining protocols result in the displacement of otherwise adherent cells from the plastic wells [363]. This happens most when LNCaP cells are very confluent; the more confluent the cells, the more easily they detach; thus, interpreting the crystal violet assay results is difficult.

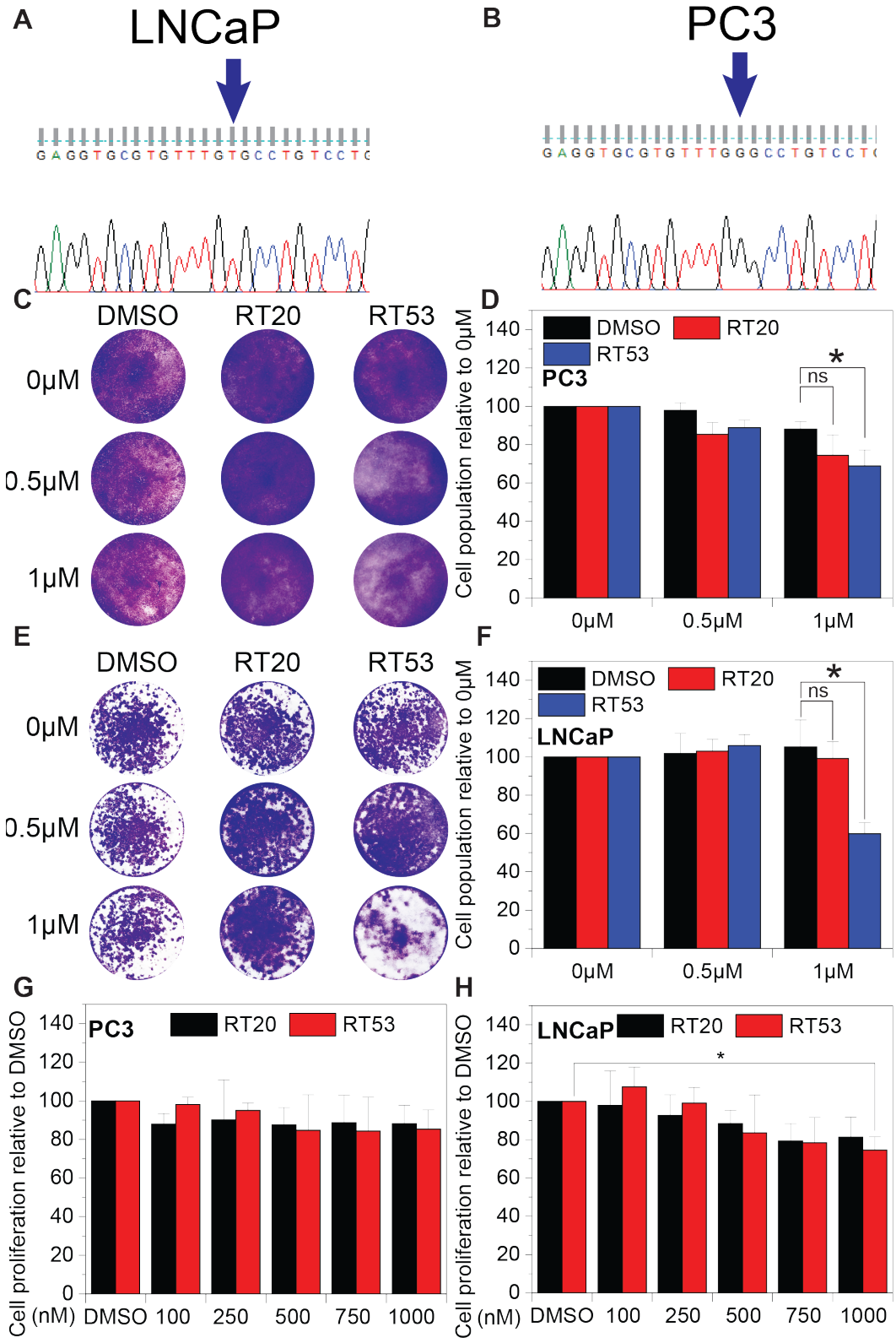


***Figure 4.1**: RT53 leads to enhanced loss of cellular proliferation in vitro in prostate cancer cells. (**A**) Sequencing results showing p53 genotype of LNCaP cells. LNCaP cells express WT p53. Arrows show site of mutation in PC3 and WT base in LNCaP cells. (**B**)*

*Sequencing results showing p53 genotype of PC3 cells. PC3 cells express mutant p53. Arrows show site of mutation in PC3 and WT base in LNCaP cells. (**C**) Representative images of crystal violet-stained wells following the indicated treatments in PC3 cells in 10% FBS medium. 0.01% v/v DMSO was included as a negative control. (**D**) Crystal violet quantification following treatment with RT20 and RT53 for 12 days in PC3 cells in 10% FBS medium. N = 3 biological replicates. 0.01% v/v DMSO was included as a negative control. Mean cellular proliferation relative to 0 μM shown ± standard deviation. Statistical significance was determined using a two-tailed Students t-test. * = p < 0.05. (**E**) Representative images of crystal violet-stained wells following the indicated treatments in LNCaP cells in 10% FBS medium. 0.01% v/v DMSO was included as a negative control. (**F**) Crystal violet quantification following treatment with RT20 and RT53 for 12 days in LNCaP cells in 10% FBS medium. 0.01% v/v DMSO was included as a negative control. N = 3 biological replicates. Mean cellular proliferation relative to 0 μM shown ± standard deviation. Statistical significance was determined using a two-tailed Students t-test. * = p < 0.05. (**G**) PC3 cells were treated for 48 h with indicated concentrations of RT20 and RT53. N = 3 biological replicates. Proliferation normalised to DMSO (0.01% v/v) proliferation value. Mean cellular proliferation shown ± standard deviation. Statistical significance was determined using a two-tailed Students t-test. * = p < 0.05. (**H**) LNCaP cells were treated for 48 h with indicated concentrations of RT20 and RT53. N = 3 biological replicates. Proliferation normalised to DMSO (0.01% v/v) proliferation value. Mean cellular proliferation shown ± standard deviation. Statistical significance was determined using a two-tailed Students t-test. * = p < 0.05.*

To confirm this observation from the crystal violet assay in an orthogonal manner, an MTT assay was carried out, in which PC3 and LNCaP cells were treated with increasing concentrations of RT20 and RT53. Figure 4.1G shows that the crystal violet observations from Figures 4.1C-4.1D could not be recapitulated, suggesting that PC3 is not sensitive to

BET inhibition. LNCaP cells showed a significant loss of cell viability when treated with RT53 (Figure 4.1H), suggesting that these cells are, indeed, more sensitive to BET inhibition via RT53 than PC3. Overall, these data demonstrate that RT53 is a more potent inhibitor than RT20 *in vitro* in both LNCaP and PC3 cell lines (Figure 4.1C-4.1F) and LNCaP, the AR-signalling-positive cell line [34], is a more sensitive cell line to RT53 than the AR-signalling-negative cell line [34], PC3. It appears that WT p53 may correlate with sensitivity of prostate cancer cell lines to BET BRD inhibition; however, more cell lines would need to be tested in order to confirm this. Having established that RT53 leads to loss of cell viability *in vitro*, the next investigation was to establish the mechanism by which this occurs.

4.2.2 Loss of cellular proliferation induced by novel BET BRD inhibitor is independent of cell death in prostate cancer

Loss of cellular proliferation can often indicate cell death. To ascertain how RT53 leads to loss of cellular proliferation in LNCaP cells, the more sensitive of the two cells lines tested in Figure 4.1, cells were examined for activators of apoptosis. Apoptosis is a form of cell death, and activation of apoptotic signalling can be indicated by PARP cleavage [211, 214]. BET BRD inhibition mediated by (+)-JQ1, another chemically distinct pharmacological BET BRD inhibitor, leads to the up-regulation of apoptotic signalling, including PARP cleavage in LNCaP cells [34], hence the selection of the apoptotic marker in this experiment.

LNCaP cells were treated with RT20, RT53 and (+)-JQ1 for the indicated times (Figure 4.2). (-)-JQ1 was used as a negative control for (+)-JQ1 as it is the negative stereoisomer of (+)-JQ1, and thus, does not bind to BET BRDs. DMSO was used as negative control with regards to both BET BRD inhibitors, as it is the solvent in which both inhibitors are dissolved. GAPDH is used as the loading control; it has been used previously investigating

the role of BET attenuation in prostate cancer [34, 147]. Given that (+)-JQ1 treatment leads to PARP cleavage in LNCaP cells [34], it used as a positive control. Figure 4.2 shows that 48 h of (+)-JQ1 treatment induces PARP cleavage, whereas 24 and 48 h of treatment with RT20 or RT53 fails to do so.

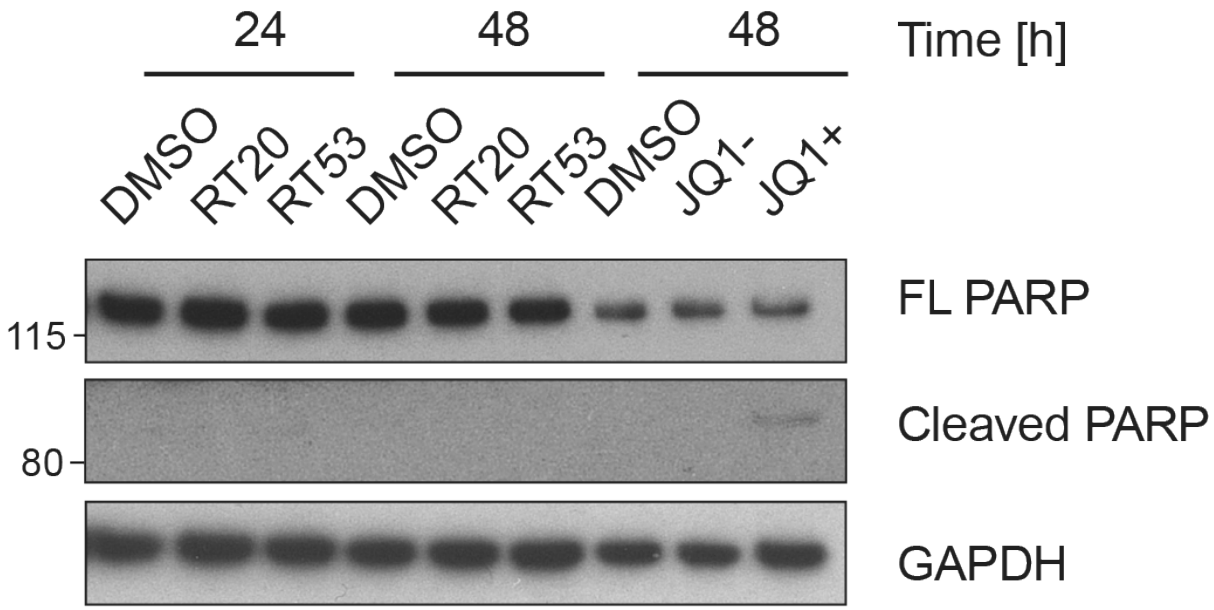


***Figure 4.2**: Immunoblot showing that neither RT20 nor RT53 induce PARP cleavage in LNCaP cells. Cells were treated with 24 or 48 h, as indicated, with 1 μM RT20 or RT53. Cells were also treated with 1 μM (-)-JQ1 or (+)-JQ1. Cells were treated with 0.1% DMSO v/v as a negative control.*

These results are not surprising, as (+)-JQ1 leads to PARP cleavage in LNCaP cells, whereas RT20 does not [34, 146]. The discrepancy in PARP cleavage induction may relate to differences in cell permeability, or perhaps quantities of inhibitors used, as RT20 and RT53 can both form racemic mixtures, as the Kd values of the BET BRD inhibitors are very similar (Table 4.1). Perhaps if the quantities of RT20 and RT52 were increased, PARP cleavage may also be observed.

Compound	Kd
(+)-JQ1	50 nM, first BRD of BRD4, 90 nM, second BRD of BRD4 [71]
RT20	52 nM [72]. In our hands, BRD4/BD1: 42 nM and BRD4/BD2: 62 nM*
RT53	BRD4/BD1: 14 nM and BRD4/BD2: 21 nM*
Table 4.1: Kd values of BET BRD inhibitors. * = Courtesy of Dr Sarah Picaud	

Further investigations into cell death were planned (see Chapter 7.3.2); however, Figure 4.2 indicates that while (+)-JQ1 elicits PARP cleavage, treatment with neither RT53 nor RT20 does. Further investigations into the mechanism by which RT53 causes loss of cellular proliferation are required.

4.2.3 Loss of prostate tumour growth is independent of loss of AR signalling

Our collaborators showed that LNCaP tumours *in vivo* regress in response to RT53 treatment (data not shown). Our collaborators have also been investigating the possibility of targeting RT53 specifically to prostate cancer cells, and have trialled the resulting compounds in murine models. Tumours regressed most dramatically when RT53 was targeted to the prostate cancer tumour (data not shown). The targeted inhibitor has the RT53 warhead but has an additional cleavable module that is cleaved upon inhibitor entry into specifically prostate cancer cells. This leads to elevated concentrations of the inhibitor in prostate cancer cells compared with non-malignant cells, which enables the circumventing of toxicity.

To understand more fully how the tumours regress, which would help to shed light on how cells die *in vitro* following treatment with RT53, the mice were sacrificed and RNA was extracted from the tumours, which was sent to me. I converted the RNA to cDNA, and ran

qPCR, with the aim of examining whether treatment with RT53, whether targeted or not, led to the reduction of AR or AR-V7 expression, and downstream signalling. Expression of genes was normalised to 18S rRNA expression, which is routinely used as an internal control in qPCR experiments [285], and then to expression values of genes of interest from control xenografts, treated with vehicle. SDHA expression was measured as an additional control, as it has been published that BET BRD inhibition does not lead to a change in SDHA expression [152]. AR-V7 is a splice variant of AR and is generated through the splicing of exon 3 to cryptic exon 3, which forms a unique C-terminal domain and lacks the ligand binding domain, which renders it impervious to the effects of androgen deprivation therapies [356, 364]. It is associated with unique transcriptional activity that promotes cellular proliferation, and its expression is associated with poor patient prognosis and resistance to androgen deprivation therapies [364-366]. BET BRD inhibition has been previously described to lead to down-regulation of AR-V7 and downstream signalling *in vitro*, including loss of MYC expression; therefore, it is possible that this is the mechanism by which RT53 acts [147].

Figure 4.3A shows that RT53 does not cause down-regulation of FL *AR* (as denoted by AR-FL -1 and -2 as two pairs of primers were used to detect AR expression), *AR-V7* (as denoted by AR-V7 -1 and -2 as two pairs of primers were used to detect AR-V7 expression), *ETV-1*, or *MYC*, whether targeted or not. ETV-1 is a transcription factor whose expression can be driven by AR and forms oncogenic fusions with TMPRSS2 and ERG in prostate cancer [367, 368]. The tumours harboured by mice are formed through injection of LNCaP cells, which do not express AR-V7 [355, 357]; therefore, it is not a surprise that *AR-V7* expression does not decrease further with RT53 treatment, rather *AR-V7* and FL *AR* increase in expression, which is unexpected. The data presented in Figure 4.3A suggest that RT53 does not act through disruption of AR signalling, given that both variants of AR and two downstream targets, *MYC* and *ETV-1*, do not decrease in

expression, whether RT53 is targeted or not. In fact, AR, both FL and -V7, increase in expression following treatment; therefore, an alternative mechanism of action accounts for tumour regression.

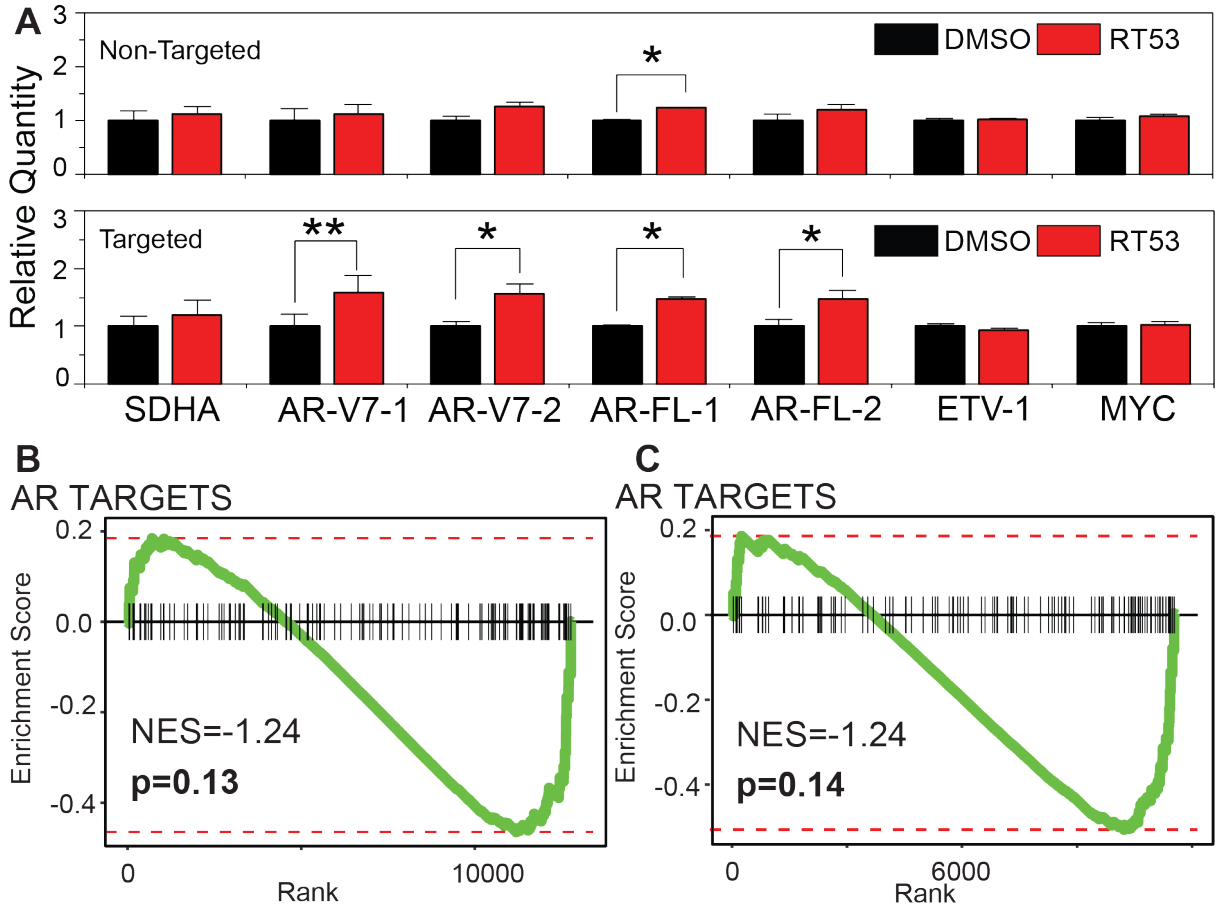


***Figure 4.3**: AR expression is not perturbed in vivo by RT53, and AR target expression is not significantly differentially regulated by RT53 in vitro. (**A**) qPCR following RT53 treatment in mice using RNA extracted from tumours. Top panel shows expression in xenograft following treatment with non-targeted RT53. Bottom panel shows expression in xenograft following treatment with targeted RT53. Two individual sets of primers were used that targeted an AR splice variant, AR-V7 (AR-V7 -1, and -2) and FL AR (AR-FL -1 and -2). In both panels, black bars represent expression in tumours treated with the control compound, DMSO, and the red bars represent expression in tumours treated with non-targeted (upper) or targeted (lower) RT53. Expression normalised to 18S rRNA expression, and then to the expression of the gene of interest in control xenografts. Mean*

*expression values shown, ± standard deviation. N = 3 biological replicates. Statistical significance was determined using a two-tailed Students t-test. * = p < 0.05, ** = p < 0.01. Collaborators carried out cell treatment and sample harvesting and sequencing. I carried out RNA-seq data analysis. GSEA of the previously defined AR targets signature [34] in LNCaP cells following 48 h treatment with (**B**) RT53 or (**C**) RT20. NES = normalised enrichment score. P value represents adjusted p value.*

Our collaborators collected mRNA samples and performed RNA-seq following treatment of LNCaP with RT20 and RT53 for 48 h. Analysis of this data shows that AR targets are not significantly regulated following RT53 (Figure 4.3B) or RT20 (Figure 4.3C). This is in agreement with the *in vivo* data, which suggests that AR signalling is not perturbed by RT53. However, LNCaP cells down-regulate AR targets in response to (+)-JQ1 treatment [34], which further highlights the differences between the BET BRD inhibitors, which was discussed in Chapter 4.2.2.

4.2.4 BET BRD inhibition leads to up-regulation of autophagy in LNCaP cells

In Chapter 3 it was established that BET BRD inhibition in melanoma cell lines led to up-regulation of autophagic flux. It is also possible that the same occurs in this malignant context. As outlined in Chapter 3.2.4, autophagy is a response to cellular stress, normally in the form of nutrient deprivation [296].

Further analysis of the RNA-seq data generated by our collaborators shows that RT53 lead to up-regulation of autophagy-related gene sets in LNCaP cells (Figure 4.4A and 4.4B). mTORC1 signalling regulates protein anabolism and catabolism [310]. Under nutrient rich conditions, mTORC1 increases translation and decreases lysosome biogenesis and autophagy through ULK1 serine 757 phosphorylation [309, 310]. Under starvation conditions, this phosphorylation mark on ULK1 is lost; thus, protein catabolism is promoted; therefore, a reduction of mTORC1 signalling is indicative of increased

autophagic signalling [310]. Formation of the autophagosome is a central process in autophagy; therefore, its up-regulation is also indicative of increased autophagic signalling [305]. Encouragingly, RT20 also elicits similar transcriptomic changes (Figure 4.4C-4.4D). Therefore, autophagy up-regulation potentially plays a role in mediating the effects of RT53 treatment.

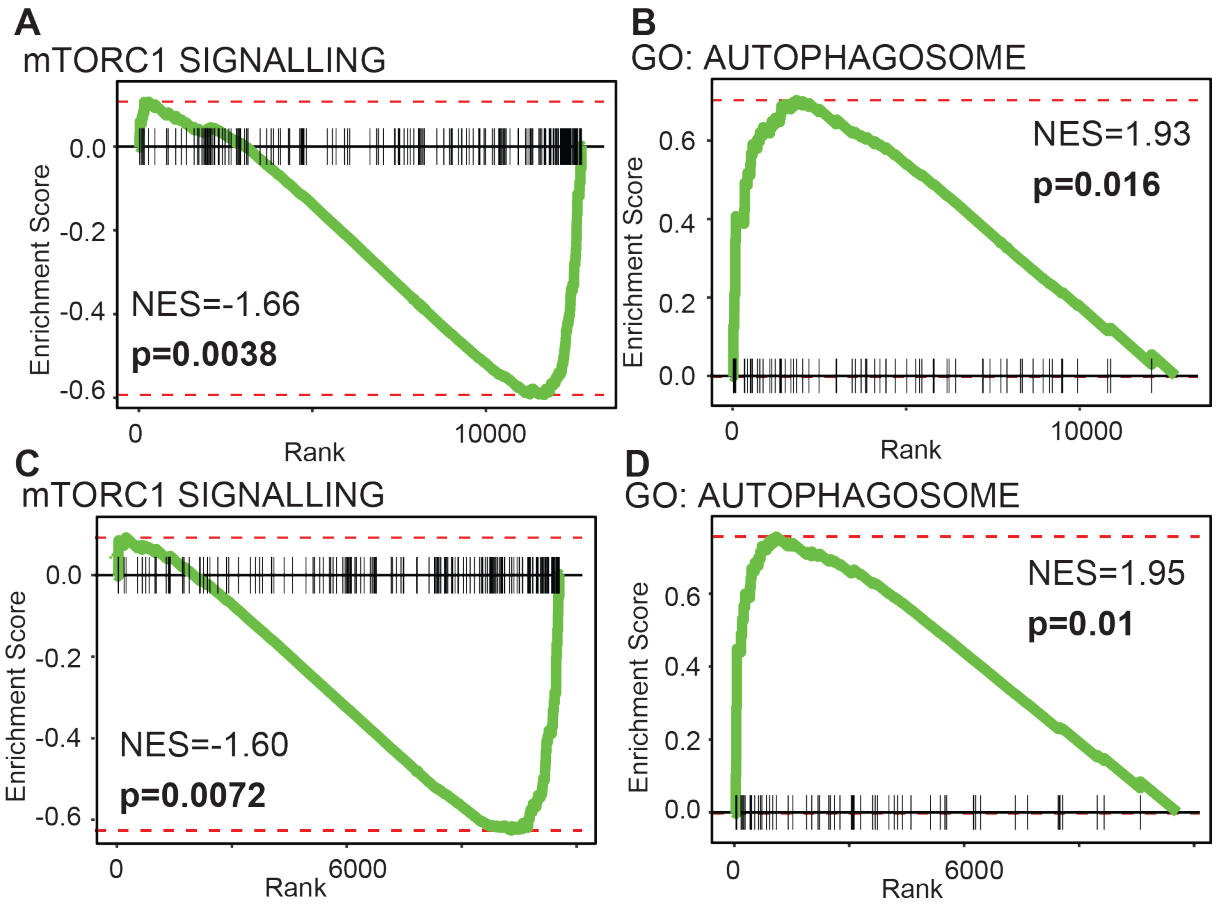
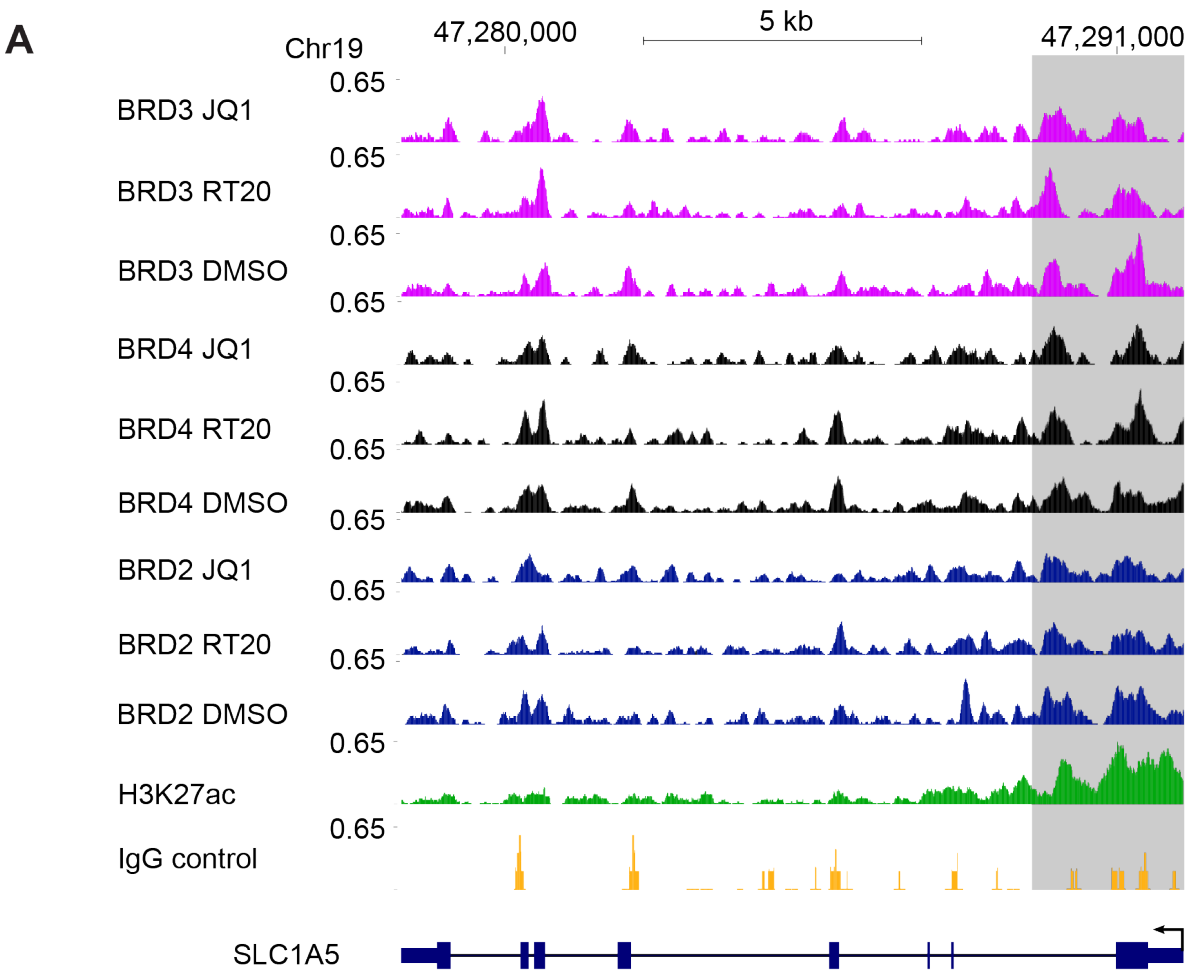


***Figure 4.4**: RT53 or RT20 treatment leads to up-regulation of autophagy-related gene sets. LNCaP cells treated with RT53 and RT20. Collaborators carried out cell treatment and sample harvesting and sequencing. I carried out RNA-seq data analysis. GSEA plots of autophagy-related gene sets ("HALLMARK_MTORC1_SIGNALING" and "GO_AUTOPHAGOSOME"), either following 48 h treatment with RT53 in LNCaP cells compared with DMSO (**A**) and (**B**), or following 48 h treatment with RT20 in LNCaP cells compared with DMSO (**C**) and (**D**). Computational analysis was carried out using DESeq2*

[243] to identify differentially expressed genes, which were used for GSEA analysis in R [244]. NES = normalised enrichment score. P value represents adjusted p value.

Autophagy can be stimulated by the loss of SLC proteins. SLC1A5 is a solute channel that transports L-glutamine into the cell. SLC7A5 forms a heterodimer with SLC3A2 and together they enable the export of L-glutamine in exchange for extracellular L-leucine [297]. Down-regulation of SLC1A5 or SLC7A5/SLC3A2 can lead to a deficit of amino acids, which leads to loss of phosphorylation of mTOR and subsequent up-regulation of autophagy [297, 298]. BET inhibition may induce autophagy through the displacement of BETs from SLC1A5 or SLC3A2 gene promoters, thereby resulting in a reduction in SLC1A5 and SLC3A2 expression. To confirm whether or not BETs occupy these promoters, and if so, are displaced following BET BRD inhibition, previously published ChIP-sequencing (ChIP-seq) data was analysed. ChIP-seq experiments were carried out in VCaP prostate cancer cells, examining BRD -2, -3, and -4 occupation of chromatin in the absence and presence of BRD inhibitors [34].

Figure 4.5A shows that BET BRD inhibitors (+)-JQ1 and RT20 displace BRD -2 and -3 from the SLC1A5 gene. Figure 4.5B shows that BET BRD inhibition displaces BRD -2, -3 and -4 from the upstream peak, and BRD -2 and -3 are displaced from the downstream peak of SLC3A2. Interestingly, BRD4 occupation of chromatin only appears to be minimally disrupted in the case of both genes, rather BRD3 occupation is most disrupted. This suggests that BRD3 regulates SLC1A5 and SLC3A2 gene expression in VCaP cells, which is a novel notion, as the role of BRD3 in prostate cancer remains largely elusive. Since this experiment was conducted in VCaP cells, the results may be context specific; however, it suggests that BET displacement from chromatin may account for loss of SLC expression and any subsequent autophagy activation in LNCaP cells.


A
Chr19
47,280,000
5 kb
47,291,000
BRD3 JQ1
BRD3 RT20
BRD3 DMSO
BRD4 JQ1
BRD4 RT20
BRD4 DMSO
BRD2 JQ1
BRD2 RT20
BRD2 DMSO
H3K27ac
IgG control
0.65
SLC1A5

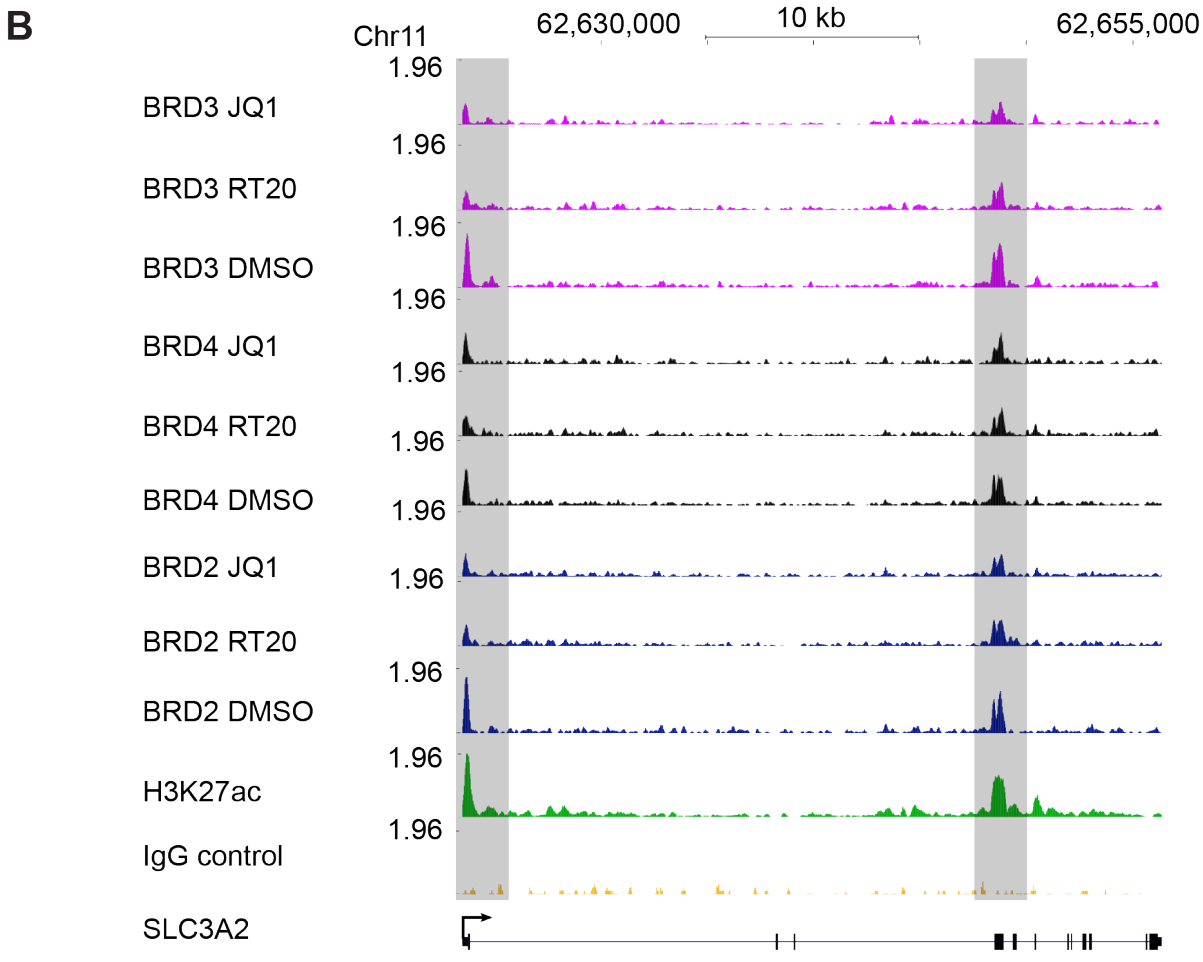

B
Chr11
62,630,000
10 kb
62,655,000
BRD3 JQ1
BRD3 RT20
BRD3 DMSO
BRD4 JQ1
BRD4 RT20
BRD4 DMSO
BRD2 JQ1
BRD2 RT20
BRD2 DMSO
H3K27ac
IgG control
1.96
SLC3A2

***Figure 4.5**: BET occupation of SLC1A5 and SLC3A2 genes is perturbed by BET BRD inhibitors. Previously published data from [34]. Briefly, VCaP cells were treated for 12 h with 500 nM (+)-JQ1 or RT20, with DMSO as the negative control. Cells were cross-linked and lysed before ChIP DNA was isolated. (**A**) BRD -2, -3, -4 occupation of the SLC1A5 gene, when cells were treated with (+)-JQ1 or RT20. (**B**) BRD -2, -3, -4 occupation of the SLC3A2 gene, when cells were treated with (+)-JQ1 or RT20. Grey box indicates H3K27ac peaks. IgG track shown as control.*

To confirm that autophagy is up-regulated following RT20 and RT53 treatment, protein expression levels of components of the autophagic pathway were analysed using immunoblotting. Of the two surveyed cell lines in Figure 4.1, LNCaP cells were the most responsive to RT53. Therefore, these cells were used to investigate the effects of this novel inhibitor. Cells were treated with 1 μM RT20 or RT53, for 48 h. DMSO was used as a negative control. RT20, also known as I-BET762 [72] was included for comparison with RT53. GAPDH is the loading control used in this experiment, as it has been used previously investigating the role of BET attenuation in prostate cancer [34, 147].

It was first ascertained whether SLC1A5 or SLC3A2 expression changed in response to BET BRD inhibition. Figure 4.6A shows that the expression of SLC1A5 and SLC3A2 is down-regulated when cells are treated with RT20 and RT53. Quantification in Figure 4.6F shows that only RT53 down-regulates both solute channels significantly; however, this suggests the autophagic pathway may be activated due to displacement of BETs from SLC1A5 and SLC3A2 promoters (Figure 4.5), whereupon SLC1A5 and SLC3A2 expression is lost [369, 370]. This is in concordance with previously published data showing treatment with BET BRD inhibitors or BRD4 knockdown led to a decrease in SLC3A2 mRNA expression in breast and lung cancer cell lines [371].

The aim of the immunoblots in Figures 4.6B-4.6E was to trace the activation of autophagic signalling. The next level down in the signalling cascade are events leading to a loss of mTOR phosphorylation. There are several ways in which loss of mTOR phosphorylation can be achieved, one of which is through AKT. AKT is activated through phosphorylation by the mTORC2 complex [372], which in turn phosphorylates tuberin (TSC2) at threonine 1462. This phosphorylation mark on TSC2 is inhibitory to its function, and prevents it from acting as a suppressor of mTOR [373, 374]. When activated, the TSC2 complex inhibits mTOR phosphorylation and activation [374]. Thus, TSC2 T1462 phosphorylation inhibits the TSC2 complex, resulting in mTOR phosphorylation and activation [374]. If mTOR phosphorylation is lost via this mechanism, a loss of AKT phosphorylation and a decrease in TSC2 T1462 phosphorylation would be expected.

However, from this point onward the transduction of the autophagic signalling cascade is less clear. Figure 4.6B shows there is an increase in AKT phosphorylation, and Figure 4.6C shows there is loss of mTOR phosphorylation, and there is a concomitant reduction in pTSC2 T1462. It is not surprising a loss of TSC2 phosphorylation coincides with loss of mTOR phosphorylation; however, the concomitant increase in AKT phosphorylation is unexpected and suggests that the loss of phosphorylation occurs in an AKT-independent manner. Quantification in Figure 4.6F shows that the up-regulation of AKT phosphorylation and down-regulation of pTSC2 1462 are non-significant across multiple biological replicates, suggesting that this arm of signalling is not significantly perturbed by RT20 or RT53 treatment.

Another way in which loss of mTOR phosphorylation is achieved is through AMPK phosphorylation and subsequent activation. AMPK phosphorylation and activation under conditions of nutrient deprivation results in subsequent phosphorylation of TSC2 S1387, which serves as an activation signal for the TSC2 complex [375-377]. When activated, the TSC2 complex inhibits the activation and phosphorylation of mTOR [375, 378]. Figure

4.6C shows that despite loss in mTOR phosphorylation, there is neither an increase in AMPK phosphorylation, nor TSC2 S1387 phosphorylation, suggesting that mTOR phosphorylation loss and the activation of the autophagy signalling cascade is AMPK-independent [379]. In fact, quantification of AMPK signalling in Figure 4.6F shows that there was no significant change in AMPK expression or phosphorylation, and TSC2 S1387 phosphorylation decreases with RT20 treatment, although is not significantly changed following RT53 treatment. These findings further suggest that loss of mTOR phosphorylation is independent of AMPK signalling.

An alternative explanation is that mTOR phosphorylation status can be directly affected by amino acid deprivation through Rag-GTPases [380]. When amino acids are abundant, mTOR is phosphorylated and activated by Rag-GTPases; when amino acids are depleted, mTOR phosphorylation is lost [380]. This possible explanation could account for the down-regulation of SLC1A5 and SLC3A2 and loss of mTOR phosphorylation without clear signalling in between via AMPK or AKT. A statistically significant decrease in mTOR phosphorylation follows RT53 treatment, demonstrating that although the cause this is unclear, RT53 disrupts autophagic signalling.

Downstream of loss of mTOR phosphorylation, in the event of autophagy up-regulation, loss of p70S6K phosphorylation [381], changes in ULK phosphorylation [309, 382]and up-regulation of Beclin1 expression [383, 384] are expected. However, only a modest decrease in p70s6k phosphorylation can be seen in Figure 4.6C, which is non-significant (Figure 4.6F). However, there is a decrease in p70s6k expression following RT53 treatment, suggesting RT53 perturbs p70s6k expression rather than phosphorylation.

Loss of mTOR phosphorylation and autophagy activation should coincide with a loss of ULK1 S757 phosphorylation [309], and an increase in ULK1 S555 phosphorylation [382]. However, no changes in ULK1 phosphorylation or expression are observed (Figure 4.6D,

4.6F). Additionally, no change in Beclin1 expression is observed, despite its necessity in autophagy up-regulation (Figure 4.6E-4.6F) [383, 384]. The lack of change in p70S6K phosphorylation, ULK1 phosphorylation and Beclin1 expression observed in Figure 4.6C-4.6F shows that the way in which autophagic signalling is transduced is unclear.

Cargoes destined for degradation are loaded into autophagosomes. The number of autophagosomes within the cell is indicative in the rate of autophagic flux [305]. As previously mentioned, LC3BII is cleaved and conjugated to PE on autophagosomes; therefore, the expression level of LC3BII is reflective of the number of autophagosomes within the cells [305, 385]. Since Figures 4.6A-4.6F are inconclusive with regards to how RT20 and RT53 affect autophagy signalling, LC3BII expression following RT20 and RT53 treatment was examined. Figure 4.6G shows that LC3BII is up-regulated following RT20 and RT53 treatment, and this increase is further exacerbated following treatment with autophagy inhibitor, BafA [304, 305], with quantification from 3 biological replicates shown in Figure 4.6H. BafA inhibits autophagy through prevention of autophagosome degradation [304, 305]. An increase in LC3BII expression in the absence of BafA suggests an increase in autophagosome formation; however, it is unclear whether this is due to their accumulation because of a deficit in degradation capabilities, or a genuine increase in autophagosome number. Concomitant BafA and RT20 or RT53 treatment leads to a further increase in LC3BII expression, demonstrating that an even greater accumulation of autophagosomes occurs when autophagosome degradation is inhibited, compared with RT20 or RT53 treatment alone.

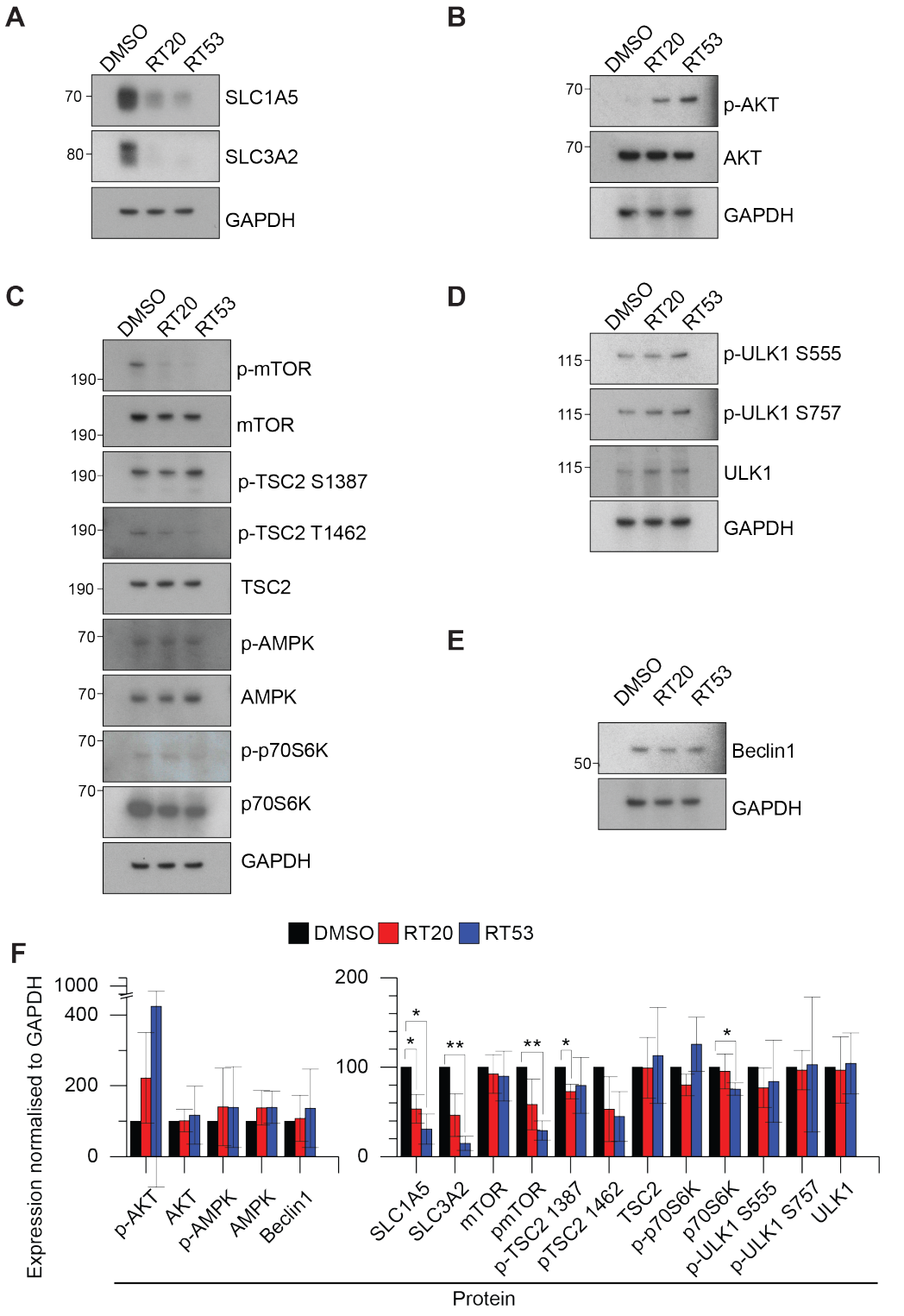

A
DMSO
RT20
RT53
70
SLC1A5
80
SLC3A2
GAPDH
B
70
p-AKT
70
AKT
GAPDH
C
190
p-mTOR
190
mTOR
190
p-TSC2 S1387
190
p-TSC2 T1462
190
TSC2
70
p-AMPK
70
AMPK
70
p-p70S6K
70
p70S6K
GAPDH
D
115
p-ULK1 S555
115
p-ULK1 S757
115
ULK1
GAPDH
E
50
Beclin1
GAPDH
F
DMSO
RT20
RT53
Expression normalised to GAPDH
1000
400
200
0
200
100
0
p-AKT
AKT
p-AMPK
AMPK
Beclin1
SLC1A5
SLC3A2
mTOR
pmTOR
p-TSC2 1387
pTSC2 1462
TSC2
p-p70S6K
p70S6K
p-ULK1 S555
p-ULK1 S757
ULK1
Protein
G
3 h BafA
-
+
DMSO
RT20
RT53
15
LC3B I
LC3B II
GAPDH
H
-BafA
+BafA
LC3BII expression normalised to GAPDH
2.5
2.0
1.5
1.0
0.5
0.0
DMSO
RT20
RT53

***Figure 4.6**: BET BRD inhibition leads to up-regulation of autophagy in LNCaP prostate cancer cells. (**A**) Representative immunoblot showing the downegulation of SLC1A5 and SLC3A2 expression following 1 μM RT20 or RT53 treatment for 48 h. 0.01% v/v DMSO is a negative control. N = 3 biological replicates. (**B**) Representative immunoblot showing the perturbation of the autophagic pathway following 1 μM RT20 or RT53 treatment for 48 h. 0.01% v/v DMSO is a negative control. N = 3 biological replicates. (**C**) Representative immunoblot showing the perturbation of the autophagic pathway following 1 μM RT20 or RT53 treatment for 48 h. 0.01% v/v DMSO is a negative control. N = 3 biological replicates. (**D**) Representative immunoblot showing the perturbation of the autophagic pathway following 1 μM RT20 or RT53 treatment for 48 h. 0.01% v/v DMSO is a negative control. N = 3 biological replicates. (**E**) Representative immunoblot showing the perturbation of the autophagic pathway following 1 μM RT20 or RT53 treatment for 48 h. 0.01% v/v DMSO is a negative control. N = 3 biological replicates. (**F**) Quantification of p-AKT, AKT, p-AMPK, AMPK, Beclin1, SLC1A5, SLC3A2, mTOR, pmTOR, p-TSC2 S1387, p-TSC2 T1462, TSC2, p-p70s6k, p70s6k, p-ULK1 S555, p-ULK1 S757 and ULK1 expression levels as determined by immunoblotting, relative to GAPDH following treatment with 0.01% v/v DMSO (negative control), or 1 μM RT20 or RT53 for 48 h. N = 3 biological replicates. Mean protein expression shown ± standard deviation. Statistical significance was determined using a two-tailed Students t-test. * = $p < 0.05$, ** = $p < 0.01$. (**G**) Representative immunoblot showing that LC3BII increases following treatment with 1 μM RT20 or RT53 for 48 h. 0.01% v/v DMSO is negative control. Cells were treated ± 10 nM BafA for 3 h. N = 3 biological replicates.*

In summary, following RT53 treatment there is clear down-regulation of SLC1A5 and SLC3A2, which could potentially be due to loss of BET chromatin occupancy, and loss of mTOR phosphorylation; however, Figures 4.6B-4.6F show that the route of autophagic signalling transduction is unclear. Upstream of mTOR phosphorylation, but downstream of

SLC1A5 and SLC3A2, it is expected that loss of TSC2 T1462 phosphorylation would coincide with loss AKT phosphorylation [373, 374], or TSC2 S1387 phosphorylation would coincide with AMPK phosphorylation [375-377]; however, neither of these arms of signalling are clearly activated. Downstream of mTOR phosphorylation, loss of p70S6K phosphorylation is expected [381], alongside decreases in ULK1 S757 phosphorylation and increases in ULK1 S555 phosphorylation [309, 382], and an increase in Beclin1 expression [383, 384]. However, none of these events are observed. Notwithstanding this lack of clarity, Figures 4.6G-4.6H show that autophagosome formation increases following RT53 treatment, which increases further upon treatment with BafA. There is perhaps a difference in the extent to which autophagy is up-regulated by each compound. Figure 4.1F suggests that RT53 induces significant loss of cellular proliferation, whereas loss of cellular proliferation induced by RT20 is not statistically significant. In line with this, Figure 4.6H shows that there is a more significant increase in expression of LC3BII following RT53 treatment, compared with the LC3BII expression induced following RT20 treatment, suggesting a greater up-regulation of autophagy by RT53.

While Figures 4.6G-4.6H show significant up-regulation of LC3BII, this experiment was only performed in one cell line, so in this context, there is confidence that autophagy is up-regulated by RT20 and RT53. However, it cannot be said RT20 and RT53 universally up-regulate autophagy throughout prostate cancer; more cell lines of varying genetic backgrounds would need to be tested in order to confirm this. It is also difficult to conclude that down-regulation of solute channels are responsible for the activation of autophagy signalling when the signalling pathway that connects the two events is not clearly activated. To show orthogonally that RT20- and RT53-mediated BET inhibition leads to autophagy up-regulation, genetic perturbation of BET proteins could be induced. If this also leads to autophagy up-regulation, it is less likely that the increase in autophagic flux observed here is due to off-target effects of pharmacological BET inhibition. While it has

been established that SLC1A5 and SLC3A2 targeting can lead to decreased p70S6K phosphorylation and increased autophagy [297, 386, 387], examination of autophagic signalling following specific targeting of of SLC1A5 and SLC3A2 would also help to confirm whether the loss of mTOR phosphorylation and increase in LC3BII expression observed in Figure 4.6, was, indeed, downstream of SLC1A5 and SLC3A2 loss in this context.

Autophagy up-regulation allows cells to meet the demands of stressful stimuli. As such, its up-regulation can prevent cell death and can be associated with increases in invasive cellular behaviour or metastasis [388, 389]. Therefore, it is possible that other indicators of increased invasiveness, such as changes in morphology or motility, may be affected by RT53 treatment. It is important to understand the effect of RT53 on unwanted cellular behaviour, as this could raise concerns surrounding patient safety. Therefore, the influence of RT53 on these phenotypes was evaluated next.

4.2.5 BET BRD inhibition yields changes in cell morphology and motility, underpinned by autophagy, in LNCaP prostate cancer cells

Autophagy functions to remove damaged organelles and misfolded proteins, allowing the cells to respond to various stressful stimuli and avoid cell death [390, 391]. Autophagy up-regulation can also lead to increased invasiveness, motility and metastasis and can promote tumour progression [388, 389, 392, 393]. Increases in invasiveness can manifest in a number of cellular phenotypes including changes in cellular morphology [248, 394-396], and increased motility [394, 397]. *In vitro*, motility is attenuated when autophagy is inhibited using autophagy inhibitor CQ [334, 392, 393]. *In vivo*, prevention of autophagy in conjunction with AR down-regulation led to a reduction in metastasis formation [393]. It is important to understand whether and how RT53, the novel BET inhibitor, affects invasive phenotypes, as this could have catastrophic *in vivo* effects. Therefore, the effects of RT53 on cellular morphology, a marker of invasive behaviour, will be evaluated in this section.

First, the influence of RT53 on transcriptional programs relating to cellular morphology was examined. This was achieved by running GSEA on the RNA-seq data generated by our collaborators, examining the gene ontologies affected. Table 4.2 shows the gene sets related to cellular morphology, migration, motility and cytoskeleton remodelling significantly affected by RT53 or RT20 treatment.

	RT53		RT20	
Pathway	Normalised p value	NES	Normalised p value	NES
GO_MICROTUBULE_BASED_PROCESS	0.01	-1.54	0.01	-1.64
GO_MICROTUBULE_CYTOSKELETON_ORGANIZATION	0.01	-1.84	0.01	-1.88
GO_NEGATIVE_REGULATION_OF_CYTOSKELETON_ORGANIZATION	0.01	-1.73	0.01	-1.87
GO_REGULATION_OF_MICROTUBULE_POLYMERIZATION_OR_DEPOLYMERIZATION	0.01	-1.88	0.01	-1.96
GO_MICROTUBULE_CYTOSKELETON	0.01	-1.61	0.01	-1.60
GO_MICROTUBULE_ORGANIZING_CENTER	0.01	-1.71	0.01	-1.65
GO_TAXIS	0.01	1.88	0.01	1.79
GO_CELL_MORPHOGENESIS_INVOLVED_IN_NEURON_DIFFERENTIATION	0.01	1.75	0.01	1.79
GO_NEURON_PROJECTION_MORPHOGENESIS	0.01	1.66	0.02	1.61
GO_REGULATION_OF_MICROTUBULE_BASED_PROCESS	0.01	-1.69	0.01	-1.77
GO_MICROTUBULE_ORGANIZING_CENTER_PART	0.01	-1.71	0.01	-1.68
GO_NEURON_PROJECTION_DEVELOPMENT	0.01	1.49	0.01	2.01
GO_CELL_PART_MORPHOGENESIS	0.01	1.52	0.02	1.49

Table 4.2: Gene ontologies related to cellular morphology, migration, motility and cytoskeleton remodelling affected by RT53 and RT20 in LNCaP cells. LNCaP cells were treated with RT53 or RT20 for 48 h. Collaborators carried out cell treatment and sample harvesting and sequencing. I carried out RNA-seq data analysis. GSEA results showing gene ontologies affected, following treatment with RT53or RT20 in LNCaP cells compared with DMSO. NES = normalised enrichment score. Computational analysis was carried out using DESeq2 [243] to identify differentially expressed genes, which were used for GSEA analysis in R [244].

Table 4.2 shows that RT53 and RT20 lead to the differential expression of transcription programs involved in changes in cellular morphology, which signals changes in migration and invasion. While RT20 is chemically distinct from RT53, both inhibitors target BET BRDs; therefore, it is unsurprising that similar transcription perturbations are observed.

To validate that changes in cellular morphology took place following RT53 treatment, cells were treated with DMSO, RT20 or RT53 for 48 h, after which, cells were stained with phalloidin, which enabled visualisation of F-actin, a component of cellular cytoskeleton. Using confocal microscopy, this enabled assessment of the cellular morphology. RT20, also known as I-BET762 [72], is used as comparison, as a known BET inhibitor. Figure 4.7A shows that following treatment with either RT20 or RT53, LNCaP cells adopted a dendritic morphology, with increased branching processes. The morphology changes exhibited by LNCaP cells following RT20 and RT53 are indicative of neuroendocrine differentiation [398]. LNCaP cells displaying signs of differentiation display reduced colony formation, and so it is possible that this change in morphology represents a less invasive phenotype [398].

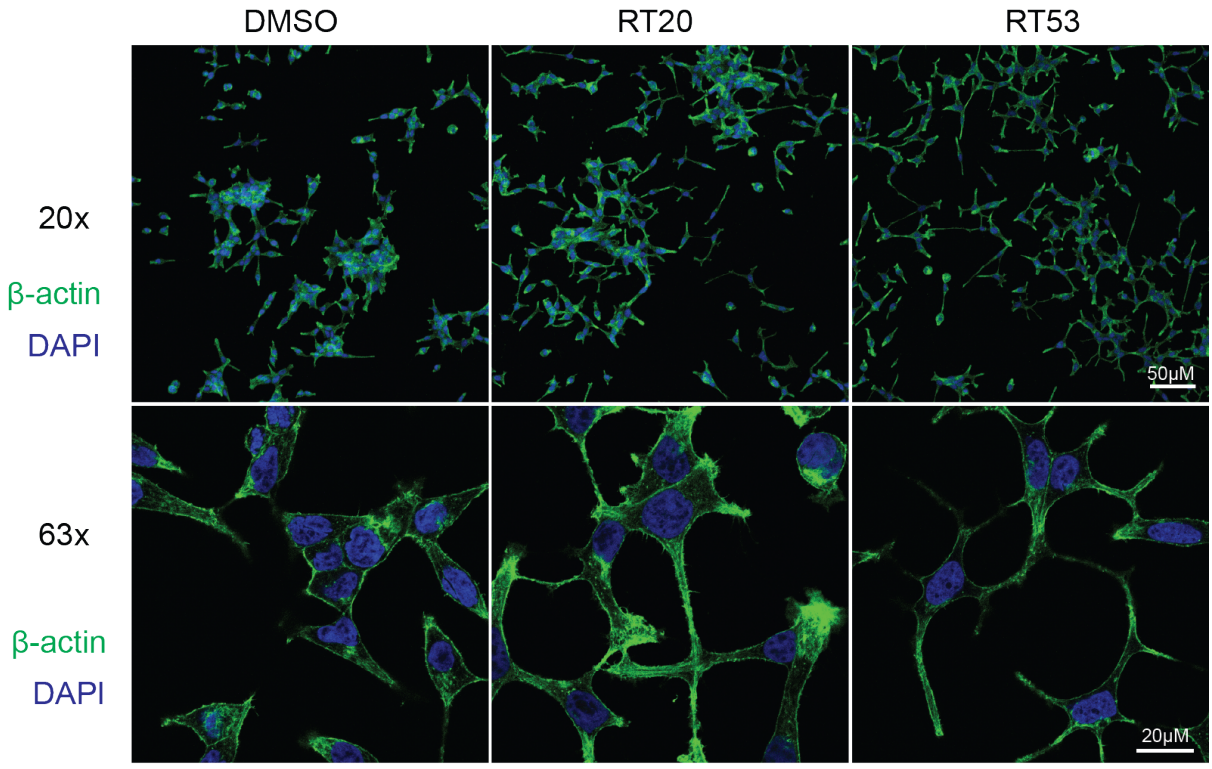


***Figure 4.7**: BET BRD inhibition yields autophagy-dependent changes in cell morphology and motility. BET BRD inhibition leads to changes in cellular morphology in prostate cancer cells. LNCaP cells were treated with 0.01% v/v DMSO or 1 μM RT20 or RT53 for 48 h and then stained with phalloidin and DAPI (blue). DMSO is used as the negative control. N = 3 biological replicates.*

Bicalutamide, an AR antagonist, induces cellular morphology changes such as increased branched processes that resemble neuronal morphology, and this coincides with increased autophagic flux in LNCaP cells [399]. Autophagosomes are generated throughout the cytoplasm but fusion with lysosomes occurs at centrosomes, and the cytoskeleton facilitates their transportation to the centrosomes [399]. Thus, lysosomal positioning may affect cellular morphology, and so it is possible that autophagy lies upstream of morphological changes [399]. While there are previous reports of AR signalling perturbation following BET BRD inhibition [34, 147], AR signalling was not perturbed in this context, despite RT53-mediated changes in AR expression (Figure 4.3A). Nonetheless, RT53 induces autophagy (Figure 4.6), therefore, is it possible that the morphology changes observed in Figure 4.7 are downstream of autophagy.

To ascertain whether autophagy activation plays a role in inducing such morphology changes, cells were treated with CQ concomitantly with RT20 and RT53. CQ is a treatment for malaria, but has been shown to inhibit autophagy through preventing the fusion of lysosomes with autophagosomes [305]. Using confocal microscopy, Figure 7.5A presents preliminary data showing that upon BET inhibition using either RT20 or RT53 and concomitant autophagy inhibition, the changes in cellular morphology were attenuated. Additionally, cellular motility was examined. Increases in cellular motility are an indicator of increasingly invasive cellular behaviour [394, 397], which can be measured using a scratch

wound healing assay [400]. Figure 7.5B shows that wound healing capacity is increased when LNCaP cells are treated with BET BRD inhibition alone, compared with DMSO. When cells were treated concomitantly with CQ, the speed at which the wound healed was reduced. Figures 7.5A and 7.5B suggest that LNCaP cells become more motile and invasive following BET BRD inhibition, and this increase in motility is potentially attenuated upon concomitant autophagy inhibition; however, Figure 7.5 represents preliminary data (see Chapter 7.3.2) and more work must be done to confirm this.

In vivo data from our collaborators show that there are fewer metastases in mice treated with targeted RT53 compared with control mice, suggesting that RT53 reduced the invasiveness of prostate cancer cells. If the cellular morphology changes observed in Figure 4.7 are, indeed, a sign of differentiation and reduced colony formation capacity, this is in line with *in vivo* findings [398]. The *in vivo* tumours constitute LNCaP cells, which at first glance might suggest a direct comparison between *in vitro* and *in vivo* data is possible, but during the *in vivo* experiments, the mice were treated with the targeted RT53, which suggests that the tumours were subject to a much higher dose of RT53 than the cells in Figures 4.7. Therefore, the *in vitro* and *in vivo* results are not directly comparable.

Having identified that autophagy activation may be linked to invasive behaviours in prostate cancer, it was important to determine the way in which autophagy affects cell proliferation. It is possible that autophagy activation underpins loss of cell proliferation, which was observed in melanoma in Figure 3.14A; up-regulation of autophagic signalling in LNCaP cells can coincide with increased loss of cellular proliferation [401]. Testing how autophagy inhibition impacts upon proliferation would also help to gain a broader insight into the role of autophagy in solid tumours following BET BRD inhibition with respect to cellular proliferation.

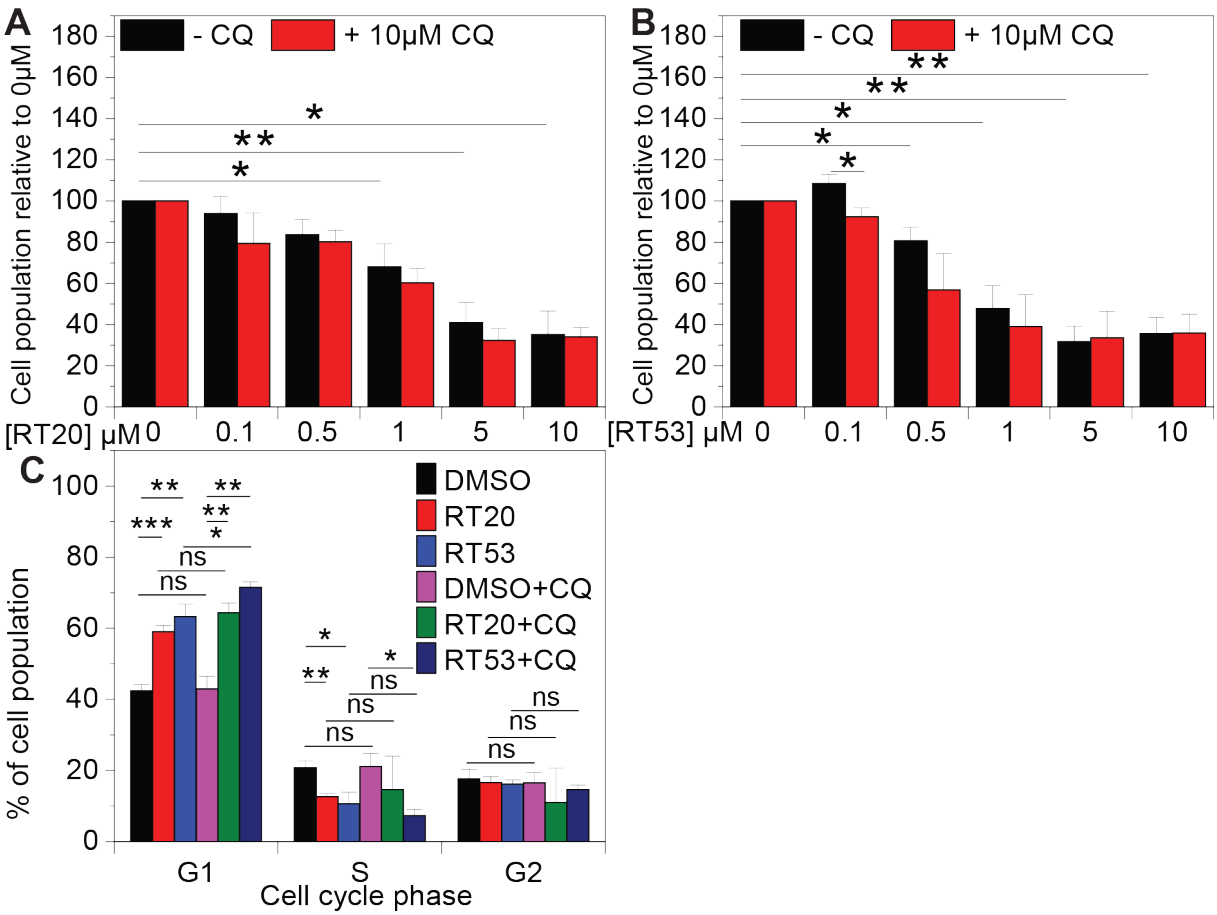
4.2.6 Concomitant BET BRD inhibition and blockade of the autophagic pathway increases loss of cellular proliferation and G1 cell cycle arrest in LNCaP prostate cancer cells

In Chapter 3, I presented evidence showing that autophagy likely plays a role in mediating the effects of BET BRD inhibitors on cellular proliferation in melanoma (Figure 3.14A). In prostate cancer, AR signalling represses autophagy and the suppression of AR signalling led to the up-regulation of autophagic signalling [393, 399, 401]. Combinatorial targeting strategies involving AR down-regulation and concomitant inhibition of autophagy can lead to greater cell death and cell cycle arrest than either agent alone *in vitro* or *in vivo* [392, 399, 401]. Moreover, sensitivity to chemotherapeutic agent docetaxel can be restored through autophagy inhibition [399], showing that autophagy can play a role in resistance to therapies, and may be cytoprotective following treatment [392, 402].

BET BRD inhibition can down-regulate AR signalling [34, 147]. Figure 4.6 shows that RT53 treatment led to autophagy up-regulation, but the data in Figure 4.3B suggest this autophagy up-regulation is AR-independent. It is possible that autophagy up-regulation represents a mechanism by which cells can mediate the stresses of BET BRD inhibition and facilitate survival. To assess the role of autophagy in relation to sensitivity to BET inhibition, the cellular proliferation of LNCaP cells was measured following concomitant treatment with BET BRD inhibitors and an autophagy inhibitor.

Cells were treated with DMSO ± CQ as the negative control, and the cellular proliferation observed in this condition is displayed as 0 μM. Cellular proliferation measurements were normalised to this value. Cells were also treated with RT20 ± CQ, to compare to the potency of RT53 ± CQ. As expected, both RT20 and RT53 alone show dose-dependent loss of cell viability (Figure 4.8A-4.8B), but there was minimal change in cell viability when cells were treated with RT20 + CQ compared with RT20 alone (Figures 4.8A). The addition

of CQ to RT53-treated LNCaP cells led to a further decrease in cell viability, compared with RT53 alone at 0.1 μM (Figures 4.8B). In agreement with Figures 4.1D and 4.1E, RT53 alone appears to induce a greater loss of cellular proliferation in comparison with RT20 alone. The data in Figures 4.8B suggest that autophagy appears to mitigate RT53-induced stress, and its up-regulation appears to be a pro-survival.



***Figures 4.8**: Concomitant RT53 treatment and blockade of the autophagic pathway increases loss of cellular proliferation and G1 cell cycle arrest. Cellular proliferation of LNCaP cells is affected by RT20 treatment alone but is not further affected by concomitant treatment of RT20 and CQ, while cellular proliferation of LNCaP cells is decreased further by concomitant treatment of RT53 and CQ. Cells were treated with the indicated concentrations of RT20 (**A**) and RT53 (**B**) for 96 h ± 10 μM CQ treatment. Cellular proliferation was measured using an MTT assay and normalised to the proliferation*

*observed in cells following treatment with DMSO ± 10 μM CQ. N = 3 biological replicates. Mean cellular proliferation shown ± standard deviation. Statistical significance was determined using a two-tailed Students t-test. * = p < 0.05, ** = p < 0.01. (**C**) Concomitant autophagy inhibition and BET BD inhibition lead to greater cell cycle arrest. LNCaP cells were treated with 0.01% v/v DMSO (negative control), or 1 μM RT20 or RT53 ± 10 μM CQ. After 72 h cells were harvested and stained with PI, after which cell cycle analysis was carried out. N = 3 biological replicates. Mean cell population shown ± standard deviation. Statistical significance was determined using a two-tailed Students t-test. * = p <0.05, ** = p < 0.01, *** = p < 0.001.*

To show orthogonally that cellular proliferation is reduced following RT53 and CQ treatment, cells were treated with BET BRD inhibitors RT20 and RT53 ± CQ and cell cycle was analysed. Figures 4.8C shows that, compared to DMSO, RT20 and RT53 lead to a G1 cell cycle arrest, with significantly fewer cells in S phase. When comparing cells treated with RT53 alone and RT53 + CQ, RT53 + CQ leads to a significantly greater population of cells in G1 phase. When comparing DMSO or RT20 to DMSO + CQ or RT20 + CQ, respectively, there was no increase in cells in G1 phase. Therefore, the concomitant blockade of autophagy using CQ leads to a modest but significant increase in G1 cell cycle arrest only following treatment with RT53.

Figures 4.8 shows that potent BET BRD inhibition via RT53 reveals a vulnerability in the prostate cancer cells to concomitant autophagy inhibition. These results suggest that autophagy plays a cytoprotective role. In the context of the *in vivo* findings from our collaborators, if autophagy is cytoprotective, this may put the cells in a check-mate scenario: if cells increase autophagy, macrophage-recruiting signals are released [347, 348]. In doing so, this leads to tumour shrinkage, and if cells down-regulate autophagy they may no longer be able to cope with the stress of BET inhibition, unless they completely rewire as an escape mechanism. Autophagy has been shown to mitigate the

stress induced on LNCaP cells following treatment with bicalutamide and docetaxel [399], and perhaps autophagy also mitigates the stresses induced by RT53 treatment. These data provide a rationale for use of a combinatorial therapeutic regimens; concomitant BET BRD and autophagy inhibition could yield a more clinically beneficial response than either treatment alone.

While the aim of a combinatorial strategy may be to reduce the dose required of either BET BRD inhibitor or autophagy inhibitor, these data suggest that with a reduction in the potency of BET BRD inhibition, or perhaps the inhibitor's ability to up-regulate autophagy, the additional increase in loss of cell cycling is lost induced by CQ. RT53 significantly reduced cell viability of LNCaP cells where RT20 failed to do so (Figure 4.1H), and induced autophagy to a greater extent than RT20 (Figure 4.6H), suggesting it has greater potency *in vitro*. Moreover, CQ did not yield additional loss of cellular proliferation when cells were concomitantly treated with RT20 (Figures 4.8A). Likewise, when cell cycle analysis was carried out, no increase in the population of cells in G1 phase was observed, when comparing RT20 with RT20 + CQ (Figures 4.8C). An alternative explanation to ability to activate autophagy, is that exacerbated loss of cellular proliferation when combined with CQ, compared to BET BRD inhibition alone, may potentially be specific to RT53. Figure 4.2 demonstrates that different BET BRD inhibitors lead to difference cellular responses, and perhaps Figure 4.8 further illustrates this. However, it is important to remember that CQ may have off-target effects [334]; therefore, there may not be a link between autophagy and cellular proliferation or cell cycling. Further investigations involving orthogonal pharmacological and genetic inhibition of different points in the signalling cascade would be needed to conclude that concomitant inhibition of autophagy increases sensitivity to BET BRD inhibition.

It is unclear why in Figures 4.8B CQ does not induce more cell death at all concentrations of RT53 treatment. It may, in fact, be beneficial, not just in terms of reducing side effects,

but in terms of loss of tumour cell cycling, to reduce BET BRD inhibitor dose, and there may be a window in which BET BRD inhibition leads to greater loss of cellular proliferation when cells are treated concomitantly with an inhibitor of autophagy. If the RT53 dose is too high, the effects of concomitant autophagy inhibition may be overshadowed by the obliterative effects of widespread BET BRD inhibition, and this would lead to greater risk of adverse effects. However, if BETs are inhibited to a lesser extent, the benefit of concomitant autophagy inhibition can be observed.

4.3 Discussion

The aims of the work undertaken in this chapter were to investigate whether the novel BET BRD inhibitor, RT53, would induce potent loss of cellular proliferation *in vitro*, and to investigate the mechanism by which this occurs. BET BRD inhibitor (+)-JQ1 causes loss of cellular proliferation, both *in vitro* and *in vivo*, through the loss of AR signalling, and subsequent down-regulation of MYC and the oncogenic fusion protein TMPRSS2-ERG [34, 147]. In this chapter I have shown that RT53 was, indeed, effective in reducing cellular proliferation in a cell line that positive for AR signalling, LNCaP [34] (Figure 4.1). PC3 cells, which do not utilise AR signalling [34], showed a modest loss of cellular proliferation compared to LNCaP cells (Figure 4.1). These *in vitro* data recapitulate the *in vivo* findings from our collaborators (not shown).

Having shown RT53 induced loss of cell viability *in vitro*, the next aim was to determine the mechanism by which this was achieved. Figure 4.2 shows that cells do not cleave PARP in response to RT53, or RT20 treatment. Published data describe how LNCaP prostate cancer cells cleave PARP and undergo apoptosis in response to (+)-JQ1-mediated BET BRD inhibition [34]. The inclusion of (+)-JQ1 as a positive control in Figure 4.2 when testing for PARP cleavage allows for speculation about possible differences between the BET BRD inhibitors.

BET inhibition via (+)-JQ1, and specifically BRD4 inhibition, leads to a reduction in AR signalling *in vitro* and *in vivo*, and AR-V7 expression, which underpins the mechanism by which AR-positive prostate cancer cells lose viability [34, 147]. However, the data presented in this chapter suggest that LNCaP prostate cells decrease in viability in an AR-independent manner. Figure 4.3A demonstrates that AR target, ETV-1 and MYC, do not decrease in expression, and nor do the expression levels of *AR-V7* or *AR*, *in vivo* following RT53 treatment. *In vitro,* neither RT53 nor RT20 treatment lead to down-regulation of AR

targets (Figures 4.3B- 4.3C) . This suggests that RT53 does not act via perturbation of AR signalling, and acts via a different mechanism to (+)-JQ1 [34]. In fact, the RNA expression of WT AR and AR-V7 increased in response to targeted RT53, yet there was no change in downstream target expression (Figure 4.3). LNCaP cells do not express AR-V7 [355, 357]; therefore, AR-V7-driven gene expression was eliminated as a possible mechanism by which LNCaP cells lost viability following BET BRD inhibition.

It is intriguing that RT53 appears to act in an AR-independent manner, and yet has a greater effect on cellular proliferation in AR-signalling-positive LNCaP cells, compared with AR-signalling-negative PC3 cells. Only RNA expression was examined in this study; however, an increase in WT AR protein expression levels in LNCaP cells following (+)-JQ1 treatment has been observed, while AR target genes concomitantly decreased [34]. Although this paradoxical observation remains to be explained, the rise in AR transcript expression levels observed in Figure 4.3 in response to RT53 treatment is reminiscent of this finding, and indicate that perhaps the mechanisms by which (+)-JQ1 and RT53 act to reduce cellular proliferation overlap more than the data in Figure 4.2 suggest.

The mechanism as to how LNCaP cells stop proliferating still requires further investigation (see Chapter 7.3.2); however, this study has uncovered that LNCaP cells up-regulate autophagic signalling upon targeted BET BRD inhibition, seemingly as a cytoprotective response. There is significant up-regulation of autophagy-related gene sets following treatment with RT53 (Figure 4.4A), suggesting a repressive role with regards to autophagy gene expression under basal conditions. Indeed, in pancreatic cancer cells BRD4 recruits histone methyltransferase G9a to autophagy gene loci, which in turn leads to silencing of autophagy genes [68]. When BRD4 and, consequently, G9a are displaced by (+)-JQ1, the autophagy gene expression is de-repressed and subsequently resumes [68]. It is possible this mechanism plays a role in autophagy up-regulation in prostate cancer cells (see Chapter 7.3.2).

In LNCaP cells, the autophagic signalling cascade may be triggered by direct transcriptional down-regulation of SLC1A5 and SLC3A2, which results in a reduction in SLC1A5 and SLC3A2 protein expression (Figure 4.6A) and amino acid uptake [369, 370]. BRD4 expression correlates with SLC3A2 in pan-cancer patients [371]; therefore, it is plausible that BRD4 directly regulates the expression of SLC3A2 in this context, although ChIP-seq data in Figure 4.5 suggest BRD -2 and -3 may contribute more to the regulation of SLC3A2 than BRD4. There is also a loss of mTOR phosphorylation (Figure 4.6C); while activation of the signalling cascade requires further elucidation downstream of mTOR in these cells, it is clear that it culminates in significant up-regulation of LC3BII expression (Figures 4.6G-4.6H). This indicates that autophagy is, indeed, up-regulated following BET BRD inhibition. When cells are treated concomitantly with RT20, or RT53 and BafA, the increase in LC3BII is increased, which is again indicative of an increase in autophagic flux, as opposed to inhibition [304, 305]. It is intriguing to observe an increase in autophagic signalling, seemingly without a decrease in AR signalling (Figure 4.3); suppression of AR signalling has been shown to up-regulate autophagy in prostate cancer cells [393, 399]. Perhaps this represents a novel BRD-dependent, AR-independent mechanism by which autophagy can be up-regulated in prostate cancer cells.

RT53 leads to changes in morphology, which are potentially underpinned by autophagy and may represent differentiation of prostate cancer cells into neuroendocrine cells. A previously published study demonstrated that BET BRD inhibition combined with androgen deprivation leads to differentiation of LNCaP cells into neuroendocrine cells [398, 399]. The differentiated cells exhibited slower clonogenic growth than their non-differentiated counterparts [398]. In another study, pharmacological AR antagonism induced increased branched processes that resemble neuronal morphology and this coincided with an increase in autophagy [399]. However, in the context of the current study, while cells treated with RT53 adopt a neuronal appearance (Figures 4.7A) and up-regulate autophagy

(Figure 4.6), AR signalling was not down-regulated following BET BRD inhibition (Figure 4.3). Therefore, in response to BET BRD inhibition, LNCaP cells potentially differentiate, and subsequently display neuronal morphology, which coincides with an AR-independent up-regulation of autophagy.

Lastly, upon concomitant RT53 treatment and autophagy inhibition, cellular proliferation further decreased (Figures 4.8B) and cell cycle G1 arrest further increased (Figures 4.8C) compared with RT53 treatment alone; therefore, the increase in autophagic flux induced by RT53 is cytoprotective. Seemingly, autophagy is up-regulated as a mechanism by which the stress induced by BET BRD inhibition is mitigated, and this has been uncovered as a point of vulnerability for the cells. This serves as a rationale to employ a combinatorial approach to therapeutic regimens, which has been shown to be effective in a liquid malignancy. AML cells that were resistant to BET BRD inhibition were rendered more sensitive when this was combined with autophagy inhibition [101], and in prostate cancer concomitant inhibition of autophagy leads to the re-sensitisation of cells to chemotherapeutic agents docetaxel and bicalutamide [399]. Therefore, the combination of BET BRD inhibitors with autophagy inhibitors may prove effective in prostate cancer, and could even allow for reduction of BET BRD dose; thus, further lowering the risk of potential toxicities.

These data collectively bring to light a BET-BRD-dependent, yet AR-independent mechanism by which autophagy is up-regulated in prostate cancer, which alleviates the stress induced by BET BRD inhibitors. Thus, a new vulnerability in prostate cancers has been revealed, which serves as a rationale for further testing of this novel combinatorial strategy. Further work is needed to clarify the link between BET BRD inhibition, autophagy and invasiveness, and the mechanism by which RT53 leads to loss of cellular proliferation.

Chapter 5: Targeting of BET proteins via the ET-domain leads to autophagy-dependent senescence in a melanoma model

5.1 Introduction

Having evaluated the effects of BET BRD inhibition in melanoma and prostate cancer models, I next assessed the impact of inhibiting the function of the ET-domain. Melanoma was used as a model so as to compare directly the phenotypes induced by BET inhibition via different domains. Given that BRD inhibition is effective but induces side effects, a method to target BETs without the associated toxicity is highly desirable [91, 161, 359]. Therefore, targeting the ET-domain, another domain common to the members of the BET protein family, represents a potential novel, therapeutic strategy.

The ET-domain is responsible for mediating Kac-independent interactions, often between BET proteins and recruited transcriptional machinery, histone modifiers and negative regulators of transcription [15, 28, 31, 397]. Also, the ET-domain is capable of driving PTEF-b-independent transcription through the recruitment of NSD3, JMJD6 and GLTSCR1 [40]. Therefore, inhibiting the ET-domain function will prevent the recruitment of these protein binding partners. Two features of the ET-domain function suggest that its inhibition could lead to fewer toxicities compared with targeting the BRDs *in vivo*. Firstly, targeting the ET-domain should perturb PTEF-b-independent transcription and alter the expression of potentially a smaller subset of genes when compared with global PTEF-b-dependent transcription [40]. Secondly, when targeting the ET-domain the BET proteins, in theory, remain bound to chromatin. When BETs are displaced from chromatin, the subsequently exposed acetylated lysine residues on histone tails become available for binding. It is possible that, following BET displacement by BET BRD inhibition [71], other chromatin binders may bind to chromatin previously occupied by BETs, which may result in aberrant

modulation of gene expression or chromatin remodelling. Inhibiting BET function(s) whilst maintaining their chromatin occupation should prevent this, and thus, could reduce toxicity.

Less is known about inhibition of Kac-independent (than Kac-dependent) functions of BETs, so further investigation into its function will provide novel insight into its role in cell viability in melanoma and its suitability as a therapeutic target. The C-terminal domain of the integrase enzyme from the murine leukaemia virus (MLV) binds to the ET-domain of BETs, which enables integration of the viral genome into transcriptionally active sites of the host genome [403, 404]. Our lab showed that a peptide, referred to as “PepX”, mimicking the C-terminus of the MLV integrase binds to the ET-domain of BETs, thereby outcompeting endogenous ET-domain interactors. Using this polypeptide competitive inhibitor of the ET-domain, the aim of the work presented in this chapter is to establish if a phenotype arises as a result of ET-domain inhibition, and any underlying mechanism.

5.2 Results

5.2.1 Generation and validation of stable, doxycycline-inducible PepX expression in a melanoma cell line

Targeting the BET BRDs can lead to a decrease in cellular proliferation (Table 3.1) and changes in downstream gene expression (Figure 3.5), begging the question as to whether ET-domain inhibition can yield the same phenotype. Initially, attempts were made to add linear or circularised PepX peptide to cells in the same way as a pharmacological inhibitor. However, as neither linear nor circularised PepX peptides permeated the cell membrane (data not shown), the strategy chosen for these experiments was to induce the expression of PepX and control peptides in a doxycycline-dependent manner within the 501mel melanoma cell line. Using the 501mel cell line would enable direct comparison between the effects of BRD and ET-domain inhibition within the same cell line, as Chapter 3 details the effect of BET BRD inhibition in 501mel cells.

A polyclonal cell line, which expresses doxycycline-inducible PepX fused to a blue fluorescent protein (BFP) and a nuclear localisation signal (NLS), PepX-BFP-NLS (hereafter referred to as “PepX”), was generated using the Tet-on piggybac system [405, 406]. As well as this cell line, three additional polyclonal cell lines were generated: one expressing doxycycline-inducible BFP-NLS (hereafter referred to as “NLS”), one expressing doxycycline-inducible KRR-BFP-NLS (hereafter referred to as “KRR”), and one expressing doxycycline-inducible LIL-BFP-NLS (hereafter referred to as “LIL”). KRR and LIL are mutants of PepX which either nullify the positive charge or the peptide’s hydrophobicity, respectively (Figure 5.1A). Expression of the constructs was stimulated using doxycycline.

Several attempts were made to generate the doxycycline-inducible PepX-, NLS-, KRR- and LIL-expressing cell lines as there were problems with stochastic induction of BFP expression and leaky BFP expression. As PepX outcompetes interactors of the ET-domain (*in vitro* data, not shown), its expression was hypothesised to affect cellular proliferation. To ascertain the concentrations of doxycycline that parental 501mel cells could tolerate before declining in proliferation, 501mel cells were treated with increasing concentrations of doxycycline up to 1 μM for 48 h, at which point cells were stained with crystal violet. Plates were scanned and cell viability at each concentration was calculated. From these values an EC_{50} value, the concentration of doxycycline at which cellular proliferation is equidistant between the maximum and minimum proliferation values, was calculated. Figure 5.1B shows that cell viability begins to decrease when cells are treated with 100 nM doxycycline. Therefore, when selecting polyclonal doxycycline-inducible PepX-, NLS-, KRR- and LIL-expressing cell lines, only those which expressed PepX, NLS, KRR or LIL following < 100 nM doxycycline treatment would be suitable for further experiments.

When doxycycline was titrated using increasing concentrations in regular increments, the subsequent increases in BFP expression were not equal between PepX-, NLS-, KRR- and LIL- expressing cell lines. Thus, the ultimate level of BFP expression in each of the PepX-, NLS-, KRR- and LIL-expressing cell lines following treatment with any given doxycycline concentration was difficult to predict, and cell lines expressing different constructs treated with the same concentration of doxycycline yielded drastically different levels of BFP expression. Due to this unpredictable nature of the constructs' expression in response to doxycycline treatment, possibly owing to the site of integration of the expression cassette, it was necessary to identify the concentration of doxycycline required for each cell line to yield similar construct expression. This reduced the variation of doxycycline-inducible construct expression levels between cell lines, thereby allowing comparison of phenotypes induced by PepX or control construct expression in their respective cell lines. From this

point onwards in all experiments, the concentrations of doxycycline used to induce construct expression can be seen in Table 5.1.

Validation of these cell lines showing dose-dependent BFP expression can be seen in the immunoblot in Figure 5.1C. BFP is visualised as two distinct bands (Figure 5.1C); therefore, quantification of immunoblotting involved measuring the density of both upper and lower BFP bands, and using the loading control density for normalisation (Figure 5.1D). KRR- and LIL-expressing cells treated with “high” doxycycline lack the expression of the higher molecular weight band, which suggests that these two controls alter BFP degradation or PTM deposition. Owing to the different concentrations of doxycycline used to induce the expression of each construct throughout this chapter, the negative control, DMSO, was diluted to different extents depending on the peptide being expressed. DMSO was used as a negative control as this is the solvent in which doxycycline is dissolved. DMSO was added to the medium at the same volume by volume (v/v) percentage as the doxycycline needed to achieve the “high” doxycycline concentration. The resulting DMSO negative control concentrations can be seen in Table 5.1.

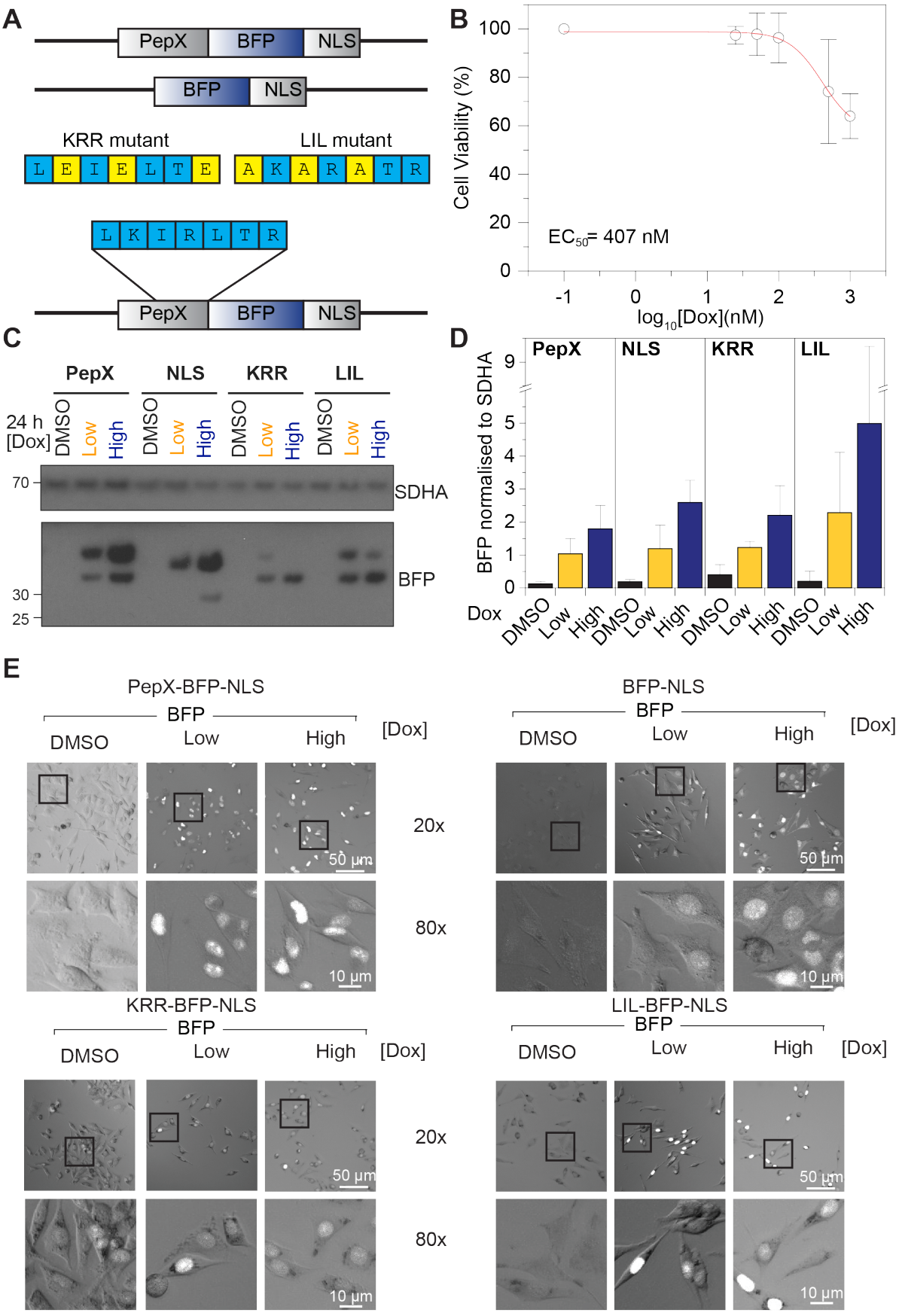

A
PepX
BFP
NLS
BFP
NLS
KRR mutant
L E I E L T E
LIL mutant
A K A R A T R
L K I R L T R
PepX
BFP
NLS
B
Cell Viability (%)
100
80
60
40
20
0
EC50= 407 nM
-1
0
1
2
3
log10[Dox](nM)
C
PepX
NLS
KRR
LIL
24 h
[Dox]
DMSO
Low
High
70
SDHA
30
25
BFP
D
BFP normalised to SDHA
9
5
4
3
2
1
0
PepX
NLS
KRR
LIL
Dox
DMSO
Low
High
E
PepX-BFP-NLS
BFP
DMSO
Low
High
[Dox]
20x
80x
50 µm
10 µm
BFP-NLS
KRR-BFP-NLS
LIL-BFP-NLS

***Figure 5.1**: PepX and control peptides are doxycycline-inducible in 501mel melanoma polyclonal cell lines and their expression is constrained to the nucleus. (**A**) Doxycycline-inducible peptides expressed in 501mel cells. BFP = blue fluorescent protein, NLS = nuclear localisation signal. (**B**) Treatment with doxycycline leads to a reduction in cellular proliferation in 501mel cells. Cells were treated with increasing concentrations of doxycycline up to 1 μM for 48 h, which was followed by crystal violet staining. Plates were scanned and cell proliferation at each concentration was calculated, normalised to the level of proliferation that was observed following treatment with DMSO, the negative control. EC_{50}= nM 407 ± 62.7 nM. Error bars represent standard deviation. N = 3 biological replicates. (**C**) Immunoblot showing comparable doxycycline-inducible expression of PepX and the three control peptides after 24 h. Both bands represent BFP; antibody recognises BFP that may have been degraded in cell lysate preparation. BFP-NLS is a lower molecular weight than PepX-, KRR- and LIL-BFP-NLS as it lacks the PepX or mutant peptide. SDHA was used as a loading control, as its expression changed minimally following BET BRD pharmacological inhibition [152]. DMSO was the negative control according to the concentrations shown in Table 5.1. (**D**) Quantification showing comparable doxycycline-inducible expression of PepX and the three control peptides in 4 different genetically modified polyclonal 501mel cell lines after 24 h. Orange bars show BFP expression following treatment with is low concentrations of doxycycline, blue bars indicate BFP expression following treatment with high concentrations of doxycycline. Quantification of BFP expression was normalised to the loading control, SDHA. DMSO was the negative control according to the concentrations shown in Table 5.1. Mean protein expression shown ± standard deviation. N = 3 biological replicates. (**E**) Representative confocal microscopy images showing visualisation of BFP after 24 h doxycycline treatment, showing that expression of BFP-tagged peptides in 501mel cells is confined to*

the nucleus. DMSO was the negative control according to the concentrations shown in Table 5.1. N = 3 biological replicates.

An additional concern of the PepX, NLS, KRR or LIL expression was off-target effects. A mass spectrometry experiment carried out by our collaborators showed that PepX interacts with BETs and mitochondrial proteins (data not shown), which could potentially induce off-target effects. However, BETs do not interact with mitochondrial proteins under normal conditions [36, 97]. Thus, to avoid off-target effects, it is necessary to constrain PepX expression to the nucleus. To minimise interactions with cytosolic proteins, the function of the nuclear localisation signal is to constrain the expression of the peptides to the nucleus. Confocal microscopy was used to examine the sub-cellular locations in which BFP signal could be detected. Figure 5.1E shows that the expression of the BFP-constructs is constrained to the nucleus in all four cell lines, indicating that any effects are unlikely to be due to off-target binding of cytosolic proteins.

Construct name	Low doxycycline concentration (nM)	High doxycycline concentration (nM)	DMSO concentration used as negative control (% v/v of cell growth medium)
PepX	40	50	0.05
NLS	20	30	0.03
KRR	6	8	0.008
LIL	40	60	0.06

Table 5.1: Low and high concentrations of doxycycline used to induce construct expression in modified 501mel cells.

Many attempts were made to identify concentrations of doxycycline that would yield similar expression levels of PepX, NLS, KRR or LIL. Additionally, lentiviral transduction as a method of integrating constructs into the 501mel genome was trialled, as well as extensive optimisation of the transfection step in the Tet-on system. Although lentiviral transduction resulted in a more homogenous cell population, BFP expression induction following

doxycycline treatment was minimal until 1 μM doxycycline was used. Given the effects of doxycycline alone on 501mel cell viability (Figure 5.1B), this was not deemed a suitable system in which to test the effects of PepX. The results shown in Figure 5.1 represent the most suitable cell lines generated using either lentiviral transduction or optimisation of the Tet-on system.

Figure 5.1D shows that, with the exception of LIL, similar levels of BFP expression were observed across different cell lines, but the standard deviation across different experiments was high, particularly for LIL-expressing cells. In addition to potential differential PTM deposition on BFP in KRR- and LIL- expressing cells, this necessitated that NLS-, KRR- and LIL- expressing cells were included as controls in experiments to determine the effect of PepX on cellular proliferation.

5.2.2 PepX-mediated ET-domain inhibition decreases cell proliferation in 501mel melanoma cells

Having validated the doxycycline-inducible expression of the PepX, NLS, KRR, and LIL constructs in Tet-on piggybac 501mel cell lines, the next step was to ascertain whether PepX expression had an effect on cellular proliferation. The PepX-expressing 501mel cells lines were treated with doxycycline to induce PepX expression, as were the KRR-, LIL- and NLS-expressing control cell lines. Cell proliferation was observed after 48 and 72 h using crystal violet staining. DMSO was used as a negative control according to the concentrations shown in Table 5.1.

Representative wells stained with crystal violet can be seen in Figure 5.2A, showing cellular proliferation after 72 h of doxycycline treatment is drastically reduced in PepX cells compared with the three control lines. Quantification of proliferation is shown, measured using crystal violet staining, following doxycycline treatment for 48 h (Figure 5.2B) and 72 h (Figure 5.2C). Figures 5.2B-5.2C show that the effect of PepX on cellular proliferation is

time- and dose-dependent; after 48 h PepX induced significant loss of cellular proliferation only following treatment with high doxycycline; however, this loss of cellular proliferation was exacerbated following 72 h doxycycline treatment. While NLS expression led to a decrease in cell proliferation (Figure 5.2C), potentially due to non-specific binding with BRD4 or another BET protein (Figure 7.7), the most drastic change in cell proliferation is observed when cells express PepX for 72 h (Figure 5.2C). This effect is abolished when either the positive charge or the hydrophobicity of the PepX peptide is removed, as shown by the lack of inhibition of proliferation when cells express KRR or LIL (Figures 5.2B-5.2C), suggesting that this effect is, indeed, due to perturbation of the BET protein ET-domain.

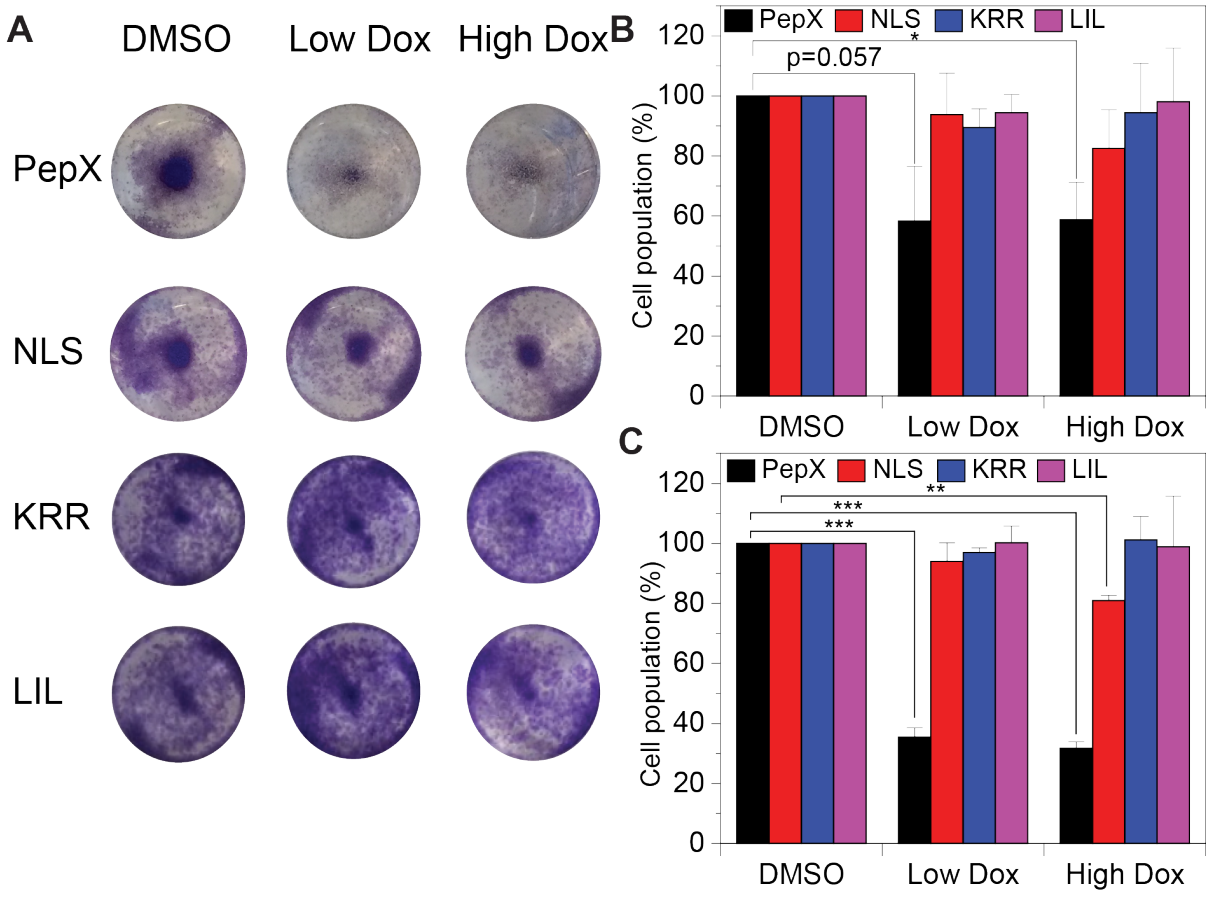


***Figure 5.2**: ET-domain inhibition leads to loss of cellular proliferation in a dose- and time-dependent manner. (**A**) Representative wells stained with crystal violet following doxycycline treatment for 72 h. DMSO was used as a negative control treatment, as well as including the NLS-, KRR-, and LIL- expressing control cell lines. DMSO was the*

*negative control according to the concentrations shown in Table 5.1. Quantification of crystal violet staining of cells after 48 h (**B**), or 72 h (**C**) doxycycline treatment. Cell proliferation following doxycycline treatment was normalised to the proliferation observed following treatment with DMSO, the negative control. DMSO was the negative control according to the concentrations shown in Table 5.1. N = 3 biological replicates. Mean crystal violet staining shown ± standard deviation. Statistical significance was determined using a two-tailed Students t-test.* = p <0.05, ** = p <0.01, *** = p < 0.001.*

5.2.3 Loss of cellular proliferation following PepX expression may be p53-independent and p21-independent

As seen in Chapter 3, 501mel parental cells harbour a mutation in p53 which correlates with the induction of autophagy-induced senescence following BET BRD inhibition. Integration of the PepX construct into the 501mel cell genome is random and could have perturbed the p53 gene by integrating at the p53 locus. To confirm the PepX-expressing cells also harbour this mutation, and whether the loss of cellular proliferation is p53-dependent, RNA was extracted, converted to cDNA, and PCR was carried out using p53-specific primers. The PCR product was then sequenced. Figure 5.3A shows that the PepX cell line does, indeed, harbour the same C275W p53 mutation as 501mel parental cells.

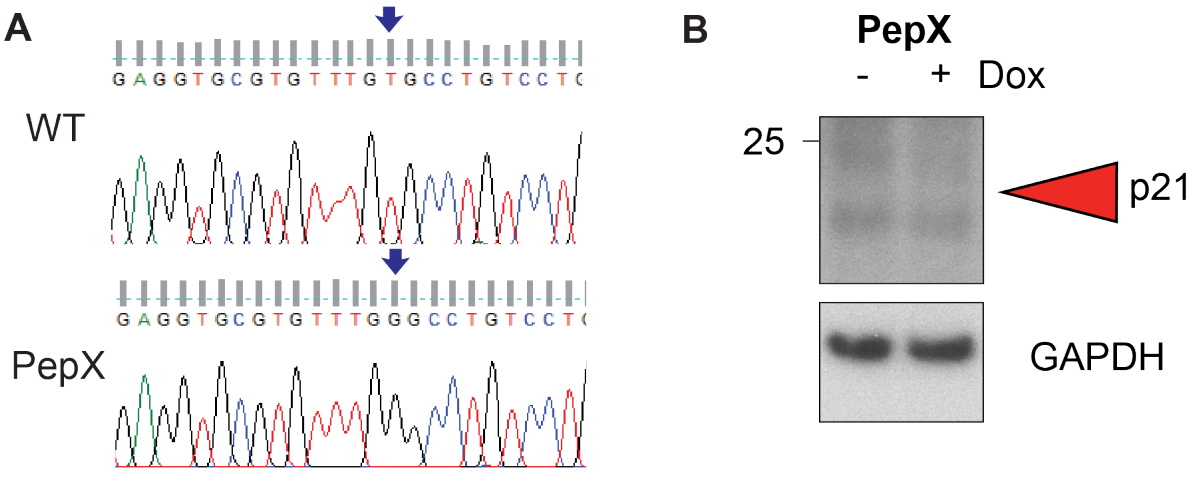


***Figure 5.3**: PepX-expressing 501mel cells harbour a C275W p53 mutation and do not up-regulate p21 expression following PepX expression. (**A**) 501mel cell lines, including the PepX and parental cell lines, express mutant p53. Arrows show site of mutation. (**B**) p21 staining in 501mel PepX cells normalised to GAPDH expression after treatment for 72 h with 0.05% v/v DMSO (negative control) or 50 nM doxycycline. N = 3 biological replicates. Red arrow points to where the p21 band should be (Figure 7.1). GAPDH was used as a loading control as its expression remained unchanged following BET BRD inhibition in melanoma [152].*

As shown previously, 501mel cells did not up-regulate p21 expression following BET BRD treatment (Figure 3.2D). This mutation may prevent binding of p53 to DNA and subsequent up-regulation of target genes, such as p21 [254, 282, 283, 340]. To determine whether ET-domain BET inhibition causes p21-up-regulation, cells were treated with doxycycline and immunoblots were carried out examining p21 expression. Figure 5.3B shows that p21 is not up-regulated following PepX expression. Thus, 501mel cells with doxycycline-inducible PepX expression retain the C275W p53 mutation and the inability to up-regulate p21 protein expression, which may be due to the mutant p53.

5.2.4 ET-domain inhibition of BETs induces cell cycle arrest

As PepX-expressing 501mel cells harbour a p53 mutation and do not up-regulate p21 expression following PepX expression, the mechanism by which cells stop proliferating remains elusive. A perturbation of cell cycle may account for the cessation in proliferation observed in Figure 5.2. Accordingly, PepX-, NLS-, KRR- and LIL-expressing cells were treated with DMSO, low or high concentrations of doxycycline for 48 or 72 h and stained with PI to enable cell cycle analysis by flow cytometry.

Figure 5.4A shows that after 48 h there was a significant accumulation of cells in G1 cell cycle phase, and a significant decrease of cells in S phase following PepX expression,

which was further exacerbated after 72 h. Figure 5.4B shows representative flow cytometry profiles, showing increasing G1 cell populations with increasing doxycycline-induced PepX expression. There was no change in cell cycle progression when any of NLS, KRR or LIL were expressed for 48 or 72 h using low or high concentrations of doxycycline (Figure 5.4A). Representative flow cytometry profiles and quantification suggest that ET-domain inhibition has a dose-dependent effect on cell cycle arrest at the longer time point (Figure 5.4A-5.4B).

As an additional control to ensure the doxycycline alone did not affect cell cycle progression, parental 501mel cells were treated with doxycycline for 72 h. Figure 5.4C shows there was no change in 501mel cells following doxycycline treatment. Therefore, neither doxycycline alone, nor KRR, LIL nor NLS expression cause any change in cell cycle progression, and ET-domain inhibition leads to G1 cell cycle arrest in a time- and dose-dependent manner.

The cell cycle arrests undergone by PepX-expressing cells are not complete, ~30% of cells remain in S phase (Figures 5.4A). This could be due to the heterogeneity of PepX expression in cells following the addition of doxycycline, or perhaps cells arrest in S phase due to DNA damage [407]. The heterogeneous nature of PepX, NLS, KRR, and LIL expression can be seen in Figures 5.1C-5.1E. In the case of PepX expression, this likely leads to different extents of ET-domain inhibition, and thus, different extents of transcriptional perturbation and cell cycle arrest.

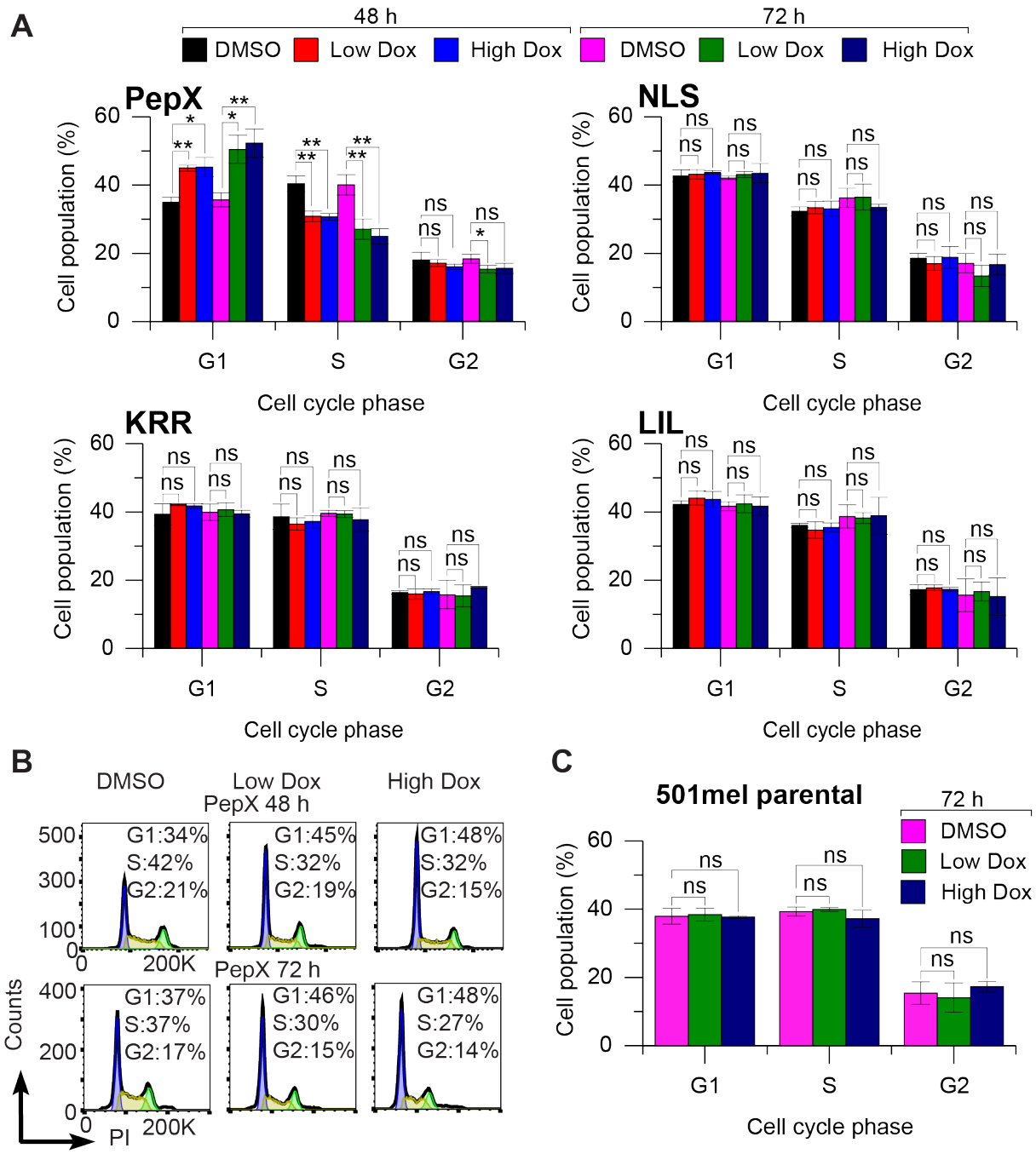


***Figure 5.4**: ET-domain inhibition causes G1 cell cycle arrest. (**A**) Percentage of cells at each stage of the cell cycle following PI staining and cell cycle analysis in PepX-expressing cells (upper left), NLS-expressing cells (upper right), KRR-expressing cells (lower left), and LIL-expressing cells (lower right) following treatment with DMSO (negative control), low and high concentrations of doxycycline as described in Table 5.1 for 48 or 72 h. N = 3 biological replicates. Mean cell population shown ± standard deviation. Statistical significance was determined using a two-tailed Students t-test. ns = non-significant*

difference, = p <0.05, ** = p <0.01. (**B**) flow cytometry profiles of PepX cells following 48 or 72 h treatment with 0.05% v/v DMSO (negative control), low or high concentrations of doxycycline. Purple indicates G1 phase, yellow indicates S phase, green indicates G2/M phase. (**C**) Percentage of cells at each stage of the cell cycle following PI staining and cell cycle analysis in 501mel parental cells 72 h following treatment with 0.05% v/v DMSO (negative control), low doxycycline and high doxycycline according to concentrations used for PepX cells described in Table 5.1. N = 3 biological replicates. Mean cell population shown ± standard deviation. Statistical significance was determined using a two-tailed Students t-test. ns = non-significant difference.*

The ET-domain is required for PTEF-b-independent transcription [40]. Given that perturbation of its function leads to a reduction in cellular proliferation (Figure 5.2), investigating a transcriptional response following its attenuation may shed light on the way in which the cell cycle is blocked. It will also provide insight into differential BET protein gene regulation; comparison of gene sets affected by BET BRD or ET-domain inhibition should provide insight into Kac- dependent and -independent mechanisms of BET protein regulation of gene expression.

Prior to preparation of samples for RNA-seq, it was important to establish the most suitable conditions for treating cells which would allow the dissection of the direct transcriptional repercussions of ET-domain inhibition. A longer duration of treatment than the treatment of cells with (+)-JQ1 in the RNA-seq experiment presented in Chapter 3 was required owing to the need for doxycycline to enable construct expression before any changes gene expression could be induced, which took at least 8 h (data not shown). However, an excessively long treatment duration should be avoided to minimise the risk of observing off-target effects of PepX. Figure 5.2B showed that after 48 h there was a reduction in cellular proliferation, indicating that PepX had potentially affected transcription following this treatment duration. Moreover, Figures 5.4A-5.4B show that a cell cycle arrest

begins following 48 h of PepX expression. Therefore, 48 h was selected as the time point at which samples were harvested for RNA-seq, using DMSO as a negative control. In addition, the expression of NLS, KRR and LIL construct was induced using “high” concentrations of doxycycline, and NLS-, KRR- and LIL-expressing cells were also treated with DMSO as additional negative controls. Following RNA extraction, all samples were subject to RNA-seq. Figure 5.5A shows the global changes in gene expression following PepX expression compared with DMSO; 31 genes were significantly up-regulated (pink dots), and 19 genes were significantly down-regulated (blue dots). No significant changes in gene expression were induced following 48 h of expression of KRR or LIL, and only the expression of 1 gene was significantly affected by NLS expression (Figure 7.6).

To determine whether PepX causes cell cycle arrest in a BET-dependent manner, the LFCs of changes in gene expression following PepX expression (compared with DMSO treatment of PepX-expressing 501mel cells) were correlated with LFCs in gene expression induced following pharmacological and genetic BET protein inhibition (compared with cells treated with (-)-JQ1 or transfected with negative control siRNA (siNC), respectively, RNA-seq experiment detailed in Chapter 3.2.3) in scatter plots. Genes with significant (adjusted p value ≤ 0.05) LFCs following both treatments were highlighted in red. Genes with significant (adjusted p value ≤ 0.05) LFCs the treatment shown on the x or y axis were highlighted in orange or blue, respectively. Genes with non-significant (adjusted p value > 0.05) LFCs following both treatments were represented by a grey dot. The correlation between genes that are significantly differentially regulated by both treatments is shown by the linear regression line and is indicated by the R^2 values shown.

Figure 5.5B shows the correlation between LFCs in gene expression when cells are treated with doxycycline to induce PepX expression, compared with (+)-JQ1 treatment. Figure 5.5C shows the correlation between LFCs in gene expression when cells are treated with doxycycline to induce PepX expression, compared with simultaneous siRNA-

mediated pan-BET knockdown (siBETs). In Figure 5.5B many genes are depicted as red dots, showing that both PepX and (+)-JQ1 leads to significant differential regulation of many of the same genes. In Figure 5.5C many genes are depicted as blue dots, showing that the expression of many genes is only significantly regulated by PepX, and not significantly regulated by siBETs. Nevertheless, both (+)-JQ1 and siRNA-mediated pan-BET knockdown lead to similar correlation of significant changes in gene expression compared with PepX, as indicated by the R^2 values, suggesting that PepX acts in a BET-dependent manner.

To determine which BET protein mediates the effects of PepX, the LFCs of changes in gene expression following PepX expression (compared with DMSO treatment of PepX-expressing 501mel cells) were correlated with LFCs in gene expression induced following individual siRNA-mediated BET knockdown (compared with 501mel cells transfected with siNC, RNA-seq experiment detailed in Chapter 3.2.3). The correlations between LFCs in gene expression when cells are treated with doxycycline to induce PepX expression compared with siRNA-mediated BRD2 knockdown (siBRD2), siRNA-mediated BRD3 knockdown (siBRD3) and siRNA-mediated BRD4 knockdown (siBRD4) are shown in Figures 5.5D, 5.5E and 5.5F, respectively. Intriguingly, there appears to be most correlation between the genes affected by PepX and siBRD2, as indicated by the R^2 values (Figures 5.5D-5.5F). It is also not surprising that the effects of BRD4 knockdown correlate with the effects of PepX expression, as PepX binds to BRD4 in the cellular environment (Figure 7.7). Figure 5.5E shows that, of BRD -2, -3, and -4 knockdowns, significant changes in gene expression following siRNA-mediated knockdown of BRD3 show the least correlation with significant changes in gene expression following PepX expression, as indicated by the R^2 value. BRD2 and BRD4 are up-regulated in melanoma, suggesting they facilitate the initiation or maintenance of malignancy [151]; however, the role of BRD3 in melanoma is unclear; therefore, this finding is not unexpected. Of Figures

5.5D-F, Figure 5.5F depicts the most genes as orange dots, indicating that BRD4 knockdown leads to significant changes in gene expression when PepX does not. This is not unexpected, as BRD4 harbours a CTM (Figure 1.1A) and facilitates PTEF-b-dependent transcription [37]. Thus, BRD4 knockdown likely perturbs PTEF-b-dependent transcription, whereas PepX expression theoretically does not disrupt this transcription mechanism.

It is unclear why some genes undergo significant changes in expression in opposing directions following PepX expression compared to other BET protein inhibition strategies. This could relate to off-target effects of one or both treatments, or perhaps the different modes of BET inhibition disrupt different transcription mechanisms. Nevertheless, the data in Figure 5.5 indicate that PepX induces changes in gene expression through BET protein perturbation. Specifically, effect of PepX appears to be exerted through inhibition of BRD2 and BRD4.

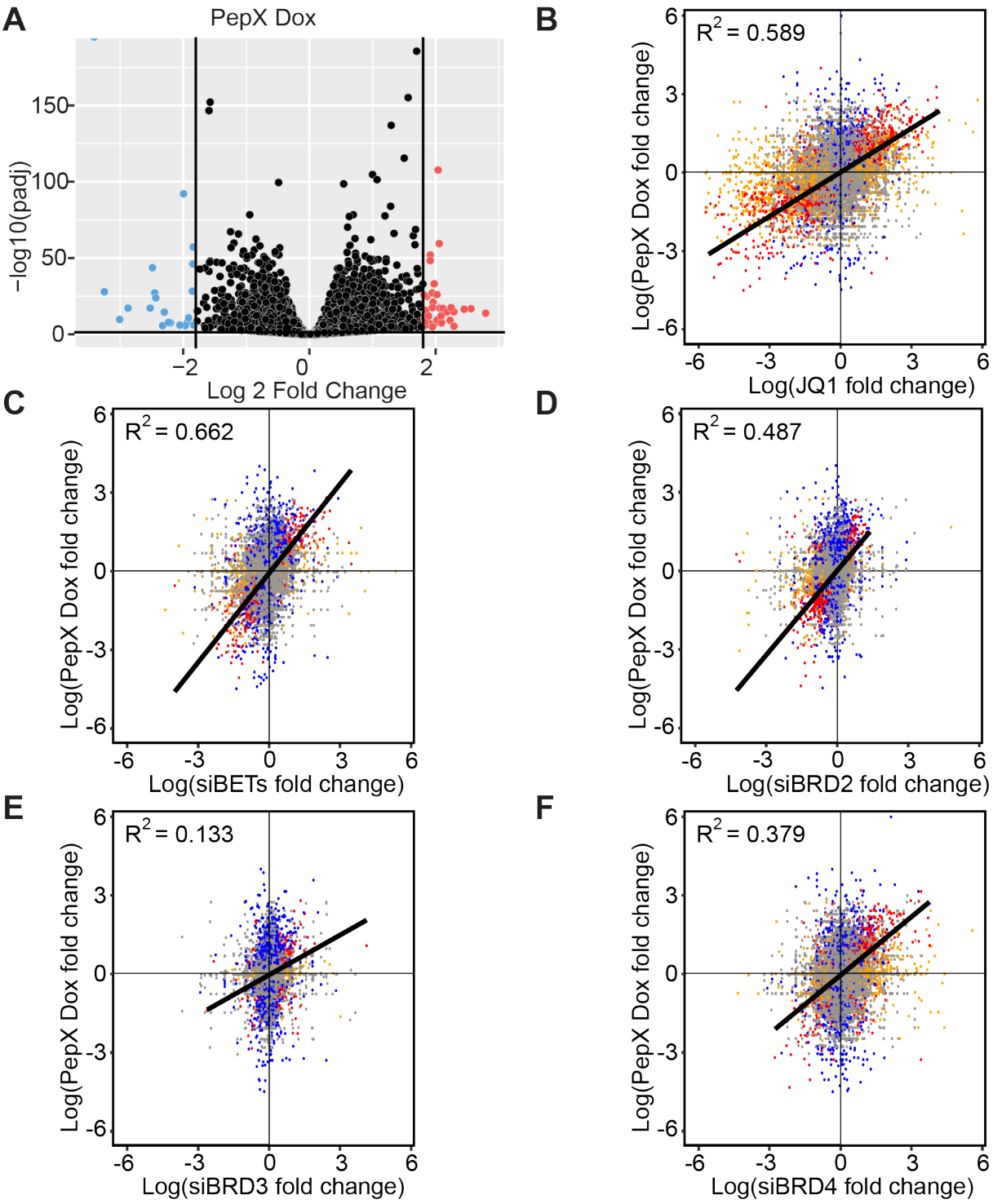


***Figure 5.5**: PepX induces BET-dependent changes in gene expression. (**A**) Changes in gene expression following induction of PepX expression by 50 nM doxycycline 48 h treatment compared with 0.05% v/v DMSO represented in a volcano plot. Blue dots represent genes with an LFC ≤ -1.8 and an adjusted p value ≤ 0.05, pink dots represent genes with an LFC ≥ 1.8 and an adjusted p value ≤ 0.05. Vertical black lines indicate 1.8*

*LFCs, which has been previously defined as the parameter by which up- and down-regulated genes are identified [152]. Horizontal black line indicates an adjusted p value ≤ 0.05. N = 4 biological replicates. Scatter plots depicting the correlation between LFCs in expression induced by PepX (compared with DMSO) compared with LFCs in expression induced by (+)-JQ1 (compared with (-)-JQ1) (**B**), siBETs (compared with siNC) (**C**), siBRD2 (compared with siNC) (**D**), siBRD3 (compared with siNC) (**E**) or siBRD4 (compared with siNC) (**F**) in 501mel cells. Genes are depicted as dots. The colour of the dot signifies the significance of the LFC: if LFC adjusted p value ≤ 0.05 for both treatments, the dot is red, if LFC adjusted p value ≤ 0.05 for treatment on the x axis, the dot is orange, if LFC adjusted p value ≤ 0.05 for treatment on the y axis, the dot is blue, if LFC adjusted p value > 0.05 for both treatments, the dot is grey. Linear regression line shows the correlation between genes that are significantly differentially regulated by both treatments. R^2 values shown.*

As PepX had an effect on transcription, the gene sets which were differentially regulated as a result of PepX expression were investigated as this may indicate how ET-domain inhibition led to a cessation of cellular proliferation. As mentioned in Chapter 3.2.3, E2F promotes transition from G1 to S phase of cell cycle [291], and MYC promotes cell cycle progression through the expression of advancers of the cell cycle and the inhibition of proteins that apply the brakes to cell cycle progression [292]. GSEA results presented in Figure 5.6 show that E2F targets, MYC targets and G2M checkpoint genes are down-regulated by PepX expression, which indicates that the PepX-induced cell cycle arrests observed in Figure 5.4 are underpinned by transcriptional events. This finding is reminiscent of GSEA results following (+)-JQ1 treatment and siRNA targeting BRD4 in 501mel cells (Figures 3.8A and 3.8C).

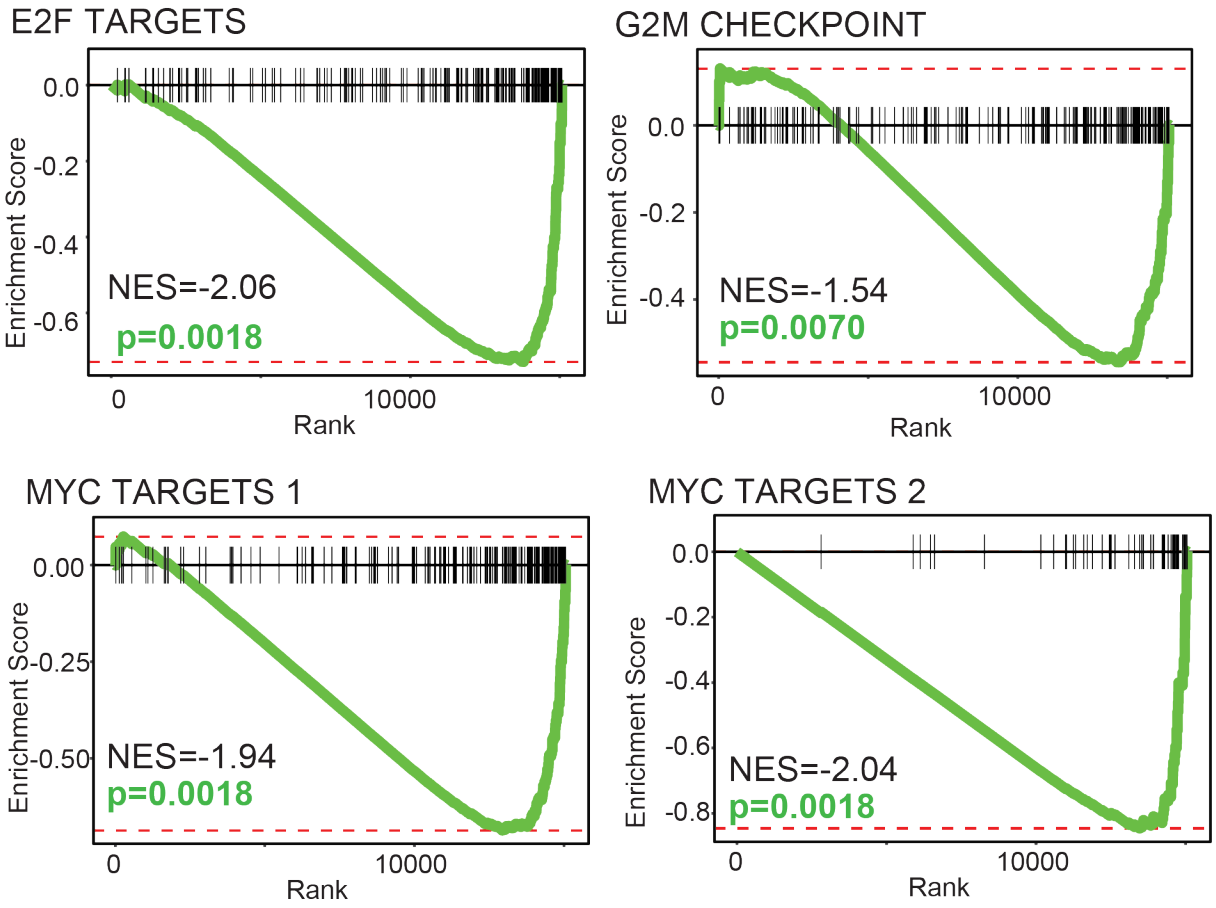


***Figure 5.6**: GSEA showing down-regulation of cell cycle related gene sets ("HALLMARK_E2F_TARGETS", upper left, "HALLMARK_G2M_CHECKPOINT", upper right, "HALLMARK_MYC_TARGETS_V1", lower left,"HALLMARK_MYC_TARGETS_V2", lower right) compared with 0.05% v/v DMSO (negative control) following 50 nM doxcycline treatment, inducing PepX expression for 48 h in 501mel cells. Computational analysis was carried out using DESeq2 [243] to identify differentially expressed genes, which were used for GSEA analysis in R [244]. NES = normalised enrichment score. P value represents adjusted p value.*

The p53 pathway was neither up-regulated following BET BRD inhibition in 501mel cells nor in p53 WT A375M cells; therefore, it is anticipated that ET-domain inhibition will also fail to up-regulate this pathway in 501mel cells. To confirm this, the p53 pathway was analysed using the RNA-seq data. Figure 5.7A shows that the p53 pathway is up-regulated following PepX expression. This indicates that perhaps the cell cycle arrest

observed in Figure 5.4 and transcriptional changes observed in Figure 5.6 are p53-dependent, but p21-independent (Figure 5.3B). This was unexpected given that (+)-JQ1 did not lead to up-regulation of the p53 pathway in 501mel cells, or in p53 WT A375M cells (Figure 3.9).

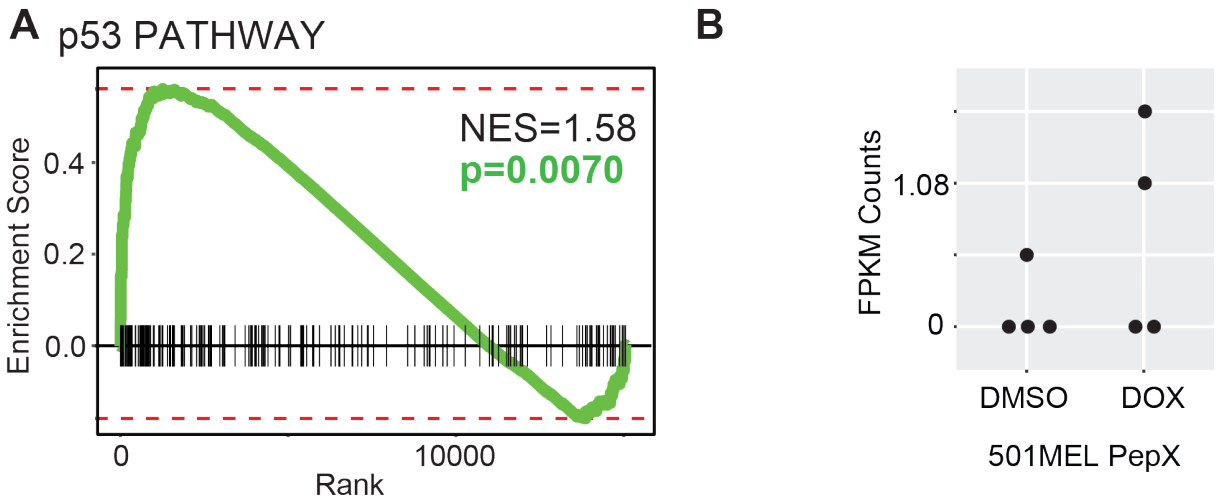


***Figure 5.7**: p53 pathway is up-regulated but CDKN1A is not following PepX expression. (**A**) GSEA showing up-regulation of the p53 pathway gene set ("HALLMARK_P53_PATHWAY") following 50 nM doxycycline treatment for 48 h to induce PepX expression compared with 0.05% v/v DMSO in 501mel cells. Computational analysis was carried out using DESeq2 [243] to identify differentially expressed genes, which were used for GSEA analysis in R [244]. NES = normalised enrichment score. P value represents adjusted p value. (**B**) Normalised FPKM of CDKN1A (p21) following RNA-seq in 501mel cells. Counts in each biological replicate of each cell line is represented by a black dot. Cells were treated with 50 nM doxycycline for 48 h before RNA was extracted and subject to sequencing. 0.05% v/v DMSO was used as a negative control. N = 4 biological replicates per condition. No statistical significant difference between the expression of CDKN1A when cells are treated with DMSO or doxycycline.*

In 501mel cells, neither p21 protein nor mRNA expression are up-regulated following BET BRD inhibition (Figures 3.2D and 3.3B). Following ET-domain inhibition, the p53 pathway is unexpectedly up-regulated. There is no up-regulation of p21 protein; however, this does not guarantee a lack of increase in p21 mRNA. Since 3 targets of p53 are up-regulated following PepX expression: IER5, FUCA1 and ATF3 [408], it is possible that there is also an up-regulation of p21 mRNA. To verify if p21 mRNA increased, RNA-seq data was analysed to ascertain how p21 (*CDKN1A*) expression is affected by PepX expression. Figure 5.7B shows that p21 expression is not affected by PepX expression; therefore, the cell cycle arrest is p21-independent, and potentially p53-dependent. Since all but 3 of the differentially regulated genes in the p53 pathway did not lie downstream of p53 [408], a lack of p53 activation due to the mutation would explain why there is up-regulation of the p53 pathway without p21 up-regulation.

BET BRD inhibition induced senescence in 501mel cells in potentially p53-independent manner; however, p53 often plays a role in the induction of senescence [409, 410]. A significant subset of the genes comprising the leading edge in the p53 pathway, including FOXO3, GADD45A, TP53, CDKN2B, ZFP36L1, and TGFB1, are involved in the KEGG cellular senescence pathway, suggesting ET-domain inhibition leads to cellular senescence (data not shown). Therefore, to gain more insight into the way in which 501mel cells stop proliferating following PepX expression, it was investigated whether ET-domain inhibition induced a senescence phenotype.

5.2.5 BET ET-domain inhibition induces autophagy-dependent senescence

To elucidate further how the cells stop proliferating, further analysis of RNA-seq data was undertaken. This revealed an up-regulation of FOXO4 targets, which indicates the activation of senescence (Figure 5.8A); Ectopic expression of FOXO4 in three $BRAF^{V600E}$ mutant melanoma cell lines led to the induction of senescence [411]. Given that 501mel

parental cells express mutant $BRAF^{V600E}$, up-regulation of FOXO4 in this context may also result in senescence. Senescent cells secrete cytokines as part of the senescence-associated secretary phenotype (SASP) [412]. Interferon gamma and TNFα are pro-inflammatory cytokines and their up-regulation can lead to the onset of senescence and the SASP in melanocytes [413-415]. Therefore, the up-regulation of TNFα and interferon gamma cytokine signalling, as indicated by the transcriptional changes in Figure 5.8B, signal the onset of senescence.

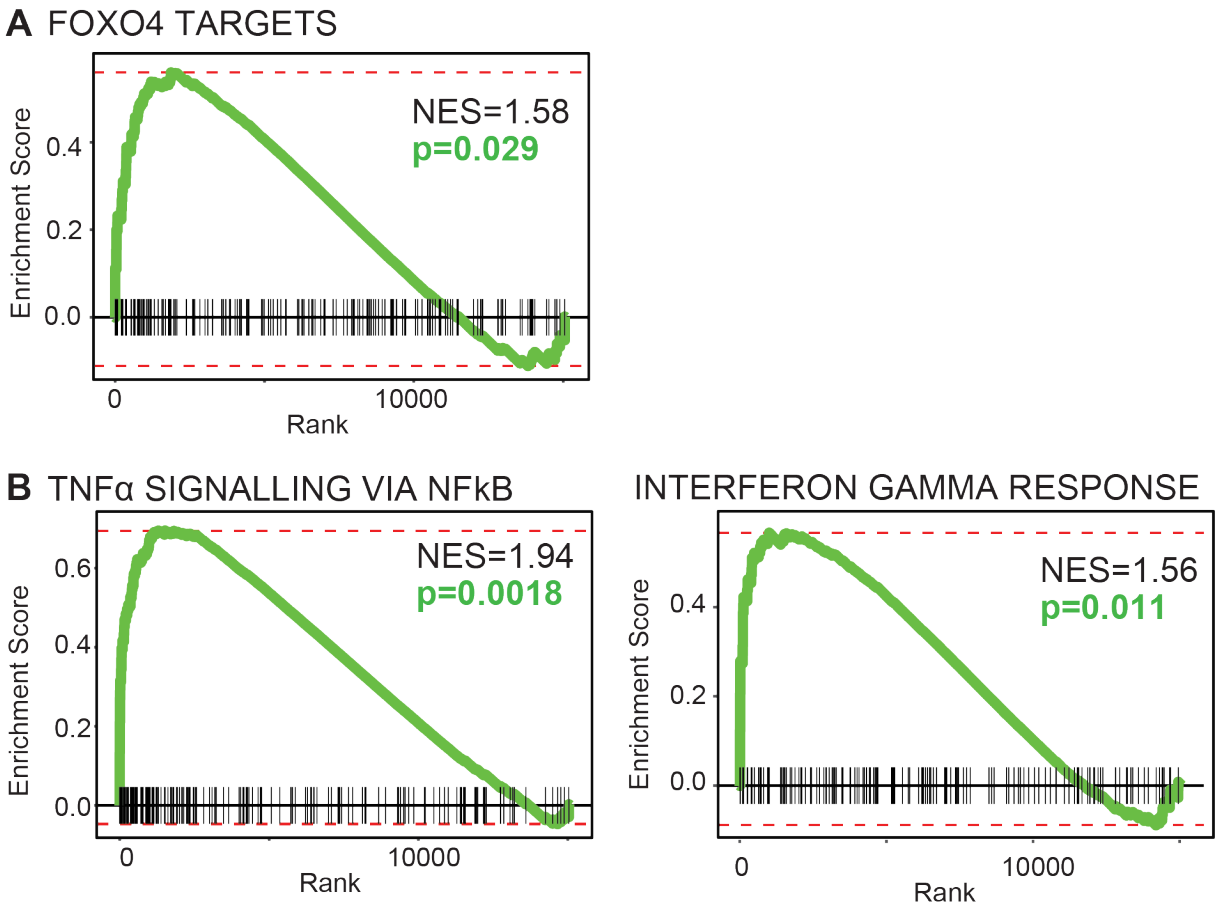


***Figure 5.8**: PepX induces the up-regulation of senescence-related gene sets. (**A**) GSEA showing up-regulation of FOXO4 targets c3 gene set ("FOXO4_01") (upper left), (**B**) TNFα signalling via NFkB ("HALLMARK_TNFA_SIGNALING_VIA_NFKB") (lower left), and interferon response ("HALLMARK_INTERFERON_GAMMA_RESPONSE") (lower right) following 50 nM doxycycline treatment for 48 h to induce PepX expression compared with 0.05% v/v DMSO in 501mel cells. Computational analysis was carried out using DESeq2*

[243] to identify differentially expressed genes, which were used for GSEA analysis in R [244]. NES = normalised enrichment score. P value represents adjusted p value.

To determine whether cells undergo senescence and to validate the RNA-seq findings presented in Figure 5.8, cells were examined for markers of cellular senescence. 501mel cells were treated with doxycycline for 48 h to induce PepX expression and were stained for β-galactosidase expression, a marker of senescence, with DMSO as a negative control. Figure 5.9A shows that PepX expression led to a moderate increase in β-galactosidase activity, which was quantified in Figure 5.9B.

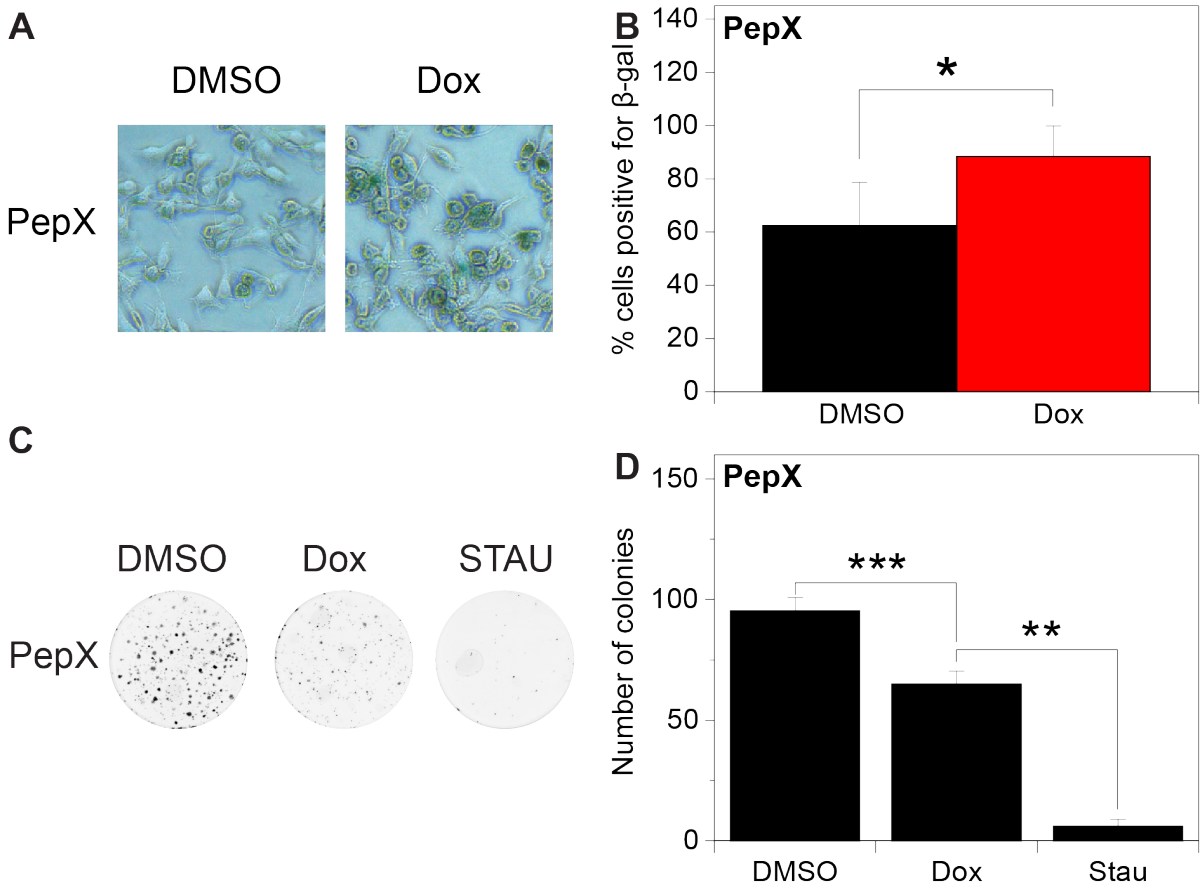


***Figure 5.9**: ET-domain inhibition induces senescence in 501mel cells. (**A**) 501mel cells show increased β-galactosidase staining following 48 h PepX expression induced using 50 nM doxycycline. 0.05% v/v DMSO was the negative control. (**B**) Quantification of β-galactosidase staining in 501mel cells following 48 h PepX expression induced using 50*

*nM doxycycline. 0.05% v/v DMSO was the negative control. N = 3 biological replicates. Mean percentage of cells stained positive for β-galactosidase shown ± standard deviation. Statistical significance was determined using a two-tailed Students t-test. * = p < 0.05. (**C**) 501mel cell colonies formed following 50 nM doxycycline-induced PepX expression for 48 h. The negative control was 0.05% v/v DMSO and the positive control was 0.1% v/v staurosporine. Cells were treated with the indicated compound for 48 h then subsequently re-plated and grew for 1 week in normal medium before staining with crystal violet. (**D**) Quantification of 501mel cell colonies formed following 50 nM doxycycline-induced PepX expression for 48 h. The negative control was 0.05% v/v DMSO and the positive control was 0.1% v/v staurosporine. N = 3 biological replicates.*

Senescence is defined as permanent cell cycle arrest whereas quiescence is a “reversible non-proliferating state” [416, 417]. While there is increased β-galactosidase staining, this is not sufficient to prove senescence, as it is possible that the cells entering a quiescent state, and β-galactosidase staining can be indicative of increased lysosomal function [418]. In order to show that the cells have irreversibly arrested their cell cycle, a clonogenicity assay was performed. Briefly, cells were treated with doxycycline for 48 h, then re-plated as single cells, which grew into colonies over the course of 1 week in normal media. Thus, throughout the week of growth, doxycycline was withdrawn. DMSO was used as a negative control. Staurosporine, a known inducer of cell death, was used as a positive control [324]. Figure 5.9C shows that the number of colonies that form following PepX expression is reduced compared with DMSO, and this is quantified in Figure 5.9D. Therefore, the phenotype induced by PepX expression is not reversible. Some cells are senescent when DMSO is added (Figure 5.9B), which may be due to leaky expression of PepX. Heterogeneity of PepX expression may account for the significant but only partial loss in colony formation capacity observed in Figure 5.9D (Figures 5.1D-5.1E).

Nonetheless, Figure 5.9 shows that 501mel cells become senescent following ET-domain inhibition.

If PepX induces cellular senescence in a homogenous cell population, there should be no induction of cell death. To confirm that PepX expression did not induce cell death, caspase signalling was examined. As detailed in Chapter 3.2.5, caspase activation converges on PARP cleavage and is indicative of the onset of apoptosis [211, 213, 214]. To detect caspase activation, cells were stained with a fluorescent reagent that binds to the cleaved caspase at the site of cleavage. The same samples were also stained with a dye specific for dead cells. The cell staining was subsequently analysed using flow cytometry. During flow cytometry analysis, cells were divided into four categories: negative for both stains (lower left quadrant), positive for dead cell stain only (upper left quadrant), positive for caspase activation (lower right quadrant) and cells positive for both caspase activation and dead cell stain (upper right quadrant). The lower and upper right panels were assigned as populations of cells which display caspase activation. Figure 5.10A shows that caspase 3/7 activation was not up-regulated following PepX expression in 501mel cells, which was quantified from 3 biological replicates in Figure 5.10B. Immunoblots were carried out to confirm the lack of caspase activation by examining PARP cleavage. Figure 5.10C shows that following the addition of doxycycline, there is no PARP cleavage. Staurosporine was included as positive control that induces PARP cleavage. Immunoblotting was also used to confirm the lack of caspase 3 activation, which is indicated through caspase 3 cleavage. Figure 5.10C confirms that caspase 3 cleavage did not take place on addition of doxycycline. Finally, to eliminate the possibility of cells undergoing cell death via non-apoptotic mechanisms, such as necrosis and pyroptosis, annexin V staining was examined. Figure 5.10D shows that there was a small increase in annexin V staining following ET-domain inhibition. However, Figure 5.10E shows that the increase in the population of cells positive for annexin V staining is not significant when expression of

PepX is induced; therefore, cells do not die following PepX expression. While it is possible that, due to the heterogeneity of the PepX expression following doxycycline addition (Figure 5.1E), a small population of PepX-expressing cells die following the addition of doxycycline, which would account for the small rise in the cell population positive for annexin V, the lack of statistical significance in this result reinforces the findings in Figure 5.10A-5.10C showing that cell death was not triggered following PepX expression in 501mel cells.

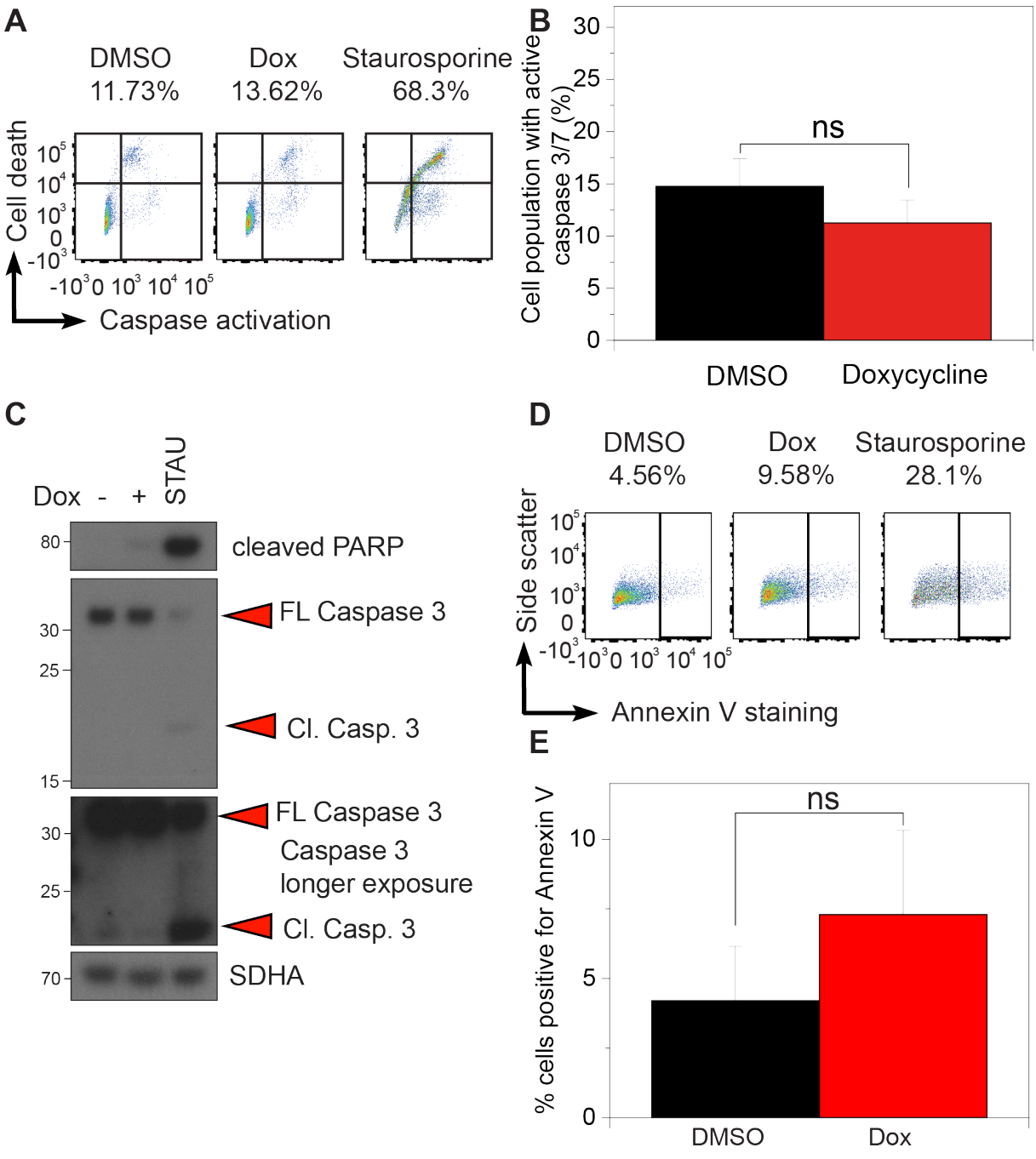


***Figure 5.10**: ET-domain inhibition does not induce cell death. (**A**) Cell staining showing caspase 3/7 activation staining of PepX-expressing 501mel cells after 72 h treatment with 50 nM doxycycline. 0.1% v/v Staurosporine is a positive control. 0.05% v/v DMSO is the negative control. (**B**) Quantification of caspase 3/7 activation in PepX-expressing 501mel cells following treatment with 50 nM for 72 h. Negative control is 0.05% v/v DMSO. N = 3 biological replicates. Mean percentage of cells stained positive for active caspases 3/7 shown ± standard deviation. Statistical significance was determined using a two-tailed Students t-test. ns = non-significant difference. (**C**) Representative immunoblot showing caspase 3 is not cleaved following BET ET inhibition in 501mel cells. PepX expression was induced following 50 nM doxycycline treatment for 72 h. SDHA was used as a loading control. 0.05% v/v DMSO was the negative control, and 0.1% v/v staurosporine (stau) was the positive control. N = 3 biological replicates. (**D**) Representative annexin V staining in 501mel cells. 501mel cells do not die following induction of PepX using 50 nM doxycycline treatment for 72 h. Annexin-V-positive cell population highlighted in box at the right of each sample. Staurosporine is positive control. 0.05% v/v DMSO is a negative control. N = 3 biological replicates. (**E**) Quantification of annexin V staining in 501mel cells following following induction of PepX using 50 nM doxycycline treatment for 72 h. N = 3 biological replicates. 0.05% v/v DMSO is a negative control Mean percentage of cells stained positive for annexin V shown ± standard deviation. Statistical significance was determined using a two-tailed Students t-test. ns = non-significant difference.*

BET BRD inhibition leads to induction of autophagy-dependent senescence in 501mel cells (Figure 3.14A). As detailed in Chapter 3.2.5, there are documented links between senescence induction and autophagy [311]; therefore, 501mel cells were tested for signs of autophagic perturbation following BET ET-domain inhibition. RNA-seq data analysis showed potential up-regulation of FOXO1 and FOXO3 targets (Figure 5.11A), which

suggests autophagy may be up-regulated underpinned by transcriptional events [419-422]. The overlap over the genes within the leading edges of these two gene sets was approximately 1/3, suggesting these gene sets were likely up-regulated independently. For plans to validate autophagy-related genes were up-regulated following PepX expression, see Chapter 7.3.3. To validate the RNA-seq data suggesting that autophagy was up-regulated, LC3BII expression was observed, with and without PepX expression. LC3BII is a marker of autophagic flux [305, 385], when its expression is coupled with the use of an inhibitor of autophagy such as BafA [304, 305], as previously described in Chapter 3.2.4 and Chapter 4.2.4. Figure 5.11B shows that LC3BII increases following PepX expression, both with or without treatment with BafA, which is quantified in Figure 5.11C, and is indicative of an increase in autophagic signalling [304, 305]. Therefore, autophagy is activated following ET-domain inhibition in 501mel cells and is potentially underpinned by transcriptional events.

The small but highly significant increase in LC3BII expression indicates that autophagy is potentially highly up-regulated in a small proportion of cells. It is impossible to determine the proportion of the cell population in which LC3BII is up-regulated using immunoblot, but could be determined using a flow cytometry experiment. LysoTracker staining would enable the detection of the lysosomal content of individual cells, which would clarify the proportion of cells in which autophagy is up-regulated by PepX expression. BFP expression could be detected using flow cytometry; therefore, it would be possible to determine if autophagy is up-regulated as a function of BFP and, therefore, PepX expression.

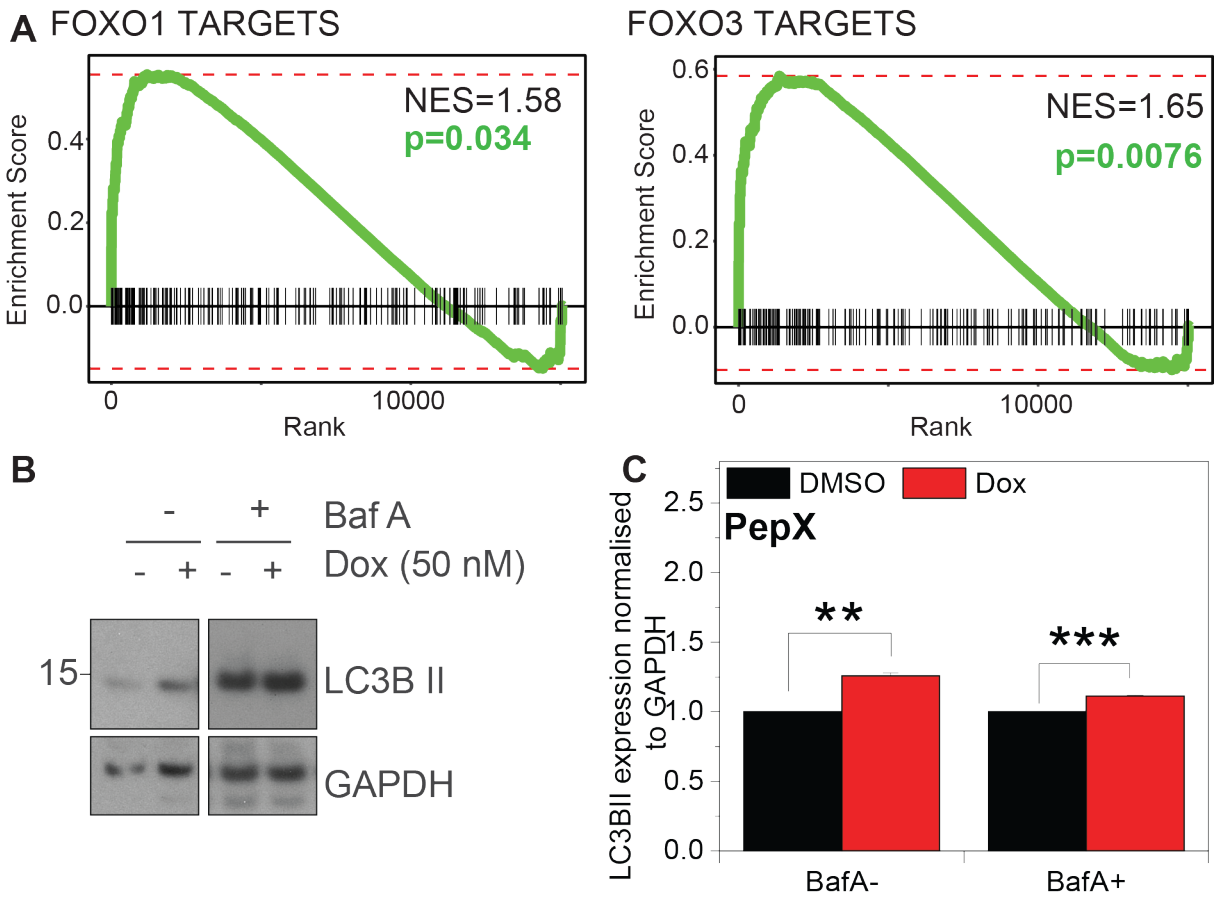


***Figure 5.11**: ET-domain inhibition leads to the up-regulation of autophagy in 501mel cells. (**A**) GSEA showing up-regulation of FOXO1 targets c3 gene set ("FOXO1_02") (left), and FOXO3 targets c3 gene set ("FOXO3_01") (right) following 50 nM doxycycline treatment for 48 h to induce PepX expression compared with 0.05% v/v DMSO in 501mel cells. Computational analysis was carried out using DESeq2 [243] to identify differentially expressed genes, which were used for GSEA analysis in R [244]. NES = normalised enrichment score. P value represents adjusted p value. (**B**) Immunoblot of LC3BII staining in 501mel PepX cells after 24 h treatment with 0.05% v/v DMSO (negative control) or 50 nM doxycycline, with or without 3 h of 10 nM BafA. GAPDH was used as a loading control. (**C**) Quantification of LC3BII staining in PepX-expressing 501mel cells normalised to GAPDH expression following treatment with 0.05% v/v DMSO (negative control) or 50 nM doxycycline for 24 h, ± 3 h of treatment with 10 nM BafA. N = 3 biological replicates. Mean protein expression shown ± standard deviation. Statistical significance was determined using a two-tailed Students t-test. * = $p < 0.05$, ** = $p < 0.01$, *** = $p < 0.001$.*

Pharmacological inhibition of BET BRD leads to loss of cell proliferation in 501mel through the onset of senescence, which can be bypassed upon inhibition of autophagy. To test whether attenuation of autophagy rescued 501mel cells from senescence induced following ET-domain inhibition, cells were concomitantly treated with doxycycline and CQ. As detailed in Chapter 3.2.5, CQ inhibits autophagy through the prevention of lysosomal acidification [305]. Figure 5.12 shows that cellular proliferation significantly decreases following PepX expression with low or high doxycycline concentrations, as expected. When cells were concomitantly treated with CQ, cellular proliferation is somewhat rescued. This suggests that the anti-proliferative effects exerted by PepX may be partly dependent upon autophagy activation, and thus, PepX induces a cessation of proliferation through the onset of autophagy-dependent senescence.

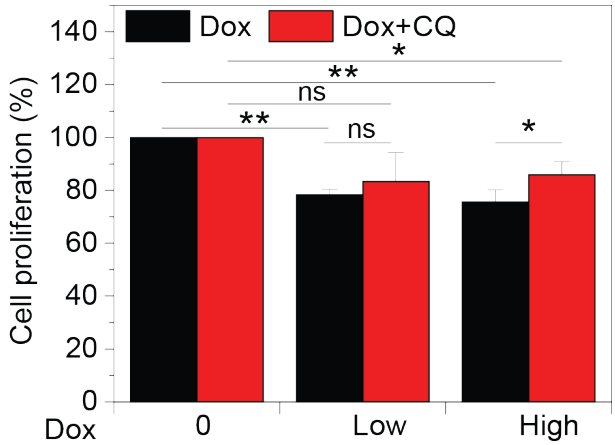


***Figure 5.12**: PepX expressing 501mel cells were treated with indicated concentrations of doxycycline for 72 h, with (red bars) and without (black bars) 10 μM CQ. Cellular proliferation measured using MTT assay, with values normalised to proliferation observed when cells were treated without any treatment (black 0 bar) or with 10 μM CQ alone (0 red bar). N = 3 biological replicates. Mean cellular proliferation shown ± standard deviation. Statistical significance was determined using a two-tailed Students t-test. ns = non-significant difference, * = $p < 0.05$, ** = $p < 0.01$.*

5.3 Discussion

In this chapter I have demonstrated for the first time that ET-domain inhibition of BET proteins leads to loss of cellular proliferation in melanoma. Perturbation of ET-dependent, and potentially PTEF-b-independent, transcription leads to loss of cell cycle gene expression (Figure 5.2), and induction of autophagy- and senescence-related genes (Figures 5.8 and 5.11A). The data in this chapter show that PepX induces onset of senescence, which can be bypassed using concomitant autophagy attenuation, providing proof of principle that Kac-independent targeting of BETs leads to loss of cellular proliferation, and a mechanism as to how this occurs.

However, these data are not without limitations. The leakiness of PepX-, NLS-, KRR- and LIL-expression, and heterogeneity of their expression within the polyclonal 501mel cell lines render the results less reliable. There is also a small amount of PepX expression in the absence of doxycycline, in cells treated with DMSO (data not shown). Therefore, the baseline is different from 501mel parental cells. This was clear when observing senescence: ~20% parental 501mel cells were senescent following treatment with (-)-JQ1 or DMSO, as indicated by β-galactosidase staining (Figure 3.12K). However, ~60% PepX-expressing cells were senescent when treated with DMSO (Figure 5.9B). The leakiness is not restricted to the PepX-expressing 501mel cell line, the expression of NLS, KRR and LIL is also leaky (Figure 5.1B). Two-plasmid Tet-on systems are notoriously leaky [423-425]; therefore, it is no surprise that leakiness is observed in this study.

Heterogeneous expression of PepX increases uncertainty as to whether results, such as those that are gained from immunoblotting, represent a small subset of the cellular population that display an extreme phenotype, or if they are truly representative of the whole population. Additionally, the expression levels of PepX-, NLS-, KRR- and LIL were variable between biological replicates, (Figure 5.1D). However, given that PepX still

induced significant effects in experiments throughout this chapter, and the control peptides did not, it seems likely that the variability in PepX-, NLS-, KRR- and LIL-expression had little biological impact. To ensure PepX-, NLS-, KRR- and LIL-expression were as consistent as possible, BFP expression was routinely observed using microscopy (data not shown). Moreover, fresh aliquots of doxycycline were used to ensure that any deterioration of doxycycline potency did not have any effect on PepX-, NLS-, KRR- and LIL-expression. To solve the problem of heterogeneity of expression within and between cell lines, perhaps multiple monoclonal PepX-, NLS-, KRR- and LIL-expressing lines should be used. While use of polyclonal cell lines has disadvantages, such as heterogeneity and perhaps the emergence of dominant clones over time, resulting in a changing population, polyclonal lines were used in these experiments to ensure that the population of cells were as closely matched to 501mel parental cells as possible and the findings did not reflect the effects of PepX on a small number of, potentially abnormal, monoclones. This enables a more direct comparison between the PepX-induced effects observed in this chapter and the (+)-JQ1-induced effects observed in 501mel cells in Chapter 3.

The leakiness and heterogeneity of the PepX expressing cells called for suitable controls. The NLS-, KRR- and LIL- expressing polyclonal cells experience the same problems of the leakiness and heterogeneity of expression as the PepX expressing cells. Therefore, they were included as controls to show that, despite the leakiness and heterogeneity of construct expression, only PepX had any significant effect on cell proliferation, transcription and cell cycle arrest. Initially, there were concerns that NLS affected cellular proliferation (Figure 5.2B); however, these concerns were allayed when cell cycle analysis data confirmed that only PepX expression induced cell cycle arrest, and RNA-seq analysis confirmed only PepX had an effect on cell cycle gene expression.

Additionally, when using the piggybac system, the site of integration of the expression cassette into the cellular genome is random, and non-uniform between different cell lines,

which may account for different basal proliferation rates of the modified cell lines. For example, if the integration of the piggybac cassette disrupts a tumour suppressor, the resulting cells may have a proliferative advantage over cells in which a pro-proliferative gene was disrupted upon integration. Perhaps to circumvent the issues of leakiness, heterogeneity, and to control the locus at which the piggybac expression cassette integrates within the cellular genome, CRISPR editing could have enabled insertion of Flp-In sites at known genomic loci, which would be subsequently used to integrate the piggybac expression cassette into the cellular genome [426-428].

It was interesting to note that an up-regulation of the p53 pathway (Figure 5.7A) coincided with changes in cell cycle gene expression (Figure 5.6) and cell cycling arrest (Figure 5.4), but no up-regulation of *CDKN1A* expression (Figure 5.7B) or p21 expression (Figure 5.3B). This suggests that cell cycle arrest following ET-domain inhibition may occur in a p53-dependent but p21-independent manner. This is an intriguing notion as this indicates that p53 retained partial functionality despite the C275W mutation harboured by 501mel cells (Figures 3.2A and 5.3A).

The gene expression findings presented in this chapter elevate the importance of ET-dependent, potentially PTEF-b-independent, transcription regulation. In order to show that PepX disrupted transcription in a ET-dependent and PTEF-b-independent manner, see Chapter 7.3.3. ET-domain-dependent, PTEF-b-independent transcription is less well studied than the PTEF-b-dependent counterpart, but represents a mechanism by which the expression of fewer genes can be perturbed compared with BET BRD inhibition or PTEF-b-dependent transcription inhibition, whilst inducing anti-tumour transcriptional effects. This indicates that BET protein Kac-independent functions, a relatively unexplored aspect of BET function, have a novel role in maintaining cell proliferation. Indeed, to yield cell cycle arrest and a reduction in cell cycle gene expression, the data presented in this chapter suggest it is sufficient to prevent the assembly of transcriptional machinery on the

BET protein platform, rather than inhibiting docking of the BET protein to chromatin. Therefore, the binding of BETs to chromatin via BRDs is necessary but not sufficient to sustain cellular proliferation.

Much evidence points to BRD4 as the most important BET family member in driving malignancy [96, 98, 151]; however, PTEF-b-independent transcription is driven through interactors that bind to the ET-domain of BRD4, which is common to BRD -2, -3, and -4 [40]. BRD2 and BRD3 possess an ET-domain with <80% sequence homology compared with the BRD4 ET-domain [40]. Additionally, BRD2 binds to two of the PTEF-b-independent drivers of transcription, JMJD6 and NSD3 [36, 40]. Indeed, Figure 5.5D-5.5F show that of BRD -2, -3 and -4, significant LFCs in gene expression induced by BRD2 knockdown correlate most with significant LFCs in gene expression compared to PepX. This indicates that the changes in transcription induced by PepX are most similar to those induced by BRD2 knockdown; thus, the effects of PepX are potentially mainly mediated through BRD2. This contradicts the notion that BRD4 is the most important member of the BET protein family for driving transcription and maintaining cell viability in the context of malignancy [96, 98, 151], and highlights BRD2 as a potential drug target candidate. Additional studies are needed to fully elucidate the roles of BRD2 and BRD3 with respect to these putative functions; however, it is possible that BET family members may play non-redundant roles in driving PTEF-b-independent transcription and malignancy.

Figure 5.8 shows that senescence-related gene sets are up-regulated [411, 413-415], and Figure 5.11A shows that autophagy-related gene sets are up-regulated [419-422] following PepX expression. The up-regulation of these gene sets suggests that BETs have a suppressive role in regulating gene expression. Indeed, the de-repression of gene expression induced by BET inhibition has been previously observed [36, 284, 429, 430]. Additionally, all BET protein inhibition strategies lead to gene up-regulation, whether via BRD or ET inhibition, or genetic individual or pan- BET inhibition (Figure 5.5). However,

this is the first time that specifically ET-domain BET inhibition has been shown to lead to gene up-regulation, suggesting that preventing docking of interactors to BETs is sufficient to stimulate locus-specific transcription. It is possible that PepX binding to the ET-domain outcompetes negative regulators of transcription, and prevents their binding to BETs at genomic loci. In pancreatic cancer, BRD4 guides the histone methyltransferase, G9a, to the promoters of autophagy-related genes, whereupon histones are methylated [68]. This leads to gene silencing, despite BETs being poised to activate transcription. Once G9a and BRD4 are displaced from chromatin by (+)-JQ1, transcription is de-repressed, which enables activation of autophagy gene expression [68]. Further work is required to determine if G9a displacement from BETs is involved in autophagy up-regulation in the context of melanoma, and whether G9a can be displaced from chromatin through ET-domain inhibition rather than BET BRD inhibition. If ET-domain inhibition is sufficient to displace BET-bound suppressors of gene expression, such as G9a, this would explain how PepX expression leads to gene up-regulation.

Overall, the data from this chapter have shown that targeting BETs via the ET-domain represents a novel strategy that leads to potential anti-tumour effects *in vitro*. In 501mel cells, ET-domain inhibition leads to autophagy-dependent senescence induction, similar to BET BRD inhibition, as shown in Chapter 3. *In vivo*, it is predicted there will be fewer toxicities compared with BET BRD inhibition, as fewer genes are perturbed following ET-domain inhibition. Additionally, in theory, ET-domain inhibition results in retention of BET chromatin occupation which prevents erroneous binding and activity of chromatin modifying enzymes and other chromatin interactors that can wreak havoc following BET displacement from chromatin. The findings in this chapter highlight PepX as a tool by which BET function in Kac-independent manner can be modulated, but more work is required to understand the mechanistic aspects of PepX-BET targeting, and to render Kac-independent BET-targeting applicable to patient care.

Chapter 6: Discussion

BET BRD inhibition leads to loss of cellular proliferation in a variety of malignancies, utilising a range of mechanisms. To ensure that BET BRD inhibitors are utilised in patients who will benefit most from them, it is important to understand the factors that drive the cellular response. In melanoma the factors underpinning sensitivity require further clarification; however, the data in this thesis suggest that p53 mutation status correlates with cellular response. BET BRD inhibition induces autophagy-dependent senescence in p53 mutant 501mel melanoma cells, and autophagy-independent senescence in A375M p53 WT melanoma cells.

Patients involved in phase 1 trials using BET BRD inhibitors experience adverse side effects [91, 160, 161]. To circumvent this issue whilst still targeting BETs, alternative targeting of BETs has been explored. In prostate cancer, RT53 leads to a reduction of cellular proliferation *in vitro*, and BET BRD inhibition leads to AR-independent autophagy up-regulation. Autophagy appears to act in a cytoprotective manner, as concomitant inhibition of autophagy and BET BRDs leads to exacerbated loss of cellular proliferation. In melanoma targeting the ET-domain represents a novel mechanism of BET inhibition: ET-domain inhibition yields therapeutically beneficial responses, providing proof-of-principle, that alternative targeting of BETs in melanoma may represent a viable targeting strategy.

6.1 Role of autophagy following BET inhibition

Autophagy is a mechanism by which nutrient availability within the cell is increased through the catabolism of damaged organelles and other lysosomal protein substrates. Furthermore, autophagy also helps to combat nutrient deficits when cells are in starvation or hypoxic conditions [431]. While BRD4 can both promote and suppress autophagy,

seemingly in a context-dependent manner [68, 432, 433], it is no surprise that throughout this thesis we find that BET inhibition affects autophagic flux.

6.1.1 Autophagy is up-regulated in prostate cancer and melanoma following BET inhibition

The role of BETs in autophagy activation appears to be context-dependent: in pancreatic cancer, BRD4 expression suppresses autophagy [68]; however, BRD4 promotes autophagy through transcription of autophagy-related genes in AML, potentially through interactions with transcription factor CEBPβ, or NPM1 [432, 433] and treatment with BET BRD inhibitors (+)-JQ1 and I-BET151 leads to down-regulation of autophagy [432].

The findings in this thesis show that since BET inhibition leads to autophagy up-regulation in both melanoma and prostate cancer, BETs suppress autophagy. In prostate cancer, autophagy is up-regulated following suppression of AR-signalling [393, 399], but the data presented in this thesis suggest that autophagy is up-regulated in prostate cancer cells, yet AR signalling is not down-regulated (Figure 4.3).

At time of writing, this is the first report of BET inhibition leading to autophagy up-regulation in prostate cancer and melanoma, either through BRD or ET-domain inhibition. To reconcile these findings with indications from AML that BETs promote autophagy, I would hypothesise that BETs occupy chromatin at the sites of autophagy-related gene promoters [68], or enhancers as observed in AML [433], in a range of malignancies. However, it is the milieu of context-dependent BET protein interactors that determine autophagy gene expression, and the influence of BET inhibition on autophagy, rather than BET protein function. As such, BETs potentially function as a platform that supports further fine-tuning of gene expression, rather than modulators of gene expression themselves.

6.1.2 The dichotomy of autophagy in cancer

Autophagy can promote or hinder the progression of tumours, seemingly in a context-dependent manner [431]. Autophagy promotes survival through withstanding anoikis, cell death following detachment from extracellular matrix. For example, autophagy is up-regulated upon detachment in breast cancer cells *in vitro*, and siRNA-mediated knockdown of autophagy-related genes leads to increased apoptosis in the detached cells [434], indicating that autophagy mediates cellular survival upon detachment. These findings suggest that *in vivo*, autophagy could promote cellular survival when cells are deprived from ECM contacts, for example in blood vessels, and thus, promote metastasis.

Autophagy up-regulation can also drive resistance to therapies. There is evidence across multiple malignancies that autophagy can serve as a cytoprotective mechanism, as observed in Figure 4.7. As previously mentioned in Chapter 4.2.6, autophagy inhibitors can enhance sensitivity of prostate cancer cells to a range of anti-cancer drugs [399]. Similarly, the sensitivity of AML cells to (+)-JQ1 was increased upon concomitant autophagy inhibition [101, 432, 435]. Unsurprisingly pancreatic cancer cells were more resistant to starvation induced death when BRD4, a suppressor of autophagy, was knocked down, thereby up-regulating autophagy. However, when autophagy genes were knocked out, cells displayed greater cell cycle arrest and cell death [68]. This suggests that the up-regulation of autophagy protected the cells from starvation-induced cell death, which could promote tumour cell longevity *in vivo*. Indeed, autophagy is up-regulated in cutaneous melanoma, suggesting that autophagy is important to melanoma survival [436]. Furthermore, autophagy is cytoprotective against MAPK-p38 inhibitors in melanoma and colorectal cancer cells [346, 437]. In the colorectal cells, inhibition of autophagy led to a switch from autophagic-cell death to apoptosis and cell death increased further [437].

However, there is evidence to suggest that autophagy can hinder tumour growth. As mentioned in Chapter 3.2.3, autophagy up-regulation is required for the onset of OIS in melanocytes, specifically following BRAF activation [318, 319]. Upon autophagy inhibition, senescence is bypassed [318, 319]. Therefore, in this context, autophagy plays a tumour suppressive role. Furthermore, a component of the autophagy pathway, Beclin1, is deemed a tumour suppressor: mice harbouring a heterozygous deletion of Beclin1 experienced a higher rate of spontaneous hepatocellular carcinomas, lymphomas and lung cancers, compared to wild-type counterparts [438]. Moreover, deletions of Beclin1 are found in breast cancers, and patients harbouring colon and oesophageal cancers with Beclin1 deletions suffer a worse 5-year survival rate compared to those with Beclin1 expression [383, 439, 440]. However, high Beclin1 expression in oesophageal cancers correlated with poorer patient outcome [441], suggesting that the influence of Beclin1 on tumour progression is context dependent.

The dichotomous role of Beclin1 exemplifies the lack of clarity surrounding the role of autophagy in tumour initiation and progression. Autophagy enables the cells to deal with stress, which serves as a double-edged sword. This may prevent oncogenic stress and prevent tumourigenesis, yet may also mitigate the stresses induction by anti-cancer therapies. The data presented throughout this thesis confirm that autophagy up-regulation has varied, context-dependent effects. BET BRD inhibition leads to autophagy up-regulation in both melanoma and prostate cancer *in vitro* models. In LNCaP prostate cancer cells concomitant pharmacological inhibition of BETs and autophagy induced a greater loss of cellular proliferation and a greater G1 cell cycle arrest compared to either inhibitor alone. Meanwhile, both BRD and ET-domain inhibition led to up-regulation of autophagy in 501mel melanoma cells. Concomitant inhibition of autophagy led to a rescue of cellular proliferation, suggesting that BET inhibition leads to activation of senescence through up-regulation of autophagy, and upon autophagy inhibition senescence is

bypassed. In A375M melanoma cells, autophagy up-regulation seemingly did not drive loss of cellular proliferation, nor was it cytoprotective, as the concomitant inhibition of autophagy and pharmacological BET BRD inhibition did not yield any change in cellular proliferation. While BET-inhibition-mediated induction of autophagy in these contexts is novel, these data are in alignment with previously published results: the role of autophagy is context-dependent and more work should be carried out to understand how better to harness it in a therapeutically beneficial manner.

6.1.3 Autophagy and p53

Transcription factor and tumour suppressor p53 also has a dual role with respect to autophagy regulation. Nuclear p53 can induce autophagy under conditions such as hypoxia, DNA damage and oncogene activation [307, 391, 431], and this can be perturbed by different mutations that affect its sub-cellular localisation. As mentioned in Chapter 3.2.3, p53 mutants that reside in the cytoplasm to a greater extent than WT p53 have a greater repressive effect on autophagy than WT [345]. Additionally, genetic or pharmacological inhibition in colorectal, neuroblastoma or cervical cancer cells led to the up-regulation of autophagy through the up-regulation of AMPK phosphorylation [257], suggesting p53 suppresses autophagy.

In melanoma, the role of autophagy in relation to cellular proliferation following BET inhibition appears to correlate with p53 mutation. However, WT p53 is expressed in both LNCaP and A375M cells; therefore, it is unlikely that the role of autophagy in relation to cellular proliferation following BET inhibition is dependent upon p53 mutation status, or perhaps it is context specific. As previously mentioned, p53 mutation status doesn't guarantee function [337], and lack of functional p53 expression does not guarantee loss of p53 pathway functionality [442]. Moreover, p38 inhibition led to autophagic-cell death in a range of colorectal cancer cell lines with varying p53 mutation statuses but induction of

autophagic-cell death did not correlate with p53 mutation status [437]. This suggests that p53 mutation status does not indicate a role of autophagy regarding cellular proliferation. Therefore, perhaps the role of autophagy in relation to cellular proliferation following BET inhibition correlates with p53 function, or pathway functionality, rather than mutation status.

More generally across cancer, p53 mutation status does not appear to universally determine cellular response to BET inhibition. Upon treatment with (+)-JQ1, resistant AML cells down-regulate genes in the p53 pathway, whereas sensitive cells up-regulate genes in the p53 pathway [102]. Conversely, sensitivity to (+)-JQ1 does not correlate with p53 mutation status in colorectal cancer cell lines [120]. While preliminary, and in need of further confirmation, my data suggest that the cellular response to BET inhibition in melanoma correlates with p53 mutation status, which has not been previously observed.

6.2 ET-domain and BRD inhibition lead to autophagy-dependent senescence in 501mel cells

BET ET-domain inhibition in melanoma gives rise the same phenotype as BET BRD inhibition; 501mel cells undergo autophagy-dependent senescence, whether inhibited through the BRD or ET domain. These results suggest that ET domain inhibition, namely, preventing assembly of transcriptional machinery on the BET protein platform is sufficient to induce a transcriptional response that culminates in autophagy-dependent senescence, rather than displacing the whole BET protein complex from chromatin.

Up-regulation of autophagy- and senescence-related gene sets following BRD and ET-domain inhibition suggests there is no need to displace BETs from chromatin to yield anti-tumour responses. Moreover, since BRD4 interacts with PTEF-b via the CTM [37], and since this interaction is theoretically not disrupted by PepX, perturbation of PTEF-b-dependent transcription is potentially unnecessary to induce a cessation in cell

proliferation. Indeed, simply the prevention of BET protein interactors on the BET protein is sufficient to yield a loss of proliferation. This is a novel strategy for BET protein inhibition and provides proof of principle that targeting Kac-independent functions of BETs yields therapeutically beneficial results.

6.2.1 Up-regulation of the p53 pathway

ET-domain inhibition provokes up-regulation of the p53 pathway in a p53 mutant cell line, when BRD inhibition in both the same cell line, and in a p53 WT melanoma cell line, failed to do so. This suggests that p53 function is only partially affected by the mutation found in these cells. However, all but 3 of the leading edge genes in the p53 pathway gene set lie upstream of p53, suggesting that p53 activation following PepX expression does not drive the up-regulation of the gene set, merely factors that lie upstream of p53 are up-regulated. This suggests that the induction of autophagy-dependent senescence is p53-independent, whether following ET-domain or BRD inhibition in 501mel cells. Further clarity is needed as to how BET BRD inhibition leads to the onset of p53-independent apoptosis in A375M melanoma cells. A wider range of cell lines and p53 mutants with defined functionalities should be surveyed to confirm this, since the data in this study show that mutation status does not necessarily correlate with p53 functionality.

6.2.2 Senescence induction

Data in this thesis show that 501mel cells undergo p21-independent senescence following BET BRD and ET-domain inhibition (Figures 3.13 and 5.9). In gastric cancer BET BRD inhibition leads to p21-dependent senescence [443]. While the *CDKN1A* promoter is highly methylated in 501mel cells [444], 501mel cells are capable of p21 expression [445]. Inhibition of DNA methyltransferases using 5-Aza-2′-deoxycytidine (Aza), combined with a block on proteosomal degradation using MG132 led to increased p21 expression [444].

Therefore, while p21 up-regulation is possible in 501mel cells, it does not occur during BET-inhibition-induced senescence.

Multiple myeloma cells enter a state of senescence following BRD4 displacement from IgH rearrangements at the *MYC* locus, induced by (+)-JQ1 treatment [103]. Furthermore, BRD4 drives induction of OIS in a BRD-dependent manner through binding to super-enhancer loci and driving SASP-associated gene expression in hepatocytes and lung cells [446]. When BRD4 is inhibited, either using a pan-BET inhibitor or through genetic knockout, senescence-associated genes are down-regulated; however, senescence-associated phenotypes such as reduced colony formation and β-galactosidase staining were maintained, suggesting that sustaining the senescence phenotype is only partly BET-dependent [446]. This emphasis on the role of BRD4 in senescence implicates PTEF-b-dependent transcription in the initiation and maintenance of senescence, since in these contexts only BRD4 (of the BET protein family members) interacts with PTEF-b. However, the data presented in this thesis indicate that PepX acts through BRD2 as well as BRD4 (Figure 5.5) and PTEF-b-independent, ET-domain inhibition is sufficient to induce senescence.

6.2.3 Transcriptional regulation by BETs in melanoma

HEXIM1 is a component of the 7SK snRNP complex, which sequesters CDK9 and suppresses its kinase activity. This prevents phosphorylation of the RNA polymerase CTM heptad repeat, and thus, curtails the transcriptional elongation capacity of PTEF-b in [447, 448]. *HEXIM1* was up-regulated by both ET-domain and BRD inhibition (RNA-seq findings, data not shown), suggesting both modes of BET inhibition could indirectly perturb PTEF-b-dependent transcription via HEXIM1. Given that BRD2 knockdown specifically leads to the up-regulation of HEXIM1 protein and mRNA in 501mel cells (Figure 7.2), this indicates that

PepX perturbs BRD2, and the effects yielded by PepX are not solely due to BRD4 perturbation.

Indeed, Figures 3.6 and 5.5 indicate that (+)-JQ1 and PepX mediate their effects primarily through BRD2 and BRD4 in 501mel cells. In fact, the R^2 values suggest that the effects of ET-domain inhibition are most similar to BRD2 knockdown, followed by BRD4 and BRD3, and the effects of BET BRD inhibition are most similar to BRD4 knockdown, followed by BRD2 and BRD3. While the contribution of BRD3 to mediating the effects of PepX appears small in comparison to BRD2 and BRD4, the R^2 value for BRD3 knockdown is larger for PepX than (+)-JQ1 (0.133 compared to 0.0026), indicating that PepX exerts more of its effects through BRD3 than (+)-JQ1 does. Additionally, the BRD4 knockdown R^2 value is bigger for (+)-JQ1 than PepX (0.406 compared to 0.379), suggesting that (+)-JQ1 exerts its effects through BRD4 to a greater extent that PepX. This suggests that (+)-JQ1 acts through perturbation of PTEF-b-dependent transcription, whereas PepX likely acts in a PTEF-b-independent manner. Lastly, The R^2 values for pan-BET siRNA mediated knockdown (siBETs) are similar for PepX and (+)-JQ1 (0.662 compared to 0.648), further reinforcing the notion that PepX acts through BETs.

The interaction of BRD4 with G9a enables the suppression of autophagy gene expression [68] and our lab has *in vitro* data showing that G9a interacts with BETs via the ET-domain (data not shown). Gene up-regulation following BET protein attenuation, either via BRD or ET-domain inhibition (Figures 3.5-3.6 and 5.5), suggests that BET proteins have under-explored negative gene expression regulatory functions. Disruption of ET-domain interactions leading to up-regulation of gene expression further indicates that it is sufficient to displace BET protein interactors from the ET-domain, rather than erasing BET occupation of chromatin in order to modulate transcription, highlighting the importance of the under-explored Kac-independent functions of BETs. Therefore, future work on BET

function should focus on exploring BET protein negative gene regulation and Kac-independent functions.

6.3 Clinical applications

501mel cells underwent senescence whether inhibited via BRDs or the ET-domain. While this is promising, senescence markers do not guarantee cells are truly senescent [449]. In fact, cells displaying β-galactosidase expression formed colonies *in vitro,* co-expression for β-galactosidase and the proliferative marker Ki67, and were able to form new tumours *in vivo* [449]. This could explain why although nearly all cells display β-galactosidase staining, colonies were formed following both (+)-JQ1 treatment and PepX expression. This suggests that perhaps BET inhibitors would be inappropriate treatment for a patient in which it is predicted that the malignant cells would respond to BET inhibition by undergoing senescence. Additionally, senescent A375 cells induce the growth of non-senescence cells both *in vitro* and *in vivo* through paracrine signalling [450]. This indicates that, if used alone, inducers of senescence would be ineffective at delivering long term results for patients and relapse should be expected. However, if used in combination with senolytics, treatments that selectively eliminate senescent cells, could be a very potent therapeutic regimens.

In melanoma, there are conflicting reports about the correlation between p53 mutation status and clinical outcome [260, 261]. Likewise, the data in Chapter 3 have demonstrated that a p53 C275W mutation would not be a suitable biomarker as it does not indicate cellular sensitivity or response to (+)-JQ1. It remains unclear why A375M cells display less sensitivity to (+)-JQ1, and yet undergo apoptosis rather than senescence like the more sensitive cell line, 501mel.

Finally, Chapter 5 provides proof of principle that targeting Kac-independent BET functions leads to potentially therapeutically beneficial results. However, pharmacological means of

inhibiting ET domain interactions are not currently available; therefore, more work is needed to make these findings relevant to patient care.

6.4 Conclusions

In conclusion this study shows that in melanoma, the cellular response to BET inhibition correlates with a specific p53 mutation: 501mel cells harbour a C275W p53 mutation and undergo autophagy-dependent senescence, and BRD inhibition yields autophagy-independent apoptosis in p53 WT A375M melanoma cells. In prostate cancer LNCaP cells, autophagy appears to have a cytoprotective, role and concomitant treatment with novel BET BRD inhibitor, RT53, and autophagy inhibitor leads to exacerbated loss of cellular proliferation. RT53 yields autophagy up-regulation in an AR-independent manner. Finally, the data in this thesis demonstrate for the first time that targeting BET protein Kac-independent functions yields loss of cellular proliferation in melanoma. ET-domain inhibition leads to the onset of senescence in 501mel cells, which is likely underpinned by autophagy.

Chapter 7: Appendix

7.1 Supplementary Figures

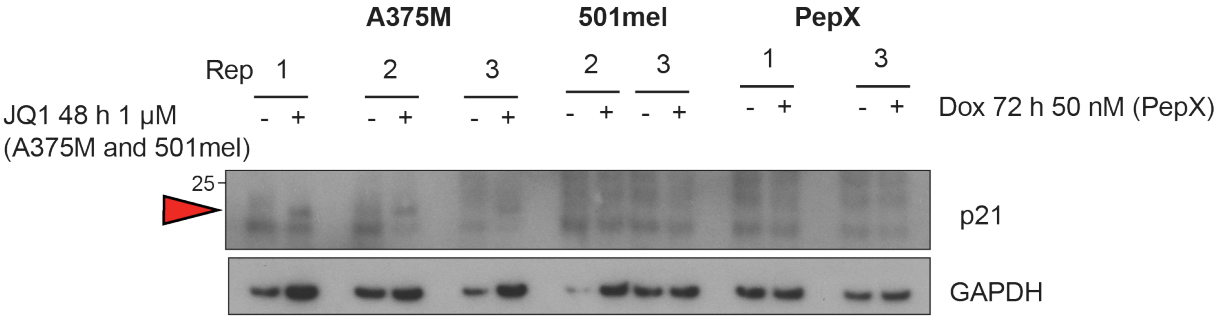


***Figure 7.1**: Immunoblot of melanoma samples side by side following 48 h (+)-JQ1 treatment (A375M and 501mel cells), or 72 h 50 nM doxycycline treatment (PepX-expressing 501mel cells cells). Red arrow indicates p21 band. (-)-JQ1 was used as a negative control in the case of (+)-JQ1. In the case of doxycycline, DMSO was used as a negative control.*

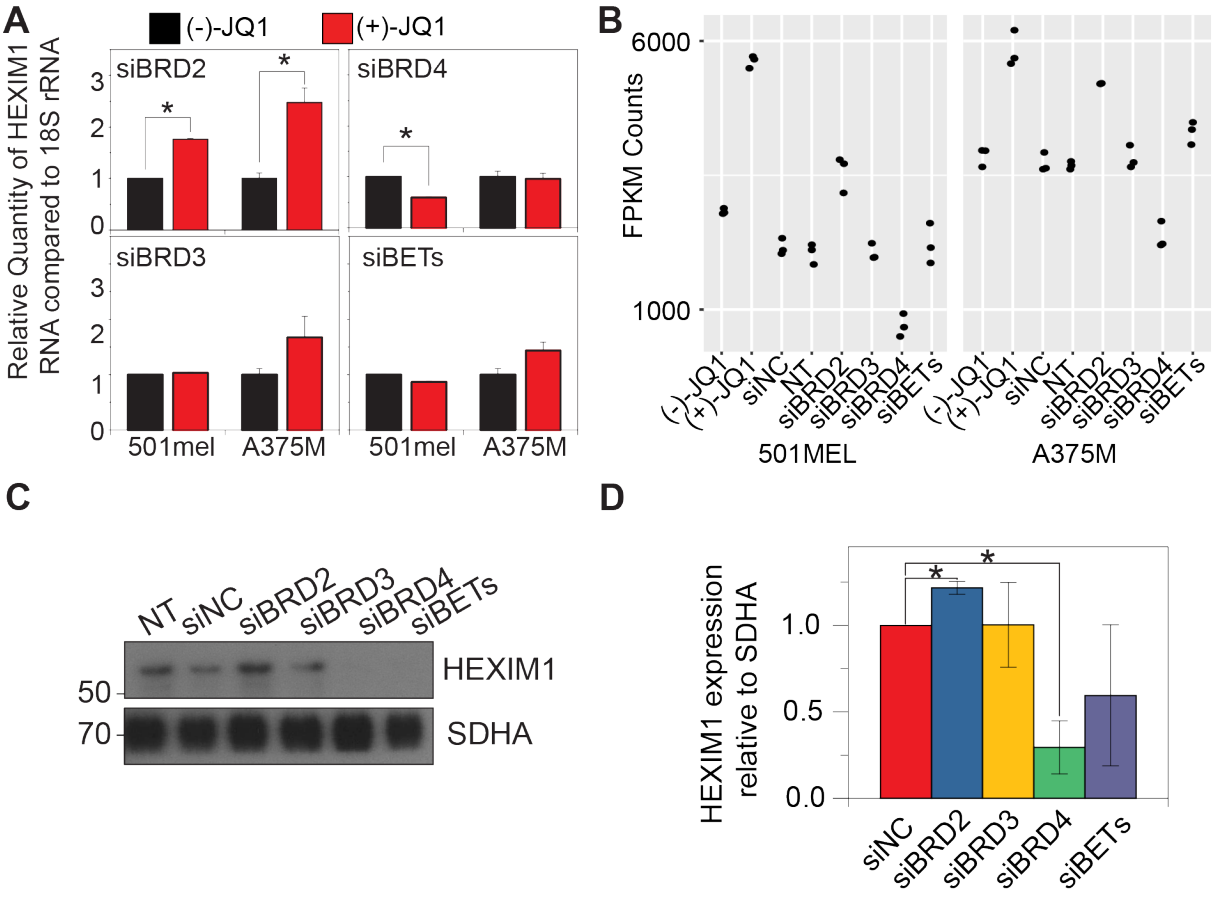


***Figure 7.2**: BRD2 knockdown leads to HEXIM1 up-regulation. (**A** 501mel cells were transfected with siRNA for 48 h. RNA was extracted, coverted to cDNA and used in qPCR. Black bars represent samples transfected with negative control siRNA, red bars represent samples transfected with the indicated siRNA. Expression of HEXIM1 was normalised to 18S rRNA and then to the expression of HEXIM1 Following transfection with negative control siRNA. N = 3 biological replicates. Mean RNA expression shown ± standard deviation. Statistical significance was determined using a two-tailed Students t-test, comparing levels of HEXIM1 expression following BET knockdown with the level of HEXIM1 expression following transfection with negative control siRNA. No stars = p > 0.05 (non-significant), * = p <0.05. (**B**) Normalised FPKM reads of HEXIM1 following RNA-seq in A375M and 501mel cells. Counts in each biological replicate of each cell line is represented by a black dot. Cells were treated with 500 nM (+)-JQ1 for 24 h before RNA was extracted and subject to sequencing. (-)-JQ1 was used as a negative control in the case of (+)-JQ1, and siNC was used as a negative control in the case of siRNA-mediated knockdown of BETs. N = 3 biological replicates per condition, per cell line. (**C**) Knockdown of BRD2 leads to an increase in HEXIM1 expression. Representative immunoblot of HEXIM1 and SDHA. 501mel cells were transfected with the indicated siRNA for 48 h. NT indicates cells that were not transfected with any siRNA. This immunoblot was carried out using the same lysates that were blotted in Figure 3.4A, showing BET knockdowns. (**D**) Knockdown of BRD2 leads to an increase in HEXIM1 expression in 501mel. Quantification of immunoblots of HEXIM1 normalised to SDHA expression. N = 3 biological replicates. Mean protein expression shown ± standard deviation. Statistical significance was determined using a two-tailed Students t-test. * = p <0.05.*

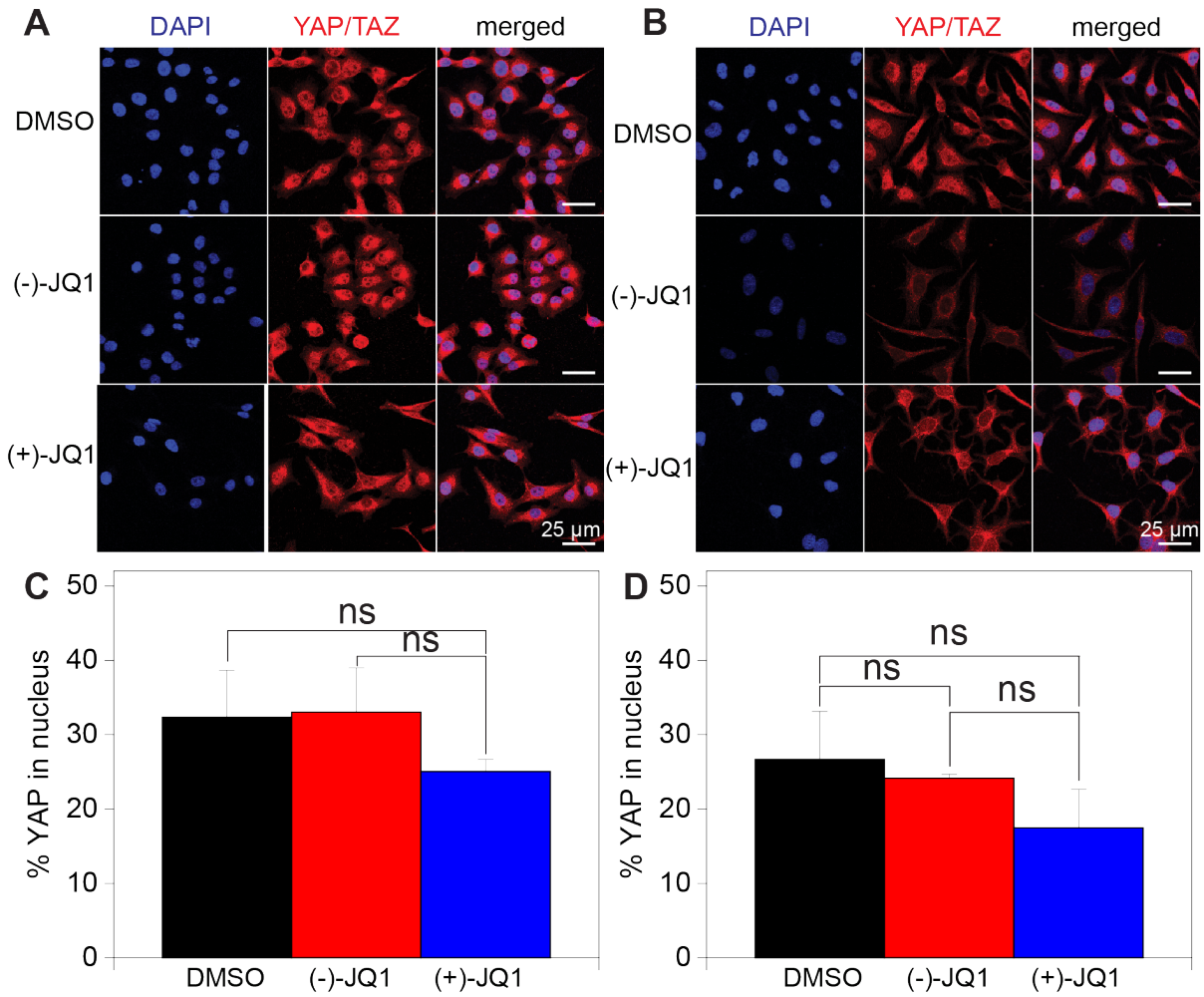


***Figure 7.3**: Cell morphology change and cell cycle arrest is YAP/TAZ independent in A375M and 501mel cells. (**A**) Representative microscopy images showing nuclei (DAPI), and YAP/TAZ subcellular localisation (red) in A375M cells following 1 µM treatment for 48 h. Images taken using confocal microscopy and 40x magnification. N = 3 biological replicates. (**B**) Representative microscopy images showing nuclei (DAPI), and YAP/TAZ subcellular localisation (red) in 501mel cells following 1 µM treatment for 48 h. Images taken using confocal microscopy and 40x magnification. N = 3 biological replicates. Quantification of YAP/TAZ nuclear localisation in A375M cells (**C**) or 501mel cells (**D**) following 48 h of 0.1% v/v DMSO, 1 µM (-)-JQ1 or (+)-JQ1 treatment. N = 3 biological replicates. 3 representative fields collected per replicate and used in 3-channel quantification analysis using ImageJ software. Mean proportion YAP/TAZ in nucleus*

shown ± standard deviation. Statistical significance was determined using a two-tailed Students t-test. ns = p > 0.05, no significant difference.

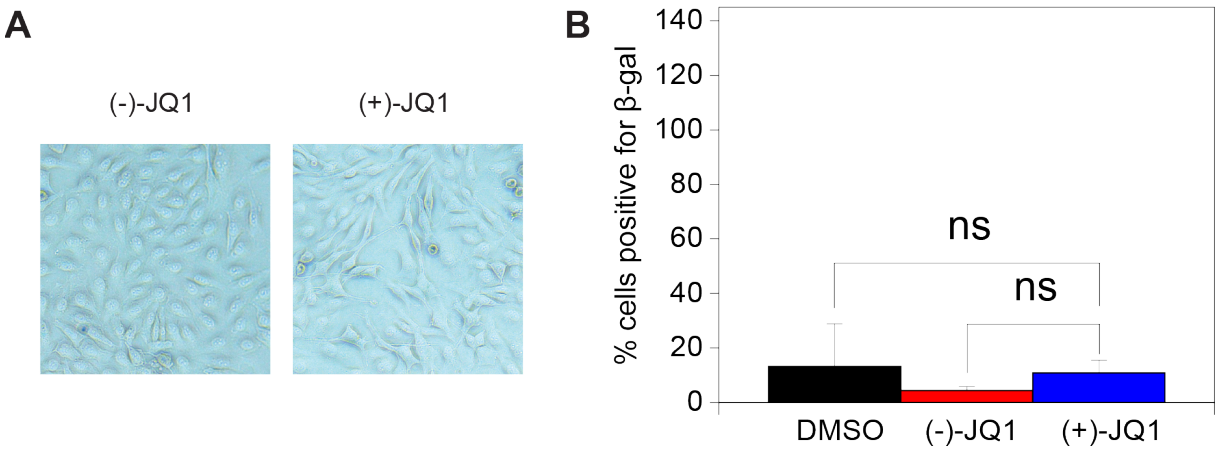


***Figure 7.4**: A375M cells do not undergo senescence in response to BET BRD inhibition. (**A**) β-galactosidase staining in A375M cells following treatment with 1 μM (-)-JQ1 or (+)-JQ1 for 48 h. (-)-JQ1 is a negative control. (**B**) Quantification of β-galactosidase staining in A375M cells after 48 h of treatment with 1 μM (+)-JQ1. 0.01% v/v DMSO and (-)-JQ1 are negative controls. N = 3 biological replicates. Mean percentage of cells stained positive for β-galactosidase shown ± standard deviation. Statistical significance was determined using a two-tailed Students t-test. ns = non-significant difference.*

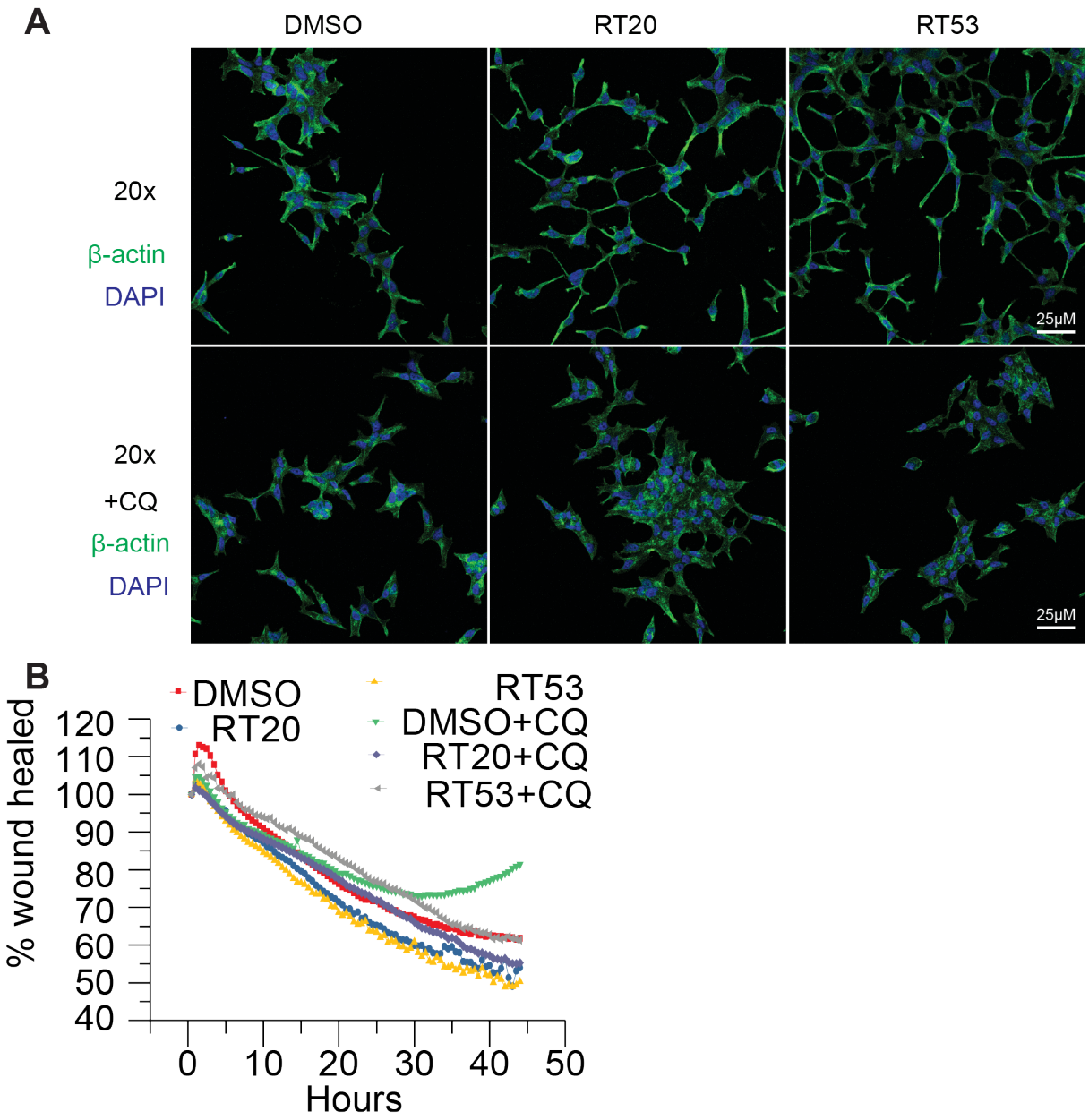


Figure 7.5: (***A***) *Cellular morphology changes of LNCaP cells is rescued following concomitant BET BRD and autophagy inhibition. Cells were treated with 1 μM RT20 or RT53 ± 10 μM CQ, 0.01% v/v DMSO was included as the negative control, for 48 h. Cells were stained with phalloidin and DAPI (blue). N = 1 biological replicate. (**B**) Scratch wound healing assay shows that LNCaP cells may lose invasive behaviours upon concomitant BET BRD and autophagy inhibition. LNCaP cells were treated with RT20 (blue) or RT53 (yellow) alone, compared with DMSO alone (red), or with CQ: RT20 (purple) or RT53 (grey) DMSO (green). The speed at which the wound healed was recorded. Cells were treated with 1 μM RT20 or RT53 ± 10 μM CQ for 48 h. 0.01% v/v DMSO was included as a*

negative control as the solvent in which RT20 and RT53 are dissolved. N = 1 biological replicate.

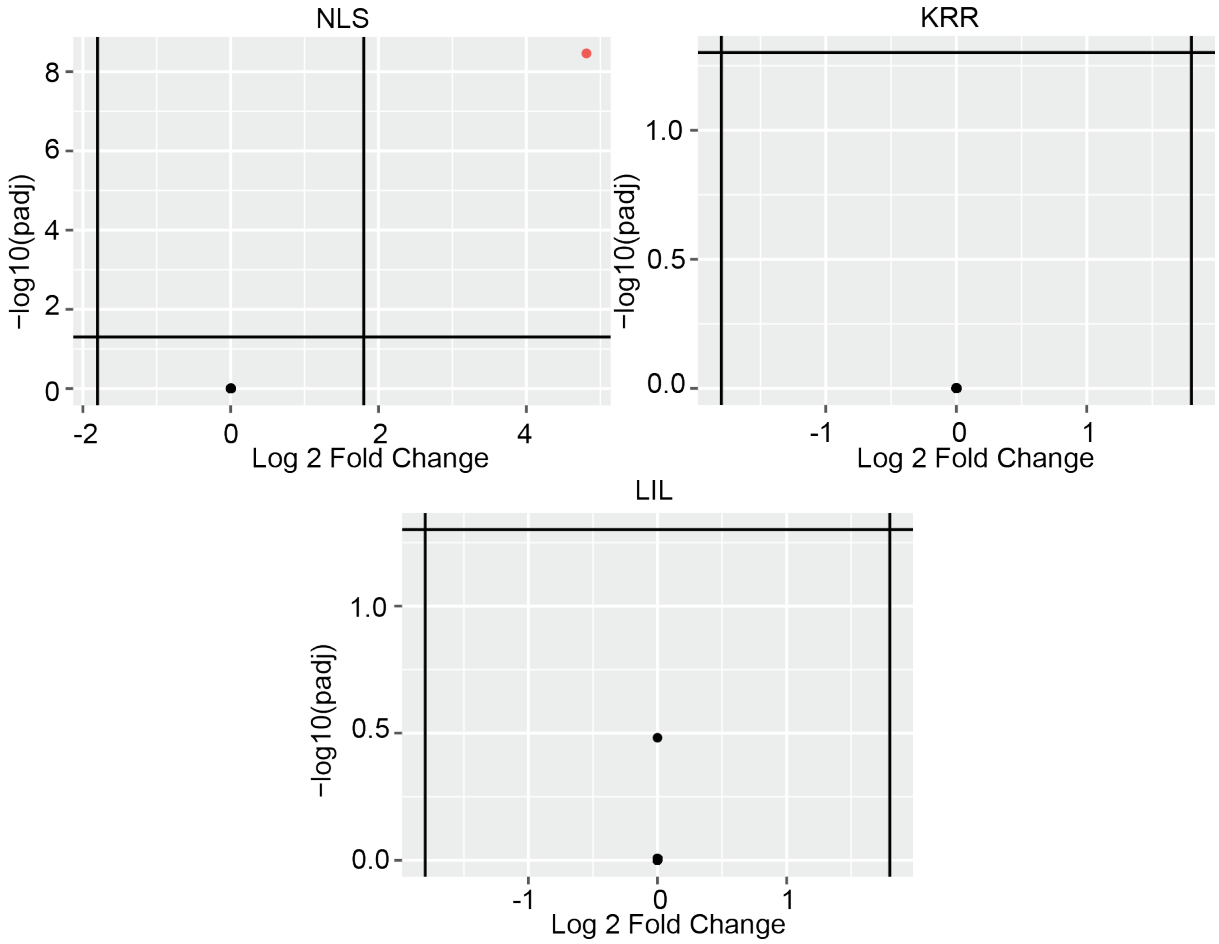


***Figure 7.6**: Volcano plots showing changes in gene expression following treatment with high doxycycline concentrations to induce expression of NLS, KRR or LIL for 48 h. Blue dots represent genes with a LFC ≤ -1.8 and an adjusted p value of ≤ 0.05, pink dots represent genes with a LFC ≥ 1.8 and an adjusted p value of ≤ 0.05. Vertical black lines indicate 1.8 LFC. Horizontal black line indicates an adjusted p value of ≤ 0.05. N = 4 biological replicates.*

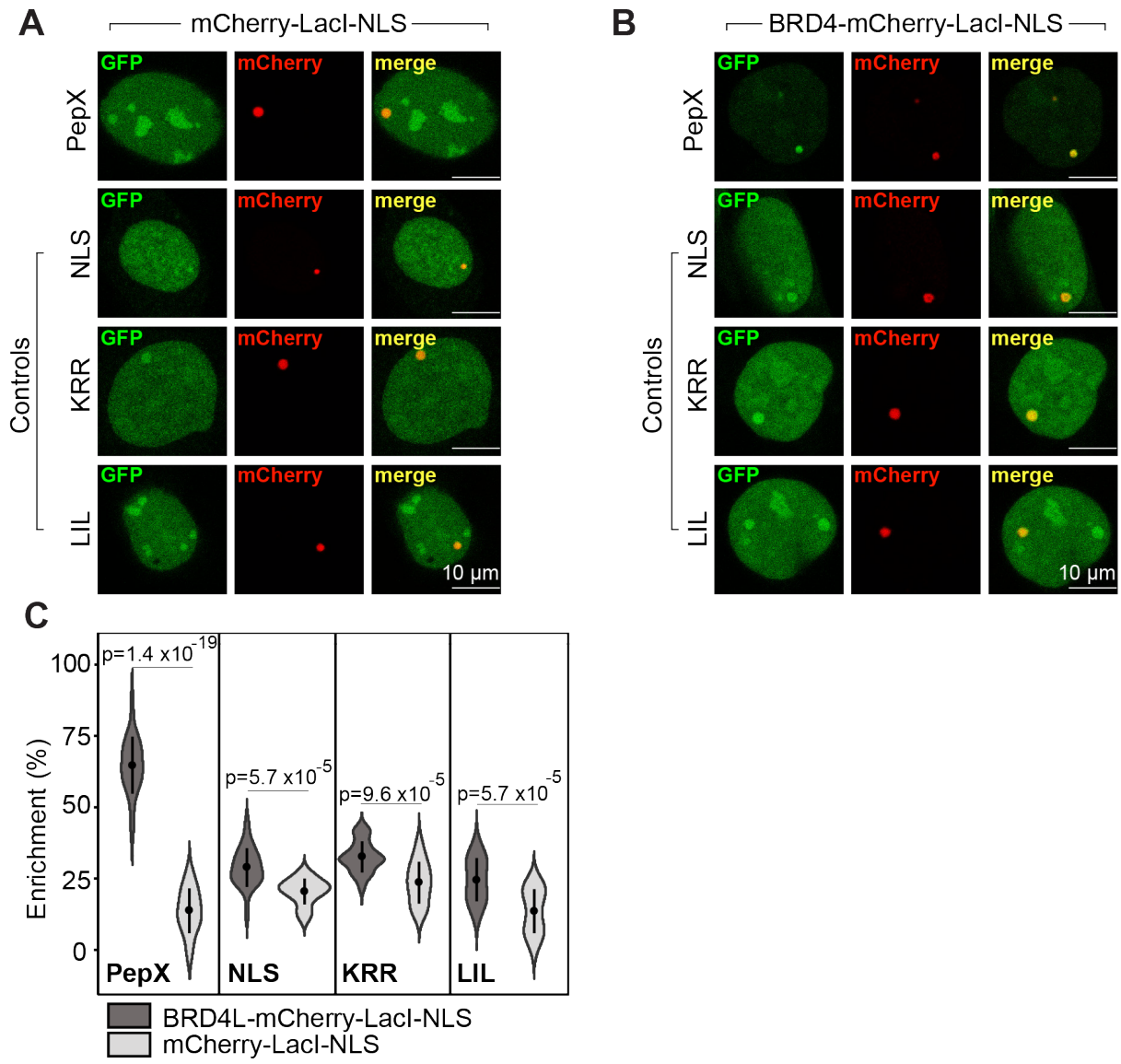


***Figure 7.7**: PepX binds to BRD4 in the cellular environment. In summary, the LacOLacI assay involves the co-transfection of U-2 OS cells expressing 256x repeats of a LacO array with two proteins of interest, one tagged with an mCherry-LacI-NLS, and the other tagged with GFP. The LacI tag immobilises the mCherry-tagged protein on the LacO repeats within chromatin. The cells are fixed then visualised using confocal microscopy. If the two fluorescent proteins co-localise then a GFP dot that overlaps with the immobilised mCherry tagged protein is visible in the nucleus of imaged cells. The extent to which this GFP signal is enriched in the dot compared to the GFP signal within the rest of the nucleus quantified for 20 cells, as previously described [451]. GFP enrichment values are then*

*plotted for each pair of co-transfected plasmids. (**A**) Representative microscopy image showing cells transfected with mCherry-LacI-NLS (negative control), and one of GFP-PepX,- NLS, -KRR, or -LIL. (**B**) Representative microscopy image showing cells transfected with BRD4-mCherry-LacI-NLS, and one of GFP- PepX,- NLS, -KRR, or -LIL. (**C**) Quantification of co-localisation of PepX-, NLS-, KRR- and LIL-GFP with BRD4L-mCherry-LacI-NLS and mCherry-LacI-NLS. The violin plots represent the GFP intensity increase over background in the mCherry foci, calculated from N = 20 cells. Mean GFP intensity shown by black dot. Quartile ranges shown by black bars. Statistical significance was determined using a two-tailed Students t-test.*

7.2 Supplemental methods

7.2.1 Time lapse microscopy

30,000 cells were seeded in a 6 well plate in 3 ml medium. 24 h later, cells were treated with 500 nM (-)-JQ1 or (+)-JQ1. Cells were transferred to a time lapse microscope incubator. Images taken every 30 min for 48 h. 3 fields of view were captured for each sample, after which the data was analysed using ImageJ software to generate images and video footage of cells.

7.2.2 Scratch wound assay

200,000 LNCaP cells were seeded in a 6 well plate in 3 ml medium. Cells were allowed to grow until they were of 100% confluency. A scratch was made in each well by dragging a 200 µL tip through the cells, across the equator of each well, thereby displacing the cells from the well. Cells were then treated with 1 µM RT20 and RT53, or 0.1% DMSO ± 10 µM CQ. Cells were then transferred to a time lapse microscope incubator. 1 well was prepared per sample, but 3 fields of view were captured for each sample. Images taken every 30 min for 48 h, after which the data was analysed using ImageJ software.

7.2.3 LacOLacI Co-localisation assay

U-2 OS cells expressing 256x repeats of a LacO array (Genetic modification performed by Dr Takao Fujisawa, a postdoctoral scientist from our lab). U-2 OS LacO Cells, previously described [452], were cultured in Dulbecco's Modified Eagle Medium (DMEM) (Thermo Fisher Scientific, cat. #31966021) supplemented with 10% FBS (v/v, Biosera, cat. #FB-1001/500) and antibiotics (1% Pencillin Streptomycin (Thermo Fisher Scientific, cat. #15070063), 1 µg/mL puromycin (Thermo Fisher Scientific, cat. #A1113803) at 37 °C and 10% CO_2. To carry out transfection, U-2 OS LacO cells were washed with PBS, trypsinised

using 0.25% trypsin-EDTA (Thermo Fisher Scientific, cat. #25200056) for 3 min at room temperature, and seeded in 24-well cell culture dishes (30,000 cells in 1 ml media per well). After incubating for 20 h at 37 °C and 10% CO2, cells were transfected with plasmids using the FuGENE6 reagent (Promega, cat #E2311) according to the manufacturer's instructions (50 ng of BRD4-mCherry-LacI-NLS plasmid, or 10 ng mCherry-LacI-NLS, 1ng GFP -PepX, -NLS, -KRR or -LIL in 20 µL OptiMem (Thermo Fisher Scientific, cat. #31985070) with 1 µL FuGENE6 per well), then incubated for 24 h at 37 °C and 10% CO_2. Transfected cells were then washed with PBS, trypsinised, and re-plated onto 8-well glass imaging chamber dishes (Thermo Fisher Scientific, cat. #155411PK) in 300 µL media. Cells were incubated for 20-24 h at 37 °C and 10% CO_2 before fixing.

Cells were washed with PBS twice before fixing at room temperature with 300 µL 4% formaldehyde for 10 min, then washed twice with PBS, and were subsequently incubated with 300 µL 0.2% Triton-X100 for 5 min at room temperature. Cells were washed with PBS three times, then incubated with 300 µL of DAPI solution for 2 min at room temperature. Cells were washed twice with PBS, and then 300 µL glycerol storage buffer was added to the cells. Cells were stored at room temperature, away from light and were imaged within one week of fixing.

Cells were imaged using a Zeiss LSM 710 scan-head (Zeiss GmbH, Jena, Germany) coupled to an inverted Zeiss Axio Observer Z1 microscope equipped with a high-numerical-aperture (N. A. 1.40) 63× oil immersion objective (Zeiss GmbH, Jena, Germany). A 405 nm excitation laser and a 410-474 nm emission filter were used to detect DAPI fluorescence. A 488 nm excitation laser and a 494-555 nm emission filter were used to detect GFP fluorescence. A 594 nm excitation laser and a 598-700 nm emission filter were used to detect mCherry fluorescence. Quantification was carried out using the

ImageJ software. Co-localisation enrichment was calculated using the following previously published formula [451]:

$$\text{Enrichment}(\%) = \frac{\frac{GFP^{\text{foci}}_{\text{Intensity}}}{GFP^{\text{foci}}_{\text{Area}}} - \frac{\left(GFP^{\text{Nucleus}}_{\text{Intensity}} - GFP^{\text{foci}}_{\text{Intensity}}\right)}{\left(GFP^{\text{Nucleus}}_{\text{Area}} - GFP^{\text{foci}}_{\text{area}}\right)}}{max\left(GFP_{\text{Intensity}}\right)} \times 100$$

7.2.4 Cloning pcDNA5-eGFP -PepX, -KRR, and -LIL

PepX, KRR and LIL were amplified from pPB-hCMV1-cHApA-MLV-TagBFP-NLS, pPB-hCMV1-cHApA-KRR-TagBFP-NLS, and pPB-hCMV1-cHApA-LIL-TagBFP-NLS plasmids using PepX-GFP-F and PepX-GFP-R primers. PCR reaction components are detailed in Table 2.22, and conditions are detailed in Table 7.1. pcDNA5-eGFP-NLS vector was linearised using HindIII-HF (New England Bio Labs, cat. #R3104S). The components of the restriction enzyme digestion are described in Table 7.2, and once assembled were incubated at 37 °C for 3 h. The products of the restriction enzyme digest and PCR products were separated on a 1% agarose gel using electrophoresis, then purified from the gel using a Gel Purification kit (Qiagen, cat. # 28704), as per the manufacturers' instructions. Each of the PCR products was combined with linearised pcDNA5-eGFP-NLS vector in a Gibson Assembly reaction [245], as detailed in Table 7.3, and was incubated at 50 °C for 1 h. 75 µL bacteria were transformed with Gibson Assembly products using method described above. Colonies were screened for successful construct transformation using a colony PCR reaction (method above) followed by resolution of resulting DNA fragments on an agarose gel. Bacteria containing the correct plasmid were used to inoculate LB medium, and were shaken at 37 °C in an incubator overnight at 225 rpm. The plasmid was purified from bacteria using a Mini-Prep kit (Qiagen, cat. #27106) as per the manufacturer's protocol. All constructs were verified by sequencing.

Temperature (°C)	Duration	Step	Cycles
98	2 min	Melting	1
98	15 seconds	Melting	25
55	15 seconds	Annealing	
72	30 seconds	Extension	
15	Continuous	Hold	1

Table 7.1: Details of PCR reaction conditions

Component	Volume (µL)
DNA	5 (1 µg)
CutSmart 2.0 Buffer (New England Bio Labs, cat. #B7204S)	2
HindIII-HF (New England Bio Labs, cat. #R3104S)	1
H_2O	12

Table 7.2: Components of HinDIII restriction enzyme digestion.

Component	Volume (µL)
Linearised pcDNA5-eGFP-NLS plasmid	0.5
PCR product	0.5
Gibson Assembly Mastermix (New England Bio Labs, cat. #E5520S)	2

Table 7.3: Components of Gibson assembly reaction

7.2.5 Cloning BRD4ΔET-mCherry-LacR-NLS

A plasmid containing WT BRD4L was passed to me by a postdoctoral scientist within our lab. The plasmid was digested using NaeI (New England Bio Labs, cat. #R0190S) by combining components detailed in Table 7.4 and incubating at 37 °C for 1 h. The products of this reaction were separated using agarose gel electrophoresis, running at 100 V for 1h and 20 min (details above). In this case, a 1% agarose gel was used and electrophoresis was run at 100 V for 1 h. This reaction produced two fragments, one of which contained the ET domain, which was 1094 bp in length, the other was the linearised vector. Both

fragments were purified from the agarose gel using a Gel Purification kit (Qiagen, cat. #28704), according to the manufacturers' instructions. Fragments were amplified by two polymerase chain reactions (PCR) using primers BRD4L-NaeIcut-F and BRD4-dET-R, and BRD4L-NaeIcut-R and BRD4-dET-F, using Herculase II Fusion DNA polymerase kit (Agilent, cat. #600677). Components of these PCR reactions were assembled according to manufacturers' instructions, and are detailed in Table 7.5, and PCR reaction conditions are detailed in Table 7.6. The resulting PCR fragments were resolved using a 1% agarose gel was used and electrophoresis was run at 100 V for 1 h, after which fragments were purified from the agarose gel using a Gel Purification kit (Qiagen, cat. #28704), according to the manufacturers' instructions. The BRD4L-NaeIcut-F and BRD4-dET-R, and BRD4L-NaeIcut-R and BRD4-dET-F PCR fragments were joined to form one PCR fragment using BRD4L-NaeIcut-F and BRD4L-NaeIcut-R primers, and conditions and components detailed in Tables 7.6 and 7.7, respectively. The resulting fragment (referred to as BRD4L-NaeIcut-F and BRD4L-NaeIcut-R fragment) was resolved using a 1% agarose gel, and purified from the gel using a Gel Purification kit (Qiagen, cat. #28704), according to the manufacturers' instructions. The BRD4L-NaeIcut-F and BRD4L-NaeIcut-R fragment was assembled with the NaeI-digested BRD4-mCherry-LacR-NLS plasmid using a Gibson Assembly reaction [245], which was run at 50 °C for 1 h, and components were as described in Table 7.8. This generated the BRD4ΔET fragment. 100 µL bacteria were transformed with plasmids as described above using 2 µL of Gibson Assembly reaction product. Colonies were screened for successful construct transformation using a colony PCR reaction (method above) followed by resolution of resulting DNA fragments on an agarose gel. Bacteria containing the correct plasmid were used to inoculate LB medium, and were shaken at 37 °C in an incubator overnight at 225 rpm. The plasmid was purified from bacteria using a Mini-Prep kit (Qiagen, cat. #27106) as per the manufacturers' protocol. BRD4ΔET was moved into the mCherry-LacR-NLS-pcDNA3-LICm destination

plasmid using an LR Clonase reaction. Components of the LR Clonase reaction can be found in Table 7.9, and once assembled, the reaction mix was incubated at room temperature for 2 h. Bacteria were transformed with the product of the clonase reaction, as detailed above. The following day, the plasmid was purified from bacteria using a Mini-Prep kit (Qiagen, cat. #27106) as per the manufacturers' protocol, and was verified by sequencing.

Component	**Volume (µL)**
DNA plasmid	43 (5 µg)
10x Tango Buffer (Thermo Fisher Scientific, cat. #BY5)	5
NaeI (New England Bio Labs, cat. #R0190S)	2
Table 7.4: Components of NaeI restriction enzyme digestion.	

Component	**Volume (µL)**
DNA template (1 ng/µL)	2.5
Primers (diluted to 10 µM)	2.5
Herculase II Fusion DNA Polymerase	1
5x Herculase Reaction Buffer	5
dNTPs (100 mM; 25 mM per dNTP)	1
H_2O	Up to 20
Table 7.5: Components of PCR reactions	

Temperature (°C)	**Duration**	**Step**	**Cycles**
98	2 min	Melting	1
98	15 seconds	Melting	25
55	15 seconds	Annealing	
72	1 min	Extension	
15	Continuous	Hold	1
Table 7.6: Details of PCR reaction conditions			

Component	Volume (µL)
BRD4L-NaeIcut-F and BRD4-dET-R PCR fragment	1
BRD4L-NaeIcut-R and BRD4-dET-F PCR fragment	1
Primers (diluted to 10 µM)	2.5
Herculase II Fusion DNA Polymerase	1
5x Herculase Reaction Buffer	5
dNTPs (100 mM; 25 mM per dNTP)	1
H_2O	Up to 20
Table 7.7: Components of PCR reactions	

Component	Volume (µL)
NaeI digested BRD4-mCherry-LacR-NLS plasmid	1
BRD4L-NaeIcut-F and BRD4L-NaeIcut-R fragment	1
Gibson Assembly Mastermix (New England Bio Labs, cat. #E5520S)	2
Table 7.8: Components of Gibson assembly reaction	

Component	Quantity
Donor vector	100 ng
Destination vector	100 ng
Gateway™ LR Clonase Mastermix (Thermo Fisher Scientific, cat. #11791020)	0.5 µL
Table 7.9: Components of LR Clonase reaction	

7.3 Future Plans relating to results chapters 3-5

7.3.1 Future plans relating to Chapter 3

- Related to Chapter 3.2.2: p21 qPCR following 500 nM 24 h (+)-JQ1 treatment in A375M and 501mel cells to confirm FPKM counts. (-)-JQ1 would be used as a negative control.

- Relating to Chapter 3.2.4: I would have conducted more repeats of qPCR of autophagy genes, and I would have expected to see statistically significant changes in the expression of these genes.

- Relating to Chapter 3.2.4: Orthogonal approaches could have been used to study autophagic flux in these cells to confirm the findings of the immunoblots presented in Figures 3.10-3.11, such as LysoTracker staining in flow cytometry experiments.

- Relating to Chapter 3.2.5: I would have tried to more robustly show that caspase activation leads to cell death following 48 h 1 μM (+)-JQ1 in A375M cells, using annexin V staining and flow cytometry analysis. I would have treated A375M cells with Z-VAD-FMK, a pan-caspase inhibitor, concomitantly with (+)-JQ1, in an attempt to rescue A375M proliferation. Negative controls would have been DMSO, (-)-JQ1 in the absence and presence of Z-VAD-FMK, and positive control would have been staurosporine. I would have also included cells treated with staurosporine and Z-VAD-FMK as a control to validate the Z-VAD-FMK as a caspase inhibitor. I would have expected Z-VAD-FMK treatment to have little effect on annexin V staining induced by (-)-JQ1 as it is a negative control that does not bind to the bromodomain binding pocket, and thus, should not impact upon BET protein function. I would have expected annexin V staining to have significantly decreased when comparing (+)-JQ1 treated

cells with (+)-JQ1 and Z-VAD-FMK treated cells, showing that caspase activation drives cell death following BET BRD inhibition in A375M cells.

- Relating to Chapter 3.2.5: Check whether CHL1 cells undergo apoptosis or senescence following (+)-JQ1 treatment using the annexin V staining analysed by flow cytometry, β-galactosidase staining and clonogenicity experiments used throughout this chapter. Negative control would be DMSO and (-)-JQ1 and staurosporine would be used as a positive control. MTT assay would have been repeated as one replicate was an outlier.

- Relating to Chapter 3.2.5: Carry out MTT assay using SK-mel-28 cells, using the method and controls detailed in Figure 3.14A, to determine if their proliferation can be rescued through concomitant BET BRD and autophagy inhibition.

- Relating to Chapter 3.2.5: In this study only two cell lines have been surveyed; more cell lines such as SK-mel-28, IGR37 and IGR39 would have been surveyed to determine whether they undergo senescence or apoptosis using the methods and controls detailed in this chapter following (+)-JQ1 treatment.

- Relating to Chapter 3.2.5: To demonstrate more robustly that autophagy up-regulation in a p53 mutant melanoma cell line leads to senescence, which can be bypassed upon concomitant inhibition of autophagy, cells would be treated with (+)-JQ1 with and without orthogonal inhibitors of autophagy. In this chapter two pharmacological inhibitors of autophagy were used to show its inhibition leads to bypass of senescence in p53 mutant cells, BafA and CQ; however, they both have off-target effects [294]. CQ induces autophagy-independent reorganisation of endosome membrane proteins and Golgi apparatus organisation [334]. While BafA does not affect the endo-lysosomal system, it also affects the morphology of Golgi apparatus lumen [334]. Use of siRNA-mediated knockdown of a key autophagy gene, such as ATG5 [318, 319, 335, 453,

454], to inhibit the autophagy pathway using genetic means in the presence of (+)-JQ1 would provide another piece of evidence to suggest autophagy up-regulation is essential for senescence induction. Conversely, perhaps treatment with an inducer of autophagy such as Torin [455] would further increase senescence induction in the presence of (+)-JQ1. Ideally, this experiment would be conducted in diverse melanoma cell lines that harbour p53 mutations.

7.3.2 Future plans relating to Chapter 4

- To complement the data in Figure 4.2, to more thoroughly rule out cell death following RT53 treatment, annexin V staining in LNCaP cells was due to be carried out. In the case of no cell death induced, senescence in LNCaP cells following RT53 treatment was going to be tested.

- Only one biological replicate for each of the experiments in Figures 7.4A-7.4B was carried out. The intention was to carry out the experiment in Figure 7.4B also using alternative pharmacological and genetic means of inhibiting autophagy, to determine the effect of autophagy on invasiveness and to eliminate the possibility of off-target effects of CQ being the underlying cause of the reversal of morphology changes.

7.3.3 Future plans relating to Chapter 5

- Related to Chapter 5.2.4: Investigate *CDKN1A* expression using qPCR to validate RNA-seq findings in Figure 5.7B. PepX-expression 501mel cells would be treated with 50 nM doxycycline to induce PepX expression for 48 h, or DMSO as the negative control. 18S rRNA would be used as the internal control to which the quantification of *CDKN1A* expression would be normalised.

- Related to Chapter 5.2.5: Show using qPCR that PepX expression leads to the up-regulation of autophagy-related genes, such as ATG5, ATG4B, ATG12, BNIP3, BNIP3L, MAP1LC3B, in order to validate RNA-seq findings. PepX-expression 501mel cells would be treated with 50 nM doxycycline to induce PepX expression for 48 h, or DMSO as the negative control. 18S rRNA would be used as the internal control to which the quantification of autophagy-related gene expression would be normalised.

- To show that PepX displaces ET-domain interactors from BETs whilst retaining BET occupation on chromatin, and that BRD4 remains bound to PTEF-b, a co-immunoprecipitation (co-IP) experiment would be carried out. PepX-expressing 501mel cells would be treated with doxycycline to induce PepX expression; DMSO treatment would be used as the negative control. RNA-seq findings show that gene expression is altered after 48 h 50 nM doxycycline treatment; therefore, I would initially use a time course, between 0 and 48 h of doxycycline treatment, as it is unknown precisely when transcription is perturbed. (+)-JQ1 causes displacement of BETs from chromatin within 1 h [36]; therefore, it is possible that PepX displaces ET-domain interactors shortly after the beginning of its expression. PepX is induced 4 h after doxycycline is added to medium (data not shown); therefore, I would initially test the time points 4, 8, 24 and 48 h. The following proteins would be blotted: H4K5ac, a modified chromatin residue to which BETs bind [23, 25, 132, 456], CDK9 and cyclin T [37], PTEF-b components,

JMJD6, and NSD3 [40], ET-domain transcriptional components, and BFP, to show that PepX, indeed, bound to the pulled down BET protein. The negative control would be DMSO and the positive control showing displacement of BETs from chromatin would be (+)-JQ1. Since (+)-JQ1 would be used in this experiment, (-)-JQ1 would be used as an additional negative control. The experiment would first be carried out using BRD4 antibodies to immunoprecipitate BRD4 and any bound proteins, to identify the time point at which PepX induces loss of ET-domain interactions. Once these conditions had been identified, I would have carried out this experiment, immunoprecipitating BRD3 and BRD2 to show that the ET-domain-mediated interactions of these proteins are also interrupted by PepX, which would highlight the importance of BRD2 and BRD3 in transcriptional regulation. The expected outcomes are summarised in Table 7.10. Following treatment with (+)-JQ1, BRD2 and BRD4 remain bound to JMJD6 [36]. Additionally, BRD4 remains bound to CDK9 [36]; therefore, with PepX expression I would expect these interactions to be maintained, and I would also expect the same of cyclin T1 given that it, like CDK9, binds to BRD4 via the CTM, and many components of PTEF-b remain bound to BRD4 in the presence of (+)-JQ1 [37, 457]. CHD4, another ET-domain interactor, remains bound to BRD4 and BRD3 despite (+)-JQ1 treatment; therefore, I would expect the interactions between JMJD6 and NSD3 and BRD3 to remain following (+)-JQ1 treatment [36]. (+)-JQ1 displaces BET protein from chromatin [36, 71]; therefore, I would expect loss of the BET-H4K5ac interaction. Once this experiment were completed in PepX-expressing 501mel cells, it would be conducted in NLS-, KRR- and LIL-expressing 501mel cells to ensure specifically ET-domain inhibition via PepX induces the break of ET-domain interactions, rather than BFP or NLS expression.

	BRD4 immunoprecipitation				BRD2 or BRD3 immunoprecipitation			
	Treatment				Treatment			
	Dox	DMSO	(+)-JQ1	(-)-JQ1	Dox	DMSO	(+)-JQ1	(-)-JQ1
JMJD6		■	■	■		■	■	■
NSD3		■	■	■		■	■	■
Cyclin T1	■	■	■	■				
CDK9	■	■	■	■				
BFP	■				■			
H4K5ac	■	■		■	■	■		■

Table 7.10: Expected outcome of co-IP experiments. DMSO and (-)-JQ1 are negative controls. 50 nM doxycycline treatment would be used, 500 nM (+)-JQ1 and (-)-JQ1 would be used. A time course experiment would be initially conducted in order to discern optimum treatment duration. Black square indicates interaction expected, grey square indicates interaction not expected.

- Related to Figure 7.7: To further validate the ET-domain-specific binding of PepX to BRD4, and the suitability of NLS, KRR and LIL as controls, I would have repeated the LacOLacI assay using BRD4ΔET-mCherry-LacI-NLS and BRD4mut-mCherry-LacI-NLS constructs, where BRD4ΔET represents BRD4 with an ET-domain deletion, and BRD4mut represents BRD4 with a mutation in the ET-domain [36]. I would predict that none of the GFP-tagged PepX, KRR, LIL or NLS peptides would show co-localisation with either of these mCherry-LacI-NLS constructs, as *in vitro* data shows that PepX binds to BRD4 via the ET-domain. I would also extend this study to BRD2 and BRD3. This would have required the cloning of BRD -2 -3 and -4S with and without ET-domains, and then I planned to use the LacOLacI assay to determine whether PepX binds to BRD -2, -3 and 4 in an ET-dependent manner. This is of particular interest to gaining further

understanding of K-ac-independent functions of BETs, and PTEF-b-independent transcription. So far, only BRD4 is known to enable PTEF-b-independent transcription; however, BRD -2, -3 and -4 all possess an ET-domain with >80% sequence homology [40]. Therefore, it is possible that all members of the BET protein family share this function. The co-localisation of PepX with BET family members via the ET-domain allows for the possibility that effects of PepX are not solely due to loss of transcription due to BRD4 perturbation, which is a novel notion in the field of melanoma.

7.4 Future Plans to extend thesis findings

7.4.1 Thesis summary

The data in this thesis show that BET BRD inhibition leads to the induction of autophagy-dependent senescence in 501mel melanoma cells, a p53-mutant cell line. In p53 WT A375M cells, autophagy-independent cell death occurs following BET BRD inhibition. Furthermore, a novel epigenetic BET inhibitor (RT53) induces loss of cellular proliferation and the induction of autophagy in prostate cancer cells. When autophagy is concomitantly inhibited, the loss of cellular proliferation is exacerbated. Lastly, in 501mel cells, PepX-mediated ET-domain inhibition led to loss of cellular proliferation through the induction of autophagy-dependent senescence.

7.4.2 Unanswered questions

There are still many unanswered questions following the data presented in this thesis:

1. How does p53 mutation status or function modulate the cellular response to BET BRD inhibition in melanoma?

   (1) Does p53 mutation correlate with function in melanoma?

   (2) What is the effect of attenuating p53 function in a p53 WT cell line, or restoring p53 WT expression in a p53 mutant cell line, on the cellular response to BET BRD inhibition?

   (3) What are the downstream targets of p53 that enable modulation of the cellular response to BET BRD inhibition?

2. What is the role of PTEF-b-independent transcription?

(1) Which BETs participate mediate PTEF-b-independent transcription?

(2) Which ET-domain interactors mediate PTEF-b-independent transcription?

(3) Is this context dependent?

(4) What is its functional relevance of this mechanism of transcription?

3. In the RNA-seq data generated in Chapters 3 and 5, many long, non-coding RNAs (lncRNAs) were differentially regulated following pan-BET or individual BET perturbation. Are there novel genes that BETs regulate that play a role in melanoma?

(1) What are the functions of these novel lncRNAs?

(2) How does their perturbation affect melanoma cellular proliferation?

(3) Do they represent viable, alternative targets?

4. Does the BET-G9a axis regulate autophagy gene expression in melanoma and prostate cells?

(1) Which BETs interact with G9a via the ET-domain in melanoma/prostate cancer?

(2) Are these interactions disrupted by ET-domain inhibition?

(3) How does ET-domain inhibition affect G9a occupancy at target gene promoters in melanoma and prostate cancer?

(4) How does G9a perturbation affect autophagy and cellular proliferation in melanoma and prostate cancer cells?

I have detailed the line of investigation of the BET-G9a axis, as this would enable the dissection of the mechanism by which autophagy is up-regulated in melanoma and prostate cancer. This thesis has shown that autophagy up-regulation can have context

dependent effects in these contexts, and therefore, further investigation into autophagy up-regulation may shed light onto how it impacts the cellular response to BET inhibition across multiple malignancies.

7.4.3 BET-G9a axis regulation of autophagy gene expression in melanoma and prostate cancer

7.4.3.1 BETs interact with G9a via the ET-domain

BETs bind to chromatin and act as a recruitment platform for activators of transcription [37, 40]; therefore, their perturbation should result in the down-regulation of genes. However, PepX-mediated ET-domain perturbation in 501mel cells leads to the significant up-regulation of 31 genes, while only 19 genes were significantly down-regulated (Figure 5.5). In the same cell line, following BET BRD inhibition, 592 genes were down-regulated, while 213 genes were up-regulated (Figure 3.5). Up-regulation of genes following BET perturbation has been observed across a range of malignancies [68, 284, 429, 430]. The precise mechanism as to genes are up-regulated happens remains to be clarified.

One possible mechanism is that BETs bind to proteins with transcriptionally-repressive function, and in binding to chromatin, guide these transcriptional repressors to sites that would otherwise be transcriptionally active. G9a, a histone lysine methyltransferase, interacts with both BRD4S and BRD4L and regulates autophagy through lysine dimethylation (H3K9me2) at sites of autophagic genes, which results in their repression [68]. When BRD4 (both the long and short variant) is displaced from chromatin in pancreatic cancer, G9a is also displaced from chromatin, which leads to autophagy gene de-repression [68]. Our group has shown G9a interacts with BRD4 via the ET domain *in vitro* (data not shown). Therefore, this interaction should be validated in the cellular environment. *In vitro* data experiments have also revealed a putative motif to which the BRD4 ET-domain may bind (data not shown); therefore, a G9a mutant with 3 mutations within this motif (I1036A, V1038A, L1040A) would be included in this experiment in an attempt to validate this binding motif.

The LacOLacI assay would be used to show that G9a binds to BETs in ET-domain-dependent manner in the cellular environment and would be carried out as described in the legend of Figure 7.7 [451, 458]. Co-localisation of G9a with both isoforms of BRD4, BRD4S and BRD4L, would be examined to demonstrate that both isoforms potentially play a role in modulating transcription through G9a. Cloning of the BRD4LΔET-mCherry-LacI-NLS (BRD4L with a deletion of the ET-domain) plasmid was completed in preparation for this experiment, and cloning of BRD4SΔET-mCherry-LacI-NLS plasmid would be carried out using the same strategy. BRD4L-mCherry-LacI-NLS and BRD4Lmut-mCherry-LacI-NLS (BRD4L with a mutation in the ET-domain) and BRD4S-mCherry-LacI-NLS and BRD4Smut-mCherry-LacI-NLS plasmids were previously cloned by a postdoctoral scientist in our group. Cloning of G9a into pcDNA5-FRTTO-eGFP-DEST vector was in progress in preparation for this experiment. Co-transfected plasmids that would be used in this experiment, along with expected results are shown in Table 7.11.

		GFP plasmids	
		GFP-G9a-WT	GFP-G9a-mut
mCherry-LacI-NLS Plasmids	BRD4S-mCherry-LacI-NLS	■	
	BRD4Smut-mCherry-LacI-NLS		
	BRD4SΔET-mCherry-LacI-NLS		
	BRD4L-mCherry-LacI-NLS	■	
	BRD4Lmut-mCherry-LacI-NLS		
	BRD4LΔET-mCherry-LacI-NLS		
	mCherry-LacI-NLS		

Table 7.11: Expected outcomes following co-transfection of plasmids in U-2 OS cells expressing 256x repeats of a LacO array. Black indicates co-localisation expected between indicated mCherry and GFP fluorescent proteins, grey indicates no co-localisation expected between indicated mCherry and GFP fluorescent proteins.

The notion that BRD4 binds to a repressor of transcription, potentially via the ET domain begs the question as to whether BRD -2 or -3 also participate in G9a-mediated gene regulation. BRD -2 and -3 share >80% sequence homology of the ET-domain with BRD4 [40], and BRD3 has been shown to interact with G9a [97]; therefore, G9a potentially also interacts with BRD -2 and -3 ET-domains. While BRD2 and BRD3 knockdown in pancreatic cells does not lead to an increase in autophagy [68], this effect may be context-specific; thus, it remains possible BRD -2 and -3 interact with G9a in melanoma, which may play a role in the regulation of autophagy-related genes. Moreover, siRNA-mediated BRD -2 and -3 knockdown led to both the up-regulation and down-regulation of genes (Figure 3.6). While it is possible this could be due to off-target effects or are secondary as opposed to direct effects of BET protein knockdown, the notion that BRD -2 and -3 may repress gene expression remains a possibility. Therefore, a LacOLacI experiment would be carried out in the same manner using BRD -2 and -3-mCherry-LacI-NLS containing plasmids. Cloning of BRD2ΔET-mCherry-LacI-NLS and BRD3ΔET-mCherry-LacI-NLS plasmids would be carried out in the same manner in which the BRD4LΔET-mCherry-LacI-NLS plasmid was cloned. BRD2-mCherry-LacI-NLS and BRD2mut-mCherry-LacI-NLS and BRD3-mCherry-LacI-NLS and BRD3mut-mCherry-LacI-NLS were previously cloned by a postdoctoral scientist in our group. Co-transfected plasmids and expected results are shown in Table 7.12.

		GFP plasmids	
		GFP-G9a-WT	GFP-G9a-mut
mCherry-LacI-NLS Plasmids	BRD2-mCherry-LacI-NLS		
	BRD2mut-mCherry-LacI-NLS		
	BRD2ΔET-mCherry-LacI-NLS		
	BRD3-mCherry-LacI-NLS		
	BRD3mut-mCherry-LacI-NLS		
	BRD3ΔET-mCherry-LacI-NLS		
	mCherry-LacI-NLS		

Table 7.12: Expected outcomes following co-transfection of plasmids in U-2 OS cells expressing 256x repeats of a LacO array. Black indicates co-localisation expected between indicated mCherry and GFP fluorescent proteins, grey indicates no co-localisation expected between indicated mCherry and GFP fluorescent proteins.

7.4.3.2 ET-domain inhibition disrupts the interaction between BETs and G9a in melanoma cells

At this point the interaction between G9a and BETs in an ET-domain-dependent manner in the cellular environment would have been validated. The next experiment would aim to show that inhibition of the ET-domain via PepX expression disrupts this interaction in melanoma cells. This would be carried out using co-IP experiments. PepX-expressing 501mel cells would be treated with doxycycline for a minimum of 8 h, as this is the length of time required for doxycycline-induced gene expression to occur when using this Tet-on system (data not shown), and for 24 and 48 h; at 24 h autophagy is up-regulated (Figure 5.12B), and at 48 h transcriptional programs related with autophagy were up-regulated (Figure 5.12A). All BET proteins, G9a, and H4K5ac would be expected to be present in all input samples. BFP would only be present in the doxycycline-treated input sample. The

BET proteins that showed co-localisation with G9a in the LacOLacI assay would be used to immunoprecipitate G9a, PepX expression would be induced to disrupt ET-domain interactions, and (+)-JQ1 would be used to disrupt BRD-mediated interactions. Table 7.13 shows the expected results when BET proteins would be immunoprecipitated, and Table 7.14 shows the anticipated results when the reciprocal experiment is carried out wherein G9a is immunoprecipitated. In Tables 7.13 and 7.14, it is presumed all BET proteins co-localise with G9a in the LacOLacI assay. IgG antibodies would be used as a negative control, and DMSO and (-)-JQ1 would be negative control treatments. It has not been demonstrated whether (+)-JQ1 would disrupt the BET-G9a interaction; however, I would expect this interaction would be maintained even in the presence of (+)-JQ1 as ET-domain interactors such as JMJD6 remain bound to BRD -2 and -4 despite (+)-JQ1 treatment [36]. However, I would expect BETs not to remain bound to acetylated chromatin, H4K5ac [23, 25, 132, 456], following (+)-JQ1 treatment.

IP	IgG				BRD -2, -3, and -4			
Treatment	50 nM Dox	DMSO	(+)-JQ1	(-)-JQ1	50 nM Dox	DMSO	(+)-JQ1	(-)-JQ1
G9a						■	■	■
BFP					■			
H4K5ac					■	■		■

Table 7.13: Expected results following co-IP of BET proteins and potential interactors. Black indicates interaction expected between indicated proteins, grey indicates no interaction expected between indicated proteins.

IP	IgG				G9a			
Treatment	50 nM Dox	DMSO	(+)-JQ1	(-)-JQ1	50 nM Dox	DMSO	(+)-JQ1	(-)-JQ1
BRD4						■	■	■
BRD3						■	■	■
BRD2						■	■	■
BFP								
H4K5ac						■		■

Table 7.14: Expected results following co-IP of G9a and potential interactors. Black indicates interaction expected between indicated proteins, grey indicates no interaction expected between indicated proteins.

These experiments would show that ET-domain perturbation leads to the loss of BET-G9a interactions, whilst BETs maintain chromatin occupancy, and BRD inhibition leads to the loss of BETs and G9a with chromatin.

7.4.3.3 ET-domain inhibition disrupts the interaction between BETs and G9a in prostate cancer cells

To show that ET-domain inhibition perturbs the BET-G9a interaction in prostate cancer cells, LNCaP cells would be co-transfected with HA-tagged FL BETs, BETs with an ET-domain deletion (ΔET) or with a mutation in the ET domain (ETmut). Co-IP experiments would be carried out, first to immunoprecipitate HA-tagged BETs, and blot for G9a. All BET proteins (HA-tagged and endogenous), G9a, and H4K5ac would be expected to be present in all input samples. An empty HA vector would be included as an additional negative control. An alternative strategy, if co-transfection of HA-tagged BETs is not viable, would be to transfect of FLAG-tagged G9a, either WT or mutant, then immunoprecipitate using anti-FLAG antibodies, and blot for endogenous BETs. All BET proteins, G9a and H4K5ac would be expected to be present in all input samples. Samples transfected with FLAG-tagged variants would also show the presence of FLAG-tagged G9a in input. An

empty FLAG vector would be included as an additional negative control. Both experimental setups would be carried out both in the presence and absence of (+)-JQ1 to show that BET BRD inhibition displaces this complex from chromatin. Only BETs that showed an interaction with G9a in the LacOLacI experiment detailed in Chapter 7.4.3.1 would be examined. Expected results can be seen in Tables 7.15 and 7.16.

IP	IgG			FL HA-BETs transfected			ΔET HA-BETs transfected			ETmut HA-BETs transfected			Empty HA vector		
Treatment	1	2	3	1	2	3	1	2	3	1	2	3	1	2	3
G9a				■	■	■									
H4K5ac				■	■		■	■		■	■				

Table 7.15: Expected results following co-IP of BET proteins and potential interactors in LNCaP cells. Treatments: 1 = DMSO, 2 = (-)-JQ1, 3 = (+)-JQ1. Black indicates interaction expected between indicated proteins, grey indicates no interaction expected between indicated proteins.

IP	IgG			G9a			FLAG (FLAG-G9a-WT transfected)			FLAG (FLAG-G9a-mut transfected)			FLAG (Empty FLAG vector transfected)		
Treatment	1	2	3	1	2	3	1	2	3	1	2	3	1	2	3
BRD -2, -3, -4				■	■	■	■	■	■						
H4K5ac				■	■		■	■							

Table 7.16: Expected results following co-IP of G9a and potential interactors in LNCaP cells. Treatments: 1 = DMSO, 2 = (-)-JQ1, 3 = (+)-JQ1. Black indicates interaction expected between indicated proteins, grey indicates no interaction expected between indicated proteins.

These experiments would show that G9a interacts with BETs in an ET-domain dependent manner in prostate cancer cells, and that this interaction with the ET-domain is necessary for G9a to bind to chromatin at BET-bound loci.

7.4.3.4 Identification of G9a targets in prostate cancer cells

Up to this point, experiments would have shown that in prostate cancer cells, G9a interacts with BETs in an ET-domain dependent manner, and (+)-JQ1 displaces both BETs and G9a from chromatin. To show that the ET-domain-dependent interaction between BETs and G9a has a functional impact on autophagy gene expression, autophagy gene expression would be observed using qPCR in the absence and presence of (+)-JQ1, and following endogenous BET knockdown with concomitant co-transfection of ΔET BETs. LNCaP Tet-on PepX-expressing cells represents an alternative strategy for ET-domain inhibition prostate cancer cells.

To identify autophagy genes likely regulated by this interaction, genes that are both regulated by G9a expression (as previously identified [68]) and whose promoters are occupied by BETs in VCaP cells but are displaced upon BET BRD inhibition (using analysis of previously published ChIP-seq data [34]) would be examined in the first instance. Such genes include MAP1LC3B (from which BRD3 is displaced), SQSTM1 (BRD -2, -3 and -4 are displaced), SGSH (from which BRD3 is displaced). Additionally, autophagy-related genes such as ATG9B, BECN1, ATG3 [459, 460], whose promoters at least one member of the BET protein family is displaced. Although these genes are not necessarily reported to be regulated by G9a [68], they would also be included as G9a chromatin occupation may be context specific, and may regulate the expression of a different subset of genes in prostate cancer, compared to the pancreatic cells in which the role of G9a in autophagy was originally discovered [68]. Interestingly, in the case of ATG9D and BECN1, BRD3 is the BET displaced from site of H3K27ac. In the case of ATG3, both BRD2 and BRD3 are displaced from the H3K27ac peak. This suggests a potential role for BRD3 in the regulation of autophagy in prostate cancer. Lastly, a third class of genes would be included: genes that are involved in autophagy, but are not regulated by G9a, and do not show loss of BET occupancy at gene promoters. These

genes include WIPI1, TPP1 and CLCN7 [68]. This would aim to detect genes that are potentially affected by unexplored BET-dependent mechanisms of negative gene regulation. BET displacement from chromatin may lead to up-regulation of autophagy gene expression, even if the precise location from which BETs are displaced is known.

7.4.3.5 Identification of G9a targets in melanoma cells

Up to this point, the interaction between G9a and BETs would have been validated in the cellular environment, and it would have been shown that ET-domain inhibition can disrupt this interaction whilst maintaining BET occupation on chromatin. In order to demonstrate the functional implications of the loss of BET-G9a interactions in melanoma, and the displacement of G9a from chromatin following (+)-JQ1 treatment, I would next show that up-regulation of G9a target genes coincides with a loss of G9a occupancy and H3K9me2 deposition at target gene promoters. BET BRD inhibition induces the expression of autophagy-related genes in melanoma cell lines 501mel and A375M (Figures 3.10A and 3.11A), and ET-domain inhibition leads to the up-regulation of autophagy gene sets (Figure 5.12A). Both forms of BET inhibition led to up-regulation of autophagy, as indicated by an increase in LC3BII expression (Figures 3.10E, 3.11D and 5.12B); therefore, further inducers of autophagy, such as starvation conditions, would not be required in these investigations.

To identity putative G9a candidate target genes in melanoma, I would examine genes whose expression is affected by G9a inhibition in other cancers, and autophagy genes in melanoma whose expression increases with BET BRD inhibition. The promoters of MAP1LC3B and SQSTM1 are both occupied by G9a in a BRD4-dependent manner in pancreatic cancer [68]. SQSTM1, MAP1LC3B and NEU1 increase following BET BRD inhibition in melanoma [152], which was also confirmed using the RNA-seq data I generated in Chapter 3 following BET BRD, and was also observed in the RNA-seq data

generated following ET-domain inhibition in Chapter 5. I would begin using these candidate genes initially. The analysis of published ChIP-seq data provides gene loci occupied by BETs [34, 152], the analysis of published RNA-seq data following the genetic silencing or pharmacological inhibition of G9a [461], and the extraction of the leading edges of differentially regulated autophagy-related gene sets in the melanoma RNA-seq datasets generated in this thesis would provide further candidate target genes which may be directly regulated by the BET-G9a axis.

7.4.3.6 ET-domain inhibition expression decreases G9a occupancy at target gene promoters in melanoma and prostate cancer cells

Once autophagy-related genes whose expression increased following BET BRD inhibition have been identified in both melanoma and prostate cancer, ChIP-qPCR experiments would be carried out, with the aim of showing that G9a no longer binds to the promoters of target genes in the presence of BRD or ET-domain inhibition.

In 501mel melanoma cells, (+)-JQ1 would be used as the BRD inhibitor, and the induction of PepX-expression would serve as the ET-domain inhibitor. Additionally, it would be important to show not just the loss of G9a, but also the loss of H3K9me2 marks at these target gene promoters coincided with an increase in their expression. IgG would be used as a negative control. DMSO and (-)-JQ1 would be used as negative controls. Expected results from experiments in melanoma can be seen in Table 7.17.

	Treatment	50 nM Dox	DMSO	(+)-JQ1	(-)-JQ1
Negative control	IgG				
Immunoprecipitated protein	G9a		■		■
	BRD4	■	■		■
	BRD3	■	■		■
	BRD2	■	■		■
	H3K9me2		■		■

Table 7.17: Expected results following ChIP-qPCR, with the immunoprecipitated proteins indicated. Black indicates expected occupancy of immunoprecipitated protein at autophagy gene promoters, grey indicates no expected occupancy of immunoprecipitated protein at autophagy gene promoters.

The ChIP-qPCR would be complemented with qPCR experiments showing the increase in G9a target expression in the presence of (+)-JQ1 or PepX. DMSO and (-)-JQ1 would be used as negative controls. These experiments would demonstrate that the interaction of G9a with the ET-domain of BETs is required for G9a to down-regulate the expression of these genes through the deposition of H3K9me2 marks at gene promoters in 501mel melanoma cells.

In the case of prostate cancer cells (+)-JQ1 would be used as the BRD inhibitor, and to show that interacting with the ET-domain is required for G9a chromatin occupancy, endogenous BET knockdown with co-transfection of ΔET BETs will be performed. Expected results from ChIP-qPCR experiments examining BET, G9a and H3K9me2 at autophagy-related gene promoters in prostate cancer can be seen in Table 7.18.

	Treatment	DMSO	(-)-JQ1	(+)-JQ1	Endogenous BET knockdown and ΔET BETs transfected
Negative control	IgG				
Immunoprecipitated protein	G9a				
	BRD4				
	BRD3				
	BRD2				
	H3K9me2				

Table 7.18: Expected results following ChIP-qPCR, with the immunoprecipitated proteins indicated. Black indicates expected occupancy of immunoprecipitated protein at autophagy gene promoters, grey indicates no expected occupancy of immunoprecipitated protein at autophagy gene promoters.

Autophagy-related genes would be expected to increase in expression following treatment with (+)-JQ1, or when endogenous BETs are knocked down with simultaneous co-transfection of ΔET BETs. This would be shown using qPCR in prostate cancer cells.

Overall, the ChIP-qPCR and qPCR experiments detailed in this section would show that when G9a is unable to occupy chromatin, either due to lack of BET chromatin occupancy or lack of available BET protein ET-domain onto which G9a can dock, H3K9me2 is lost and autophagy gene expression increases in prostate cancer and melanoma cells.

7.4.3.7 G9a knockdown and pharmacological inhibition activates autophagy

If BET inhibition, either via the BRD or ET-domain, leads to up-regulation of autophagy-related genes, and subsequent autophagy up-regulation in melanoma and prostate cancer, it stands to reason that G9a inhibition should have the same effect on autophagy and the expression of associated genes. In order to show G9a inhibition leads to the up-regulation of autophagy-related genes in 501mel and LNCaP cells, an RNA-seq

experiment would be carried out, examining the genes whose expression is significantly altered following G9a inhibition.

To identify appropriate treatment conditions prior to subjecting samples to RNA-seq, cells would be treated with wither 80 nM (IC_{50} in terms of H3K9me2 loss) or 250 nM (IC_{90} in terms of H3K9me2 loss) G9a inhibitor, UNC0638 [462], for 24 or 48 h, as these time points were used in previous RNA-seq experiments in this thesis where changes in autophagy-related genes were observed. UNC0737 would be used as a negative control [462]. At each time point, H3K9me2 protein expression would be observed using immunoblot, and the expression of mRNA of autophagy-related genes regulated by the BET-G9a axis would be monitored using qPCR. A time and duration of treatment would be selected where there is loss of H3K9me2 and an increase in autophagy gene expression. If suitable conditions cannot be identified following G9a pharmacological inhibition, perhaps siRNA-mediated knockdown of G9a or shRNA-mediated G9a knockout is an alternative approach that may have fewer off-target effects, as UNC0638 also inhibits EHMT1 [462].

Such an RNA-seq experiment would enable identification of G9a target autophagy-related genes, and perhaps additional pathways affected by G9a, which may or may not be BET-dependent. Changes in gene expression would be validated, using qPCR, and immunoblotting would be used to validate that autophagy is up-regulated in cells following inhibition of G9a.

7.4.3.8 G9a-regulates autophagy which underpins BET-inhibition induced senescence

If the outcomes of the experiments detailed in this chapter were as anticipated, the resulting data would show that G9a regulates autophagy-related gene expression through deposition of H3K9me2 marks at promoters. This activity would be dependent upon interacting with the BET ET-domain whilst BETs are bound to chromatin at autophagy

gene promoters. Lastly, to explore the role of G9a in relation to autophagy modulation and cellular proliferation, I would hypothesise that since concomitant inhibition of autophagy rescues proliferation in 501mel melanoma cells (Figures 3.14A and 5.12), then prevention of gene-de-repression through the maintenance of H3K9me2 marks should enable bypass of senescence.

LSD1 and JMJD2C demethylate H3K9me2 [463-465] and inhibition of either demethylase in melanoma leads to senescence onset [466]. Conversely, over-expression of LSD1 or JMJD2C leads to the bypass of senescence [466]. 2-PCPA-1a inhibits the H3K9 demethylation activity of LSD1; however, 2-PCPA only affects LSD1-mediated H3K4 demethylation [467]. Thus, 2-PCPA-1a treatment should result in the maintenance of H3K9me2, and subsequent repression of autophagy-related genes, whereas 2-PCPA would not affect H3K9me2 marks; therefore, autophagy genes would be expressed. IOX1 inhibits JMJD2C [466], and while JMJD2C also demethylates H3K9me3 and other histone residues, it may play a role in the removal of G9a-deposited H3K9me2 marks.

Treatment with CQ, an autophagy inhibitor [335], rescues 501mel cells from onset of senescence (Figures 3.14A and 5.12), this indicates that de-repression of autophagy genes is required for senescence. Therefore, treatment with 2-PCPA-1a or IOX1 should enable bypass of proliferation as both treatments should prevent the de-repression of autophagy genes. Concomitant treatment of cells with (+)-JQ1 and 2-PCPA-1a or IOX1 will allow BETs and G9a to be displaced from chromatin, but the effects of G9a displacement would be minimised as the repressive methylation marks would remain on the chromatin; thus, the genes would remain repressed and cell proliferation would be maintained. Likewise, PepX expression, induced by doxycycline, would prevent BET-G9a interaction, but concomitant 2-PCPA-1a or IOX1 treatment would prevent the subsequent up-regulation of autophagy genes. Expected results are detailed in Table 7.19.

The concomitant effect of LSD1 or JMJD2C inhibition would be first tested using an MTT assay to assess, its effects on cellular proliferation. Senescence onset would then be confirmed using a β-galactosidase assay. Immunoblotting would also be carried out to ensure that H3K9me2 marks are maintained upon 2-PCPA-1a or IOX1 treatment, and lost when cells are treated with 2-PCPA, irrespective of DMSO, doxycycline (dox), (-)-JQ1 or (+)-JQ1 treatment.

+ DMSO				+ 2-PCPA-1a or +IOX1				+ 2-PCPA			
1	2	3	4	1	2	3	4	1	2	3	4
	■		■		■		■		■		■

Table 7.19: Expected outcomes following experiments showing induction of senescence following treatment with the indicated compounds in 501mel cells. Treatments: 1 = DMSO, 2 = 50 nM Doxycycline, 3 = (-)-JQ1, 4 = (+)-JQ1. Black squares indicate the onset of senescence is expected; grey squares indicates bypass of the onset of senescence owing to autophagy inhibition expected, white indicates no loss of proliferation expected.

However, LSD1 and JMJD2C inhibition cause senescence in melanoma cells in a cell line-dependent manner [466]. Therefore, concomitant treatment with negative controls DMSO and (-)-JQ1 and demethylase inhibitor could induce senescence, and perhaps concomitant BET inhibition may not induce senescence bypass. As an alternative strategy G9a over-expression or knockdown could be induced in tandem with BET inhibition to further examine the effects of histone methylation modulation on autophagy-dependent senescence induction. It is predicted that G9a over-expression should lead to greater autophagy gene repression, and G9a knockdown should lead to greater autophagy gene de-repression. Thus, when combined with BET perturbation, ectopic expression of G9a should lead to senescence bypass, and G9a lockdown should not, and may even potentially lead to greater senescence induction. Expected results shown in Table 7.20.

+ DMSO				G9a over-expression				G9a knockdown			
1	2	3	4	1	2	3	4	1	2	3	4

Table 7.20: Expected outcomes following experiments showing induction of senescence following treatment with the indicated compounds and over-expression of knockdown of G9a in 501mel cells. Treatments: 1 = DMSO, 2 = 50 nM Doxycycline, 3 = (-)-JQ1, 4 = (+)-JQ1. Black squares indicate the onset of senescence is expected; grey squares indicates the bypass of the onset of senescence owing to autophagy inhibition expected, white indicates no loss of proliferation expected.

Concomitant inhibition of autophagy exacerbates loss of cellular proliferation in LNCaP prostate cancer cells (Figure 4.8B); therefore, prevention of gene de-repression through the maintenance of H3K9me2 marks should also lead to greater loss of proliferation. G9a over-expression would lead to increased deposition of H3K9me2 marks and would mimic the effects of autophagy inhibition. Conversely, knockdown of G9a potentially mimics the effects of increased autophagic flux, as this would lead to a reduction in H3K9me2 marks at autophagy gene loci and subsequent autophagy gene up-regulation. If inhibition of autophagy leads to increased loss of cellular proliferation, increased autophagy stimulation may lead to rescue of cellular proliferation. Expected results of the impact of modulation of G9a expression in conjunction with BET BRD inhibition, measured using an MTT assay, are shown in Table 7.21.

+ DMSO		G9a over-expression		G9a knockdown	
DMSO	RT53	DMSO	RT53	DMSO	RT53

Table 7.21: Expected outcomes following experiments showing loss of proliferation in LNCaP cells, following treatment with the indicated compounds and over-expression of knockdown of G9a. Black squares indicate exaggerated loss of cellular proliferation is expected; grey squares indicate moderate loss of cellular proliferation expected, white indicates no loss of proliferation expected.

If the expected results are obtained, then these experiments altogether would demonstrate that specifically BET ET-domain inhibition, rather than displacement of BETs from chromatin through BET BRD inhibition, leads to the displacement of G9a from chromatin. In 501mel melanoma cells, this in turn would lead to the de-repression of autophagy-related genes, and subsequent autophagy up-regulation and senescence induction. This up-regulation autophagy may be inhibited if histone demethylases LSD1 or JMJD2C are inhibited, or if G9a is over-expressed thereby showing that G9a-dependent deposition of H3K9me2 marks drive autophagy gene repression, and bypassing senescence. In prostate cancer LNCaP cells, G9a over-expression would lead to increased loss of cellular proliferation

7.4.3.9 Alternative mechanisms

It remains possible that G9a does not regulate autophagy gene expression in melanoma or prostate cancer cells; perhaps a different histone modifier or repressive complex is dependent upon BETs for chromatin occupancy. The work could be expanded to further cell lines in each malignancy model to confirm this gene regulation mechanism is not cell line specific. It would perhaps be prudent to begin the search for alternatives to G9a by examining ET-dependent interactors of BETs, as these would be displaced from chromatin with BETs upon treatment with a BET BRD inhibitor. For example, BETs bind to components of the transcriptionally-repressive NuRD complex; BRD3 and BRD4 bind to CHD4 and MTA3 in a (+)-JQ1-independent manner [36, 468].

Alternatively, perhaps the perturbation of topology of chromatin may led to increased gene expression. BRD2 is involved in insulation of chromatin, ensuring that two genes are not simultaneously expressed simply because they are located in physical proximity to each other [53]. BRD2 depletion leads to the increase in expression of genes owing to the loss of boundary integrity. Therefore, it is possible that this mechanism could be more

widespread and involve BRD3 and BRD4. BRD3 occupancy of chromatin overlaps with CTCF, albeit to a lesser extent than BRD2; however, perhaps BRD3 plays a role in a similar regulatory mechanism [53].

PTMs are able to modulate both Kac -independent and -dependent interactions of BRD4 [96]. BRD4 hyperphosphorylation plays a role in driving resistance in triple-negative breast cancer, with BRD4 hyperphosphorylation leading to greater nuclear retention and stability [96]. BRD4 phosphorylation affects transcription, chromatin occupation and BRD-independent interactions [96]. BET decoration with PTMs and, therefore, BET function can be fine-tuned in a context-dependent manner. It seems plausible that if PTMs modulate the activity of BRD4, then there are unexplored mechanisms by which the functions of BRD -2 and -3 are modulated by PTMs, which in turn, could lead to their modulation of autophagy-related gene expression.

Bibliography

1. Hauer, M.H. and S.M. Gasser, *Chromatin and nucleosome dynamics in DNA damage and repair.* Genes Dev, 2017. **31**(22): p. 2204-2221.

2. Luger, K., et al., *Crystal structure of the nucleosome core particle at 2.8 A resolution.* Nature, 1997. **389**(6648): p. 251-60.

3. Litt, M.D., et al., *Correlation between histone lysine methylation and developmental changes at the chicken beta-globin locus.* Science, 2001. **293**(5539): p. 2453-5.

4. Tamaru, H., *Confining euchromatin/heterochromatin territory: jumonji crosses the line.* Genes Dev, 2010. **24**(14): p. 1465-78.

5. Strom, A.R., et al., *Phase separation drives heterochromatin domain formation.* Nature, 2017. **547**(7662): p. 241-245.

6. Choudhary, C., et al., *The growing landscape of lysine acetylation links metabolism and cell signalling.* Nat Rev Mol Cell Biol, 2014. **15**(8): p. 536-50.

7. Wang, Z., et al., *Combinatorial patterns of histone acetylations and methylations in the human genome.* Nat Genet, 2008. **40**(7): p. 897-903.

8. Godfrey, L., et al., *MLL-AF4 binds directly to a BCL-2 specific enhancer and modulates H3K27 acetylation.* Exp Hematol, 2017. **47**: p. 64-75.

9. Heintzman, N.D., et al., *Histone modifications at human enhancers reflect global cell-type-specific gene expression.* Nature, 2009. **459**(7243): p. 108-12.

10. Bolden, J.E., M.J. Peart, and R.W. Johnstone, *Anticancer activities of histone deacetylase inhibitors.* Nat Rev Drug Discov, 2006. **5**(9): p. 769-84.

11. Choi, J.H., et al., *Expression profile of histone deacetylase 1 in gastric cancer tissues.* Jpn J Cancer Res, 2001. **92**(12): p. 1300-4.

12. Halkidou, K., et al., *Upregulation and nuclear recruitment of HDAC1 in hormone refractory prostate cancer.* Prostate, 2004. **59**(2): p. 177-89.

13. Zhu, P., et al., *Induction of HDAC2 expression upon loss of APC in colorectal tumorigenesis.* Cancer Cell, 2004. **5**(5): p. 455-63.

14. Fraga, M.F., et al., *Loss of acetylation at Lys16 and trimethylation at Lys20 of histone H4 is a common hallmark of human cancer.* Nat Genet, 2005. **37**(4): p. 391-400.

15. Huang, B.H., et al., *Inhibition of histone deacetylase 2 increases apoptosis and p21Cip1/ WAF1 expression, independent of histone deacetylase 1.* Cell Death Differ, 2005. **12**(4): p. 395-404.

16. Zhang, Z., et al., *Quantitation of HDAC1 mRNA expression in invasive carcinoma of the breast*.* Breast Cancer Res Treat, 2005. **94**(1): p. 11-6.

17. Wilson, A.J., et al., *Histone deacetylase 3 (HDAC3) and other class I HDACs regulate colon cell maturation and p21 expression and are deregulated in human colon cancer.* J Biol Chem, 2006. **281**(19): p. 13548-58.

18. Haynes, S.R., et al., *The bromodomain: a conserved sequence found in human, Drosophila and yeast proteins.* Nucleic Acids Res, 1992. **20**(10): p. 2603.

19. Dhalluin, C., et al., *Structure and ligand of a histone acetyltransferase bromodomain.* Nature, 1999. **399**(6735): p. 491-6.

20. Jacobson, R.H., et al., *Structure and function of a human TAFII250 double bromodomain module.* Science, 2000. **288**(5470): p. 1422-5.

21. Filippakopoulos, P. and S. Knapp, *The bromodomain interaction module.* FEBS Lett, 2012. **586**(17): p. 2692-704.

22. Fujisawa, T. and P. Filippakopoulos, *Functions of bromodomain-containing proteins and their roles in homeostasis and cancer.* Nat Rev Mol Cell Biol, 2017. **18**(4): p. 246-262.

23. Wang, C.Y. and P. Filippakopoulos, *Beating the odds: BETs in disease.* Trends Biochem Sci, 2015. **40**(8): p. 468-79.

24. Moriniere, J., et al., *Cooperative binding of two acetylation marks on a histone tail by a single bromodomain.* Nature, 2009. **461**(7264): p. 664-8.

25. Filippakopoulos, P., et al., *Histone recognition and large-scale structural analysis of the human bromodomain family.* Cell, 2012. **149**(1): p. 214-31.

26. Musselman, C.A., et al., *Perceiving the epigenetic landscape through histone readers.* Nat Struct Mol Biol, 2012. **19**(12): p. 1218-27.

27. Huang, B., et al., *Brd4 coactivates transcriptional activation of NF-kappaB via specific binding to acetylated RelA.* Mol Cell Biol, 2009. **29**(5): p. 1375-87.

28. Lamonica, J.M., et al., *Bromodomain protein Brd3 associates with acetylated GATA1 to promote its chromatin occupancy at erythroid target genes.* Proc Natl Acad Sci U S A, 2011. **108**(22): p. E159-68.

29. Shi, J., et al., *Disrupting the interaction of BRD4 with diacetylated Twist suppresses tumorigenesis in basal-like breast cancer.* Cancer Cell, 2014. **25**(2): p. 210-25.

30. Blee, A.M., et al., *BET bromodomain-mediated interaction between ERG and BRD4 promotes prostate cancer cell invasion.* Oncotarget, 2016. **7**(25): p. 38319-38332.

31. Cheung, K.L., et al., *Distinct Roles of Brd2 and Brd4 in Potentiating the Transcriptional Program for Th17 Cell Differentiation.* Mol Cell, 2017. **65**(6): p. 1068-1080 e5.

32. Schroder, S., et al., *Two-pronged binding with bromodomain-containing protein 4 liberates positive transcription elongation factor b from inactive ribonucleoprotein complexes.* J Biol Chem, 2012. **287**(2): p. 1090-9.

33. Chen, Y., et al., *ZMYND8 acetylation mediates HIF-dependent breast cancer progression and metastasis.* J Clin Invest, 2018. **128**(5): p. 1937-1955.

34. Asangani, I.A., et al., *Therapeutic targeting of BET bromodomain proteins in castration-resistant prostate cancer.* Nature, 2014. **510**(7504): p. 278-82.

35. Choudhary, C., et al., *Lysine acetylation targets protein complexes and co-regulates major cellular functions.* Science, 2009. **325**(5942): p. 834-40.

36. Lambert, J.P., et al., *Interactome Rewiring Following Pharmacological Targeting of BET Bromodomains.* Mol Cell, 2019. **73**(3): p. 621-638 e17.

37. Jang, M.K., et al., *The bromodomain protein Brd4 is a positive regulatory component of P-TEFb and stimulates RNA polymerase II-dependent transcription.* Mol Cell, 2005. **19**(4): p. 523-34.

38. Gaucher, J., et al., *Bromodomain-dependent stage-specific male genome programming by Brdt.* EMBO J, 2012. **31**(19): p. 3809-20.

39. Bisgrove, D.A., et al., *Conserved P-TEFb-interacting domain of BRD4 inhibits HIV transcription.* Proc Natl Acad Sci U S A, 2007. **104**(34): p. 13690-5.

40. Rahman, S., et al., *The Brd4 extraterminal domain confers transcription activation independent of pTEFb by recruiting multiple proteins, including NSD3.* Mol Cell Biol, 2011. **31**(13): p. 2641-52.

41. Zhang, Q., et al., *Structural Mechanism of Transcriptional Regulator NSD3 Recognition by the ET Domain of BRD4.* Structure, 2016. **24**(7): p. 1201-8.

42. Henderson, E., Filippakopoulos, P., *BET mechanisms in cancer*, in *Histone Modifications in Therapy*. 2020, Elsevier. p. 101-142.

43. *Gene Expression database of Normal and Tumour Tissues*. Available from: http://gent2.appex.kr/gent2/.

44. Park, S.J., et al., *GENT2: an updated gene expression database for normal and tumor tissues.* BMC Med Genomics, 2019. **12**(Suppl 5): p. 101.

45. Kim, M.S., et al., *A draft map of the human proteome.* Nature, 2014. **509**(7502): p. 575-81.

46. Gyuris, A., et al., *The chromatin-targeting protein Brd2 is required for neural tube closure and embryogenesis.* Biochim Biophys Acta, 2009. **1789**(5): p. 413-21.

47. Shang, E., et al., *Double bromodomain-containing gene Brd2 is essential for embryonic development in mouse.* Dev Dyn, 2009. **238**(4): p. 908-17.

48. Houzelstein, D., et al., *Growth and early postimplantation defects in mice deficient for the bromodomain-containing protein Brd4.* Mol Cell Biol, 2002. **22**(11): p. 3794-802.

49. Tsume, M., et al., *Brd2 is required for cell cycle exit and neuronal differentiation through the E2F1 pathway in mouse neuroepithelial cells.* Biochem Biophys Res Commun, 2012. **425**(4): p. 762-8.

50. Wang, F., et al., *Brd2 disruption in mice causes severe obesity without Type 2 diabetes.* Biochem J, 2009. **425**(1): p. 71-83.

51. Zang, K., et al., *Brd2 inhibits adipogenesis via the ERK1/2 signaling pathway in 3T3-L1 adipocytes.* PLoS One, 2013. **8**(10): p. e78536.

52. Dixon, J.R., et al., *Topological domains in mammalian genomes identified by analysis of chromatin interactions.* Nature, 2012. **485**(7398): p. 376-80.

53. Hsu, S.C., et al., *The BET Protein BRD2 Cooperates with CTCF to Enforce Transcriptional and Architectural Boundaries.* Mol Cell, 2017. **66**(1): p. 102-116 e7.

54. Gamsjaeger, R., et al., *Structural basis and specificity of acetylated transcription factor GATA1 recognition by BET family bromodomain protein Brd3.* Mol Cell Biol, 2011. **31**(13): p. 2632-40.

55. Stonestrom, A.J., et al., *Functions of BET proteins in erythroid gene expression.* Blood, 2015. **125**(18): p. 2825-34.

56. Shao, Z., et al., *The acetyllysine reader BRD3R promotes human nuclear reprogramming and regulates mitosis.* Nat Commun, 2016. **7**: p. 10869.

57. Zhang, L., et al., *microRNA-141 is involved in a nasopharyngeal carcinoma-related genes network.* Carcinogenesis, 2010. **31**(4): p. 559-66.

58. Bolden, J.E., et al., *Inducible in vivo silencing of Brd4 identifies potential toxicities of sustained BET protein inhibition.* Cell Rep, 2014. **8**(6): p. 1919-1929.

59. Penas, C., et al., *Time series modeling of cell cycle exit identifies Brd4 dependent regulation of cerebellar neurogenesis.* Nat Commun, 2019. **10**(1): p. 3028.

60. Dey, A., et al., *A bromodomain protein, MCAP, associates with mitotic chromosomes and affects G(2)-to-M transition.* Mol Cell Biol, 2000. **20**(17): p. 6537-49.

61. Maruyama, T., et al., *A Mammalian bromodomain protein, brd4, interacts with replication factor C and inhibits progression to S phase.* Mol Cell Biol, 2002. **22**(18): p. 6509-20.

62. Ottinger, M., et al., *Kaposi's sarcoma-associated herpesvirus LANA-1 interacts with the short variant of BRD4 and releases cells from a BRD4- and BRD2/RING3-induced G1 cell cycle arrest.* J Virol, 2006. **80**(21): p. 10772-86.

63. Dey, A., et al., *The double bromodomain protein Brd4 binds to acetylated chromatin during interphase and mitosis.* Proc Natl Acad Sci U S A, 2003. **100**(15): p. 8758-63.

64. Zhao, R., et al., *Gene bookmarking accelerates the kinetics of post-mitotic transcriptional re-activation.* Nat Cell Biol, 2011. **13**(11): p. 1295-304.

65. Wang, R., et al., *Bromodomain protein Brd4 associated with acetylated chromatin is important for maintenance of higher-order chromatin structure.* J Biol Chem, 2012. **287**(14): p. 10738-52.

66. Behera, V., et al., *Interrogating Histone Acetylation and BRD4 as Mitotic Bookmarks of Transcription.* Cell Rep, 2019. **27**(2): p. 400-415 e5.

67. Floyd, S.R., et al., *The bromodomain protein Brd4 insulates chromatin from DNA damage signalling.* Nature, 2013. **498**(7453): p. 246-50.

68. Sakamaki, J.I., et al., *Bromodomain Protein BRD4 Is a Transcriptional Repressor of Autophagy and Lysosomal Function.* Mol Cell, 2017. **66**(4): p. 517-532 e9.

69. Meyers, R.M., et al., *Computational correction of copy number effect improves specificity of CRISPR-Cas9 essentiality screens in cancer cells.* Nat Genet, 2017. **49**(12): p. 1779-1784.

70. Miyoshi, S., et al., *ANTITUMOR AGENT*. 2009, MITSUBISHI TANABE PHARMA CORPORATION. p. 1-37.

71. Filippakopoulos, P., et al., *Selective inhibition of BET bromodomains.* Nature, 2010. **468**(7327): p. 1067-73.

72. Nicodeme, E., et al., *Suppression of inflammation by a synthetic histone mimic.* Nature, 2010. **468**(7327): p. 1119-23.

73. Filippakopoulos, P. and S. Knapp, *Targeting bromodomains: epigenetic readers of lysine acetylation.* Nat Rev Drug Discov, 2014. **13**(5): p. 337-56.

74. Xu, Y. and C.R. Vakoc, *Targeting Cancer Cells with BET Bromodomain Inhibitors.* Cold Spring Harb Perspect Med, 2017. **7**(7).

75. Cochran, A.G., A.R. Conery, and R.J. Sims, 3rd, *Bromodomains: a new target class for drug development.* Nat Rev Drug Discov, 2019.

76. Martin, M.P., et al., *Cyclin-dependent kinase inhibitor dinaciclib interacts with the acetyl-lysine recognition site of bromodomains.* ACS Chem Biol, 2013. **8**(11): p. 2360-5.

77. Dittmann, A., et al., *The commonly used PI3-kinase probe LY294002 is an inhibitor of BET bromodomains.* ACS Chem Biol, 2014. **9**(2): p. 495-502.

78. Ember, S.W., et al., *Acetyl-lysine binding site of bromodomain-containing protein 4 (BRD4) interacts with diverse kinase inhibitors.* ACS Chem Biol, 2014. **9**(5): p. 1160-71.

79. Ciceri, P., et al., *Dual kinase-bromodomain inhibitors for rationally designed polypharmacology.* Nat Chem Biol, 2014. **10**(4): p. 305-12.

80. Liu, S., et al., *Structure-Guided Design and Development of Potent and Selective Dual Bromodomain 4 (BRD4)/Polo-like Kinase 1 (PLK1) Inhibitors.* J Med Chem, 2018. **61**(17): p. 7785-7795.

81. Loven, J., et al., *Selective inhibition of tumor oncogenes by disruption of super-enhancers.* Cell, 2013. **153**(2): p. 320-34.

82. Mertens, F., et al., *Successful treatment of a child with t(15;19)-positive tumor.* Pediatr Blood Cancer, 2007. **49**(7): p. 1015-7.

83. Kees, U.R., M.T. Mulcahy, and M.L. Willoughby, *Intrathoracic carcinoma in an 11-year-old girl showing a translocation t(15;19).* Am J Pediatr Hematol Oncol, 1991. **13**(4): p. 459-64.

84. French, C.A., et al., *BRD4 bromodomain gene rearrangement in aggressive carcinoma with translocation t(15;19).* Am J Pathol, 2001. **159**(6): p. 1987-92.

85. French, C.A., et al., *BRD-NUT oncoproteins: a family of closely related nuclear proteins that block epithelial differentiation and maintain the growth of carcinoma cells.* Oncogene, 2008. **27**(15): p. 2237-42.

86. Reynoird, N., et al., *Oncogenesis by sequestration of CBP/p300 in transcriptionally inactive hyperacetylated chromatin domains.* EMBO J, 2010. **29**(17): p. 2943-52.

87. Alekseyenko, A.A., et al., *The oncogenic BRD4-NUT chromatin regulator drives aberrant transcription within large topological domains.* Genes Dev, 2015. **29**(14): p. 1507-23.

88. Liao, S., et al., *Genetic modifiers of the BRD4-NUT dependency of NUT midline carcinoma uncovers a synergism between BETis and CDK4/6is.* Genes Dev, 2018. **32**(17-18): p. 1188-1200.

89. Wang, R., et al., *Uncovering BRD4 hyperphosphorylation associated with cellular transformation in NUT midline carcinoma.* Proc Natl Acad Sci U S A, 2017. **114**(27): p. E5352-E5361.

90. Wang, R., et al., *Activation of SOX2 expression by BRD4-NUT oncogenic fusion drives neoplastic transformation in NUT midline carcinoma.* Cancer Res, 2014. **74**(12): p. 3332-43.

91. Stathis, A., et al., *Clinical Response of Carcinomas Harboring the BRD4-NUT Oncoprotein to the Targeted Bromodomain Inhibitor OTX015/MK-8628.* Cancer Discov, 2016. **6**(5): p. 492-500.

92. Mertz, J.A., et al., *Targeting MYC dependence in cancer by inhibiting BET bromodomains.* Proc Natl Acad Sci U S A, 2011. **108**(40): p. 16669-74.

93. Rathert, P., et al., *Transcriptional plasticity promotes primary and acquired resistance to BET inhibition.* Nature, 2015. **525**(7570): p. 543-547.

94. Puissant, A., et al., *Targeting MYCN in neuroblastoma by BET bromodomain inhibition.* Cancer Discov, 2013. **3**(3): p. 308-23.

95. Gallagher, S.J., et al., *The epigenetic regulator I-BET151 induces BIM-dependent apoptosis and cell cycle arrest of human melanoma cells.* J Invest Dermatol, 2014. **134**(11): p. 2795-2805.

96. Shu, S., et al., *Response and resistance to BET bromodomain inhibitors in triple-negative breast cancer.* Nature, 2016. **529**(7586): p. 413-417.

97. Dawson, M.A., et al., *Inhibition of BET recruitment to chromatin as an effective treatment for MLL-fusion leukaemia.* Nature, 2011. **478**(7370): p. 529-33.

98. Zuber, J., et al., *RNAi screen identifies Brd4 as a therapeutic target in acute myeloid leukaemia.* Nature, 2011. **478**(7370): p. 524-8.

99. Fong, C.Y., et al., *BET inhibitor resistance emerges from leukaemia stem cells.* Nature, 2015. **525**(7570): p. 538-42.

100. Devaraj, S.G., et al., *HEXIM1 induction is mechanistically involved in mediating anti-AML activity of BET protein bromodomain antagonist.* Leukemia, 2016. **30**(2): p. 504-8.

101. Jang, J.E., et al., *AMPK-ULK1-Mediated Autophagy Confers Resistance to BET Inhibitor JQ1 in Acute Myeloid Leukemia Stem Cells.* Clin Cancer Res, 2017. **23**(11): p. 2781-2794.

102. Khoueiry, P., et al., *BRD4 bimodal binding at promoters and drug-induced displacement at Pol II pause sites associates with I-BET sensitivity.* Epigenetics Chromatin, 2019. **12**(1): p. 39.

103. Delmore, J.E., et al., *BET bromodomain inhibition as a therapeutic strategy to target c-Myc.* Cell, 2011. **146**(6): p. 904-17.

104. Abruzzese, M.P., et al., *Inhibition of bromodomain and extra-terminal (BET) proteins increases NKG2D ligand MICA expression and sensitivity to NK cell-mediated cytotoxicity in multiple myeloma cells: role of cMYC-IRF4-miR-125b interplay.* J Hematol Oncol, 2016. **9**(1): p. 134.

105. Suzuki, K., et al., *Antimyeloma activity of bromodomain inhibitors on the human myeloma cell line U266 by downregulation of MYCL.* Anticancer Drugs, 2016. **27**(8): p. 756-65.

106. Carew, J.S., et al., *Rational cotargeting of HDAC6 and BET proteins yields synergistic antimyeloma activity.* Blood Adv, 2019. **3**(8): p. 1318-1329.

107. Stubbs, M.C., et al., *The Novel Bromodomain and Extraterminal Domain Inhibitor INCB054329 Induces Vulnerabilities in Myeloma Cells That Inform Rational Combination Strategies.* Clin Cancer Res, 2019. **25**(1): p. 300-311.

108. Shahbazi, J., et al., *Histone deacetylase 2 and N-Myc reduce p53 protein phosphorylation at serine 46 by repressing gene transcription of tumor protein 53-induced nuclear protein 1.* Oncotarget, 2014. **5**(12): p. 4257-68.

109. Lee, S., et al., *Bromodomain and extraterminal inhibition blocks tumor progression and promotes differentiation in neuroblastoma.* Surgery, 2015. **158**(3): p. 819-26.

110. Liu, P.Y., et al., *The BET bromodomain inhibitor exerts the most potent synergistic anticancer effects with quinone-containing compounds and anti-microtubule drugs.* Oncotarget, 2016. **7**(48): p. 79217-79232.

111. Shahbazi, J., et al., *The Bromodomain Inhibitor JQ1 and the Histone Deacetylase Inhibitor Panobinostat Synergistically Reduce N-Myc Expression and Induce Anticancer Effects.* Clin Cancer Res, 2016. **22**(10): p. 2534-44.

112. Veneziani, I., et al., *The BET-bromodomain inhibitor JQ1 renders neuroblastoma cells more resistant to NK cell-mediated recognition and killing by downregulating ligands for NKG2D and DNAM-1 receptors.* Oncotarget, 2019. **10**(22): p. 2151-2160.

113. Pastori, C., et al., *BET bromodomain proteins are required for glioblastoma cell proliferation.* Epigenetics, 2014. **9**(4): p. 611-20.

114. Pastori, C., et al., *The Bromodomain protein BRD4 controls HOTAIR, a long noncoding RNA essential for glioblastoma proliferation.* Proc Natl Acad Sci U S A, 2015. **112**(27): p. 8326-31.

115. Berenguer-Daize, C., et al., *OTX015 (MK-8628), a novel BET inhibitor, displays in vitro and in vivo antitumor effects alone and in combination with conventional therapies in glioblastoma models.* Int J Cancer, 2016. **139**(9): p. 2047-55.

116. Ishida, C.T., et al., *Mitochondrial matrix chaperone and c-myc inhibition causes enhanced lethality in glioblastoma.* Oncotarget, 2017. **8**(23): p. 37140-37153.

117. Fahey, J.M., et al., *Nitric oxide antagonism to glioblastoma photodynamic therapy and mitigation thereof by BET bromodomain inhibitor JQ1.* J Biol Chem, 2018. **293**(14): p. 5345-5359.

118. Meng, W., et al., *Enhanced efficacy of histone deacetylase inhibitor combined with bromodomain inhibitor in glioblastoma.* J Exp Clin Cancer Res, 2018. **37**(1): p. 241.

119. Xu, L., et al., *Targetable BET proteins- and E2F1-dependent transcriptional program maintains the malignancy of glioblastoma.* Proc Natl Acad Sci U S A, 2018. **115**(22): p. E5086-E5095.

120. Togel, L., et al., *Dual Targeting of Bromodomain and Extraterminal Domain Proteins, and WNT or MAPK Signaling, Inhibits c-MYC Expression and Proliferation of Colorectal Cancer Cells.* Mol Cancer Ther, 2016. **15**(6): p. 1217-26.

121. Ma, Y., et al., *The MAPK Pathway Regulates Intrinsic Resistance to BET Inhibitors in Colorectal Cancer.* Clin Cancer Res, 2017. **23**(8): p. 2027-2037.

122. Nakamura, Y., et al., *Targeting of super-enhancers and mutant BRAF can suppress growth of BRAF-mutant colon cancer cells via repression of MAPK signaling pathway.* Cancer Lett, 2017. **402**: p. 100-109.

123. Bauer, K., et al., *Hitting two oncogenic machineries in cancer cells: cooperative effects of the multi-kinase inhibitor ponatinib and the BET bromodomain blockers JQ1 or dBET1 on human carcinoma cells.* Oncotarget, 2018. **9**(41): p. 26491-26506.

124. Zhang, Y., et al., *JQ-1 Inhibits Colon Cancer Proliferation via Suppressing Wnt/beta-Catenin Signaling and miR-21.* Chem Res Toxicol, 2018. **31**(5): p. 302-307.

125. Kurimchak, A.M., et al., *Resistance to BET Bromodomain Inhibitors Is Mediated by Kinome Reprogramming in Ovarian Cancer.* Cell Rep, 2016. **16**(5): p. 1273-1286.

126. Zhang, Z., et al., *BET Bromodomain Inhibition as a Therapeutic Strategy in Ovarian Cancer by Downregulating FoxM1.* Theranostics, 2016. **6**(2): p. 219-30.

127. Karakashev, S., et al., *BET Bromodomain Inhibition Synergizes with PARP Inhibitor in Epithelial Ovarian Cancer.* Cell Rep, 2017. **21**(12): p. 3398-3405.

128. Li, C., et al., *Mutational landscape of primary, metastatic, and recurrent ovarian cancer reveals c-MYC gains as potential target for BET inhibitors.* Proc Natl Acad Sci U S A, 2019. **116**(2): p. 619-624.

129. Lockwood, W.W., et al., *Sensitivity of human lung adenocarcinoma cell lines to targeted inhibition of BET epigenetic signaling proteins.* Proc Natl Acad Sci U S A, 2012. **109**(47): p. 19408-13.

130. Shimamura, T., et al., *Efficacy of BET bromodomain inhibition in Kras-mutant non-small cell lung cancer.* Clin Cancer Res, 2013. **19**(22): p. 6183-92.

131. Jahchan, N.S., et al., *Identification and Targeting of Long-Term Tumor-Propagating Cells in Small Cell Lung Cancer.* Cell Rep, 2016. **16**(3): p. 644-56.

132. Handoko, L., et al., *JQ1 affects BRD2-dependent and independent transcription regulation without disrupting H4-hyperacetylated chromatin states.* Epigenetics, 2018. **13**(4): p. 410-431.

133. Gobbi, G., et al., *The Hippo pathway modulates resistance to BET proteins inhibitors in lung cancer cells.* Oncogene, 2019.

134. Qiu, H., et al., *JQ1 suppresses tumor growth via PTEN/PI3K/AKT pathway in endometrial cancer.* Oncotarget, 2016. **7**(41): p. 66809-66821.

135. Janouskova, H., et al., *Opposing effects of cancer-type-specific SPOP mutants on BET protein degradation and sensitivity to BET inhibitors.* Nat Med, 2017. **23**(9): p. 1046-1054.

136. Bonazzoli, E., et al., *Inhibition of BET Bromodomain Proteins with GS-5829 and GS-626510 in Uterine Serous Carcinoma, a Biologically Aggressive Variant of Endometrial Cancer.* Clin Cancer Res, 2018. **24**(19): p. 4845-4853.

137. Zhang, P., et al., *BRD4 promotes tumor growth and epithelial-mesenchymal transition in hepatocellular carcinoma.* Int J Immunopathol Pharmacol, 2015. **28**(1): p. 36-44.

138. Hong, S.H., et al., *Epigenetic reader BRD4 inhibition as a therapeutic strategy to suppress E2F2-cell cycle regulation circuit in liver cancer.* Oncotarget, 2016. **7**(22): p. 32628-40.

139. Russell, J.O., et al., *Bromodomain and Extraterminal (BET) Proteins Regulate Hepatocyte Proliferation in Hepatocyte-Driven Liver Regeneration.* Am J Pathol, 2018. **188**(6): p. 1389-1405.

140. Eberherr, C., et al., *Targeting excessive MYCN expression using MLN8237 and JQ1 impairs the growth of hepatoblastoma cells.* Int J Oncol, 2019. **54**(5): p. 1853-1863.

141. Yin, Y., et al., *EGFR signaling confers resistance to BET inhibition in hepatocellular carcinoma through stabilizing oncogenic MYC.* J Exp Clin Cancer Res, 2019. **38**(1): p. 83.

142. Wang, L., et al., *JQ1, a small molecule inhibitor of BRD4, suppresses cell growth and invasion in oral squamous cell carcinoma.* Oncol Rep, 2016. **36**(4): p. 1989-96.

143. Leonard, B., et al., *BET Inhibition Overcomes Receptor Tyrosine Kinase-Mediated Cetuximab Resistance in HNSCC.* Cancer Res, 2018. **78**(15): p. 4331-4343.

144. Webber, L.P., et al., *Interference with the bromodomain epigenome readers drives p21 expression and tumor senescence.* Cancer Lett, 2019. **461**: p. 10-20.

145. Wu, Y., et al., *Therapeutic Targeting of BRD4 in Head Neck Squamous Cell Carcinoma.* Theranostics, 2019. **9**(6): p. 1777-1793.

146. Wyce, A., et al., *Inhibition of BET bromodomain proteins as a therapeutic approach in prostate cancer.* Oncotarget, 2013. **4**(12): p. 2419-29.

147. Welti, J., et al., *Targeting Bromodomain and Extra-Terminal (BET) Family Proteins in Castration-Resistant Prostate Cancer (CRPC).* Clin Cancer Res, 2018. **24**(13): p. 3149-3162.

148. Coleman, D.J., et al., *BET bromodomain inhibition blocks the function of a critical AR-independent master regulator network in lethal prostate cancer.* Oncogene, 2019. **38**(28): p. 5658-5669.

149. Hupe, M.C., et al., *The BET-inhibitor PFI-1 diminishes AR/AR-V7 signaling in prostate cancer cells.* World J Urol, 2019. **37**(2): p. 343-349.

150. Shafran, J.S., et al., *BRD4 Regulates Metastatic Potential of Castration-Resistant Prostate Cancer through AHNAK.* Mol Cancer Res, 2019. **17**(8): p. 1627-1638.

151. Segura, M.F., et al., *BRD4 sustains melanoma proliferation and represents a new target for epigenetic therapy.* Cancer Res, 2013. **73**(20): p. 6264-76.

152. Fontanals-Cirera, B., et al., *Harnessing BET Inhibitor Sensitivity Reveals AMIGO2 as a Melanoma Survival Gene.* Mol Cell, 2017. **68**(4): p. 731-744 e9.

153. Erkes, D.A., et al., *The next-generation BET inhibitor, PLX51107, delays melanoma growth in a CD8-mediated manner.* Pigment Cell Melanoma Res, 2019. **32**(5): p. 687-696.

154. Tiago, M., et al., *Targeting BRD/BET proteins inhibits adaptive kinome upregulation and enhances the effects of BRAF/MEK inhibitors in melanoma.* Br J Cancer, 2020. **122**(6): p. 789-800.

155. NIH, U.N.L.o.M.; Available from: https://clinicaltrials.gov/.

156. Cheng, Z., et al., *Inhibition of BET bromodomain targets genetically diverse glioblastoma.* Clin Cancer Res, 2013. **19**(7): p. 1748-59.

157. Di Micco, R., et al., *Control of embryonic stem cell identity by BRD4-dependent transcriptional elongation of super-enhancer-associated pluripotency genes.* Cell Rep, 2014. **9**(1): p. 234-247.

158. Korb, E., et al., *BET protein Brd4 activates transcription in neurons and BET inhibitor Jq1 blocks memory in mice.* Nat Neurosci, 2015. **18**(10): p. 1464-73.

159. Matzuk, M.M., et al., *Small-molecule inhibition of BRDT for male contraception.* Cell, 2012. **150**(4): p. 673-84.

160. Berthon, C., et al., *Bromodomain inhibitor OTX015 in patients with acute leukaemia: a dose-escalation, phase 1 study.* Lancet Haematol, 2016. **3**(4): p. e186-95.

161. Amorim, S., et al., *Bromodomain inhibitor OTX015 in patients with lymphoma or multiple myeloma: a dose-escalation, open-label, pharmacokinetic, phase 1 study.* Lancet Haematol, 2016. **3**(4): p. e196-204.

162. Shorstova, T., et al., *SWI/SNF-Compromised Cancers Are Susceptible to Bromodomain Inhibitors.* Cancer Res, 2019. **79**(10): p. 2761-2774.

163. Medina, P.P., et al., *Genetic and epigenetic screening for gene alterations of the chromatin-remodeling factor, SMARCA4/BRG1, in lung tumors.* Genes Chromosomes Cancer, 2004. **41**(2): p. 170-7.

164. Bertrand, J.U., et al., *Melanoma Risk and Melanocyte Biology.* Acta Derm Venereol, 2020. **100**(11): p. adv00139.

165. Ferlay, J., et al., *Cancer incidence and mortality worldwide: sources, methods and major patterns in GLOBOCAN 2012.* Int J Cancer, 2015. **136**(5): p. E359-86.

166. Rambow, F., J.C. Marine, and C.R. Goding, *Melanoma plasticity and phenotypic diversity: therapeutic barriers and opportunities.* Genes Dev, 2019. **33**(19-20): p. 1295-1318.

167. Lim, S.Y., A.M. Menzies, and H. Rizos, *Mechanisms and strategies to overcome resistance to molecularly targeted therapy for melanoma.* Cancer, 2017. **123**(S11): p. 2118-2129.

168. Rahmati, M., et al., *New insights on the role of autophagy in the pathogenesis and treatment of melanoma.* Mol Biol Rep, 2020. **47**(11): p. 9021-9032.

169. Domingues, B., et al., *Melanoma treatment in review.* Immunotargets Ther, 2018. **7**: p. 35-49.

170. Kim, C., et al., *Long-term survival in patients with metastatic melanoma treated with DTIC or temozolomide.* Oncologist, 2010. **15**(7): p. 765-71.

171. Fisher, R. and J. Larkin, *Vemurafenib: a new treatment for BRAF-V600 mutated advanced melanoma.* Cancer Manag Res, 2012. **4**: p. 243-52.

172. Chapman, P.B., et al., *Improved survival with vemurafenib in melanoma with BRAF V600E mutation.* N Engl J Med, 2011. **364**(26): p. 2507-16.

173. Sosman, J.A., et al., *Survival in BRAF V600-mutant advanced melanoma treated with vemurafenib.* N Engl J Med, 2012. **366**(8): p. 707-14.

174. Flaherty, K.T., et al., *Improved survival with MEK inhibition in BRAF-mutated melanoma.* N Engl J Med, 2012. **367**(2): p. 107-14.

175. Robert, C., et al., *Improved overall survival in melanoma with combined dabrafenib and trametinib.* N Engl J Med, 2015. **372**(1): p. 30-9.

176. Long, G.V., et al., *Combined BRAF and MEK inhibition versus BRAF inhibition alone in melanoma.* N Engl J Med, 2014. **371**(20): p. 1877-88.

177. Larkin, J., et al., *Combined vemurafenib and cobimetinib in BRAF-mutated melanoma.* N Engl J Med, 2014. **371**(20): p. 1867-76.

178. Grob, J.J., et al., *Comparison of dabrafenib and trametinib combination therapy with vemurafenib monotherapy on health-related quality of life in patients with unresectable or metastatic cutaneous BRAF Val600-mutation-positive melanoma (COMBI-v): results of a phase 3, open-label, randomised trial.* Lancet Oncol, 2015. **16**(13): p. 1389-98.

179. Goding, C.R. and H. Arnheiter, *MITF-the first 25 years.* Genes Dev, 2019. **33**(15-16): p. 983-1007.

180. Muller, J., et al., *Low MITF/AXL ratio predicts early resistance to multiple targeted drugs in melanoma.* Nat Commun, 2014. **5**: p. 5712.

181. Clemente, C.G., et al., *Prognostic value of tumor infiltrating lymphocytes in the vertical growth phase of primary cutaneous melanoma.* Cancer, 1996. **77**(7): p. 1303-10.

182. Atkins, M.B., et al., *High-dose recombinant interleukin-2 therapy in patients with metastatic melanoma: long-term survival update.* Cancer J Sci Am, 2000. **6 Suppl 1**: p. S11-4.

183. Kirkwood, J.M., et al., *High- and low-dose interferon alfa-2b in high-risk melanoma: first analysis of intergroup trial E1690/S9111/C9190.* J Clin Oncol, 2000. **18**(12): p. 2444-58.

184. Kawakami, Y. and S.A. Rosenberg, *Immunobiology of human melanoma antigens MART-1 and gp100 and their use for immuno-gene therapy.* Int Rev Immunol, 1997. **14**(2-3): p. 173-92.

185. Bianchi, V., et al., *A Molecular Switch Abrogates Glycoprotein 100 (gp100) T-cell Receptor (TCR) Targeting of a Human Melanoma Antigen.* J Biol Chem, 2016. **291**(17): p. 8951-9.

186. Kawakami, Y., et al., *Identification of a human melanoma antigen recognized by tumor-infiltrating lymphocytes associated with in vivo tumor rejection.* Proc Natl Acad Sci U S A, 1994. **91**(14): p. 6458-62.

187. Hodi, F.S., et al., *Improved survival with ipilimumab in patients with metastatic melanoma.* N Engl J Med, 2010. **363**(8): p. 711-23.

188. Robert, C., et al., *Nivolumab in previously untreated melanoma without BRAF mutation.* N Engl J Med, 2015. **372**(4): p. 320-30.

189. Larkin, J., et al., *Five-Year Survival with Combined Nivolumab and Ipilimumab in Advanced Melanoma.* N Engl J Med, 2019. **381**(16): p. 1535-1546.

190. Liu, L., et al., *The BRAF and MEK Inhibitors Dabrafenib and Trametinib: Effects on Immune Function and in Combination with Immunomodulatory Antibodies Targeting PD-1, PD-L1, and CTLA-4.* Clin Cancer Res, 2015. **21**(7): p. 1639-51.

191. Boni, A., et al., *Selective BRAFV600E inhibition enhances T-cell recognition of melanoma without affecting lymphocyte function.* Cancer Res, 2010. **70**(13): p. 5213-9.

192. Hooijkaas, A., et al., *Selective BRAF inhibition decreases tumor-resident lymphocyte frequencies in a mouse model of human melanoma.* Oncoimmunology, 2012. **1**(5): p. 609-617.

193. Kim, T., et al., *Combining targeted therapy and immune checkpoint inhibitors in the treatment of metastatic melanoma.* Cancer Biol Med, 2014. **11**(4): p. 237-46.

194. Rozeman, E.A. and C.U. Blank, *Combining checkpoint inhibition and targeted therapy in melanoma.* Nat Med, 2019. **25**(6): p. 879-882.

195. Woan, K.V., et al., *Targeting histone deacetylase 6 mediates a dual anti-melanoma effect: Enhanced antitumor immunity and impaired cell proliferation.* Mol Oncol, 2015. **9**(7): p. 1447-1457.

196. Gallagher, S.J., et al., *HDAC inhibitors restore BRAF-inhibitor sensitivity by altering PI3K and survival signalling in a subset of melanoma.* Int J Cancer, 2018. **142**(9): p. 1926-1937.

197. Woods, D.M., et al., *HDAC Inhibition Upregulates PD-1 Ligands in Melanoma and Augments Immunotherapy with PD-1 Blockade.* Cancer Immunol Res, 2015. **3**(12): p. 1375-85.

198. Daud, A.I., et al., *Potentiation of a topoisomerase I inhibitor, karenitecin, by the histone deacetylase inhibitor valproic acid in melanoma: translational and phase I/II clinical trial.* Clin Cancer Res, 2009. **15**(7): p. 2479-87.

199. Haas, N.B., et al., *Phase II trial of vorinostat in advanced melanoma.* Invest New Drugs, 2014. **32**(3): p. 526-34.

200. Flaherty, K.T., et al., *Inhibition of mutated, activated BRAF in metastatic melanoma.* N Engl J Med, 2010. **363**(9): p. 809-19.

201. Flaherty, K.T., et al., *Combined BRAF and MEK inhibition in melanoma with BRAF V600 mutations.* N Engl J Med, 2012. **367**(18): p. 1694-703.

202. Long, G.V., et al., *Dabrafenib and trametinib versus dabrafenib and placebo for Val600 BRAF-mutant melanoma: a multicentre, double-blind, phase 3 randomised controlled trial.* Lancet, 2015. **386**(9992): p. 444-51.

203. Robert, C., et al., *Ipilimumab plus dacarbazine for previously untreated metastatic melanoma.* N Engl J Med, 2011. **364**(26): p. 2517-26.

204. Darvin, P., et al., *Immune checkpoint inhibitors: recent progress and potential biomarkers.* Exp Mol Med, 2018. **50**(12): p. 165.

205. Davis, L.E., S.C. Shalin, and A.J. Tackett, *Current state of melanoma diagnosis and treatment.* Cancer Biol Ther, 2019: p. 1-14.

206. Fan, Y., et al., *Progress of immune checkpoint therapy in the clinic (Review).* Oncol Rep, 2019. **41**(1): p. 3-14.

207. Vardabasso, C., et al., *Histone Variant H2A.Z.2 Mediates Proliferation and Drug Sensitivity of Malignant Melanoma.* Mol Cell, 2015. **59**(1): p. 75-88.

208. Bhadury, J., et al., *BET and HDAC inhibitors induce similar genes and biological effects and synergize to kill in Myc-induced murine lymphoma.* Proc Natl Acad Sci U S A, 2014. **111**(26): p. E2721-30.

209. Gallagher, S.J., et al., *Control of NF-kB activity in human melanoma by bromodomain and extra-terminal protein inhibitor I-BET151.* Pigment Cell Melanoma Res, 2014. **27**(6): p. 1126-37.

210. Muralidharan, S.V., et al., *BET bromodomain inhibitors synergize with ATR inhibitors in melanoma.* Cell Death Dis, 2017. **8**(8): p. e2982.

211. Fink, S.L. and B.T. Cookson, *Apoptosis, pyroptosis, and necrosis: mechanistic description of dead and dying eukaryotic cells.* Infect Immun, 2005. **73**(4): p. 1907-16.

212. Lockshin, R.A. and Z. Zakeri, *Programmed cell death and apoptosis: origins of the theory.* Nat Rev Mol Cell Biol, 2001. **2**(7): p. 545-50.

213. Boatright, K.M. and G.S. Salvesen, *Mechanisms of caspase activation.* Curr Opin Cell Biol, 2003. **15**(6): p. 725-31.

214. Tewari, M., et al., *Yama/CPP32 beta, a mammalian homolog of CED-3, is a CrmA-inhibitable protease that cleaves the death substrate poly(ADP-ribose) polymerase.* Cell, 1995. **81**(5): p. 801-9.

215. Gerdes, J., et al., *Cell cycle analysis of a cell proliferation-associated human nuclear antigen defined by the monoclonal antibody Ki-67.* J Immunol, 1984. **133**(4): p. 1710-5.

216. Sun, X. and P.D. Kaufman, *Ki-67: more than a proliferation marker.* Chromosoma, 2018. **127**(2): p. 175-186.

217. Gelato, K.A., et al., *Super-enhancers define a proliferative PGC-1alpha-expressing melanoma subgroup sensitive to BET inhibition.* Oncogene, 2018. **37**(4): p. 512-521.

218. Garraway, L.A., et al., *Integrative genomic analyses identify MITF as a lineage survival oncogene amplified in malignant melanoma.* Nature, 2005. **436**(7047): p. 117-22.

219. *NCI-60 drug screen data*. [cited 2017 30th November]; Available from: https://dtp.cancer.gov/discovery_development/nci-60/.

220. Cerami, E., et al., *The cBio cancer genomics portal: an open platform for exploring multidimensional cancer genomics data.* Cancer Discov, 2012. **2**(5): p. 401-4.

221. Gao, J., et al., *Integrative analysis of complex cancer genomics and clinical profiles using the cBioPortal.* Sci Signal, 2013. **6**(269): p. pl1.

222. Paoluzzi, L., et al., *BET and BRAF inhibitors act synergistically against BRAF-mutant melanoma.* Cancer Med, 2016. **5**(6): p. 1183-93.

223. Mustafi, S., et al., *Vitamin C Sensitizes Melanoma to BET Inhibitors.* Cancer Res, 2018. **78**(2): p. 572-583.

224. Lu, J., et al., *Hijacking the E3 Ubiquitin Ligase Cereblon to Efficiently Target BRD4.* Chem Biol, 2015. **22**(6): p. 755-63.

225. Winter, G.E., et al., *BET Bromodomain Proteins Function as Master Transcription Elongation Factors Independent of CDK9 Recruitment.* Mol Cell, 2017. **67**(1): p. 5-18 e19.

226. Rathod, D., Y. Fu, and K. Patel, *BRD4 PROTAC as a novel therapeutic approach for the treatment of vemurafenib resistant melanoma: Preformulation studies, formulation development and in vitro evaluation.* Eur J Pharm Sci, 2019. **138**: p. 105039.

227. Zhang, L., et al., *Acquired Resistance to BET-PROTACs (Proteolysis-Targeting Chimeras) Caused by Genomic Alterations in Core Components of E3 Ligase Complexes.* Mol Cancer Ther, 2019. **18**(7): p. 1302-1311.

228. Yang, G.J., et al., *A 7-methoxybicoumarin derivative selectively inhibits BRD4 BD2 for anti-melanoma therapy.* Int J Biol Macromol, 2020.

229. Kollmann, K., et al., *The interplay of CDK4 and CDK6 in melanoma.* Oncotarget, 2019. **10**(14): p. 1346-1359.

230. Jenei, V., et al., *A t-butyloxycarbonyl-modified Wnt5a-derived hexapeptide functions as a potent antagonist of Wnt5a-dependent melanoma cell invasion.* Proc Natl Acad Sci U S A, 2009. **106**(46): p. 19473-8.

231. Faivre, E.J., et al., *Selective inhibition of the BD2 bromodomain of BET proteins in prostate cancer.* Nature, 2020. **578**(7794): p. 306-310.

232. Gilan, O., et al., *Selective targeting of BD1 and BD2 of the BET proteins in cancer and immunoinflammation.* Science, 2020. **368**(6489): p. 387-394.

233. Raina, K., et al., *PROTAC-induced BET protein degradation as a therapy for castration-resistant prostate cancer.* Proc Natl Acad Sci U S A, 2016. **113**(26): p. 7124-9.

234. Zakut, R., et al., *KIT ligand (mast cell growth factor) inhibits the growth of KIT-expressing melanoma cells.* Oncogene, 1993. **8**(8): p. 2221-9.

235. Fogh, J., J.M. Fogh, and T. Orfeo, *One hundred and twenty-seven cultured human tumor cell lines producing tumors in nude mice.* J Natl Cancer Inst, 1977. **59**(1): p. 221-6.

236. Yu, M., et al., *A resource for cell line authentication, annotation and quality control.* Nature, 2015. **520**(7547): p. 307-11.

237. Aubert, C., F. Rouge, and J.R. Galindo, *Tumorigenicity of human malignant melanocytes in nude mice in relation to their differentiation in vitro.* J Natl Cancer Inst, 1980. **64**(5): p. 1029-40.

238. Horoszewicz, J.S., et al., *The LNCaP cell line--a new model for studies on human prostatic carcinoma.* Prog Clin Biol Res, 1980. **37**: p. 115-32.

239. Horoszewicz, J.S., et al., *LNCaP model of human prostatic carcinoma.* Cancer Res, 1983. **43**(4): p. 1809-18.

240. Kaighn, M.E., et al., *Establishment and characterization of a human prostatic carcinoma cell line (PC-3).* Invest Urol, 1979. **17**(1): p. 16-23.

241. Vance, K.W., et al., *Tbx2 is overexpressed and plays an important role in maintaining proliferation and suppression of senescence in melanomas.* Cancer Res, 2005. **65**(6): p. 2260-8.

242. Liao, Y., G.K. Smyth, and W. Shi, *The Subread aligner: fast, accurate and scalable read mapping by seed-and-vote.* Nucleic Acids Res, 2013. **41**(10): p. e108.

243. Love, M.I., W. Huber, and S. Anders, *Moderated estimation of fold change and dispersion for RNA-seq data with DESeq2.* Genome Biol, 2014. **15**(12): p. 550.

244. Subramanian, A., et al., *Gene set enrichment analysis: a knowledge-based approach for interpreting genome-wide expression profiles.* Proc Natl Acad Sci U S A, 2005. **102**(43): p. 15545-50.

245. Gibson, D.G., et al., *Enzymatic assembly of DNA molecules up to several hundred kilobases.* Nat Methods, 2009. **6**(5): p. 343-5.

246. Luke, J.J., et al., *Targeted agents and immunotherapies: optimizing outcomes in melanoma.* Nat Rev Clin Oncol, 2017. **14**(8): p. 463-482.

247. Carreira, S., et al., *Mitf cooperates with Rb1 and activates p21Cip1 expression to regulate cell cycle progression.* Nature, 2005. **433**(7027): p. 764-9.

248. Carreira, S., et al., *Mitf regulation of Dia1 controls melanoma proliferation and invasiveness.* Genes Dev, 2006. **20**(24): p. 3426-39.

249. Hayward, N.K., et al., *Whole-genome landscapes of major melanoma subtypes.* Nature, 2017. **545**(7653): p. 175-180.

250. Savoia, P., et al., *Targeting the ERK Signaling Pathway in Melanoma.* Int J Mol Sci, 2019. **20**(6).

251. Echevarria-Vargas, I.M., et al., *Co-targeting BET and MEK as salvage therapy for MAPK and checkpoint inhibitor-resistant melanoma.* EMBO Mol Med, 2018. **10**(5).

252. Hodis, E., et al., *A landscape of driver mutations in melanoma.* Cell, 2012. **150**(2): p. 251-63.

253. Stewart, H.J., et al., *BRD4 associates with p53 in DNMT3A-mutated leukemia cells and is implicated in apoptosis by the bromodomain inhibitor JQ1.* Cancer Med, 2013. **2**(6): p. 826-35.

254. Vogelstein, B., D. Lane, and A.J. Levine, *Surfing the p53 network.* Nature, 2000. **408**(6810): p. 307-10.

255. Vousden, K.H. and X. Lu, *Live or let die: the cell's response to p53.* Nat Rev Cancer, 2002. **2**(8): p. 594-604.

256. Riley, T., et al., *Transcriptional control of human p53-regulated genes.* Nat Rev Mol Cell Biol, 2008. **9**(5): p. 402-12.

257. Tasdemir, E., et al., *Regulation of autophagy by cytoplasmic p53.* Nat Cell Biol, 2008. **10**(6): p. 676-87.

258. Collado, M. and M. Serrano, *Senescence in tumours: evidence from mice and humans.* Nat Rev Cancer, 2010. **10**(1): p. 51-7.

259. Duffy, M.J., N.C. Synnott, and J. Crown, *Mutant p53 as a target for cancer treatment.* Eur J Cancer, 2017. **83**: p. 258-265.

260. Kim, D.W., et al., *Clinicopathological features and clinical outcomes associated with TP53 and BRAF(N)(on-)(V)(600) mutations in cutaneous melanoma patients.* Cancer, 2017. **123**(8): p. 1372-1381.

261. DeLeon, T.T., et al., *Assessment of clinical outcomes with immune checkpoint inhibitor therapy in melanoma patients with CDKN2A and TP53 pathogenic mutations.* PLoS One, 2020. **15**(3): p. e0230306.

262. Vincent, K.M. and L.M. Postovit, *Investigating the utility of human melanoma cell lines as tumour models.* Oncotarget, 2017. **8**(6): p. 10498-10509.

263. Louphrasitthiphol, P., et al., *MITF controls the TCA cycle to modulate the melanoma hypoxia response.* Pigment Cell Melanoma Res, 2019. **32**(6): p. 792-808.

264. Vivas-Garcia, Y., et al., *Lineage-Restricted Regulation of SCD and Fatty Acid Saturation by MITF Controls Melanoma Phenotypic Plasticity.* Mol Cell, 2020. **77**(1): p. 120-137 e9.

265. Reifenberger, J., et al., *Frequent alterations of Ras signaling pathway genes in sporadic malignant melanomas.* Int J Cancer, 2004. **109**(3): p. 377-84.

266. Margue, C., et al., *Kinase inhibitor library screening identifies synergistic drug combinations effective in sensitive and resistant melanoma cells.* J Exp Clin Cancer Res, 2019. **38**(1): p. 56.

267. Lu, M., et al., *Restoring p53 function in human melanoma cells by inhibiting MDM2 and cyclin B1/CDK1-phosphorylated nuclear iASPP.* Cancer Cell, 2013. **23**(5): p. 618-33.

268. Ji, Z., et al., *p53 rescue through HDM2 antagonism suppresses melanoma growth and potentiates MEK inhibition.* J Invest Dermatol, 2012. **132**(2): p. 356-64.

269. Soengas, M.S., et al., *Inactivation of the apoptosis effector Apaf-1 in malignant melanoma.* Nature, 2001. **409**(6817): p. 207-11.

270. Fufa, T.D., et al., *MEK inhibition remodels the active chromatin landscape and induces SOX10 genomic recruitment in BRAF(V600E) mutant melanoma cells.* Epigenetics Chromatin, 2019. **12**(1): p. 50.

271. Sulkowski, P.L., et al., *PTEN Regulates Nonhomologous End Joining By Epigenetic Induction of NHEJ1/XLF.* Mol Cancer Res, 2018. **16**(8): p. 1241-1254.

272. van Rikxoort, M., et al., *Oncolytic effects of a novel influenza A virus expressing interleukin-15 from the NS reading frame.* PLoS One, 2012. **7**(5): p. e36506.

273. Dahl, C., et al., *Mutual exclusivity analysis of genetic and epigenetic drivers in melanoma identifies a link between p14 ARF and RARbeta signaling.* Mol Cancer Res, 2013. **11**(10): p. 1166-78.

274. Precazzini, F., et al., *Automated in vivo screen in zebrafish identifies Clotrimazole as targeting a metabolic vulnerability in a melanoma model.* Dev Biol, 2020. **457**(2): p. 215-225.

275. Felli, N., et al., *miR-126&126* restored expressions play a tumor suppressor role by directly regulating ADAM9 and MMP7 in melanoma.* PLoS One, 2013. **8**(2): p. e56824.

276. Rambow, F., et al., *New Functional Signatures for Understanding Melanoma Biology from Tumor Cell Lineage-Specific Analysis.* Cell Rep, 2015. **13**(4): p. 840-853.

277. Errico, M.C., et al., *The abrogation of the HOXB7/PBX2 complex induces apoptosis in melanoma through the miR-221&222-c-FOS pathway.* Int J Cancer, 2013. **133**(4): p. 879-92.

278. Li, L., et al., *Common cancer mutations R175H and R273H drive the p53 DNA-binding domain towards aggregation-prone conformations.* Phys Chem Chem Phys, 2020. **22**(17): p. 9225-9232.

279. Cho, Y., et al., *Crystal structure of a p53 tumor suppressor-DNA complex: understanding tumorigenic mutations.* Science, 1994. **265**(5170): p. 346-55.

280. Joerger, A.C. and A.R. Fersht, *Structure-function-rescue: the diverse nature of common p53 cancer mutants.* Oncogene, 2007. **26**(15): p. 2226-42.

281. Emamzadah, S., et al., *Reversal of the DNA-binding-induced loop L1 conformational switch in an engineered human p53 protein.* J Mol Biol, 2014. **426**(4): p. 936-44.

282. el-Deiry, W.S., et al., *WAF1, a potential mediator of p53 tumor suppression.* Cell, 1993. **75**(4): p. 817-25.

283. Wang, X., E.R. Simpson, and K.A. Brown, *p53: Protection against Tumor Growth beyond Effects on Cell Cycle and Apoptosis.* Cancer Res, 2015. **75**(23): p. 5001-7.

284. Picaud, S., et al., *RVX-208, an inhibitor of BET transcriptional regulators with selectivity for the second bromodomain.* Proc Natl Acad Sci U S A, 2013. **110**(49): p. 19754-9.

285. Schmittgen, T.D. and B.A. Zakrajsek, *Effect of experimental treatment on housekeeping gene expression: validation by real-time, quantitative RT-PCR.* J Biochem Biophys Methods, 2000. **46**(1-2): p. 69-81.

286. Brennecke, P., et al., *Accounting for technical noise in single-cell RNA-seq experiments.* Nat Methods, 2013. **10**(11): p. 1093-5.

287. Xiao, B.D., et al., *Multifaceted p21 in carcinogenesis, stemness of tumor and tumor therapy.* World J Stem Cells, 2020. **12**(6): p. 481-487.

288. Trivedi, A., et al., *Bromodomain and extra-terminal domain (BET) proteins regulate melanocyte differentiation.* Epigenetics Chromatin, 2020. **13**(1): p. 14.

289. Bretones, G., M.D. Delgado, and J. Leon, *Myc and cell cycle control.* Biochim Biophys Acta, 2015. **1849**(5): p. 506-16.

290. Engeland, K., *Cell cycle arrest through indirect transcriptional repression by p53: I have a DREAM.* Cell Death Differ, 2018. **25**(1): p. 114-132.

291. Bertoli, C., J.M. Skotheim, and R.A. de Bruin, *Control of cell cycle transcription during G1 and S phases.* Nat Rev Mol Cell Biol, 2013. **14**(8): p. 518-28.

292. Garcia-Gutierrez, L., M.D. Delgado, and J. Leon, *MYC Oncogene Contributions to Release of Cell Cycle Brakes.* Genes (Basel), 2019. **10**(3).

293. Tan, J.L., et al., *Stress from Nucleotide Depletion Activates the Transcriptional Regulator HEXIM1 to Suppress Melanoma.* Mol Cell, 2016. **62**(1): p. 34-46.

294. Zanconato, F., et al., *Transcriptional addiction in cancer cells is mediated by YAP/TAZ through BRD4.* Nat Med, 2018. **24**(10): p. 1599-1610.

295. Kim, M.H., et al., *Actin remodeling confers BRAF inhibitor resistance to melanoma cells through YAP/TAZ activation.* EMBO J, 2016. **35**(5): p. 462-78.

296. Glick, D., S. Barth, and K.F. Macleod, *Autophagy: cellular and molecular mechanisms.* J Pathol, 2010. **221**(1): p. 3-12.

297. Nicklin, P., et al., *Bidirectional transport of amino acids regulates mTOR and autophagy.* Cell, 2009. **136**(3): p. 521-34.

298. Boulter, E., et al., *Cell metabolism regulates integrin mechanosensing via an SLC3A2-dependent sphingolipid biosynthesis pathway.* Nat Commun, 2018. **9**(1): p. 4862.

299. Levy, J.M.M., C.G. Towers, and A. Thorburn, *Targeting autophagy in cancer.* Nat Rev Cancer, 2017. **17**(9): p. 528-542.

300. Zheng, K., et al., *Selective Autophagy Regulates Cell Cycle in Cancer Therapy.* Theranostics, 2019. **9**(1): p. 104-125.

301. Garbar, C., et al., *Autophagy is decreased in triple-negative breast carcinoma involving likely the MUC1-EGFR-NEU1 signalling pathway.* Int J Clin Exp Pathol, 2015. **8**(5): p. 4344-55.

302. Wartosch, L. and T. Stauber, *A role for chloride transport in lysosomal protein degradation.* Autophagy, 2010. **6**(1): p. 158-9.

303. Nicoli, E.R., et al., *Lysosomal Storage and Albinism Due to Effects of a De Novo CLCN7 Variant on Lysosomal Acidification.* Am J Hum Genet, 2019. **104**(6): p. 1127-1138.

304. Klionsky, D.J., et al., *Guidelines for the use and interpretation of assays for monitoring autophagy (3rd edition).* Autophagy, 2016. **12**(1): p. 1-222.

305. Yoshii, S.R. and N. Mizushima, *Monitoring and Measuring Autophagy.* Int J Mol Sci, 2017. **18**(9).

306. Yamamoto, A., et al., *Bafilomycin A1 prevents maturation of autophagic vacuoles by inhibiting fusion between autophagosomes and lysosomes in rat hepatoma cell line, H-4-II-E cells.* Cell Struct Funct, 1998. **23**(1): p. 33-42.

307. White, E., *Autophagy and p53.* Cold Spring Harb Perspect Med, 2016. **6**(4): p. a026120.

308. Cordani, M., et al., *Molecular interplay between mutant p53 proteins and autophagy in cancer cells.* Biochim Biophys Acta Rev Cancer, 2017. **1867**(1): p. 19-28.

309. Kim, J., et al., *AMPK and mTOR regulate autophagy through direct phosphorylation of Ulk1.* Nat Cell Biol, 2011. **13**(2): p. 132-41.

310. Rabanal-Ruiz, Y., E.G. Otten, and V.I. Korolchuk, *mTORC1 as the main gateway to autophagy.* Essays Biochem, 2017. **61**(6): p. 565-584.

311. Gewirtz, D.A., *Autophagy and senescence: a partnership in search of definition.* Autophagy, 2013. **9**(5): p. 808-12.

312. Kwon, Y., et al., *Autophagy Is Pro-Senescence When Seen in Close-Up, but Anti-Senescence in Long-Shot.* Mol Cells, 2017. **40**(9): p. 607-612.

313. Kang, C. and S.J. Elledge, *How autophagy both activates and inhibits cellular senescence.* Autophagy, 2016. **12**(5): p. 898-9.

314. Maiuri, M.C., et al., *Self-eating and self-killing: crosstalk between autophagy and apoptosis.* Nat Rev Mol Cell Biol, 2007. **8**(9): p. 741-52.

315. Marino, G., et al., *Self-consumption: the interplay of autophagy and apoptosis.* Nat Rev Mol Cell Biol, 2014. **15**(2): p. 81-94.

316. d'Adda di Fagagna, F., *Living on a break: cellular senescence as a DNA-damage response.* Nat Rev Cancer, 2008. **8**(7): p. 512-22.

317. Kuilman, T., et al., *The essence of senescence.* Genes Dev, 2010. **24**(22): p. 2463-79.

318. Liu, H., et al., *Down-regulation of autophagy-related protein 5 (ATG5) contributes to the pathogenesis of early-stage cutaneous melanoma.* Sci Transl Med, 2013. **5**(202): p. 202ra123.

319. Liu, H., Z. He, and H.U. Simon, *Autophagy suppresses melanoma tumorigenesis by inducing senescence.* Autophagy, 2014. **10**(2): p. 372-3.

320. Martin, S.J., et al., *Phosphatidylserine externalization during CD95-induced apoptosis of cells and cytoplasts requires ICE/CED-3 protease activity.* J Biol Chem, 1996. **271**(46): p. 28753-6.

321. van Engeland, M., et al., *Annexin V-affinity assay: a review on an apoptosis detection system based on phosphatidylserine exposure.* Cytometry, 1998. **31**(1): p. 1-9.

322. Segawa, K. and S. Nagata, *An Apoptotic 'Eat Me' Signal: Phosphatidylserine Exposure.* Trends Cell Biol, 2015. **25**(11): p. 639-650.

323. Kay, J.G. and G.D. Fairn, *Distribution, dynamics and functional roles of phosphatidylserine within the cell.* Cell Commun Signal, 2019. **17**(1): p. 126.

324. Zhang, X.D., S.K. Gillespie, and P. Hersey, *Staurosporine induces apoptosis of melanoma by both caspase-dependent and -independent apoptotic pathways.* 2004. **3**(2): p. 187-97.

325. Taghizadeh, R., et al., *CXCR6, a newly defined biomarker of tissue-specific stem cell asymmetric self-renewal, identifies more aggressive human melanoma cancer stem cells.* PLoS One, 2010. **5**(12): p. e15183.

326. Dolinsek, T., et al., *Electrochemotherapy with bleomycin is effective in BRAF mutated melanoma cells and interacts with BRAF inhibitors.* Radiol Oncol, 2016. **50**(3): p. 274-9.

327. Flockhart, R.J., et al., *NFAT signalling is a novel target of oncogenic BRAF in metastatic melanoma.* Br J Cancer, 2009. **101**(8): p. 1448-55.

328. Chen, B., et al., *BRAFV600E negatively regulates the AKT pathway in melanoma cell lines.* PLoS One, 2012. **7**(8): p. e42598.

329. Eskiocak, B., et al., *Biomarker Accessible and Chemically Addressable Mechanistic Subtypes of BRAF Melanoma.* Cancer Discov, 2017. **7**(8): p. 832-851.

330. Wardwell-Ozgo, J., et al., *HOXA1 drives melanoma tumor growth and metastasis and elicits an invasion gene expression signature that prognosticates clinical outcome.* Oncogene, 2014. **33**(8): p. 1017-26.

331. Fathi, Z., et al., *Distribution of KRAS, DDR2, and TP53 gene mutations in lung cancer: An analysis of Iranian patients.* PLoS One, 2018. **13**(7): p. e0200633.

332. Shajani-Yi, Z., et al., *Frequency of Somatic TP53 Mutations in Combination with Known Pathogenic Mutations in Colon Adenocarcinoma, Non-Small Cell Lung Carcinoma, and Gliomas as Identified by Next-Generation Sequencing.* Neoplasia, 2018. **20**(3): p. 256-262.

333. Frebourg, T., et al., *Germ-line p53 mutations in 15 families with Li-Fraumeni syndrome.* Am J Hum Genet, 1995. **56**(3): p. 608-15.

334. Mauthe, M., et al., *Chloroquine inhibits autophagic flux by decreasing autophagosome-lysosome fusion.* Autophagy, 2018. **14**(8): p. 1435-1455.

335. Amaravadi, R.K., et al., *Autophagy inhibition enhances therapy-induced apoptosis in a Myc-induced model of lymphoma.* J Clin Invest, 2007. **117**(2): p. 326-36.

336. Muller, P.A. and K.H. Vousden, *p53 mutations in cancer.* Nat Cell Biol, 2013. **15**(1): p. 2-8.

337. Avery-Kiejda, K.A., et al., *P53 in human melanoma fails to regulate target genes associated with apoptosis and the cell cycle and may contribute to proliferation.* BMC Cancer, 2011. **11**: p. 203.

338. Minamoto, T., et al., *Distinct pattern of p53 phosphorylation in human tumors.* Oncogene, 2001. **20**(26): p. 3341-7.

339. Yoshida, A., E.K. Lee, and J.A. Diehl, *Induction of Therapeutic Senescence in Vemurafenib-Resistant Melanoma by Extended Inhibition of CDK4/6.* Cancer Res, 2016. **76**(10): p. 2990-3002.

340. Duan, Q., et al., *BET bromodomain is a novel regulator of TAZ and its activity.* Biochim Biophys Acta, 2016. **1859**(12): p. 1527-1537.

341. Satyamoorthy, K., et al., *Aberrant regulation and function of wild-type p53 in radioresistant melanoma cells.* Cell Growth Differ, 2000. **11**(9): p. 467-74.

342. Kato, S., et al., *Understanding the function-structure and function-mutation relationships of p53 tumor suppressor protein by high-resolution missense mutation analysis.* Proc Natl Acad Sci U S A, 2003. **100**(14): p. 8424-9.

343. Leroy, B., M. Anderson, and T. Soussi, *TP53 mutations in human cancer: database reassessment and prospects for the next decade.* Hum Mutat, 2014. **35**(6): p. 672-88.

344. Abu El Maaty, M.A., et al., *Differences in p53 status significantly influence the cellular response and cell survival to 1,25-dihydroxyvitamin D3-metformin cotreatment in colorectal cancer cells.* Mol Carcinog, 2017. **56**(11): p. 2486-2498.

345. Morselli, E., et al., *Mutant p53 protein localized in the cytoplasm inhibits autophagy.* 2008. **7**(19): p. 3056-61.

346. Shang, Y.Y., et al., *Alisertib promotes apoptosis and autophagy in melanoma through p38 MAPK-mediated aurora a signaling.* Oncotarget, 2017. **8**(63): p. 107076-107088.

347. Zhang, Q., et al., *DAMPs and autophagy: cellular adaptation to injury and unscheduled cell death.* Autophagy, 2013. **9**(4): p. 451-8.

348. Zhong, Z., E. Sanchez-Lopez, and M. Karin, *Autophagy, Inflammation, and Immunity: A Troika Governing Cancer and Its Treatment.* Cell, 2016. **166**(2): p. 288-298.

349. Adeegbe, D.O., et al., *BET Bromodomain Inhibition Cooperates with PD-1 Blockade to Facilitate Antitumor Response in Kras-Mutant Non-Small Cell Lung Cancer.* Cancer Immunol Res, 2018. **6**(10): p. 1234-1245.

350. Mao, W., et al., *Immunogenicity of prostate cancer is augmented by BET bromodomain inhibition.* J Immunother Cancer, 2019. **7**(1): p. 277.

351. Visakorpi, T., et al., *In vivo amplification of the androgen receptor gene and progression of human prostate cancer.* Nat Genet, 1995. **9**(4): p. 401-6.

352. Kumar, A., et al., *Substantial interindividual and limited intraindividual genomic diversity among tumors from men with metastatic prostate cancer.* Nat Med, 2016. **22**(4): p. 369-78.

353. Chen, C.D., et al., *Molecular determinants of resistance to antiandrogen therapy.* Nat Med, 2004. **10**(1): p. 33-9.

354. Vogelzang, N.J., *Enzalutamide--a major advance in the treatment of metastatic prostate cancer.* N Engl J Med, 2012. **367**(13): p. 1256-7.

355. Hu, R., et al., *Ligand-independent androgen receptor variants derived from splicing of cryptic exons signify hormone-refractory prostate cancer.* Cancer Res, 2009. **69**(1): p. 16-22.

356. Antonarakis, E.S., et al., *AR-V7 and resistance to enzalutamide and abiraterone in prostate cancer.* N Engl J Med, 2014. **371**(11): p. 1028-38.

357. Welti, J., et al., *Analytical Validation and Clinical Qualification of a New Immunohistochemical Assay for Androgen Receptor Splice Variant-7 Protein Expression in Metastatic Castration-resistant Prostate Cancer.* Eur Urol, 2016. **70**(4): p. 599-608.

358. Urbanucci, A., et al., *Androgen Receptor Deregulation Drives Bromodomain-Mediated Chromatin Alterations in Prostate Cancer.* Cell Rep, 2017. **19**(10): p. 2045-2059.

359. Piha-Paul, S.A., et al., *First-in-Human Study of Mivebresib (ABBV-075), an Oral Pan-Inhibitor of Bromodomain and Extra Terminal Proteins, in Patients with Relapsed/Refractory Solid Tumors.* Clin Cancer Res, 2019. **25**(21): p. 6309-6319.

360. Pawar, A., et al., *Resistance to BET Inhibitor Leads to Alternative Therapeutic Vulnerabilities in Castration-Resistant Prostate Cancer.* Cell Rep, 2018. **22**(9): p. 2236-2245.

361. Stattin, P., et al., *p53 immunoreactivity as prognostic marker for cancer-specific survival in prostate cancer.* Eur Urol, 1996. **30**(1): p. 65-72.

362. Kluth, M., et al., *Clinical significance of different types of p53 gene alteration in surgically treated prostate cancer.* Int J Cancer, 2014. **135**(6): p. 1369-80.

363. Liberio, M.S., et al., *Differential effects of tissue culture coating substrates on prostate cancer cell adherence, morphology and behavior.* PLoS One, 2014. **9**(11): p. e112122.

364. Uo, T., S.R. Plymate, and C.C. Sprenger, *The potential of AR-V7 as a therapeutic target.* Expert Opin Ther Targets, 2018. **22**(3): p. 201-216.

365. Li, Y., et al., *Androgen receptor splice variants mediate enzalutamide resistance in castration-resistant prostate cancer cell lines.* Cancer Res, 2013. **73**(2): p. 483-9.

366. Wang, S., et al., *Expression of Androgen Receptor Variant 7 (AR-V7) in Circulated Tumor Cells and Correlation with Drug Resistance of Prostate Cancer Cells.* Med Sci Monit, 2018. **24**: p. 7051-7056.

367. Tomlins, S.A., et al., *Recurrent fusion of TMPRSS2 and ETS transcription factor genes in prostate cancer.* Science, 2005. **310**(5748): p. 644-8.

368. Higgins, J., et al., *Interaction of the Androgen Receptor, ETV1, and PTEN Pathways in Mouse Prostate Varies with Pathological Stage and Predicts Cancer Progression.* Horm Cancer, 2015. **6**(2-3): p. 67-86.

369. Kekuda, R., et al., *Cloning of the sodium-dependent, broad-scope, neutral amino acid transporter Bo from a human placental choriocarcinoma cell line.* J Biol Chem, 1996. **271**(31): p. 18657-61.

370. Feral, C.C., et al., *CD98hc (SLC3A2) mediates integrin signaling.* Proc Natl Acad Sci U S A, 2005. **102**(2): p. 355-60.

371. Sui, S., et al., *Ferritinophagy is required for the induction of ferroptosis by the bromodomain protein BRD4 inhibitor (+)-JQ1 in cancer cells.* Cell Death Dis, 2019. **10**(5): p. 331.

372. Sarbassov, D.D., et al., *Phosphorylation and regulation of Akt/PKB by the rictor-mTOR complex.* Science, 2005. **307**(5712): p. 1098-101.

373. Tee, A.R., et al., *Tuberous sclerosis complex-1 and -2 gene products function together to inhibit mammalian target of rapamycin (mTOR)-mediated downstream signaling.* Proc Natl Acad Sci U S A, 2002. **99**(21): p. 13571-6.

374. Mirkheshti, N., et al., *Dual targeting of androgen receptor and mTORC1 by salinomycin in prostate cancer.* Oncotarget, 2016. **7**(38): p. 62240-62254.

375. Inoki, K., T. Zhu, and K.L. Guan, *TSC2 mediates cellular energy response to control cell growth and survival.* Cell, 2003. **115**(5): p. 577-90.

376. Nellist, M., et al., *Phosphorylation and binding partner analysis of the TSC1-TSC2 complex.* Biochem Biophys Res Commun, 2005. **333**(3): p. 818-26.

377. Hardie, D.G., *AMP-activated/SNF1 protein kinases: conserved guardians of cellular energy.* Nat Rev Mol Cell Biol, 2007. **8**(10): p. 774-85.

378. Shaw, R.J., et al., *The LKB1 tumor suppressor negatively regulates mTOR signaling.* Cancer Cell, 2004. **6**(1): p. 91-9.

379. Hindupur, S.K., A. Gonzalez, and M.N. Hall, *The opposing actions of target of rapamycin and AMP-activated protein kinase in cell growth control.* Cold Spring Harb Perspect Biol, 2015. **7**(8): p. a019141.

380. Sancak, Y., et al., *The Rag GTPases bind raptor and mediate amino acid signaling to mTORC1.* Science, 2008. **320**(5882): p. 1496-501.

381. Hara, K., et al., *Amino acid sufficiency and mTOR regulate p70 S6 kinase and eIF-4E BP1 through a common effector mechanism.* J Biol Chem, 1998. **273**(23): p. 14484-94.

382. Egan, D.F., et al., *Phosphorylation of ULK1 (hATG1) by AMP-activated protein kinase connects energy sensing to mitophagy.* Science, 2011. **331**(6016): p. 456-61.

383. Liang, X.H., et al., *Induction of autophagy and inhibition of tumorigenesis by beclin 1.* Nature, 1999. **402**(6762): p. 672-6.

384. Monkkonen, T. and J. Debnath, *Inflammatory signaling cascades and autophagy in cancer.* Autophagy, 2018. **14**(2): p. 190-198.

385. Sun, A., et al., *GSK-3beta controls autophagy by modulating LKB1-AMPK pathway in prostate cancer cells.* Prostate, 2016. **76**(2): p. 172-83.

386. Hassanein, M., et al., *Targeting SLC1a5-mediated glutamine dependence in non-small cell lung cancer.* Int J Cancer, 2015. **137**(7): p. 1587-97.

387. Digomann, D., et al., *The CD98 Heavy Chain Is a Marker and Regulator of Head and Neck Squamous Cell Carcinoma Radiosensitivity.* Clin Cancer Res, 2019. **25**(10): p. 3152-3163.

388. Peng, Y.F., et al., *Autophagy inhibition suppresses pulmonary metastasis of HCC in mice via impairing anoikis resistance and colonization of HCC cells.* Autophagy, 2013. **9**(12): p. 2056-68.

389. Yun, C.W. and S.H. Lee, *The Roles of Autophagy in Cancer.* Int J Mol Sci, 2018. **19**(11).

390. White, E. and R.S. DiPaola, *The double-edged sword of autophagy modulation in cancer.* Clin Cancer Res, 2009. **15**(17): p. 5308-16.

391. Kroemer, G., G. Marino, and B. Levine, *Autophagy and the integrated stress response.* Mol Cell, 2010. **40**(2): p. 280-93.

392. Farrow, J.M., J.C. Yang, and C.P. Evans, *Autophagy as a modulator and target in prostate cancer.* Nat Rev Urol, 2014. **11**(9): p. 508-16.

393. Zhao, R., et al., *Endothelial cells promote metastasis of prostate cancer by enhancing autophagy.* J Exp Clin Cancer Res, 2018. **37**(1): p. 221.

394. Hanahan, D. and R.A. Weinberg, *Hallmarks of cancer: the next generation.* Cell, 2011. **144**(5): p. 646-74.

395. Dekervel, J., et al., *Acriflavine Inhibits Acquired Drug Resistance by Blocking the Epithelial-to-Mesenchymal Transition and the Unfolded Protein Response.* Transl Oncol, 2017. **10**(1): p. 59-69.

396. Wu, P.H., et al., *Single-cell morphology encodes metastatic potential.* Sci Adv, 2020. **6**(4): p. eaaw6938.

397. Friedl, P. and S. Alexander, *Cancer invasion and the microenvironment: plasticity and reciprocity.* Cell, 2011. **147**(5): p. 992-1009.

398. Yuan, T.C., et al., *Androgen deprivation induces human prostate epithelial neuroendocrine differentiation of androgen-sensitive LNCaP cells.* Endocr Relat Cancer, 2006. **13**(1): p. 151-67.

399. Bennett, H.L., et al., *Does androgen-ablation therapy (AAT) associated autophagy have a pro-survival effect in LNCaP human prostate cancer cells?* BJU Int, 2013. **111**(4): p. 672-82.

400. Kramer, N., et al., *In vitro cell migration and invasion assays.* Mutat Res, 2013. **752**(1): p. 10-24.

401. Colquhoun, A.J., et al., *Metformin enhances the antiproliferative and apoptotic effect of bicalutamide in prostate cancer.* Prostate Cancer Prostatic Dis, 2012. **15**(4): p. 346-52.

402. Nguyen, H.G., et al., *Targeting autophagy overcomes Enzalutamide resistance in castration-resistant prostate cancer cells and improves therapeutic response in a xenograft model.* Oncogene, 2014. **33**(36): p. 4521-30.

403. De Rijck, J., et al., *The BET family of proteins targets moloney murine leukemia virus integration near transcription start sites.* Cell Rep, 2013. **5**(4): p. 886-94.

404. Sharma, A., et al., *BET proteins promote efficient murine leukemia virus integration at transcription start sites.* Proc Natl Acad Sci U S A, 2013. **110**(29): p. 12036-41.

405. Gossen, M. and H. Bujard, *Tight control of gene expression in mammalian cells by tetracycline-responsive promoters.* Proc Natl Acad Sci U S A, 1992. **89**(12): p. 5547-51.

406. Shockett, P., et al., *A modified tetracycline-regulated system provides autoregulatory, inducible gene expression in cultured cells and transgenic mice.* Proc Natl Acad Sci U S A, 1995. **92**(14): p. 6522-6.

407. Li, H., et al., *Adapalene suppressed the proliferation of melanoma cells by S-phase arrest and subsequent apoptosis via induction of DNA damage.* Eur J Pharmacol, 2019. **851**: p. 174-185.

408. Fischer, M., *Census and evaluation of p53 target genes.* Oncogene, 2017. **36**(28): p. 3943-3956.

409. Blander, G., et al., *Superoxide dismutase 1 knock-down induces senescence in human fibroblasts.* J Biol Chem, 2003. **278**(40): p. 38966-9.

410. Murray-Zmijewski, F., E.A. Slee, and X. Lu, *A complex barcode underlies the heterogeneous response of p53 to stress.* Nat Rev Mol Cell Biol, 2008. **9**(9): p. 702-12.

411. de Keizer, P.L., et al., *Activation of forkhead box O transcription factors by oncogenic BRAF promotes p21cip1-dependent senescence.* Cancer Res, 2010. **70**(21): p. 8526-36.

412. Childs, B.G., et al., *Senescence and apoptosis: dueling or complementary cell fates?* EMBO Rep, 2014. **15**(11): p. 1139-53.

413. Schroder, K., et al., *Interferon-gamma: an overview of signals, mechanisms and functions.* J Leukoc Biol, 2004. **75**(2): p. 163-89.

414. Balkwill, F., *TNF-alpha in promotion and progression of cancer.* Cancer Metastasis Rev, 2006. **25**(3): p. 409-16.

415. Wang, S., et al., *Interferon-gamma induces senescence in normal human melanocytes.* PLoS One, 2014. **9**(3): p. e93232.

416. Yao, G., *Modelling mammalian cellular quiescence.* Interface Focus, 2014. **4**(3): p. 20130074.

417. Hernandez-Segura, A., J. Nehme, and M. Demaria, *Hallmarks of Cellular Senescence.* Trends Cell Biol, 2018. **28**(6): p. 436-453.

418. Lee, B.Y., et al., *Senescence-associated beta-galactosidase is lysosomal beta-galactosidase.* Aging Cell, 2006. **5**(2): p. 187-95.

419. Zhao, J., et al., *FoxO3 coordinately activates protein degradation by the autophagic/ lysosomal and proteasomal pathways in atrophying muscle cells.* Cell Metab, 2007. **6**(6): p. 472-83.

420. Salminen, A. and K. Kaarniranta, *Regulation of the aging process by autophagy.* Trends Mol Med, 2009. **15**(5): p. 217-24.

421. Carames, B., et al., *Autophagy is a protective mechanism in normal cartilage, and its aging-related loss is linked with cell death and osteoarthritis.* Arthritis Rheum, 2010. **62**(3): p. 791-801.

422. Matsuzaki, T., et al., *FoxO transcription factors modulate autophagy and proteoglycan 4 in cartilage homeostasis and osteoarthritis.* Sci Transl Med, 2018. **10**(428).

423. Shaikh, S. and L.F. Nicholson, *Optimization of the Tet-On system for inducible expression of RAGE.* J Biomol Tech, 2006. **17**(4): p. 283-92.

424. Costello, A., et al., *Leaky Expression of the TET-On System Hinders Control of Endogenous miRNA Abundance.* Biotechnol J, 2019. **14**(3): p. e1800219.

425. Kang, K., et al., *An improved Tet-on system in microRNA overexpression and CRISPR/Cas9-mediated gene editing.* J Anim Sci Biotechnol, 2019. **10**: p. 43.

426. Craig, N.L., *The mechanism of conservative site-specific recombination.* Annu Rev Genet, 1988. **22**: p. 77-105.

427. Sauer, B., *Site-specific recombination: developments and applications.* Curr Opin Biotechnol, 1994. **5**(5): p. 521-7.

428. Cong, L., et al., *Multiplex genome engineering using CRISPR/Cas systems.* Science, 2013. **339**(6121): p. 819-23.

429. Barrow, J.J., et al., *Bromodomain Inhibitors Correct Bioenergetic Deficiency Caused by Mitochondrial Disease Complex I Mutations.* Mol Cell, 2016. **64**(1): p. 163-175.

430. Muhar, M., et al., *SLAM-seq defines direct gene-regulatory functions of the BRD4-MYC axis.* Science, 2018. **360**(6390): p. 800-805.

431. Chen, N. and V. Karantza, *Autophagy as a therapeutic target in cancer.* 2011. **11**(2): p. 157-68.

432. Huang, M., et al., *Autophagy mediates proteolysis of NPM1 and HEXIM1 and sensitivity to BET inhibition in AML cells.* Oncotarget, 2016. **7**(46): p. 74917-74930.

433. Huang, M., et al., *Brd4 regulates the expression of essential autophagy genes and Keap1 in AML cells.* Oncotarget, 2018. **9**(14): p. 11665-11676.

434. Fung, C., et al., *Induction of autophagy during extracellular matrix detachment promotes cell survival.* Mol Biol Cell, 2008. **19**(3): p. 797-806.

435. Jang, J.E., et al., *Targeting AMPK-ULK1-mediated autophagy for combating BET inhibitor resistance in acute myeloid leukemia stem cells.* Autophagy, 2017. **13**(4): p. 761-762.

436. Lazova, R., V. Klump, and J. Pawelek, *Autophagy in cutaneous malignant melanoma.* J Cutan Pathol, 2010. **37**(2): p. 256-68.

437. Comes, F., et al., *A novel cell type-specific role of p38alpha in the control of autophagy and cell death in colorectal cancer cells.* Cell Death Differ, 2007. **14**(4): p. 693-702.

438. Qu, X., et al., *Promotion of tumorigenesis by heterozygous disruption of the beclin 1 autophagy gene.* J Clin Invest, 2003. **112**(12): p. 1809-20.

439. Chen, Y., et al., *Beclin-1 expression is a predictor of clinical outcome in patients with esophageal squamous cell carcinoma and correlated to hypoxia-inducible factor (HIF)-1alpha expression.* Pathol Oncol Res, 2009. **15**(3): p. 487-93.

440. Li, B.X., et al., *The expression of beclin 1 is associated with favorable prognosis in stage IIIB colon cancers.* Autophagy, 2009. **5**(3): p. 303-6.

441. Wan, X.B., et al., *Elevated Beclin 1 expression is correlated with HIF-1alpha in predicting poor prognosis of nasopharyngeal carcinoma.* Autophagy, 2010. **6**(3): p. 395-404.

442. Ceballos, E., et al., *c-Myc antagonizes the effect of p53 on apoptosis and p21WAF1 transactivation in K562 leukemia cells.* Oncogene, 2000. **19**(18): p. 2194-204.

443. Dong, X., et al., *BRD4 regulates cellular senescence in gastric cancer cells via E2F/ miR-106b/p21 axis.* Cell Death Dis, 2018. **9**(2): p. 203.

444. Halaban, R., et al., *Integrative analysis of epigenetic modulation in melanoma cell response to decitabine: clinical implications.* PLoS One, 2009. **4**(2): p. e4563.

445. Wansleben, S., et al., *A novel role for the anti-senescence factor TBX2 in DNA repair and cisplatin resistance.* Cell Death Dis, 2013. **4**: p. e846.

446. Tasdemir, N., et al., *BRD4 Connects Enhancer Remodeling to Senescence Immune Surveillance.* Cancer Discov, 2016. **6**(6): p. 612-29.

447. Michels, A.A., et al., *Binding of the 7SK snRNA turns the HEXIM1 protein into a P-TEFb (CDK9/cyclin T) inhibitor.* EMBO J, 2004. **23**(13): p. 2608-19.

448. Diribarne, G. and O. Bensaude, *7SK RNA, a non-coding RNA regulating P-TEFb, a general transcription factor.* RNA Biol, 2009. **6**(2): p. 122-8.

449. Webster, M.R., et al., *Wnt5A promotes an adaptive, senescent-like stress response, while continuing to drive invasion in melanoma cells.* Pigment Cell Melanoma Res, 2015. **28**(2): p. 184-95.

450. Sun, X., et al., *Senescence-associated secretory factors induced by cisplatin in melanoma cells promote non-senescent melanoma cell growth through activation of the ERK1/2-RSK1 pathway.* Cell Death Dis, 2018. **9**(3): p. 260.

451. Ivanochko, D., et al., *Direct interaction between the PRDM3 and PRDM16 tumor suppressors and the NuRD chromatin remodeling complex.* Nucleic Acids Res, 2019. **47**(3): p. 1225-1238.

452. Luijsterburg, M.S., et al., *DDB2 promotes chromatin decondensation at UV-induced DNA damage.* J Cell Biol, 2012. **197**(2): p. 267-81.

453. Mizushima, N., et al., *Dissection of autophagosome formation using Apg5-deficient mouse embryonic stem cells.* J Cell Biol, 2001. **152**(4): p. 657-68.

454. Levine, B. and D.J. Klionsky, *Development by self-digestion: molecular mechanisms and biological functions of autophagy.* Dev Cell, 2004. **6**(4): p. 463-77.

455. Thoreen, C.C., et al., *An ATP-competitive mammalian target of rapamycin inhibitor reveals rapamycin-resistant functions of mTORC1.* J Biol Chem, 2009. **284**(12): p. 8023-32.

456. LeRoy, G., B. Rickards, and S.J. Flint, *The double bromodomain proteins Brd2 and Brd3 couple histone acetylation to transcription.* Mol Cell, 2008. **30**(1): p. 51-60.

457. Yang, Z., et al., *Recruitment of P-TEFb for stimulation of transcriptional elongation by the bromodomain protein Brd4.* Mol Cell, 2005. **19**(4): p. 535-45.

458. Soutoglou, E. and T. Misteli, *Activation of the cellular DNA damage response in the absence of DNA lesions.* Science, 2008. **320**(5882): p. 1507-10.

459. Pal, D., et al., *Inhibition of autophagy prevents cadmium-induced prostate carcinogenesis.* Br J Cancer, 2017. **117**(1): p. 56-64.

460. Niture, S., et al., *TNFAIP8 promotes prostate cancer cell survival by inducing autophagy.* Oncotarget, 2018. **9**(42): p. 26884-26899.

461. Tu, W.B., et al., *MYC Interacts with the G9a Histone Methyltransferase to Drive Transcriptional Repression and Tumorigenesis.* Cancer Cell, 2018. **34**(4): p. 579-595 e8.

462. Vedadi, M., et al., *A chemical probe selectively inhibits G9a and GLP methyltransferase activity in cells.* Nat Chem Biol, 2011. **7**(8): p. 566-74.

463. Metzger, E., et al., *LSD1 demethylates repressive histone marks to promote androgen-receptor-dependent transcription.* Nature, 2005. **437**(7057): p. 436-9.

464. Cloos, P.A., et al., *The putative oncogene GASC1 demethylates tri- and dimethylated lysine 9 on histone H3.* Nature, 2006. **442**(7100): p. 307-11.

465. Perillo, B., et al., *DNA oxidation as triggered by H3K9me2 demethylation drives estrogen-induced gene expression.* Science, 2008. **319**(5860): p. 202-6.

466. Yu, Y., et al., *Targeting the Senescence-Overriding Cooperative Activity of Structurally Unrelated H3K9 Demethylases in Melanoma.* Cancer Cell, 2018. **33**(2): p. 322-336 e8.

467. Pollock, J.A., et al., *Lysine-specific histone demethylase 1 inhibitors control breast cancer proliferation in ERalpha-dependent and -independent manners.* ACS Chem Biol, 2012. **7**(7): p. 1221-31.

468. Xue, Y., et al., *NURD, a novel complex with both ATP-dependent chromatin-remodeling and histone deacetylase activities.* Mol Cell, 1998. **2**(6): p. 851-61.